Supramolecular Aspects of Fluorine Chemistry in Self-Assembled Monolayers

Harry Pinfold

A thesis submitted in partial fulfilment of the requirements for the degree of Doctor of Philosophy in Chemistry

Department of Chemistry, University of Warwick

July 2021

Table of Contents

Declarations ... **iv**

Abstract ... **v**

List of abbreviations ... **vi**

Chapter 1: Introduction ... **1**

1.1 Surface-confined supramolecular chemistry ... 2

1.2 Impact of experimental conditions ... 3

1.3 Intermolecular interactions ... 5

1.3.1 Metal–ligand coordination ... 6

1.3.2 van der Waals interactions ... 7

1.3.3 Hydrogen bonds ... 9

1.3.4 Halogen bonds ... 10

1.4 Multicomponent self-assembly ... 11

1.5 Host–guest networks ... 12

1.6 Organofluorine compounds ... 13

1.7 Hydrogen–fluorine interchange ... 16

1.8 Thesis objectives and outline ... 17

Chapter 2: Experimental background ... **19**

2.1 Basic principles of STM ... 20

2.2 STM at the solid–liquid interface ... 21

Chapter 3: Exploring the impact of fluorination on the self-assembly behaviour of isophthalic acid ... **25**

3.1 Homomolecular self-assembly behaviour of IPA ... 27

3.2 Response of IPA to the presence of coronene ... 28

3.3 Homomolecular self-assembly behaviour of F4IPA ... 29

3.4 Response of F4IPA to the presence of coronene ... 30

3.5 Conclusions ... 40

Chapter 4: Exploring the self-assembly behaviour of tripyridyltriazine isomers **42**

4.1 Potential conformations of the tripyridyltriazine isomers 43

4.2 Surface-induced chirality of 2TPTZ and 3TPTZ 44

4.3 Homomolecular self-assembly behaviour of 4TPTZ 45

4.4 Homomolecular self-assembly behaviour of 3TPTZ 46

4.5 Homomolecular self-assembly behaviour of 2TPTZ 49

4.6 Further discussion 54

4.5 Conclusions 54

Chapter 5: Exploring the impact of fluorination on the self-assembly behaviour of terephthalic acid in homomolecular and bimolecular systems **56**

5.1 Homomolecular self-assembly behaviour of TPA 59

5.2 Homomolecular self-assembly behaviour of F4TPA 60

5.3 Bimolecular self-assembly properties of TPA with 4TPTZ 60

5.4 Bimolecular self-assembly properties of F4TPA with 4TPTZ 61

5.5 Bimolecular self-assembly properties of TPA with 3TPTZ 63

5.6 Bimolecular self-assembly properties of F4TPA with 3TPTZ 64

5.7 Bimolecular self-assembly properties of TPA with 2TPTZ 65

5.8 Bimolecular self-assembly properties of F4TPA with 2TPTZ 67

5.9 Further discussion 68

5.10 Conclusions 69

Chapter 6: Fluorination as a route to the formation of 2D phenol–pyridine cocrystals **70**

6.1 Homomolecular self-assembly properties of TFHQ and HQ 72

6.2 Bimolecular self-assembly properties of TFHQ with 4TPTZ 72

6.3 Bimolecular self-assembly properties of HQ with 4TPTZ 74

6.4 Bimolecular self-assembly properties of TFHQ with 3TPTZ 75

6.5 Bimolecular self-assembly properties of HQ with 3TPTZ 76

6.6 Bimolecular self-assembly properties of TFHQ/HQ with 2TPTZ 77

6.7 Further discussion 77

6.8 Conclusions 80

Chapter 7: Exploring the interplay between fluorine activated hydrogen bonding synthons in 2D networks **81**

7.1 Homomolecular self-assembly properties of 4HTFBA 83

7.2 Bimolecular self-assembly properties of 4HTFBA with 4TPTZ 83

7.3 Bimolecular self-assembly properties of 4HTFBA with 3TPTZ 89

7.4 Bimolecular self-assembly properties of 4HTFBA with 2TPTZ 91

7.5 Conclusions 98

Chapter 8: Exploring the interplay between fluorine activated halogen and hydrogen bonds in 2D networks **99**

8.1 Homomolecular self-assembly properties of 4BTFBA 102

8.2 Bimolecular self-assembly properties of 4BTFBA with 4TPTZ 102

8.3 Bimolecular self-assembly properties of 4BTFBA with 3TPTZ 107

8.4 Conclusions 117

Chapter 9: Overall conclusions and perspectives **118**

9.1 Conclusions 118

9.2 Perspectives 120

Chapter 10: Experimental details **122**

10.1 STM setup 123

10.2 Sample preparation 124

10.3 Chemicals 124

10.4 Data analysis 125

References **126**

Declarations

This thesis has been submitted to the University of Warwick in partial fulfilment of the requirements for the degree of Doctor of Philosophy in Chemistry. All of the work presented here is entirely my own. It was performed between August 2016 and March 2020 under the supervision of Professor Giovanni Costantini. None of the work presented in this thesis has previously been submitted to any institution for a higher degree. Some of the work presented in this thesis has been published in the following articles:

Pinfold, H., Greenland, C., Pattison, G. & Costantini, G. Fluorinated carboxylic acids as powerful building blocks for the formation of bimolecular monolayers. Chem. Commun. 56, 125–128 (2020).

Pinfold, H., Pattison, G. & Costantini, G. Fluorination as a route towards unlocking the hydrogen bond donor ability of phenolic compounds in self-assembled monolayers. CrystEngComm 22, 2425–2428 (2020).

Abstract

The role of non-covalent interactions involving fluorine atoms is of significant interest in the field of supramolecular chemistry, with particular focus being invested into understanding the role such interactions have in medicinal chemistry and three-dimensional solid-state materials. Although the formation of two-dimensional surface-confined networks is largely governed by the same principles of supramolecular chemistry as the aforementioned fields, the potential value of interactions involving fluorine within these systems has been little studied. In this thesis, the supramolecular role of fluorine atoms within two-dimensional surface-confined networks is systematically explored. Scanning tunnelling microscopy is used to investigate the ability of an array of fluorinated molecular building blocks to self-assemble into two-dimensional surface-confined networks. The arrangement of the molecular building blocks within the resultant networks gives insight into the structural role of the intermolecular interactions at play. Specific insight into the significance of the fluorine atoms is obtained by comparing the self-assembly behaviour of the fluorinated building blocks with that of their unfluorinated structural analogues. Although some focus is given to simple homomolecular systems, particular emphasis is devoted to investigating the role of fluorination in promoting the formation of complex multicomponent networks. In some of the systems studied, the presence of fluorine atoms is found to have a minimal impact, with isostructural networks being observed with both the fluorinated and unfluorinated analogues. However, in other systems the fluorine atoms are found to play a very prominent role. This is rationalised as being due to a combination of weak intermolecular interactions in which the fluorine atoms can directly partake and the ability of fluorination to augment other intermolecular interactions, such as hydrogen bonds. In particular, fluorination is found to promote the formation of carboxyl–pyridyl and phenol–pyridyl hydrogen bonding interactions, the former of which is rarely observed in two-dimensional surface-confined networks and the latter of which has hitherto not been observed.

List of abbreviations

2D	Two-dimensional
3D	Three-dimensional
UHV	Ultra-high vacuum
DBA	Dehydrobenzo[12]annulene
TMA	Trimesic acid
4TPB	1,3,5-tri(4-pyridyl)benzene
TITFB	1,3,5-triiodotrifluorobenzene
3N	1,3,5-tris(pyridine-4-ylethynyl)benzene
DIP	Diindenoperylene
F_{16}CuPc	Copper hexadecafluorophthalocyanine
TCNQ	Tetracyanoquinodimethane
F4-TCNQ	Tetrafluorotetracyanoquinodimethane
IPA	Isophthalic acid
F4IPA	Tetrafluoroisophthalic acid
STM	Scanning tunnelling microscopy
SEM	Scanning electron microscopy
HOPG	Highly oriented pyrolytic graphite
TPTC	p-terphenyl-3,5,3',5' -tetracarboxylic acid
2TPTZ	2,4,6-tri(2-pyridyl)-*s*-triazine
3TPTZ	2,4,6-tri(3-pyridyl)-*s*-triazine
4TPTZ	2,4,6-tri(4-pyridyl)-*s*-triazine
DFT	Density functional theory
TPA	Terephthalic acid
F4TPA	Tetrafluoroterephthalic acid
HQ	Hydroquinone
TFHQ	Tetrafluorohydroquinone
4HTFBA	4-hydroxytetrafluorobenzoic acid
4BTFBA	4-bromotetrafluorobenzoic acid
4MeTFBA	4-methyltetrafluorobenzoic acid

Chapter 1: Introduction

Within this chapter, surface-confined supramolecular chemistry is introduced. The molecular building blocks used to form two-dimensional (2D) networks on surfaces and the prototypical non-covalent interactions used to govern their supramolecular organisation are discussed. Particular focus is given to complex multicomponent structures and the various routes towards their formation. Lastly, the supramolecular aspects of fluorine chemistry in surface-confined systems is reviewed and contrasted with that of conventional three-dimensional (3D) systems, which reveals a rich area for further research in this seemingly niche topic.

1.1 Surface-confined supramolecular chemistry

2D networks formed via the spontaneous organisation of molecular building blocks on atomically flat solid surfaces (see schematic in figure 1) have been extensively studied. The formation of these networks provides a promising bottom-up strategy for the nanoscale functionalisation of solid surfaces. Within these systems, the organisation of the molecular building blocks is primarily governed by a complex balance between the lateral intermolecular interacts between them and the interaction between the building blocks and the underlying surface.

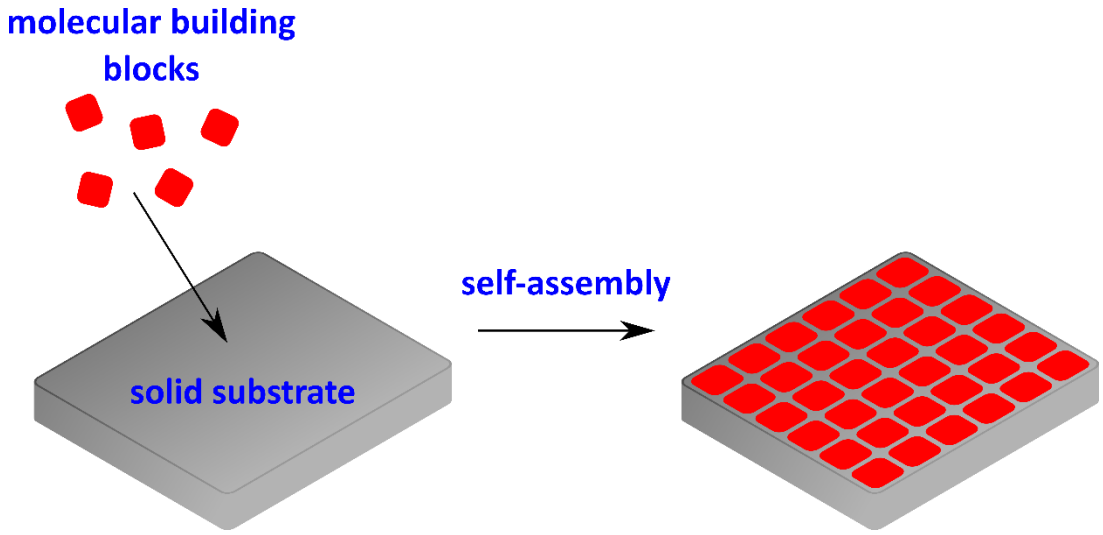

Figure 1: Simple schematic representation highlighting how molecular building blocks can spontaneously organise on the surface of a solid support into an ordered network.

Surface-confined 2D molecular assemblies can be broadly classified into two categories: chemisorbed and physisorbed systems. Within chemisorbed systems, the involved molecules are strongly bound (adsorption energy approximately 20–400 kJ/mol[1]) to the substrate's surface via chemical bonds. As a result, the interactions between the building blocks and the underlying surface typically plays a determinant structural role in the organisation of the molecules on the surface. Conversely, in physisorbed systems the molecules are not attached to the underlying surface via chemical bonds, and accordingly the association between the molecular building blocks and the underlying surface, which is typically mediated by van der Waals interactions, is much weaker (adsorption energy approximately 10–40 kJ/mol[1]). This weaker interaction with the surface means that lateral intermolecular interactions between the building blocks normally plays a more significant role in organising the molecules in physisorbed systems. As a result, physisorbed networks are ideal model systems on which to explore the influence of intermolecular interactions in 2D networks. Physisorbed networks and the intermolecular interaction which help stabilise them are the focus of this thesis.

1.2 Impact of experimental conditions

There is a wide range of different experimental conditions under which 2D surface-confined networks have been studied. Many of these networks are formed under ultra-high vacuum (UHV) conditions and the samples are held at cryogenic temperatures whilst being studied. At the other end of the spectrum are experiments conducted under ambient conditions. One particularly interesting environment in which such ambient conditions experiments are routinely conducted is the solid–liquid interface. The formation of 2D networks at this interface is typically achieved by simply depositing a volume of solution containing appropriate molecular building blocks onto the surface of a solid substrate. 2D surface-confined networks can then spontaneously form at the interface between the deposited solution and the surface of the substrate. The solid–liquid interface is a particularly thermodynamically challenging environment in which to form 2D surface-confined networks. Firstly, the solvent molecules themselves can adsorb on the surface; therefore, the self-assembly of the molecular building blocks on the surface must be favourable enough that they can outcompete the solvent molecules for surface adsorption. Secondly, the solution phase presents a competitive environment in the sense that it may be energetically favourable for the molecular building blocks to remain in solution rather than self-assemble on the surface. The use of ambient temperatures also presents challenges, particularly when compared with the cryogenic temperature routinely used in UHV studies. At low temperatures there is little thermal energy available to the molecular building blocks, and consequently weak non-covalent interactions can dominate their organisation. Conversely, at room temperature such weak interactions may no longer be sufficient. As a result, the use of stronger lateral intermolecular interactions is typically required to control the organisation of molecules at the solid–liquid interface. At the same time, the presence of strong non-covalent interactions within the 2D network can further increase the favourability of its formation and help to overcome the aforementioned issues associated with substrate–solvent and molecule–solvent interactions. This thesis is centred around the significance of intermolecular interactions within 2D surface-confined networks. Consequently, the solid–liquid interface under ambient conditions was chosen as the environment of study since the challenges associated with it present an acid test which gives valuable insight into the efficacy of the intermolecular interactions under investigation.

There are a number of different experimental conditions which can influence the organisation of a given molecular building block at the solid–liquid interface under ambient conditions. These include the identity of the substrate, the identity of the solvent and the concentration of the deposited solution. Within the following, these variables are briefly discussed and examples of the significance of each are given.

The nature of the substrate can significantly influence the self-assembly properties of molecular building blocks. Although this variable has been more significantly investigated under UHV conditions, where the number of available substrates is much more extensive, it can also play a prominent role at the solid–liquid interface. So that the surface is stable to processes such as oxidation, the use of inert substrates is required for experiments conducted under ambient-conditions at the solid–liquid interface. This, and a number of other factors which will be further discussed in section 2.2, severely limits the range of suitable substrates, and accordingly the only substrates which find routine use under these conditions are graphite and Au(111). These two surfaces both have a similar hexagonal arrangement of atoms on their surfaces. Despite this, due to differences in the interfacial interactions between adsorbed molecules and the two substrate materials, the organisation of molecular building blocks on them can differ significantly.[2–5] Also of note is the use of modified surfaces. Of particular significance are HOPG substrates which have been modified via the electrochemical grafting of diazonium compounds.[6] The presence of these covalently grafted species can significantly influence the way molecules will organise themselves on the surface when compared with unmodified HOPG.

The concentration of the solution can also play a significant role in influencing the self-assembly behaviour of molecular building blocks at the solid–liquid interface. One way in which the influence of the concentration manifests itself is through concentration-dependant polymorphism, i.e., the organisation of the molecular building blocks on the surface can differ depending on their concentration in solution. The first observation of the behaviour was reported in the seminal work of Lei et al.[7] They found that the a series of alkoxylated dehydrobenzo[12]annulene (DBA) derivatives can form two distinct structures at the 1,2,4-trichlorobenzene/graphite interface and that which of the two structures is observed depends on the concentration of DBA derivative in the solution. In the higher concentration regime, the formation of a densely packed linear structure is preferred, whereas in the lower concentration regime a porous hexagonal structure is preferred. Since its initial observation, concentration-dependant polymorphism is now routinely reported for systems studied at the solid–liquid interface, with the formation of lower density structures at lower concentrations being the typical observation.

The final factor which will be discussed is the role of the identity of the solvent. There are a wide range of systems in which solvent identity is significant and there are a variety of different mechanisms through which it can influence the structure of 2D networks.[8] The prototypical example of a 2D surface-confined system in which solvent identity is significant occurs with the molecule trimesic acid (TMA). TMA can self-assemble into two polymorphs at the interface between fatty acid solvents and a graphite substrate.[9] When using the short chain fatty acid solvents butanoic acid, pentanoic acid and hexanoic acid, the so-called flower polymorph is observed. Alternatively, with the longer chain

solvents, octanoic acid and nonanoic acid, TMA self-assembles into the less densely packed 'chicken-wire' structure. When heptanoic acid, which has an intermediate chain length, is used as the solvent,

both polymorphs coexist on the surface. Overall, what is seen is that as the length of the chain of the solvent is increased the networks formed with TMA transition from the flower polymorph to the chicken-wire polymorph. One suggested explanation for this behaviour is that the solvent impacts on the formation of precursor seed units in solution which in turn impacts on the structure of the networks observed. An alternative explanation is solvent coadsorption, with the idea being that the coadsorbed solvent molecules may be present in one or both of the polymorphs and that different solvents stabilise the formation of different structures. However, the exact mechanism for the solvent-induced polymorphism observed with TMA remains unclear, particularly when it is noted that the solubility of TMA in each of the solvents differs and that no concentration-dependant measurements were undertaken to explore the significance of this, with only saturated solutions being tested. Although there is no unambiguous evidence for its role in the networks formed with TMA, solvent-coadsorption is the most direct route through which solvent identity can influence network morphology, and there are several other systems in which this is clearly observed.[8] Within these systems, the coadsorbed solvent molecules can be thought of as molecular building blocks which coassemble with the solute molecules on the surface. By simply changing the structure of one of the building blocks, i.e., the solvent, the structure of the assembly can accordingly be altered.

1.3 Intermolecular interactions

One of the most significant challenges in surface-confined supramolecular chemistry is predicting the arrangement of 2D architectures based on the structure of the molecular building blocks from which they are constructed. However, due to the complex balance between the different non-covalent interactions in which a given building block can normally partake and the influence of the underlying surface, accurate predictions of how the molecules will arrange themselves can be extremely challenging. One way to circumvent this issue is to utilise strong intermolecular interactions which are capable of dominating the self-assembly process. Knowledge of which intermolecular interactions can be reliably utilised in this manner allows chemists to design molecular building blocks which self-assemble in a more predictable manner.

Various different non-covalent interactions have been used to organise molecular building blocks within surface-confined systems. These include metal–ligand coordination[10], van der Waals

interactions[11], hydrogen bonds[12–15] and halogen bonds[16]. These four interactions and their utility in surface-confined supramolecular chemistry is discussed in the following.

1.3.1 Metal–ligand coordination

Coordination chemistry is the study of molecular systems in which metal atoms/cations are directly bound to surrounding molecules/anions known as ligands. Although this chemistry has historically been primarily utilised for the formation of 3D structures, it has recently found routine use for the formation of 2D surface-confined networks[10]. Within these networks, metal atoms/cations serve as nodes whilst the ligands act as linkers which bridge these nodes. Due to the inherent directionality of the metal–ligand interactions, the ligands are typically attached to the metal centres at well-defined angles. Furthermore, the nodes typically coordinate with a particular number of ligands. These properties can control the spatial arrangement of the ligands and metal atoms/cations on the surface, resulting in the formation of ordered 2D networks.

The use of coordination chemistry is a versatile approach which can be used for the fabrication of a diverse array of structures.[10] One way to control the organisation of the assembly is by adjusting the structure of the ligands. By adjusting the dimensions of the backbone of the ligand, the separation and angle between different nodes can be adjusted. Furthermore, changing the functional groups which directly coordinate to the metal centres can also modify the arrangement of the assembly. Different ligands can interact with the same metal centre via different coordination geometries. Such local changes in the arrangement of ligands around the nodes can result in significant modification to the overall arrangement of the assembly. The arrangement of the ligands around the nodes also depends on the identity of the metal atoms/cations being used as the nodes. One such example, reported by Shi et al., occurs when the molecule 1,3,5-tri(4-pyridyl)benzene (4TPB, figure 2) is employed as a ligand.[17] When deposited together onto a gold surface, 4TPB and copper atoms coassemble into a porous chicken-wire network (see figure 2). The formation of this chicken-wire assembly is mediated by Cu···N(pyridyl) coordination interactions between the copper atoms and the 4TPB molecules. Within this assembly, each of the copper atoms interacts with two 4TPB molecules via a linear coordination motif. When 4TPB is deposited alongside iron atoms rather than copper atoms, a new structure is observed. In this case, the assembly is mediated by Fe···N(pyridyl) coordination interactions and its structure differs markedly from that observed with copper (see figure 2). Rather than the linear twofold coordination observed with copper, each iron atom interacts with three 4TPB molecules via a threefold-symmetric coordination motif. These different coordination motifs, which

come about due to differences in the identity of the metal atoms being used as nodes, result in markedly different supramolecular arrangements being observed with the two metals.

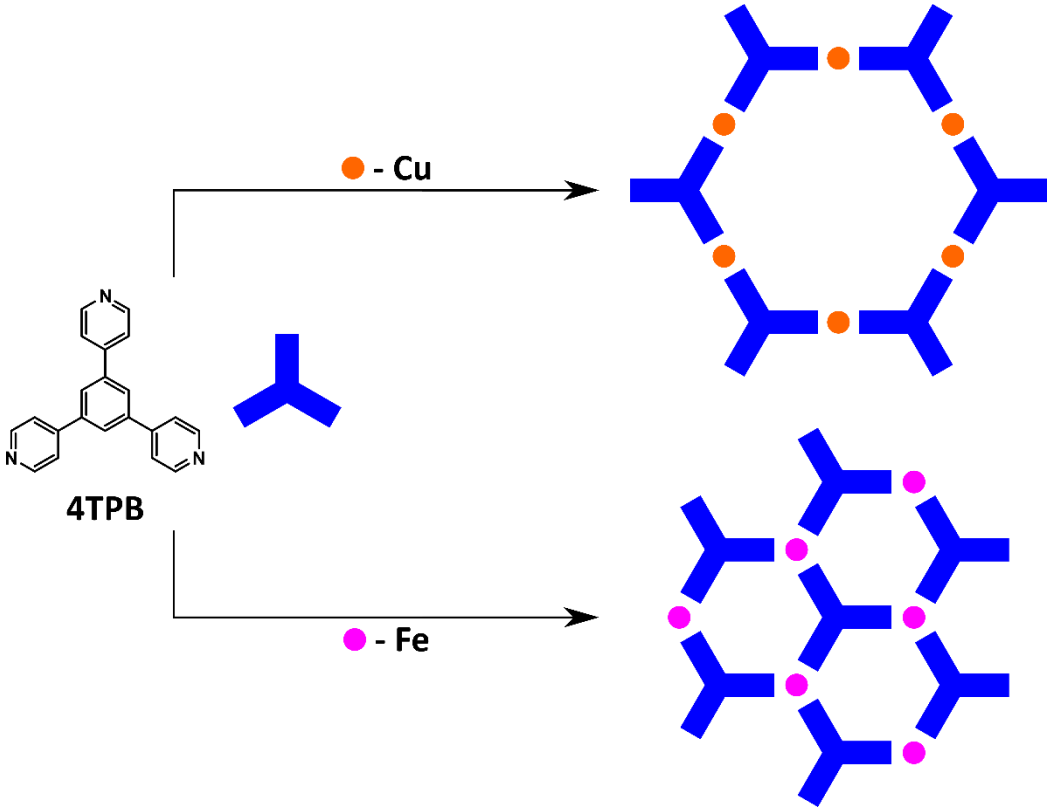

Figure 2: Schematic representation of the different self-assembled structures observed when 4TPTB is codeposited with copper and iron.

1.3.2 van der Waals interactions

Although van der Waals interactions are typically quite weak and are not inherently directional, through judicious design of the molecular building blocks used, these interactions can be a powerful tool for the formation of stable, ordered networks. This approach typically relies on the favourable interdigitation of long alkyl chains. Alkyl chains themselves are not functionalised such that they can partake in any particularly strong non-covalent interactions. Despite this, simple straight chain alkanes are observed to self-assemble into 2D networks on solid surfaces.[18–45] Within these networks, the alkyl chains typically pack together side-by-side on the surface into lamella structures. The driving force for this organisation is a combination of the lateral van der Waals interactions between adjacent alkyl chains and the van der Waals interactions between the chains and the underlying surface. The significance of the surface is particularly prominent when graphite is employed as the substrate due to the preferential alignment of straight chain alkanes with the $\langle 11\bar{2}0 \rangle$ directions of the graphite surface.[18]

Although as isolated compounds alkyl chains are of limited interest in terms of their ability to self-assemble on surfaces, their chemistry can be used to control the organisation of other compounds. By functionalising molecular building blocks with long alkyl chains, the van der Waals driven interdigitation of the attached chains can be used to control the arrangement of the molecules on the surface. This approach has been pioneered by the De Feyter group at KU Leuven, in collaboration with the Tobe group at Osaka University.[11] They have extensively studied the surface-confined self-assembly of a library DBAs and various derivatives thereof. Many of the DBAs studied have their rigid triangular core peripherally functionalised with alkyl/alkoxy chains (see figure 3). Although a range of different structures can be formed based on the precise experimental conditions and the exact structure of the DBA used, the van der Waals mediated side-by-side packing of the chains is consistently observed to play a dominant role in the organisation of these molecules. One seminal example is the formation of a porous honeycomb type network with the molecule DBA-C10. DBA-C10 is a DBA derivative in which the rigid triangular centre is functionalised with six straight chain alkyl groups, each of which is ten carbon atoms long (see figure 3). As is shown schematically in figure 3, the van der Waals driven interdigitation of these alkyl chains organises the DBA-C10 molecules into a honeycomb network. This same pattern has also been observed for a range of other DBA derivatives with different length chains.

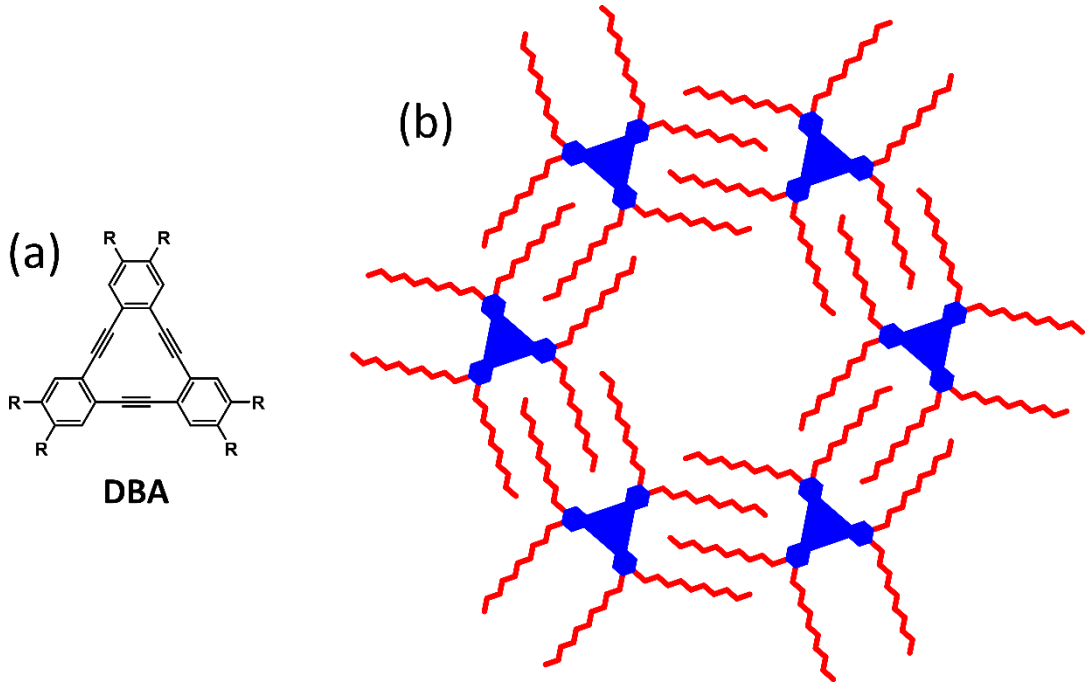

Figure 3: (a) Molecular structure of DBA. The R groups represent unbranched alkyl or alkoxy chains. **(b)** Schematic representation of the porous hexagonal structure formed via the self-assembly of DBA-C10. The blue shapes highlight the cores of the DBA molecules. The alkyl chains are highlighted in red.

1.3.3 Hydrogen bonds

Hydrogen bonds are perhaps the most extensively utilised intermolecular interaction in the context of surface-confined supramolecular chemistry.[12–15] They are both strong and directional, properties which are ideal for the formation of stable, ordered networks. Likely the most widely studied molecular building blocks for the formation of hydrogen-bond-controlled 2D networks are carboxylic acids.[14,15] Although carboxylic acids are capable of interacting via a range of different hydrogen bonding motifs, the most extensively observed is the $\mathrm{R}_2^2(8)$ hydrogen bonding junction (see figure 4). Within this motif, two carboxyl groups, which act as both hydrogen bond donors and acceptors, interact via two strong hydrogen bonds. Other classes of molecular building blocks that are routinely used also often involve functional groups which interact via multiple hydrogen bonds as, for example, between imide moieties and the molecule melamine.[12] Within this motif, the imide groups interact with the melamine molecules via triple hydrogen bonds (see figure 4). The use of motifs which are mediated via multiple hydrogen bonds likely increases the efficacy of these interactions compared to cases where only single hydrogen bonds are used.

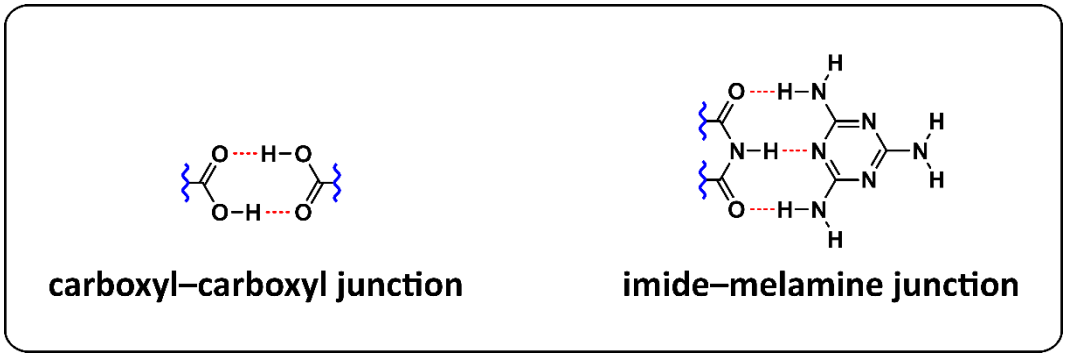

Figure 4: Schematics showing the $R_2^2(8)$ hydrogen bonding junction formed between two carboxyl groups and the triple hydrogen bonding junction formed between imides and melamine.

The previously discussed self-assembly of the molecule TMA (see section 1.2) is an archetypal example of how hydrogen bonds can be used to control the formation of surface-confined networks. The molecules within both networks into which TMA self-assembles, namely the flower and chicken-wire structures, are organised via hydrogen bonding interactions between their carboxyl groups. These strong hydrogen bonding interactions are sufficient to stabilise these structures under a range of different conditions, including ambient conditions at the solid–liquid interface[9]. The chicken-wire network, which is highlighted schematically in figure 5, is a clear example of the efficacy of the aforementioned $\mathrm{R}_2^2(8)$ hydrogen bonds, which are the only intermolecular interactions present between the TMA molecules within this structure.

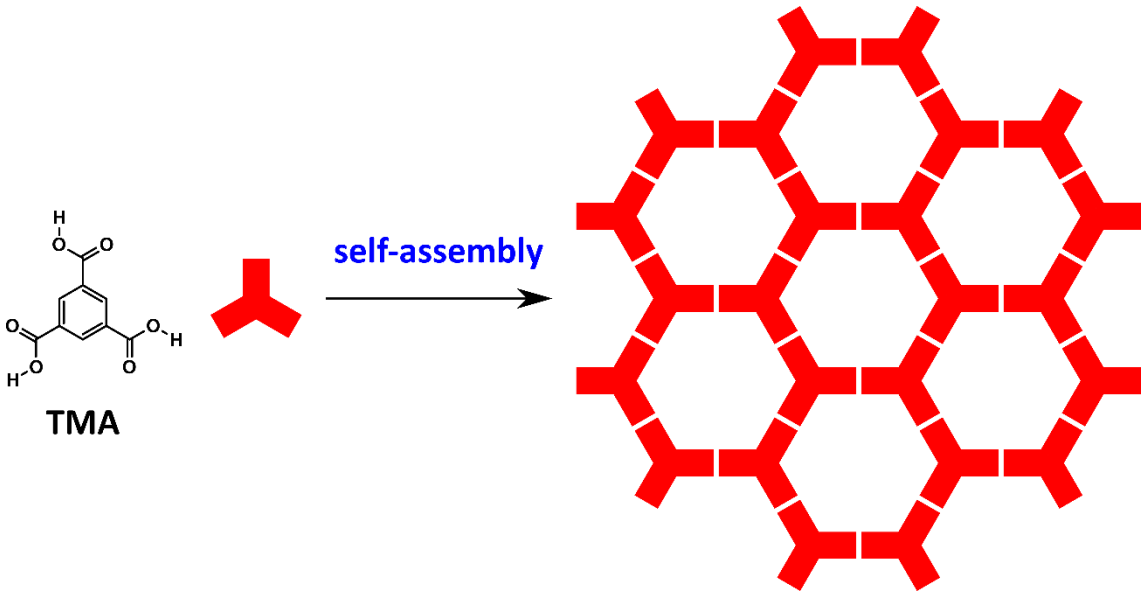

Figure 5: Schematic representation of the chicken-wire structure formed via the self-assembly of TMA.

1.3.4 Halogen bonds

Of the four non-covalent interactions highlighted, halogen bonds are the least frequently encountered. Despite this, recent results clearly demonstrate the efficacy that these interactions have for controlling the formation of 2D networks.[16] When a halogen atom is attached to an electron withdrawing group, the electron density surrounding it can become polarised. As a result of this polarisation, an electrophilic region associated with the halogen atom forms. This electrophilic region, which is known as a σ-hole[46], is centred at the antipode of the covalent bond attaching the halogen atom to the electron withdrawing group. The σ-hole typically manifests itself clearly in the electrostatic potential energy distribution surrounding the halogen atom (see figure 6).[47,48] It is the interaction between the σ-hole of a halogen atom and a nucleophilic site that constitutes a halogen bond. As the strength of the halogen bond typically correlates with the extent of the polarisation of

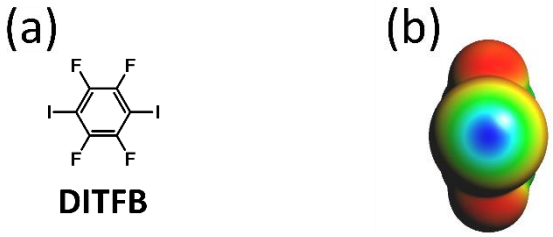

Figure 6: (a) Chemical structure of 1,4-diiodotetrafluorobenzene (DITFB), which is a prototypical halogen bond donor. **(b)** Electrostatic potential map of DITFB viewed along the axis of one of the C–I bonds. The σ-hole on the iodine atom can be clearly seen as a concentrated region of positive electrostatic potential (region shown in blue).

the partaking halogen atom, the heavier, more polarisable halogen atoms typically form stronger halogen bonds, i.e., halogen bond strength increases as the identity of the halogen bond donating atom changes according to the following sequence: F < Cl < Br < I.

Like hydrogen bonds, halogen bonds can be both strong and directional, and these properties have been similarly exploited for the formation of 2D structures on surfaces.[16] The most compelling examples are networks formed under the thermodynamically challenging conditions present at the solid–liquid interface. These systems are often stabilised by strong I···N(pyridyl) halogen bonds.[49–51] Zheng et al. have reported on the formation of number of such systems, amongst which is a seemingly porous chicken-wire structure.[49] This chicken-wire structure is formed using two different building blocks, namely 1,3,5-triiodotrifluorobenzene (TITFB, figure 7) and 1,3,5-tris(pyridine-4-ylethynyl)benzene (3N, figure 7). The TITFB molecules serve as halogen bond donating building blocks which each interact with three 3N molecules via I···N(pyridyl) halogen bonds. As is shown schematically in figure 7, these interactions organise the TITFB and 3N molecules into a porous hexagonal array. This structure is of particular interest as I···N(pyridyl) halogen bonds appear to be the only direct intermolecular interaction between the TITFB and 3N molecules, which exemplifies the dominant structural role that halogen bonds can have in surface-confined networks.

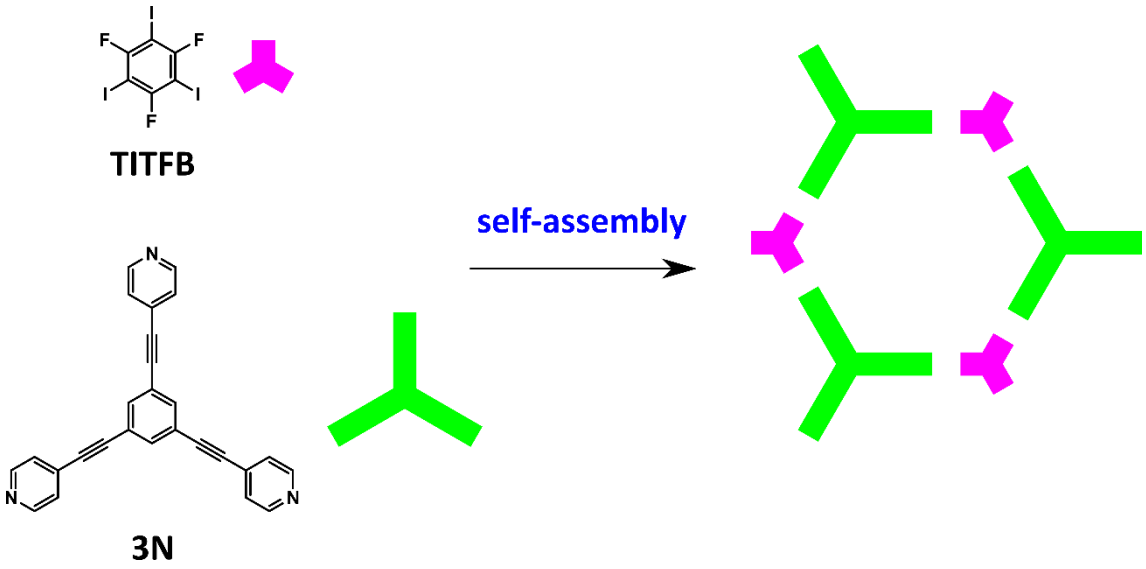

Figure 7: Schematic representation of the chicken-wire structure formed via the coassembly of TITFB and 3N.

1.4 Multicomponent self-assembly

Multicomponent networks are a special class of systems constructed using two or more chemically distinct molecular building blocks. The simultaneous use of multiple building blocks increases the potential complexity of the networks which can be formed. Despite extensive research in this area,

the controlled formation of multicomponent networks remains particularly challenging. In order to reliably form such systems, the stability of the desired multicomponent system must exceed that of the homomolecular assembly of all of the individual components and that of any other multicomponent structures formed using a submaximal number of the available building blocks. Designing molecular building blocks which behave in such a manner requires an extremely clear understanding of the non-covalent interactions which govern molecular recognition.

The difficulty in constructing multicomponent networks increases with the number of building blocks used. Consequently, bimolecular networks are routinely observed, trimolecular networks[5,52–60] are much less frequently encountered, and tetramolecular networks have only been constructed in a handful of exceptional cases[60–63]. An example of a bimolecular system is the coassembly of TITFB and 3N that was discussed in section 1.3.4. More interesting are the handful of reported tetramolecular system, with four distinct building blocks being the maximum number which has thus far been observed in a single surface-confined 2D network. The formation of these highly complex systems relies on a delicate balance between complementary intermolecular interactions coupled with highly specific size and shape complementarity between the involved building blocks.

1.5 Host–guest networks

Host–guest networks are a special class of multicomponent structures comprised of two distinct components: guest molecules and a porous host network which accommodates them. The guest molecules, which adsorb within the pores of the host network, serve no determinant role in the structure of the assembly, and their organisation is controlled by the position and structure of the pores within the host network. In order for a host network to effectively capture guest molecules, the shape and size of its pores must be complementary with the dimensions of the desired guest. Furthermore, the chemical functionality lining the pores must be complementary with that on the periphery of the desired guest such that there are no repulsive interactions which may disrupt guest capture. The favourable adsorption of the guest molecules on the surface and lateral van der Waals interactions between them and the interior of the pores are often sufficient to facilitate effective guest capture. Although these van der Waals interactions are typically sufficient, efforts have been made to improve guest capture systems by functionalising the pores such that they can interact with the desired guests via specific non-covalent interactions.[64]

By exploiting the kind of non-covalent chemistry discussed in section 1.3, a library of different host–guest structures have been constructed.[64–67] Amongst this library of systems, the successful capture

of a range of different guest species has been observed. One prototypical example relates to the molecule TMA. As was discussed in section 1.3.3, TMA self-assembles into a porous chicken-wire structure (see figure 5). As was demonstrated by Griessl et al., this chicken-wire structure is an effective host structure for the capture of the polycyclic aromatic hydrocarbon coronene (see schematic in figure 8).[68] This process relies on the precise shape and size complementarity between the pores of the chicken-wire structure and the dimension of the coronene guest molecules.

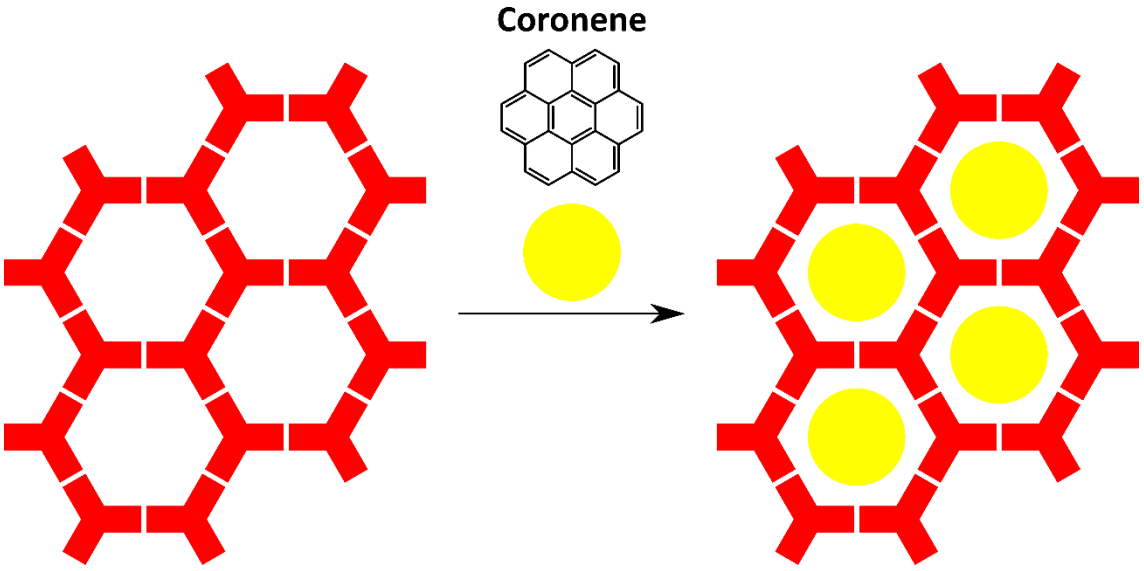

Figure 8: Schematic representation showing how coronene molecules can be captured within the pores of the chicken-wire structure of TMA.

1.6 Organofluorine compounds

Fluorinated compounds represent a particularly interesting class of molecules within the context of supramolecular chemistry. This is of particular note in the field of 3D crystal engineering, where interactions involving fluorine atoms have gained significant interest.[69–71] Although the non-covalent interactions in which fluorine atoms can directly partake are typically quite weak, as is discussed in the following, these interactions have been shown to play a determinant role in a variety of supramolecular systems.

Even amongst the diverse array of elements present on the periodic table, fluorine is particularly unique. It is the most electronegative element and is further characterised by its compact size and low polarisability. One of the most striking aspects of the supramolecular chemistry of organic fluorine is its inability to readily partake in any particularly strong non-covalent interactions. Fluorine atoms within organic molecules possess three lone pairs of electrons and, due to the electronegativity of fluorine, have a high density of negative charge. Intuitively, these properties should make fluorine atoms effective acceptor sites for the formation of strong hydrogen bonds. However, there is little

evidence to support this, and strong hydrogen bond donor sites, such as N−H and O−H sites, rarely hydrogen bond to organic fluorine atoms.[71–74] More commonly observed are C−H···F interactions,[71,72] which although weak can play a significant role in supramolecular systems[75]. The role of fluorine atoms as hydrogen bond acceptors is generally a controversial topic and remains an active area of research.

Another interaction in which fluorine may be expected to partake in, by virtue of its position on the periodic table, are halogen bonds. As was discussed in section 1.3.4, the formation of halogen bonds typically requires that the halogen bond donating atom is polarised via attachment to an electron withdrawing group. However, due to the low polarisability of fluorine its ability to act as an effective halogen bond donor site is clearly limited. Despite this, such interactions have been reported.[76] In order to achieve this, the halogen bond donating fluorine atoms must be attached to particularly strong electron withdrawing groups in order for sufficient polarisation to be achieved. However, even under these conditions the interactions observed are typically very weak. Furthermore, whether or not these seldom encountered interactions can truly be classified as halogen bonds remains controversial.[77] Although the direct participation of fluorine in halogen bonds is limited, fluorine chemistry still has significant utility in this area. The strong electron withdrawing influence of fluorine can be used to polarise the electron density of the heavier halogens, thereby activating them towards halogen bonding. A classic example occurs with halobenzenes, for which halogen bond donor strength dramatically increases upon fluorination of the aromatic core.[78] This effect is exploited in the coassembly of TITFB and 3N discussed in section 1.3.4. Within this system, the iodine atoms of the halogen bond donating building block, TITFB, are polarised by the electron withdrawing influence of the fluorine substituents of its central benzene ring.

In addition to the interactions discussed above, other interactions in which organic fluorine atoms have been reported to directly partake include F···F, F···π_F and F···metal interactions.[69–71] One general characteristic of interactions directly involving organic fluorine atoms is that they are quite weak. Although these interactions are generally not sufficient to dominate the organisation of supramolecular systems on their own, they often play a significant supporting role.

Despite general interest in the field of supramolecular chemistry, research into the role of interactions involving organic fluorine atoms in surface-confined 2D networks is far from comprehensive. However, there are a number of studies which do offer some insight in this area.[58,63,79–114] A range of different interactions have been suggested to be of significance in surface-confined 2D systems. These include C−F···π[79,80], F···F[80–83] and C−H···F[58,81–100] interactions. Of these, C−H···F interactions are by far the most extensively observed and evidence that these weak interactions can play a significant role in surface-confined 2D systems is particularly compelling. One prominent example, which has served as

the foundation for a number of further studies, is the coassembly of diindenoperylene (DIP) and copper hexadecafluorophthalocyanine (F_{16}CuPc). As was shown by Barrena et al.,[92] DIP and F_{16}CuPc are able to coassemble into highly ordered bimolecular networks on both copper and gold substrates under UHV conditions. The organisation of the molecules within these bimolecular networks is controlled by C–H···F interactions between the hydrogen atoms on the periphery of the DIP molecules and the fluorine atoms on the periphery of the F_{16}CuPc molecules. C–H···F interactions also seem to be capable of influencing the organisation of molecules within 2D networks formed at the solid–liquid interface. One particularly clear-cut example[87] occurs with the tripodal molecule shown in figure 9. This molecule consists of a 1,3,5-tri(phenylethynyl)benzene core which is further functionalised on its periphery by pentafluorobenzyl groups which are attached to the core via diacetylene linkages. As is

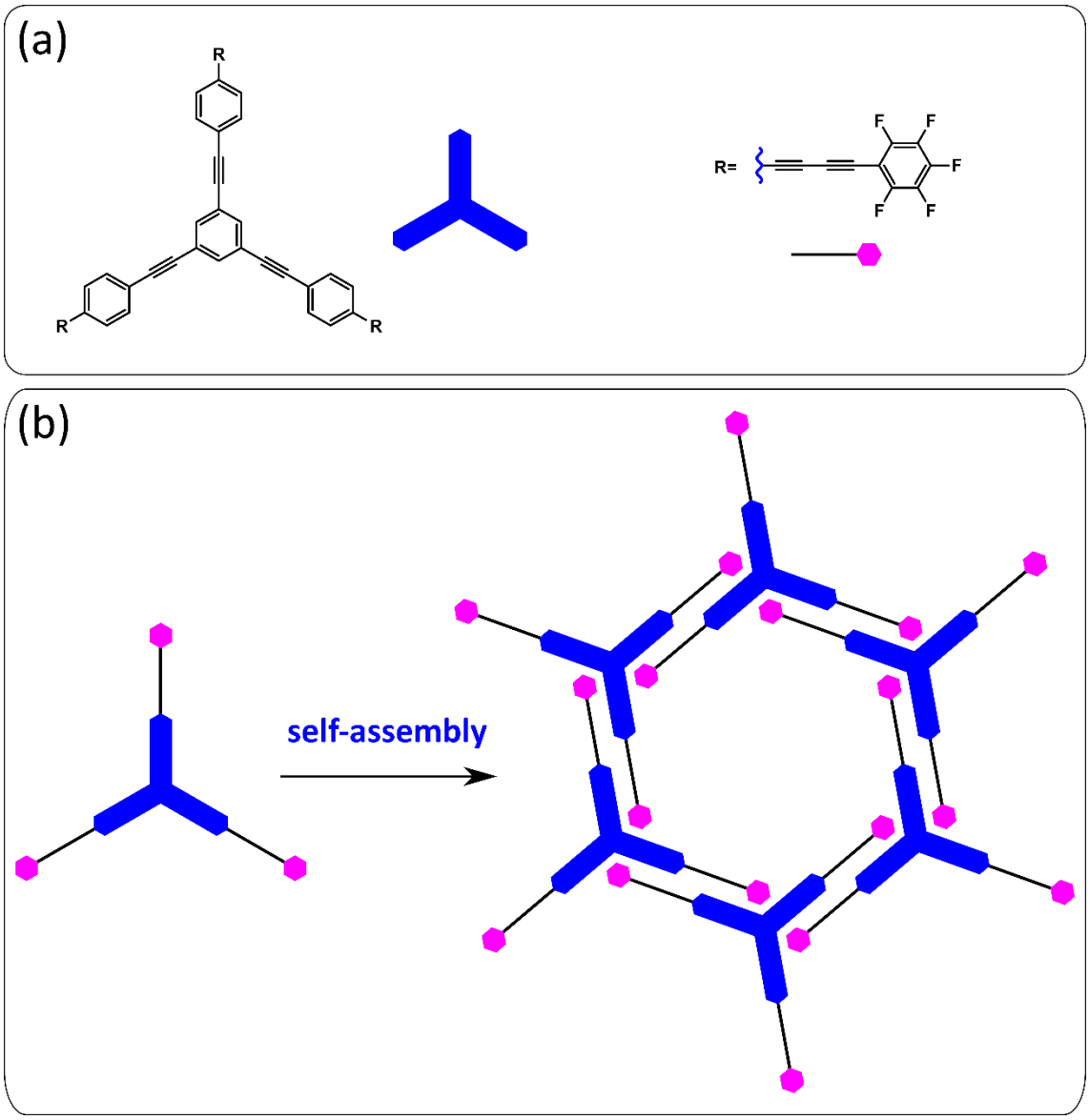

Figure 9: (a) Structure of the tripodal molecular building block. **(b)** Schematic representation of the porous hexagonal structure formed via the self-assembly of the tripodal molecule shown in (a).

shown schematically in figure 9, the molecules are organised into a porous structure via C–H···F interactions between the fluorine atoms of the pentafluorophenyl groups and the hydrogen atoms of the 1,3,5-tri(phenylethynyl)benzene core.

1.7 Hydrogen–fluorine interchange

Exchanging hydrogen atoms for fluorine atoms is a particularly interesting and well explored structural transformation. The van der Waals radii of hydrogen (1.20 Å[115]) and fluorine (1.47 Å[115]) are not dissimilar. Accordingly, the interchange of these two elements does not typically have a significant steric impact. At the same time, differences in the properties of hydrogen and fluorine, of which the extreme difference in electronegativity is particularly significant, mean that interchanging these two elements can significantly alter a compound's chemical properties. Overall, the exchange of hydrogen and fluorine can be used to modify a compound's chemical properties without significantly modifying its dimensions. This transformation is of extreme importance in the field of medicinal chemistry as it allows the chemical properties of drug candidates to be modified without majorly disrupting the sterics required for shape complementarity with the target molecule.[116] Albeit to a much lesser extent, the impact of the interchange of hydrogen and fluorine has also been studied in in the field of 3D crystal engineering.[69,71] As is discussed in the review by Berger et al.,[69] the general observation is that the introduction of fluorine offers the potential for different intermolecular interactions which results in different crystal structures being observed with fluorinated and unfluorinated analogues.

There are a number of studies in which the influence of the interchange of hydrogen and fluorine atoms on the organisation of molecular building blocks within 2D surface-confined systems has been explored. Within some of these studies, interchanging hydrogen and fluorine is not found to significantly impact upon the organisation of the molecular building blocks, with isostructural networks being formed with both the fluorinated and unfluorinated analogues.[106–108] The fact that such isostructural networks can be observed is testament to the minimal steric impact associated with interchanging hydrogen and fluorine. However, in the majority of examples, the structure of the 2D surface-confined networks formed with fluorinated and unfluorinated analogues are found to differ.[63,83–88,101–106] In most cases this seems to occur due to the different intermolecular interactions in which the two analogues can partake. One such example occurs with the previously discussed tripodal molecule shown in figure 9. As was shown in section 1.6, C–H···F interactions between the between the fluorine atoms of its pentafluorophenyl groups and the hydrogen atoms of its 1,3,5-tri(phenylethynyl)benzene core mediate the supramolecular organisation of this tripodal molecule into ordered networks. Within the study by Mu et al. which demonstrated this,[87] the self-assembly of

the unfluorinated analogue, i.e., the same structure but with phenyl groups instead of pentafluorophenyl groups, was also studied. Interestingly, the unfluorinated version was not observed to self-assemble into surface-confined 2D networks under the same conditions that were successful with its fluorinated analogue. This was ascribed to the inability of the unfluorinated analogue to partake in C−H···F interactions. A similar situation has been observed when comparing the self-assembly of the molecule para-sexiphenyl with that of two partially fluorinated analogues.[86] Para-sexiphenyl does not self-assemble into 2D supramolecular structures when deposited onto a silver substrate at low coverage. Conversely, with the two partially fluorinated analogues aggregation into 2D supramolecular structures is observed at low coverage, which is attributed to the ability of these molecules to favourably interact via C−H···F interactions. Although in the examples discussed thus far fluorination is found to play an advantageous role in organising molecular building blocks into 2D surface-confined structures, in some cases it can play a more disruptive role.[84,103] One such example occurs when comparing the self-assembly behaviour of the electron acceptor tetracyanoquinodimethane (TCNQ) and its fluorinated analogue tetrafluorotetracyanoquinodimethane (F4-TCNQ).[103] When deposited onto a layer of graphene grown on iridium, TCNQ self-assembles into an ordered structure due to C−H···N interactions. However, these interactions are no longer possible in F4-TCNQ, where the hydrogen atoms are replaced with fluorine atoms. Furthermore, repulsion involving the negatively charged fluorine and nitrogen atoms on the periphery of the F4-TCNQ molecules disfavours close packing, and accordingly the formation of compact supramolecular networks is not observed with F4-TCNQ.

1.8 Thesis objectives and outline

This thesis addresses the supramolecular aspects of fluorine chemistry in 2D surface-confined systems formed at the solid–liquid interface, with the aim of exploring how the supramolecular potential of fluorine can be utilised in this setting. The impact of intermolecular interactions involving fluorine on the self-assembly properties of a range of different molecular building blocks is investigated. Particular focus is given to the role of fluorine in augmenting other interactions such as hydrogen and halogen bonds. Using this approach, the potential role of fluorine in stabilising the formation hydrogen bonding motifs which are not typically observed in 2D surface-confined systems is explored. Throughout these studies, the supramolecular significance of the fluorine atoms is investigated by studying analogous systems in which they have been replaced with hydrogen atoms. In the latter two results chapters of this thesis, attention is refocused away from the direct role of fluorine and towards the hydrogen and halogen bonding interactions which fluorine mediates, with a particular focus on

understanding the interplay between these interactions. A brief outline of each of the results chapters is given below.

Chapter 3: A comparative study on the self-assembly properties of the molecule isophthalic acid (IPA) and its fluorinated analogue (F4IPA) is presented. Differences in the homomolecular self-assembly properties of these two molecules are studied and discussed. Furthermore, the steric impact associated with interchanging hydrogen and fluorine is evaluated by exploring the ability of both IPA and F4IPA to form coronene-templated cyclic hexamers: a process which requires precise shape and size complementarity between the IPA/F4IPA and coronene molecules.

Chapter 4: The self-assembly properties of a series of tripyridyltriazine isomers is studied at the solid–liquid interface. The impact of both the identity of the solvent and the concentration of the solutions on the self-assembly behaviour of these molecules is explored. The tripyridyltriazine isomers do not contain fluorine, and the results in this chapter are not directly related to the main aims of this thesis. However, these molecules are utilised as acceptors for both halogen and hydrogen bonds for the formation of complex multicomponent structures in the subsequent chapters, and the structure of the networks formed using only the tripyridyltriazine isomers provides a useful point of comparison.

Chapter 5: The impact of fluorination on both the homomolecular and bimolecular self-assembly properties of a simple dicarboxylic acid are explored. The bimolecular systems of interest are prepared by coupling the dicarboxylic acid and its fluorinated analogue with a series of tripyridyltriazine isomers, with the aim of constructing bimolecular networks driven by carboxyl–pyridine hydrogen bonding interactions.

Chapter 6: The ability of fluorination to stabilise the formation of previously unobserved 2D surface-confined phenol–pyridine cocrystals is explored.

Chapter 7: The interplay between carboxyl–pyridine and phenol–pyridine interaction modes is explored. Within some systems competition between these two interaction modes is observed whilst in others they cooperate to synergistically control the organisation of the molecules within the observed 2D surface-confined networks. Factors which influence the balance between these two behaviours are explored.

Chapter 8: The ability of halogen and hydrogen bonds to cooperatively control the supramolecular organisation of the molecular building blocks within 2D surface-confined networks is investigated.

Chapter 2: Experimental background

Scanning tunnelling microscopy (STM) has remained the principle experimental tool used to study atomic scale phenomena on surfaces since its Nobel-prize-winning development in 1981. This versatile technique is capable of operating in a wide range of different experimental conditions, and it is the main tool used to explore all of the solid–liquid interface systems studied in this thesis. Within this chapter, the basic theoretical background of STM and some of the key components required for its successful operation at the solid–liquid interface are briefly discussed.

2.1 Basic principles of STM

Figure 10 shows a basic schematic representation highlighting the core components of an STM. During operation, the apex of a sharp, conductive tip is brought into extremely close proximity to the surface of a conductive sample whilst a bias voltage is applied between the two. The separation between the apex of the tip and the surface of the sample (d in figure 10) is typically on the order of ~5 Å. At these distances, the electronic orbitals of the apical atom of the tip and of the underlying surface meaningfully overlap and the bias voltage causes electrons to tunnel between the tip and the sample. Although this so-called tunnelling current is very small, typically in the range of pA to nA, it is measurable. The tunnelling current decreases exponentially as the separation between the apex of the tip and the surface of the sample increases. Furthermore, the magnitude of the tunnelling current is also proportional to the number of available electronic states through which tunnelling can occur. By scanning the STM tip across a sample and monitoring the tunnelling current as a function of the lateral position of the tip, the surface of the sample can be imaged. The contrast within the generated STM image reflects both the topography and the local density of states of the sample.

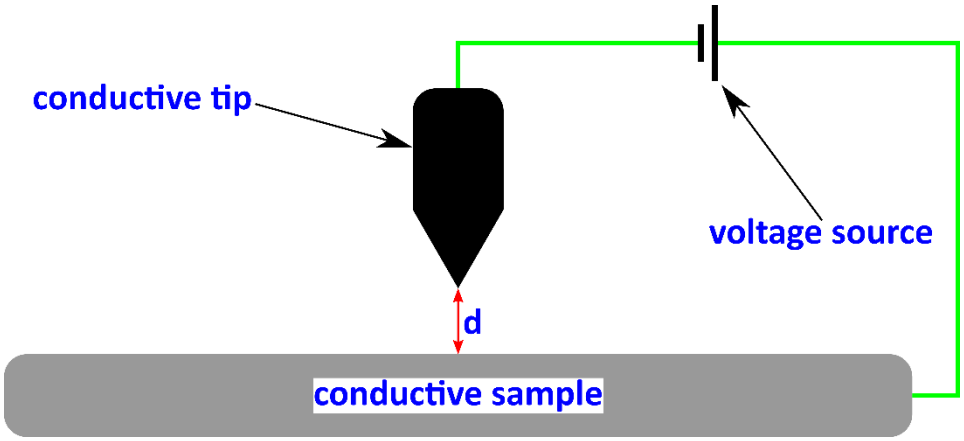

Figure 10: Simple schematic representation of a typical STM setup.

There are two modes in which STM data can be acquired: constant height mode and constant current mode (see figure 11). In constant height mode the absolute vertical position of the tip is maintained during scanning and the tunnelling current is plotted as a function of the lateral position of the tip. Conversely, in constant current mode the vertical position of the tip changes during imaging such that the measured tunnelling current remains constant and the vertical displacement of the tip required to maintain this current is plotted as a function of the lateral position of the tip. The use of constant current mode can be advantageous as when imaging in this mode the tip follows the contours of the sample, meaning it is less likely to crash into the surface of the sample. This can be particularly beneficial in the unstable environment present at the solid–liquid interface.

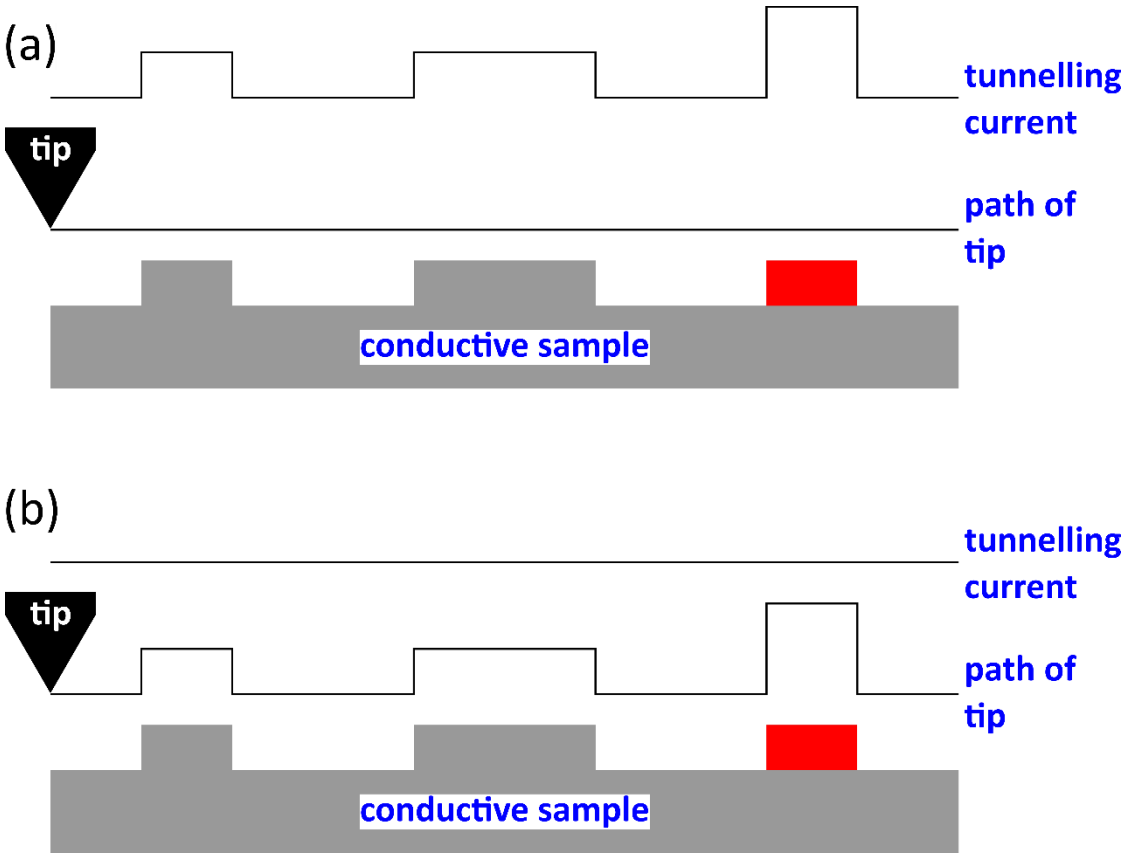

Figure 11: (a) Simple schematic representation highlighting the path of the tip and the behaviour of the tunnelling current as the tip is scanned across a sample in constant height mode. **(b)** Simple schematic representation highlighting the path of the tip and the behaviour of the tunnelling current as the tip is scanned across a sample in constant current mode. In both figures the red section of the sample represents a region with an elevated local density of available states through which tunnelling can occur.

2.2 STM at the solid–liquid interface

STM is the primary experimental technique used to study 2D surface-confined phenomena at the solid–liquid interface. As is shown schematically in figure 12, within these experiments the STM tip is directly submerged in a droplet of solution which is placed onto the surface of the substrate. This situation presents some practical challenges, one of which is the selection of the solvent. Ideally, the solvent used should have a low vapour pressure so that significant evaporation does not occur during the extended periods of time over which STM experiments are typically conducted. Furthermore, the solvent is also required to have a very low electrical conductivity. This is to ensure that current does not flow between the tip to the sample through the solution rather than via tunnelling. These restrictions significantly limit the range of useable solvents, and only a small number of solvents, such as heptanoic acid, 1-phenlyoctane and trichlorobenzene, are routinely used.

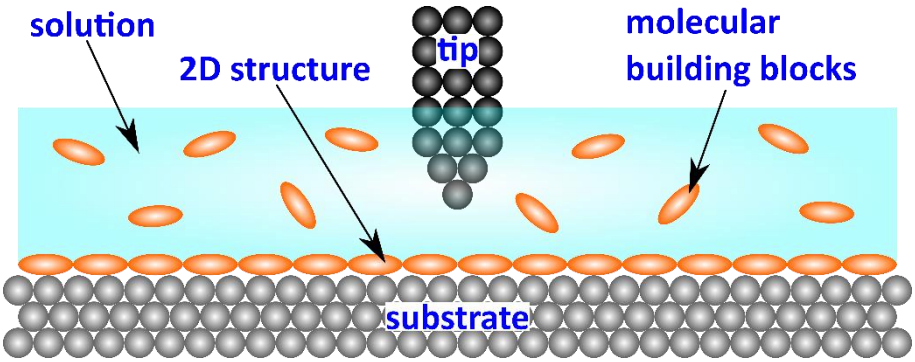

Figure 12: Schematic representation showing the configuration of an STM experiment conducted at the solid–liquid interface.

In addition to solvent selection, the material from which the tip is constructed is also an important consideration. Ideally, the STM tip should be atomically sharp, i.e., the apex of the tip should be terminated by a single atom. STM tips used in UHV conditions are typically made from tungsten and are prepared via electrochemical etching procedures. However, under ambient conditions tungsten is no longer suitable as it is not sufficiently inert meaning an insulating layer of oxide rapidly forms on its surface. The typical material used to construct STM tips for use under ambient conditions is a platinum–iridium alloy. Platinum is extremely inert and, unlike tungsten, does not oxidise under ambient conditions. Alloying the platinum with a small amount of iridium results in a material which is harder than pure platinum. This hardness means the alloy can be readily mechanically sheared, which is the primary method through which platinum–iridium STM tips are prepared. Figure 13 shows typical scanning electron microscopy (SEM) images of an STM tip prepared by mechanically shearing 80:20 Pt:Ir wire.

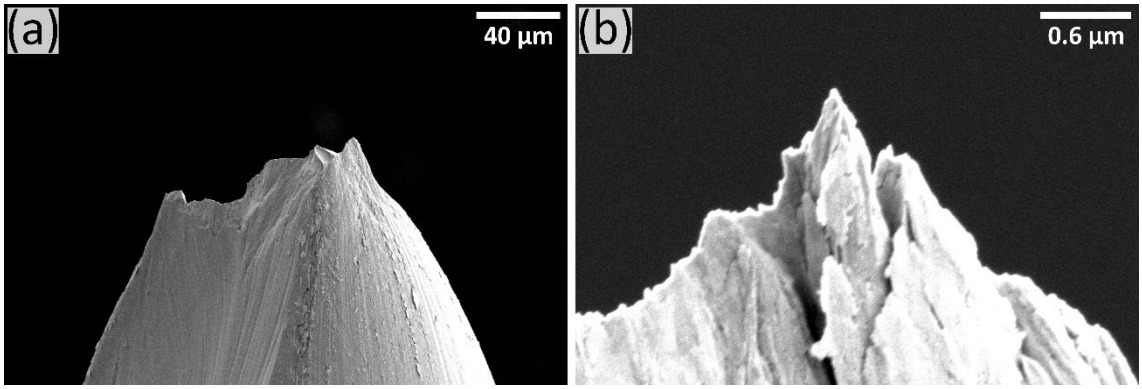

Figure 13: (a) SEM image of a 80:20 Pt:Ir wire STM tip prepared by mechanical shearing. **(b)** SEM image showing a higher magnification image of the apex of the STM tip shown in (a).

The final major component of STM experiments which will be discussed is the substrate. In order to successfully conduct STM experiments under ambient conditions at the solid–liquid interface, judicious selection of the substrate material is required. The substrate needs to be conductive whilst also being inert enough that it is stable under ambient conditions. Furthermore, STM imaging requires

the surface to be flat on an atomic scale. These conditions are difficult to fulfil and only a limited range of materials are appropriate. Of these, by far the most frequently encountered, and the substrate that is used throughout this thesis, is graphite. Graphite substrates used in STM experiments are a highly crystalline form of synthetic graphite known as highly oriented pyrolytic graphite (HOPG). In addition to their conductivity, inertness, and atomic scale flatness, HOPG samples also have the additional advantage that they are straightforward to prepare for STM experiments. Furthermore, atomic

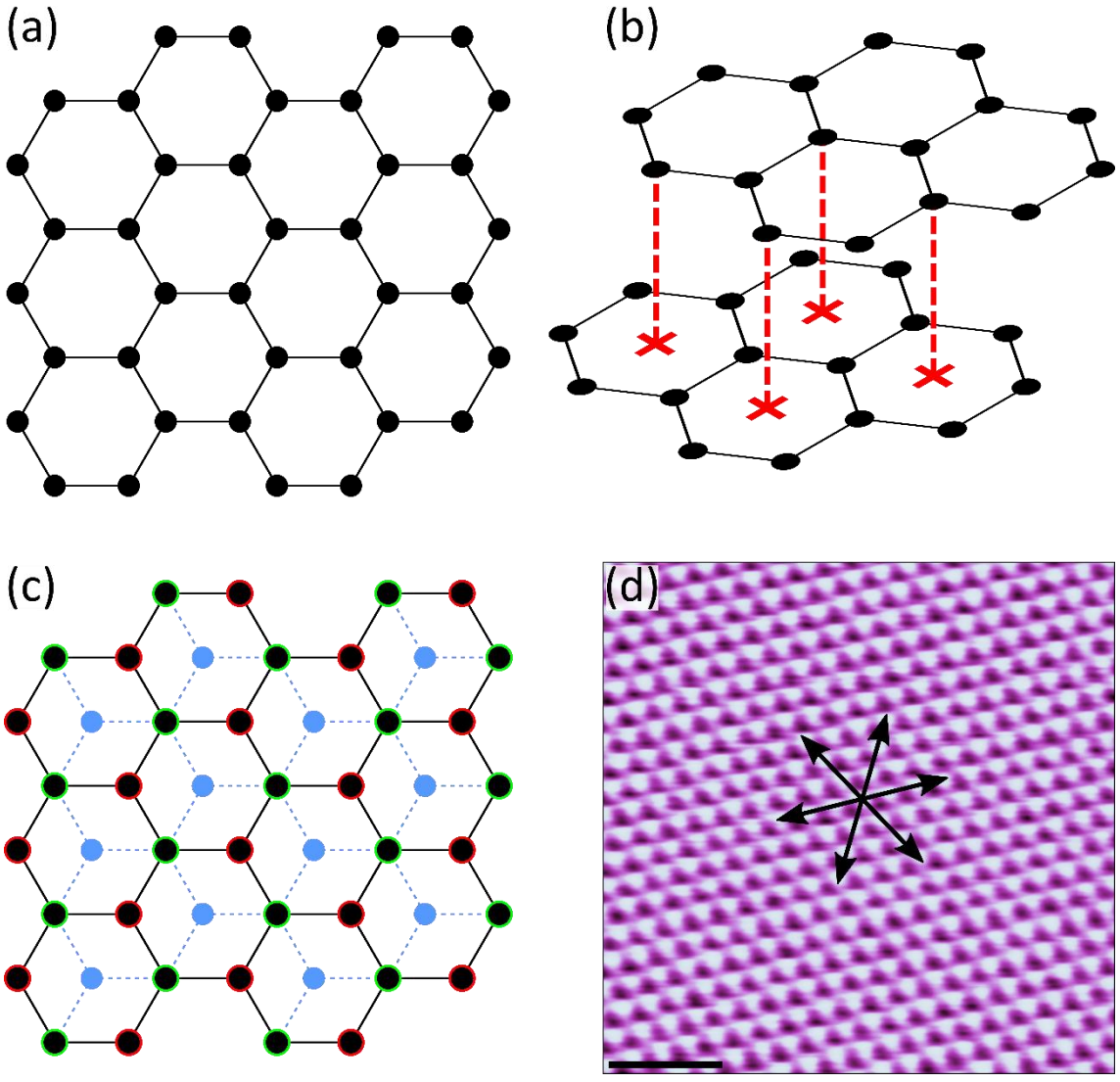

Figure 14: (a) Schematic highlighting the honeycomb arrangement of the carbon atoms in one of the 2D carbon sheets present in graphite. **(b)** Schematic highlighting the staggered layering of adjacent sheets in the crystal structure of graphite. **(c)** Structure of graphite when viewed perpendicularly to the plane of the sheets. The carbon atom in the uppermost layer are shown in black, whilst the carbon atoms in the layer below are shown in blue. The carbon atoms in the uppermost layer which are circled in green have a carbon atom of the layer below directly beneath them, whilst those circled in red do not. **(d)** STM image showing atomic resolution of HOPG. Tunnelling parameters: V_{bias} = +5 mV, I_{set} = 900 pA. Scale bar = 1 nm. The radial arrows show the main symmetry axis of the surface.

resolution of HOPG is particularly easy to achieve during STM experiments, which allows for the precise calibration of experimental data.

Graphite is an allotrope of carbon in which the carbon atoms are arranged into a hexagonal structure. Each carbon atom is covalently bound to three neighbouring carbon atoms which are positioned 120° apart. This organises the carbon atoms into 2D sheets which have a honeycomb structure (see figure 14a). These 2D sheets are then stacked together one on top of the other to form the 3D structure of graphite. There are no covalent bonds between the sheets, and their stacking is mediated simply by van der Waals interactions. Neighbouring sheets are not stacked such that their carbon atoms are positioned directly above those in the layer below; rather, as is highlighted in figure 14b, each sheet is positioned such that half of its carbon atoms are positioned directly above the centre of each of the hexagons in the sheet below. As a result of this arrangement, when viewed perpendicularly to the plane of the sheets, half of the carbon atoms in a given sheet have a carbon atom from the sheet below located directly beneath them, whilst the other half do not. Within the sheets, these two inequivalent sites adopt an alternating pattern, i.e., each carbon atom is inequivalent to its three nearest neighbours within the honeycomb structure. This structure is highlighted schematically in figure 14c. The surface used in STM experiments is prepared by cleaving a graphite substrate along the plane of the 2D sheets, i.e., it corresponds to the uppermost layer shown in figure 14c. An STM image showing atomic resolution of this surface is shown in figure 14d. It should be noted that within STM images of this surface, only half of the constituent atoms are typically resolved. These atoms are thought to correspond to those which do not have a carbon atom located directly beneath them.[117,118] Such atomic resolution can be easily achieved and, as the dimensions of the lattice are precisely known, can be used for calibration purposes. The main symmetry axes of this surface along which there is a characteristic lattice spacing of 0.246 nm, are highlighted in figure 14d.

Chapter 3: Exploring the impact of fluorination on the self-assembly behaviour of isophthalic acid

Isophthalic acid (IPA) is a prototypical molecule used to study the formation of hydrogen-bond-controlled self-assembled monolayers. IPA, the structure of which is shown in figure 15a, is composed of a central benzene ring functionalised with two carboxyl groups positioned meta to one another. The self-assembly of this molecule into ordered networks at the solid–liquid interface has been extensively investigated.[53,119] Homomolecular networks of IPA can be readily formed at the interface between fatty acid solvents, such as heptanoic acid[119] and octanoic acid[53], and HOPG substrates. Within these networks, $R_2^2(8)$ hydrogen bonding interactions between the carboxyl groups of adjacent molecules arrange the IPA molecules into extended zigzag chains. The formation of these chains is shown schematically in figure 15b.

One of the most interesting properties regarding the self-assembly of IPA is its response to the molecule coronene.[53] As is shown schematically in figure 15, coronene serves as a template around which six IPA molecules can arrange themselves into cyclic hexameric units stabilised via $R_2^2(8)$ hydrogen bonds between their carboxyl groups. The templating influence of coronene relies on precise shape and size complementarity between the coronene and IPA molecules: the 120° angle

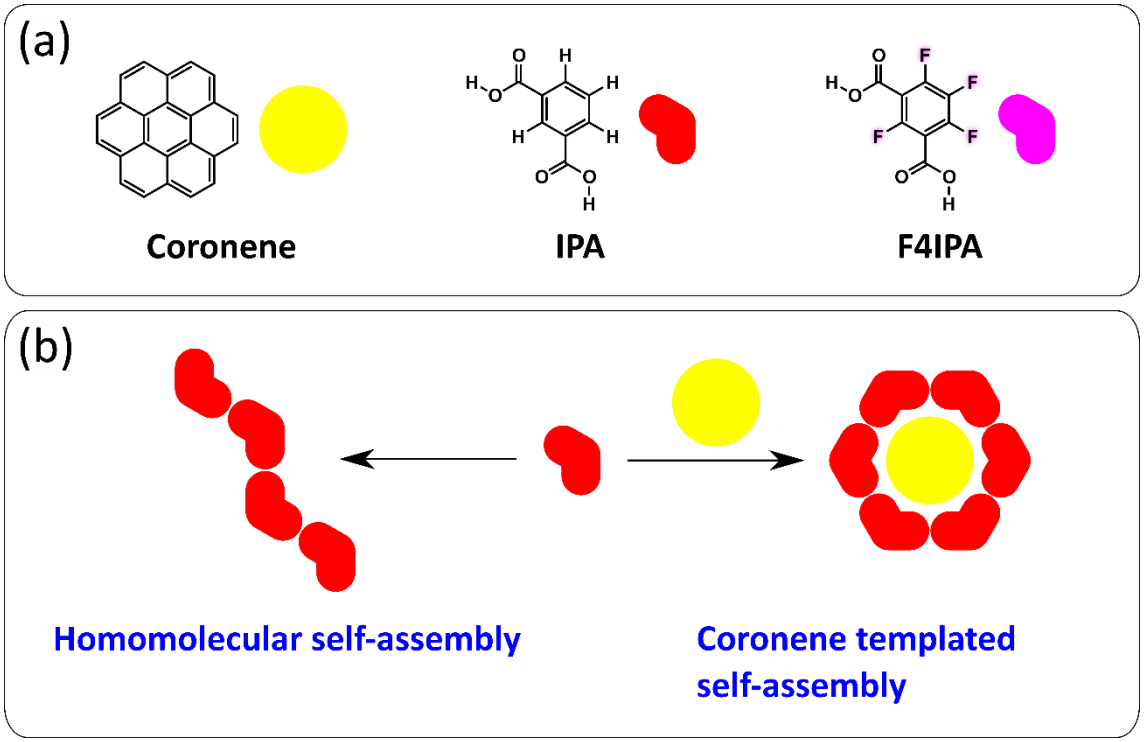

Figure 15: (a) Molecular structures alongside schematic representations of coronene, isophthalic acid (IPA) and tetrafluoroisophthalic acid (F4IPA). **(b)** Schematic illustrations of the homomolecular self-assembly of IPA into zigzag chains, and the coronene templated self-assembly of IPA into its cyclic hexameric arrangement.

between their carboxyl groups allows six IPA molecules to arrange themselves into a hexagon with an internal pore size that is of ideal size to confine a single coronene molecule. The central coronene molecule and the surrounding IPA molecules interact via favourable van der Waals interactions.[53] The coronene-templated formation of this cyclic hexameric motif has been utilised in an array of other monolayer systems.[5,53,61,120–125]

The simplicity of IPA makes it an ideal model system on which to explore the impact of fluorination. The formation of the previously discussed zigzag chains of IPA present in its homomolecular assembly relies on the specific bent geometry of the IPA molecules. Furthermore, as discussed above, for coronene to act as an effective template for the formation of the cyclic hexameric arrangement of IPA molecules, the dimensions of the IPA and coronene molecules must be complementary. Exchanging the aromatic hydrogen atoms of IPA for fluorine atoms is not expected to significantly alter the molecule's dimensions. Therefore, the fluorinated analogue (F4IPA, see figure 15) should be geometrically capable of self-assembling into both the zigzag chain and cyclic hexameric motifs. However, the presence of fluorine atoms is expected to impact on the intermolecular interactions in which the molecular building blocks are able to partake. This could significantly influence the observed self-assembly behaviour.

In order to explore these ideas, the self-assembly of F4IPA has been investigated at the heptanoic acid/HOPG interface. Both the homomolecular self-assembly of F4IPA and its response to the presence of coronene were investigated and systematically compared with the corresponding behaviour observed with IPA.

3.1 Homomolecular self-assembly behaviour of IPA

The homomolecular self-assembly of IPA has previously been explored at the heptanoic acid/HOPG interface.[119] As expected, these results were extremely easily reproduced. Deposition of a saturated solution of IPA onto a freshly cleaved HOPG substrate leads to the formation of a self-assembled monolayer at the heptanoic acid/HOPG interface (see figure 16).

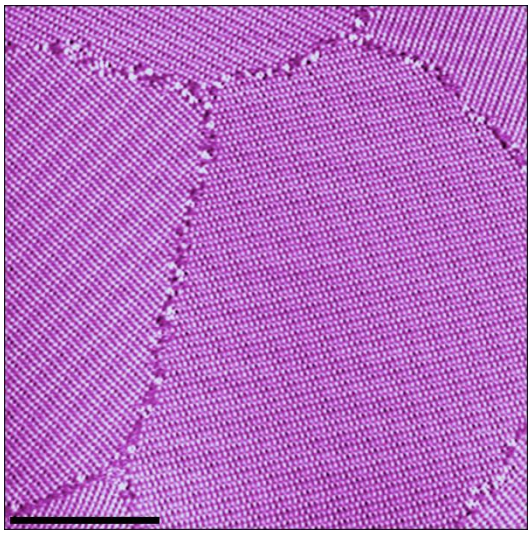

Figure 16: Large-scale STM image showing the homomolecular assembly of IPA at the heptanoic acid/HOPG interface. Tunnelling parameters: V_{bias} = −1.2 V, I_{set} = 50 pA. Scale bar = 20 nm.

Within high-resolution images of the assembly, such as that shown in figure 17a, the individual IPA molecules can be clearly resolved. These molecules are arranged into the expected zigzag chains via $R_2^2(8)$ hydrogen bonds between their carboxyl groups. Individual chains are aligned in a parallel

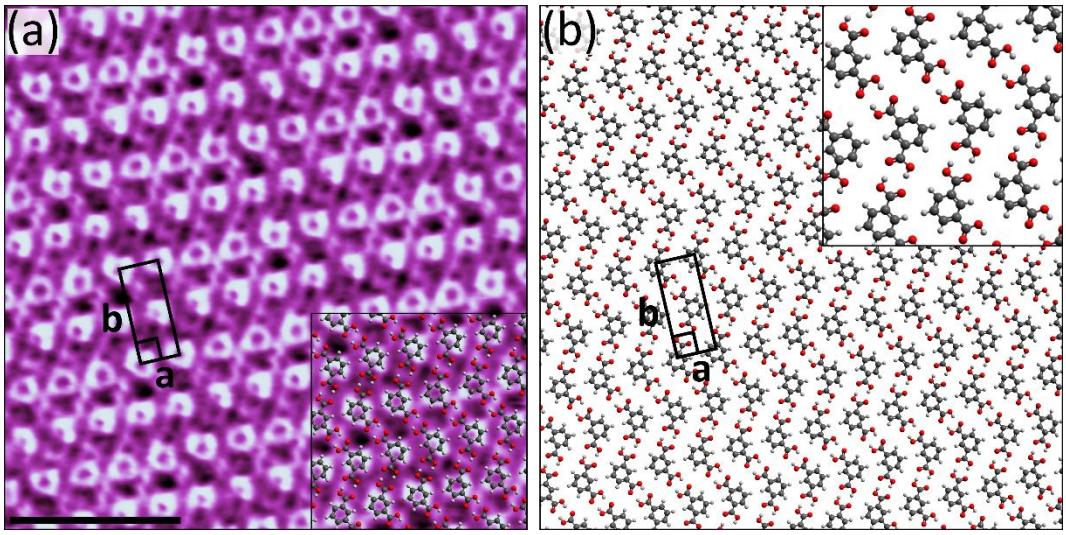

Figure 17: (a) STM image showing the homomolecular assembly of IPA at the heptanoic acid/HOPG interface. Tunnelling parameters: V_{bias} = −1.2 V, I_{set} = 300 pA. Unit cell parameters: a = 0.72 ± 0.05 nm, b = 1.7 ± 0.1 nm, angle = 90 ± 2°. Scale bar = 3 nm. **(b)** Proposed model for the assembly.

manner within a given domain. These chains are packed together side-by-side on the surface, resulting in the formation of an ordered monolayer. In addition to the van der Waals interactions that seem to dominate the dense side-by-side packing of the chains, there may also be some contribution from weak interchain C–H···O interactions. The proposed model for the assembly is given in figure 17b.

3.2 Response of IPA to the presence of coronene

The coronene-templated self-assembly of IPA into a hexagonal array based on the formation of cyclic hexameric arrangements has previously been investigated at the octanoic acid/HOPG interface.[53] These results could be readily reproduced at the heptanoic acid/HOPG interface. There was no notable difference in the results obtained in the two solvents. Deposition of solutions containing IPA at a concentration of 4×10^{-3} M and coronene at a concentration of 5×10^{-5} M leads to the formation of an ordered bimolecular network at the heptanoic acid/HOPG interface (see figure 18).

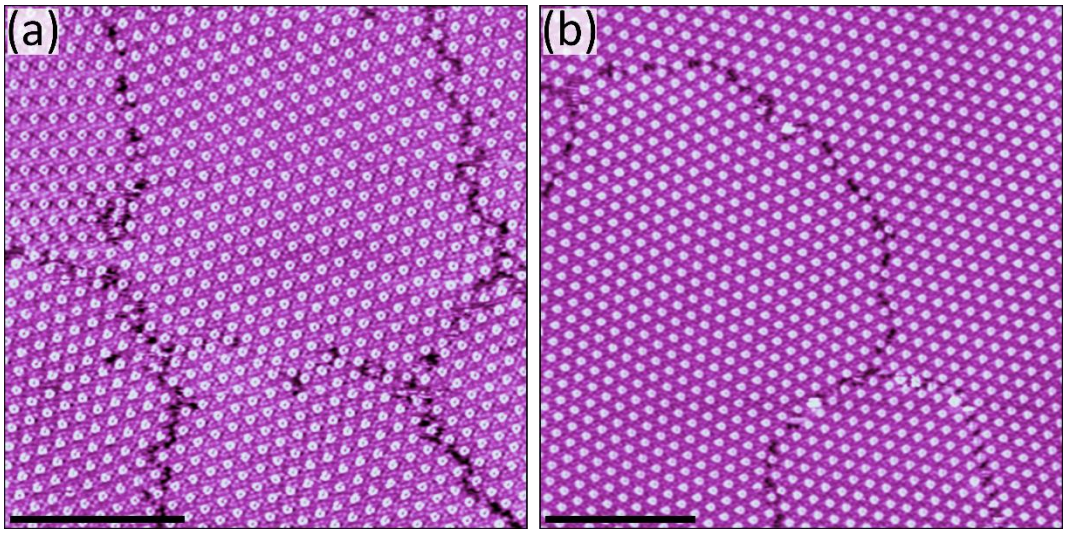

Figure 18: Large-scale STM images showing the coassembly of IPA and coronene at the heptanoic acid/HOPG interface. Tunnelling parameters: (a) V_{bias} = −0.9 V, I_{set} = 200 pA, (b) V_{bias} = −1.2 V, I_{set} = 300 pA. Both scale bars = 20 nm.

High-resolution STM images of the assembly, such as that shown in figure 19a, demonstrate the strong templating influence that coronene has. Within these images, the individual coronene molecules can be clearly resolved. Surrounding each of the coronene molecules, six IPA molecules, clearly organised into their cyclic hexameric arrangement, can be seen. These coronene centred cyclic hexameric arrangements are packed together on the surface into an ordered hexagonal array. Simple van der Waals interactions between the peripheries of adjacent cyclic hexameric structures appears to dominate the dense packing of these structures into an ordered array on the surface. There may also be some contribution from weak C–H···O interactions. The proposed model for this assembly is given

in figure 19b. The unit cell dimensions for the assembly, a = b = 2.3 ± 0.1 nm and θ = 60 ± 2° (see figure 19), are consistent with those reported at the octanoic acid/HOPG interface[53]. Furthermore, the unit cell vectors for the assembly are found to be rotated by 11 ± 1° with respect to the principle lattice vectors of the underlying HOPG substrate, which is again consistent with the assembly observed at the octanoic acid/HOPG interface[53].

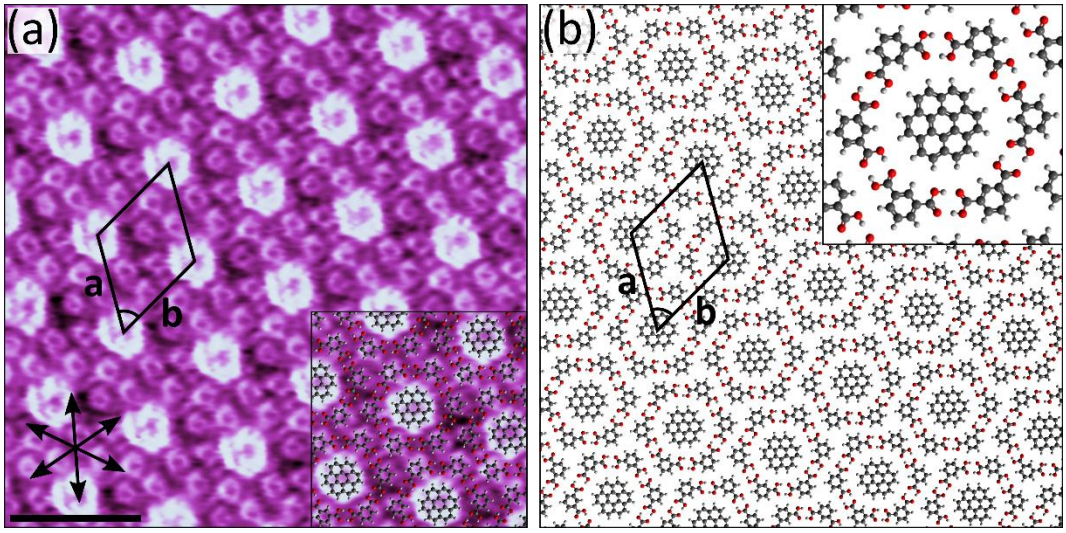

Figure 19: (a) STM image showing the coassembly of IPA and coronene at the heptanoic acid/HOPG interface. Tunnelling parameters: V_{bias} = −0.8 V, I_{set} = 500 pA. Unit cell parameters: a = b = 2.3 ± 0.1 nm, angle = 60 ± 2°. Scale bar = 3 nm. The radial arrows in the lower left corner show the principle crystallographic directions of the underlying HOPG substrate. **(b)** Proposed model for the assembly.

3.3 Homomolecular self-assembly behaviour of F4IPA

The homomolecular self-assembly of F4IPA was explored in exactly the same manner as that used with IPA. F4IPA (solubility > 8×10^{-2} M) was observed to have a markedly higher solubility in heptanoic acid than IPA. Deposition of solutions in which the concentration of F4IPA was comparable to that used with IPA did not result in the formation of any self-assembled structure at the heptanoic/acid HOPG interface. Even after increasing the F4IPA concentration to its saturation point, no evidence of any assembly could be observed at the heptanoic acid/HOPG interface. Overall, F4IPA solutions with concentrations ranging from 10^{-4} M to saturated were tested. The absence of any assembly on the surface was consistent throughout the explored concentration range.

The absence of any assembly with F4IPA, compared with the ability of IPA to readily form self-assembled monolayers, indicates that the presence of the fluorine atoms disrupts the self-assembly of F4IPA. The carboxyl groups within the two molecules are positioned in an equivalent manner; therefore, F4IPA could in principle self-assemble into the same zigzag chains observed with IPA. However, the fluorine atoms may disrupt the side-by-side packing of the zigzag chains. As was

discussed in section 3.1, with IPA it seems that there may be some contribution from weak C–H···O interactions in packing the zigzag chains side-by-side. However, with F4IPA these interactions are not possible due to the fact that the hydrogen atoms of the central benzene ring of IPA are replaced by fluorine atoms in F4IPA. This may be a significant factor in the absence of self-assembly with F4IPA.

3.4 Response of F4IPA to the presence of coronene

Although neither of the individual components form self-assembled monolayers in isolation, deposition of solutions containing both F4IPA and coronene does lead to the formation of stable bimolecular structures at the heptanoic acid/HOPG interface. Using solutions in which the concentration of F4IPA is 4×10^{-2} M and the concentration of coronene is 5×10^{-5} M leads to the formation of a seemingly hexagonal assembly. Extended domains of this assembly could be observed covering essentially the entire surface of the sample (see figure 20).

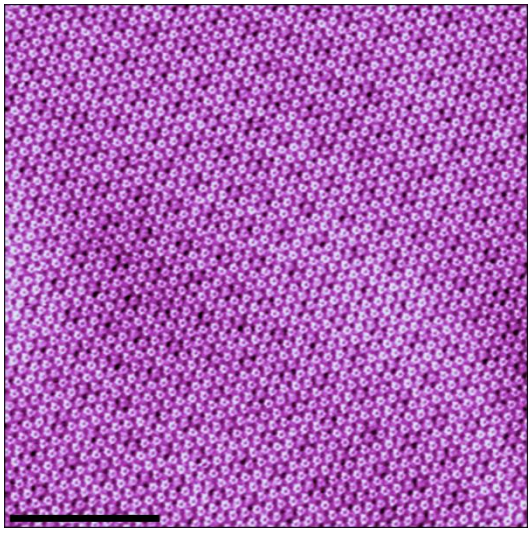

Figure 20: Large-scale STM image showing the coassembly of F4IPA and coronene at the heptanoic acid/HOPG interface. Tunnelling parameters: V_{bias} = −1.2 V, I_{set} = 100 pA. Scale bar = 20 nm.

Within high-resolution images of the assembly, such as that presented in figure 21a, both the coronene and F4IPA molecules can be resolved. The coronene molecules, which appear as large, approximately circular protrusions, are organised into a hexagonal array. This hexagonal array has a unit cell with dimensions of a = b = 1.7 ± 0.1 nm and θ = 60 ± 2°. As is highlighted in the overlay shown in figure 21a, the F4IPA molecules are positioned in the interstices between the coronene molecules in one of two inequivalent sites. These inequivalent sites alternate, i.e., a given site is inequivalent to its three nearest neighbours. This arrangement is highlighted schematically in figure 21b. There are three different directions, each of which is separated by 120°, in which the carboxyl groups of the

individual F4IPA molecules can be orientated such that they can hydrogen bond to neighbouring F4IPA molecules via $R_2^2(8)$ hydrogen bonds. Note that these directions differ by 60° between the two inequivalent sites. These directions are highlighted in the schematic shown in figure 21b. Although there are three available directions in which the carboxyl groups of each of the F4IPA molecules can be orientated, the F4IPA molecules only have two carboxyl groups, meaning that each can only occupy two of these directions. If an F4IPA molecule is positioned on one of the sites with its carboxyl groups aligned along two of the directions highlighted in figure 21b, the F4IPA molecules on the neighbouring sites towards which the carboxyl groups of the of the first molecule are aligned can adopt one of two orientations. These two orientations, which are shown schematically in figures 21c and 21d, occur when the neighbouring F4IPA molecules are related by either a 60° or 180° rotation. By ordering the F4IPA molecules based on these two possible interneighbour relationships, an infinite number of

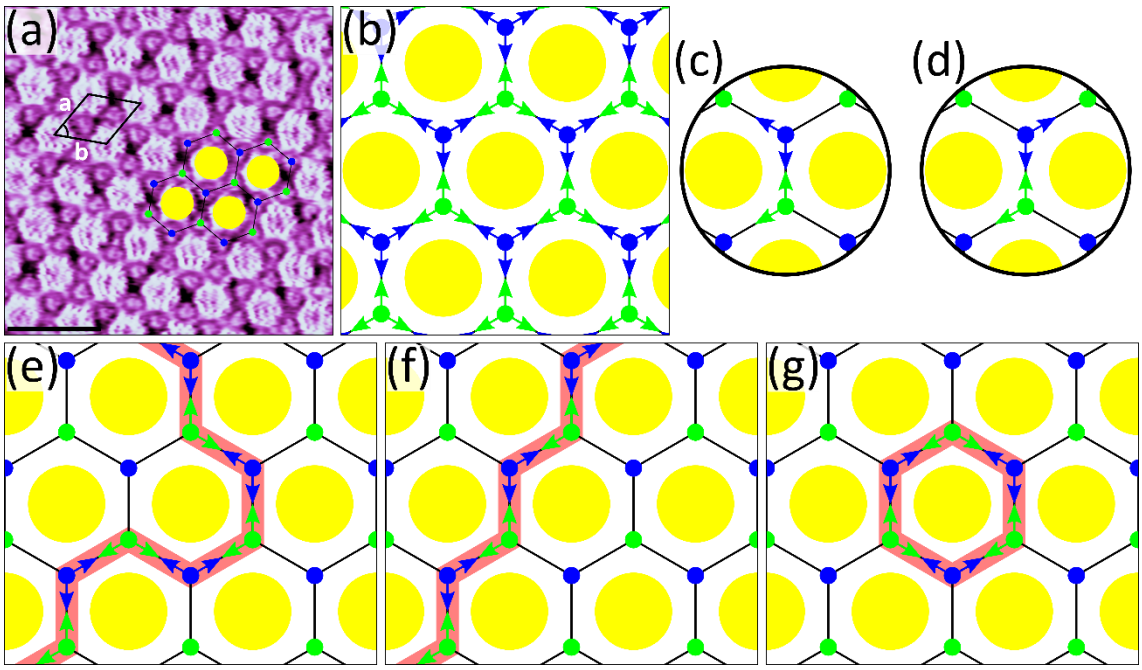

Figure 21: (a) STM image showing the coassembly of F4IPA and coronene at the heptanoic acid/HOPG interface. Tunnelling parameters: V_{bias} = −0.9 V, I_{set} = 80 pA. Unit cell parameters: a = b = 1.7 ± 0.1 nm, angle = 60 ± 2°. Scale bar = 3 nm. A schematic representation is overlaid to highlight the position of the coronene molecules (large yellow circles) and the position of the F4IPA molecules (small green and blue circles). Two different colours are used to represent the F4IPA molecules to highlight the positions of the two inequivalent sites on which they are located. **(b)** Schematic representation consistent with that overlaid in (a), but with the three directions in which the carboxyl groups of the F4IPA molecules can be aligned shown with arrows. **(c)** Schematic representation showing two neighbouring F4IPA molecules related by a 60° rotation. **(d)** Schematic representation showing two neighbouring F4IPA molecules related by a 180° rotation. **(e)** Schematic representation showing an irregular chain of F4IPA molecules formed from a random sequence of the two possible relative rotations of neighbouring molecules shown in (c) and (d). **(f)** Schematic representation showing a zigzag chain of F4IPA molecules formed from a continuous sequence of the interneighbour relationship shown in (d). **(g)** Schematic representation showing a cyclic hexamer of F4IPA molecules formed from a continuous sequence of the interneighbour relationship shown in (c).

possible supramolecular chain and/or ring structures can be formed. For example, figure 21e shows an irregular chain constructed based on a random combination of the two possible interneighbour relationships. Furthermore, by using a repeating pattern of these two interneighbour relationships, ordered structures are also possible. As is shown in figures 21f and 21g, these include the zigzag chain motif observed in the homomolecular self-assembly of IPA (see section 3.1) and the cyclic hexameric arrangement observed in the coronene-templated self-assembly of IPA (see section 3.2).

Due to the infinite number of possible combinations, unambiguously understanding how the F4IPA molecules are arranged in a given STM image is particularly challenging. Assuming that each F4IPA molecule interacts with two of its nearest neighbours via $\mathrm{R}_2^2(8)$ hydrogen bonds, each molecule must be rotated such that the fluorine atom positioned meta to its carboxyl groups is orientated towards the corresponding fluorine atom on a neighbouring F4IPA molecule. Overall, as is highlighted in the schematic shown in figures 22a and 22b, there are two different ways a given F4IPA molecule can interface with its three neighbouring F4IPA molecules: two equivalent $\mathrm{R}_2^2(8)$ hydrogen bonding junctions (labelled **a** in figures 22a and 22b) or a single "junction" in which the meta fluorine atoms of neighbouring F4IPA molecules are orientated towards one another (labelled **b** in figures 22a and 22b). In principle, these two different junctions should resolve in a different manner within the STM images. Close inspection of high-resolution STM images (such as that shown in figure 22c) indeed reveals that there are often distinct dark depressions located between neighbouring F4IPA molecules (highlighted by red arrows in figure 22c). As each F4IPA molecule typically only has a single depression neighbouring it, these depressions are assumed to correspond to the junctions labelled **b** in figures 22a and 22b. Based on this assumption, the arrangement of the F4IPA molecules within the assembly can be deduced. Within the high-resolution STM image shown in figure 22c, a sequence of neighbouring F4IPA molecules are labelled with the numbers 1–9. By appropriately positioning each of these molecules such that the fluorine atoms meta to their carboxyl groups are orientated towards their neighbouring depressions, it becomes clear that the nine F4IPA molecules are arranged into the irregular chain shown schematically in figure 22d. This same procedure can (generally) be followed for every F4IPA molecule within the assembly, and an irregular ordering of the F4IPA molecules is consistently observed (see full analysis of the STM image in figure 22e). Although the orientation of F4IPA molecules can be identified in most cases, in some instances their orientation is unclear. These F4IPA molecules generally appear to have either no neighbouring dark depressions or two neighbouring depressions (see circled F4IPA molecules in figure 22e), rather than the single depression associated with each of the F4IPA molecules within the irregular sequences. One possible explanation for some of these anomalous molecules is that they are positioned at the terminal position of a chain. Within the preceding analysis, it was assumed that every F4IPA molecule interacts with two others via

$R_2^2(8)$ hydrogen bonds; however, for this to be true the irregular chains observed would either have to have infinite lengths or be arranged into closed loops. Rather, it is more likely that chains of $R_2^2(8)$ hydrogen bonded molecules with finite lengths are present. In this case, the F4IPA molecules at the terminal positions of the chains should interface with one of their neighbouring F4IPA molecules by having one of their carboxyl groups orientated towards the meta fluorine atom of said neighbouring F4IPA molecule. It is unclear how this junction, which differs from either of the junctions highlighted in figures 22a and 22b, should resolve within the STM images. Were this junction to appear as a dark depression, then the terminal molecules would be expected to have two neighbouring depressions, and they may correspond to the anomalous molecules that resolve in this manner within the images.

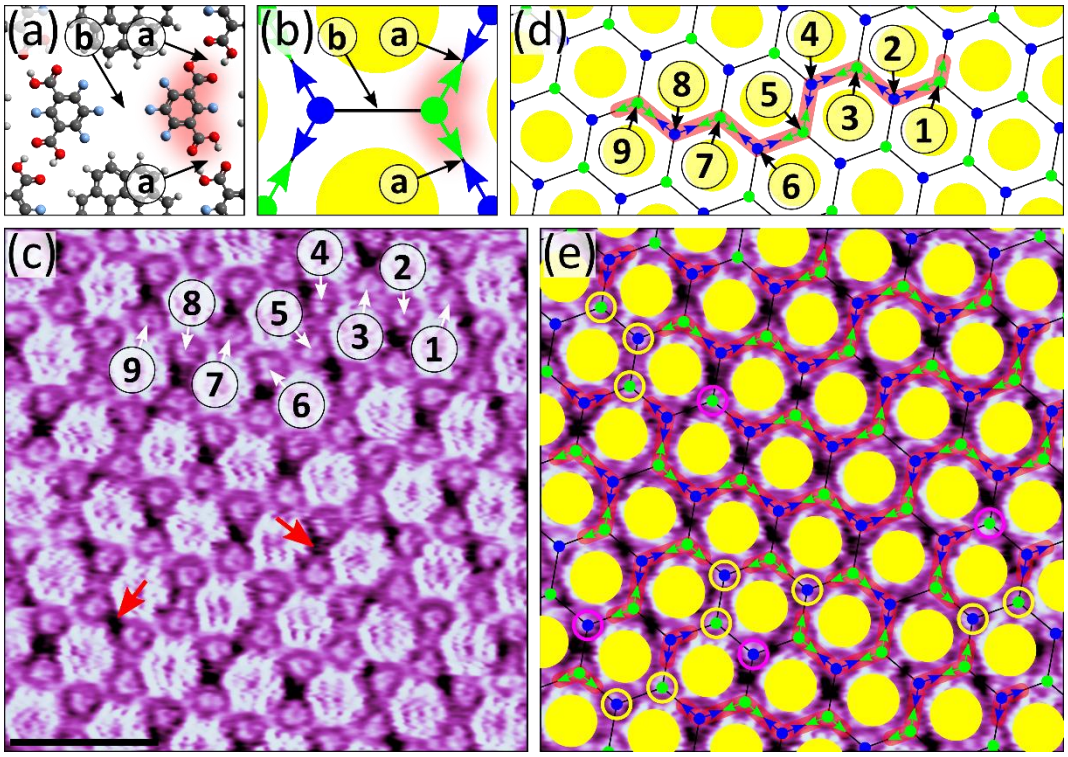

Figure 22: (a) Model showing how the F4IPA molecule highlighted in red (right hand side) interfaces with its three neighbouring F4IPA molecules. The two $R_2^2(8)$ hydrogen bonding junctions involving the highlighted molecule are labelled **a**. The junction in which the meta fluorine atoms of two neighbouring F4IPA molecules are orientated towards one another is labelled **b**. **(b)** Schematic representation equivalent to that shown in (a). **(c)** The same STM image as that shown in figure 21a, but with a sequence of connected F4IPA molecules labelled with the numbers 1–9. The red arrows highlight two examples of the dark depressions observed between neighbouring F4IPA molecules. **(d)** Schematic representation showing how the sequence of nine F4IPA molecules highlighted in (c) is arranged into the irregular chain highlighted in red. **(e)** The same STM image as that shown in (c), but with the orientations of the F4IPA molecules, deduced by the location of their neighbouring dark depressions, highlighted in the overlaid schematic. The chains of F4IPA molecules are highlighted in red. F4IPA molecules which appear to have two neighbouring dark depressions are highlighted with purple circles. F4IPA molecules which appear to have no neighbouring dark depressions are highlighted with yellow circles.

Another extremely significant factor that has not yet been considered is the potential mobility of the F4IPA molecules. As there is an infinite number of possible arrangements, it seems possible that the F4IPA molecules within the assembly may rearrange themselves over time. In order to explore this idea, sequential STM images of the same region of the surface were recorded. Two such STM images, recorded 41 seconds apart, are shown in figures 23a and 23c. As is highlighted in the corresponding analysis shown in figures 23b and 23d, the arrangement of the F4IPA molecules changes almost entirely between the two images, which hints at a highly fluctuant assembly. However, such

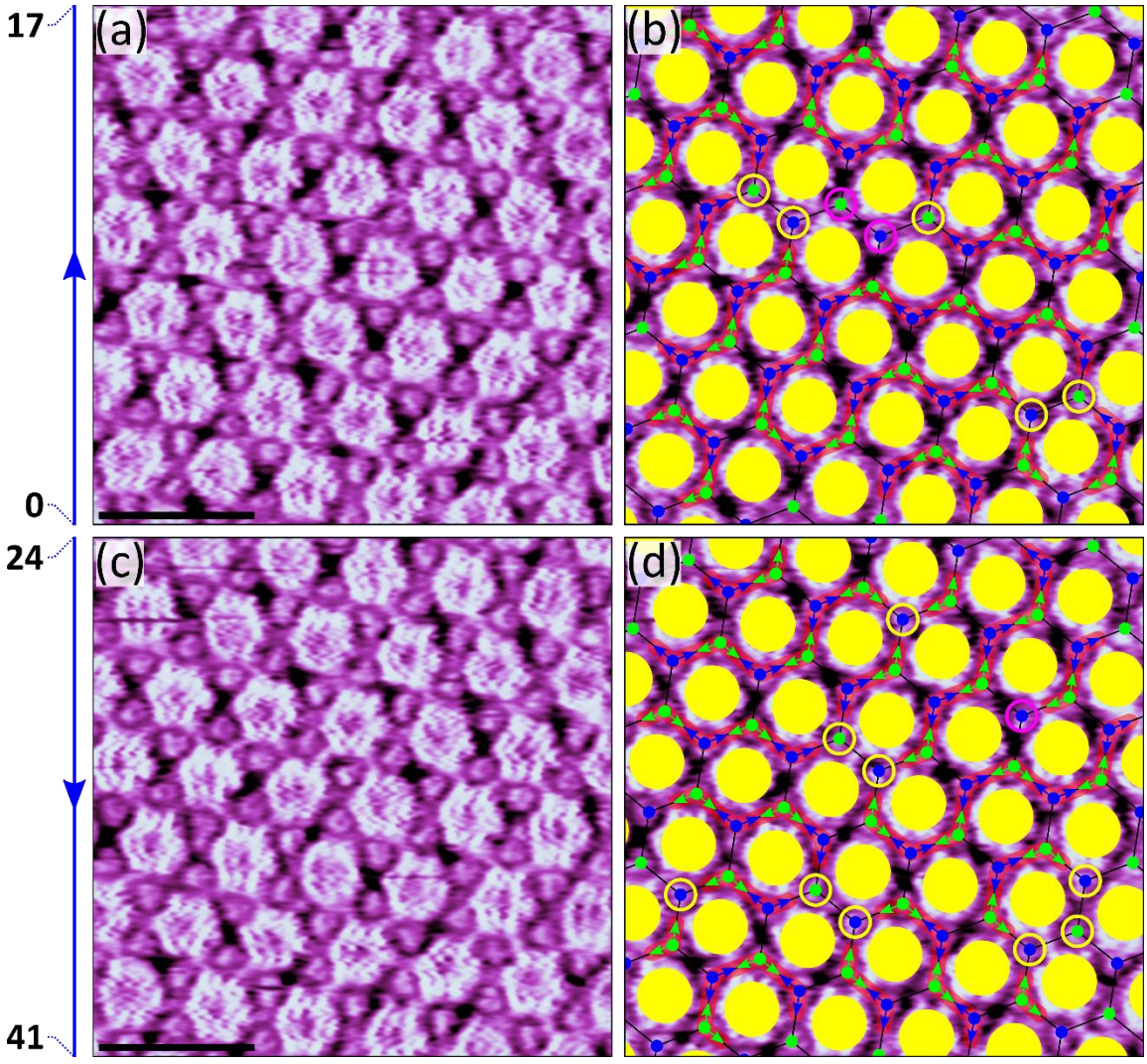

Figure 23: (a) STM image showing the coassembly of F4IPA and coronene at the heptanoic acid/HOPG interface. Tunnelling parameters: V_{bias} = −0.9 V, I_{set} = 80 pA. Scale bar = 3 nm. The blue arrow to the left of the image highlights the slow scan direction and the time in seconds between the start and end of the scan. **(b)** Schematic representation highlighting the arrangement of the molecules in the image shown in (a). **(c)** STM image showing the coassembly of F4IPA and coronene at the heptanoic acid/HOPG interface. The image is recorded in the same location, with the same dimensions and the same tunnelling parameters as the image shown in (a). The blue arrow to the left of the image highlights the slow scan direction and the time in seconds between the start and end of the scan. **(d)** Schematic representation highlighting the arrangement of the molecules in the image shown in (c).

observations were not consistent. Figure 24 shows another pair of sequential STM images, recorded 42 seconds apart, alongside the corresponding analysis highlighting the arrangement of the molecules within them. In this case, the arrangement of the F4IPA molecules appears to be largely preserved between the two images. It is not entirely clear why the F4IPA molecules appear to rearrange much more rapidly in some cases than in others. One potential explanation is that the scanning process

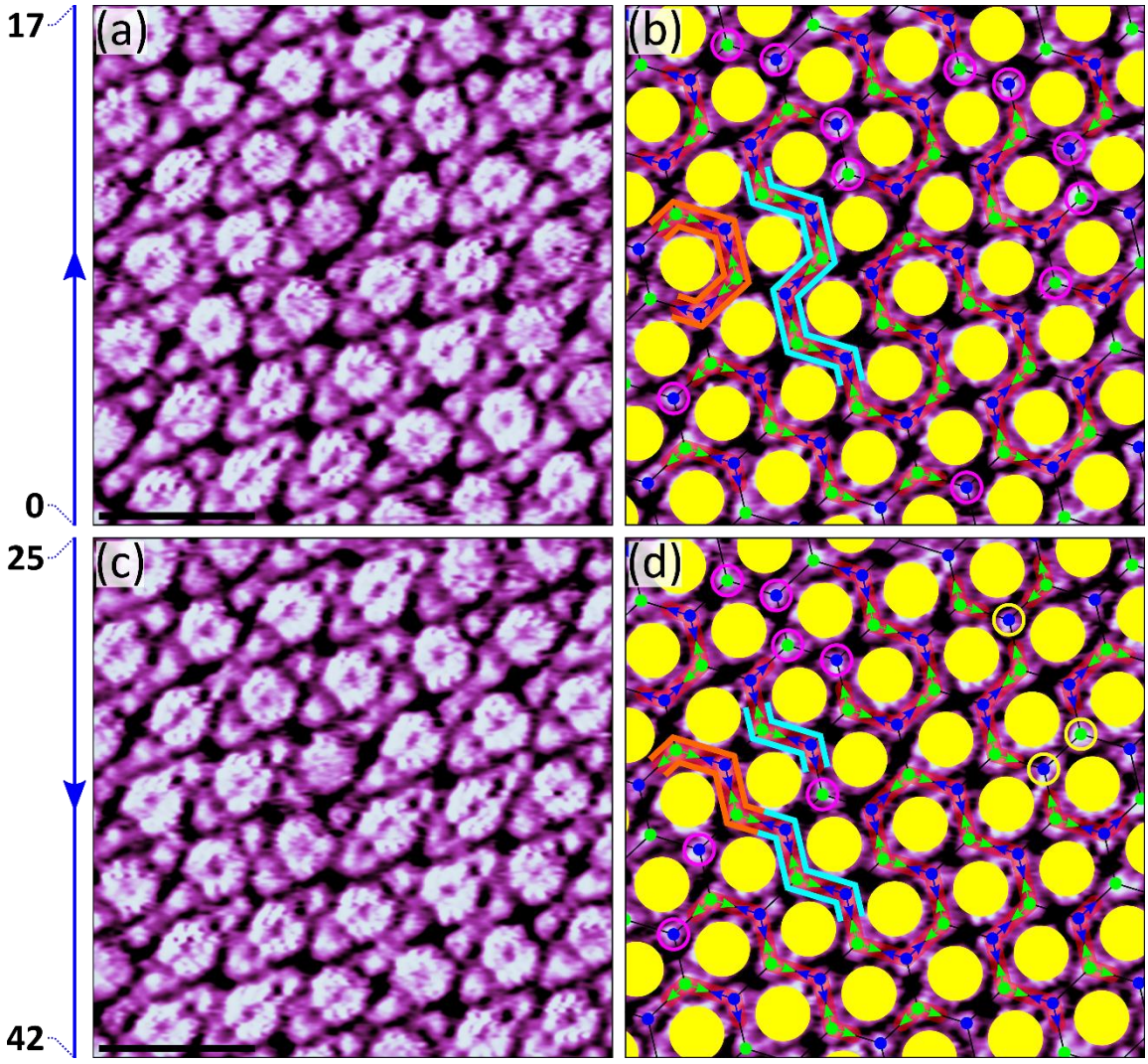

Figure 24: (a) STM image showing the coassembly of F4IPA and coronene at the heptanoic acid/HOPG interface. Tunnelling parameters: V_{bias} = −1.2 V, I_{set} = 300 pA. Scale bar = 3 nm. The blue arrow to the left of the image highlights the slow scan direction and the time in seconds between the start and end of the scan. **(b)** Schematic representation highlighting the arrangement of the molecules in the image shown in (a). Two neighbouring chain sections are outlined in orange and blue. **(c)** STM image showing the coassembly of F4IPA and coronene at the heptanoic acid/HOPG interface. The image is recorded in the same location, with the same dimensions and the same tunnelling parameters as the image shown in (a). The blue arrow to the left of the image highlights the slow scan direction and the time in seconds between the start and end of the scan. **(d)** Schematic representation highlighting the arrangement of the molecules in the image shown in (c). The rearranged configuration of the chains outlined in (b) is highlighted. The involved F4IPA molecules are outlined in the same colour as they are in their parent chains in (b).

disrupts the assembly to some extent and that in cases where rapid rearrangement is observed, the scanning conditions (structure of the STM tip, V_{bias} and I_{set}) are such that they more significantly disrupt the assembly. It should be noted that some rearrangement was observed in all cases. The mobility associated with this rearrangement may account for the aforementioned anomalous F4IPA molecules for which the orientation cannot be defined, i.e., the anomalous F4IPA molecules may have reoriented during imaging, resulting in them adopting an irregular appearance which is consistent with a combination of orientations.

Instances where the rearrangement is not observed to be too rapid potentially give some insight into the mechanism for this rearrangement. Within figure 24b, two unconnected neighbouring sections of chains of F4IPA molecules are highlighted. As can be seen in figure 24d, within the subsequent image these two chains rearrange such that a new chain, containing regions of the two original chains, forms. The new connection between the two chains forms between two neighbouring F4IPA molecules which were both involved in two $\mathrm{R}_2^2(8)$ hydrogen bonding junctions within their respective preceding chains, i.e., they are not at the terminal positions of their chains. In order for these two neighbouring F4IPA molecules to interact with one another, one of the $\mathrm{R}_2^2(8)$ hydrogen bonding junctions that each was involved in must be broken and the F4IPA molecules must both reorientate such that their carboxyl groups which were involved in the broken junctions are now orientated towards one another. This process is highlighted schematically in figure 25. Of particular interest are the F4IPA molecules which were involved in the broken $\mathrm{R}_2^2(8)$ hydrogen bonding junctions which are not involved in the new hybrid chain structure. In principle, after the rearrangement these two molecules should be located at the terminal position of chains. Accordingly, as can be seen in figures 24c and 24d, these molecules resolve with two neighbouring dark depressions following the rearrangement. This supports the previous conjecture that the anomalous F4IPA molecules with two neighbouring depressions may correspond to those at the terminal position of the chains. However, due to the limited quantity of

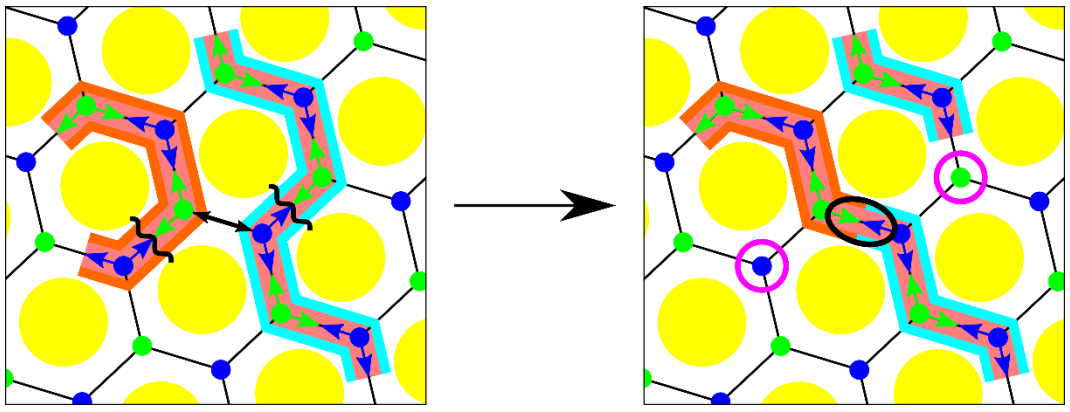

Figure 25: Schematic representation showing the rearrangement of the chains highlighted in figures 24a and 24b into the configuration observed in figures 24c and 24d. The black wavy lines highlight the $\mathrm{R}_2^2(8)$ junctions which break. The new $\mathrm{R}_2^2(8)$ junction that forms is circled in black.

available data, establishing any statistically concrete conclusions regarding this is not possible. Furthermore, it also seems very likely that there are other mechanisms for rearrangement of the molecules, particularly mechanisms which directly involve the F4IPA molecules at the terminal positions of chains. However, again due to the limited quantity of experimental data, such possibilities are not explored and the understanding of the rearrangement routes within the assembly presented here is very likely incomplete.

Although the structure of the coassembly of F4IPA with coronene seems highly unusual, it actually shows several similarities with the assembly of p-terphenyl-3,5,3′,5′-tetracarboxylic acid (TPTC, see figure 26a) at the nonanoic acid/HOPG interface, first reported in the seminal work of Blunt et al.[126] . Within this assembly, each of the TPTC molecules adopts one of three separate orientations. The three separate orientations of the TPTC molecules are then packed together on the surface into a porous network which possesses hexagonal orientational order but lacks translational symmetry. The hexagonal orientational order manifests itself in the location of the pores, which are positioned in a simple hexagonal array, but the network of TPTC molecules which delineates them possesses no translational order. By representing each of the TPTC molecules as rhombuses, it becomes clear that this network can be mapped as a so-called random rhombus tiling in which adjacent TPTC molecules interact via $\mathrm{R}_2^2(8)$ hydrogen bonds between their carboxyl groups.

Clear parallels can be drawn between the homomolecular assembly of TPTC and the coassembly of F4IPA with coronene. Like its TPTC counterpart, the coassembly of F4IPA with coronene possesses

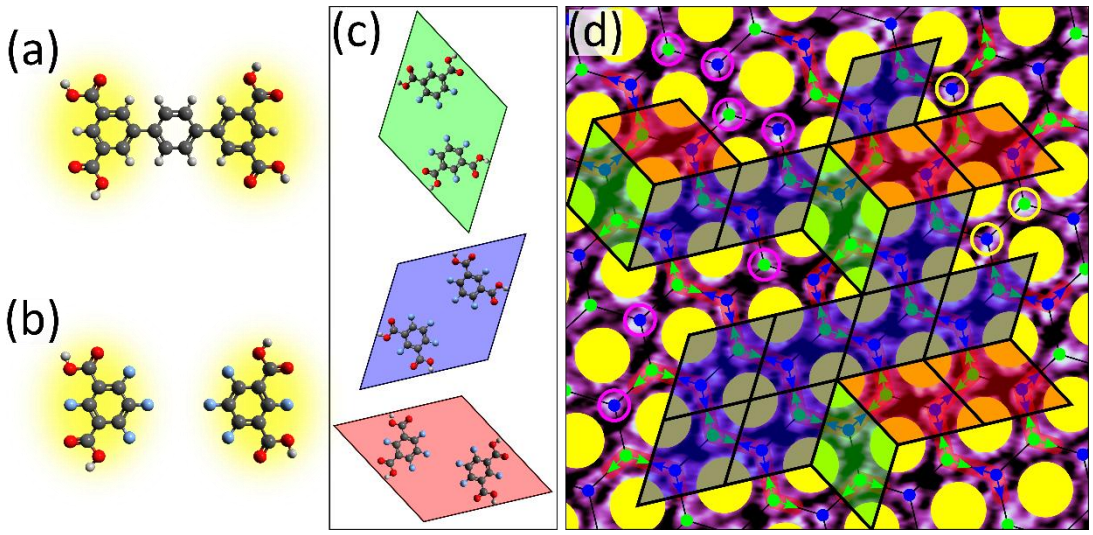

Figure 26: (a) Molecular structure of TPTC. **(b)** Structure of the F4IPA dimer which mimics the structure of TPTC. **(c)** Three different orientations of the F4IPA dimers highlighted by the coloured rhombuses used to represent them. **(d)** The same schematic representation as that shown in figure 24b, but with the rhombus representation outlined in (c) overlaid to highlight the tiling of the dimers on the surface.

hexagonal orientational order but lacks translational symmetry. The former manifests itself in the location of the coronene molecules (instead of the hexagonal array of pores observed with TPTC). Furthermore, similarly to what was observed for the TPTC molecules surrounding the pores, the network of F4IPA molecules which surrounds the coronene molecules lacks translational order. At this point, it is useful to compare the structure of TPTC with that of F4IPA. As is highlighted in figures 26a and 26b, a single F4IPA molecule closely mimics one of the dicarboxyl functionalised terminal benzene rings of the terphenyl moiety of TPTC. If two F4IPA molecules are positioned such that the fluorine atoms meta to their carboxyl groups are orientated towards one another, i.e., the manner in which the molecules are arranged within the assembly (see figure 26b), the resulting dimer structure clearly resembles the structure of TPTC. Accordingly, like TPTC, these dimers can be represented using a rhombus. Like in the homomolecular assembly of TPTC, these rhombuses adopt three different orientations, which are related to each other by 120° rotations. These three different orientations are shown in figure 26c, with each being represented using a different colour for clarity. Figure 26d shows the same STM image as figure 24c, but with the coloured rhombus representation for the F4IPA dimers overlaid. Although the extent of the resultant tiling is significantly limited/disrupted due to the presence F4IPA molecules without obvious orientations, all three possible orientations of the rhombuses are present, and they seem to be organised in a random manner. Although this crude analysis is far from statistically concrete, it does hint at a situation which is clearly comparable to the random rhombus tiling observed with TPTC.

The coassembly of coronene with F4IPA discussed above clearly differs markedly from that observed with IPA and coronene (see section 3.2). However, the ratio of IPA to coronene in the coassembly of these two molecules is 6:1, whereas the corresponding ratio in the coassembly of F4IPA and coronene discussed thus far is only 2:1. Therefore, it seems plausible that increasing the relative concentration of F4IPA to coronene may be required for F4IPA and coronene to coassemble in an isostructural manner to that observed with IPA and coronene. Accordingly, solutions in which the concentration of F4IPA is 7.6×10^{-2} M and the concentration of coronene is 2.0×10^{-6} M were tested. These solutions were found to result in the formation of a structure at the heptanoic acid/HOPG interface which is clearly distinct from that discussed previously. As is shown in figure 27, particularly large domains of this new assembly could be readily observed.

High resolution STM images of the new assembly (see figure 28a) clearly indicate that the coronene molecules effectively template the self-assembly of F4IPA into cyclic hexameric units in the same manner that was observed with IPA. Each coronene molecule can clearly be resolved surrounded by six F4IPA molecules arranged into the characteristic cyclic hexameric motif. These coronene centred arrangements are closely packed on the surface into an extended hexagonal array in the same manner

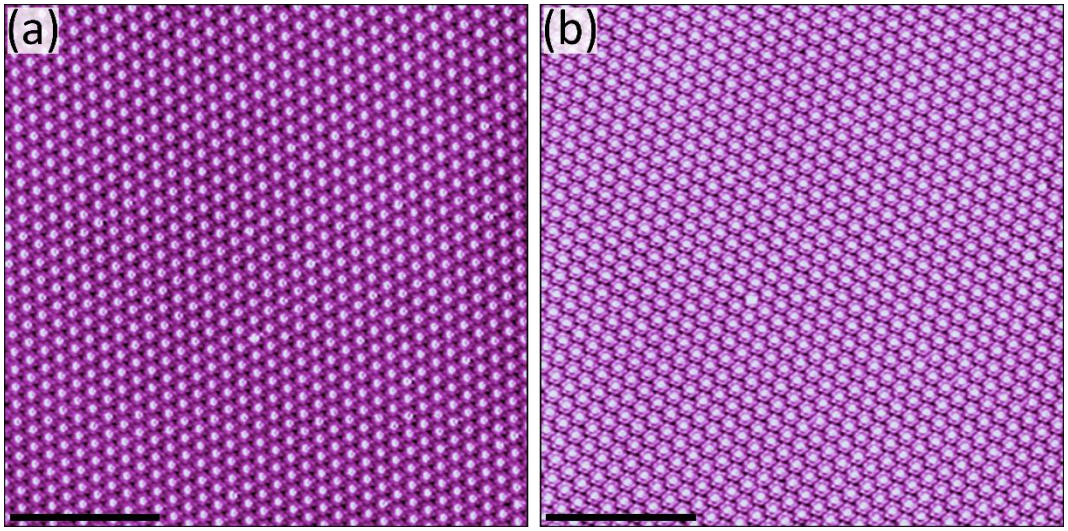

Figure 27: Large-scale STM images showing the coassembly of F4IPA and coronene at the heptanoic acid/HOPG interface, that emerges upon increasing the relative concentration of F4IPA to coronene. Tunnelling parameters: (a) V_{bias} = −0.9 V, I_{set} = 150 pA, (b) V_{bias} = −0.9 V, I_{set} = 200 pA. Both scale bars = 20 nm.

that was observed in the analogous IPA based system. However, as can be seen by comparing figure 18 with figure 27, the domain size with F4IPA is significantly larger. Furthermore, given that no strong interactions involving the fluorine atoms on the outer edges of the hexameric arrangements seem to be possible, it is likely that van der Waals interactions dominate the organisation of these structures into a hexagonal array on the surface. Also note that, due to the presence of peripheral fluorine atoms rather than hydrogen atoms, the weak the C−H···O interactions that may occur between the outer

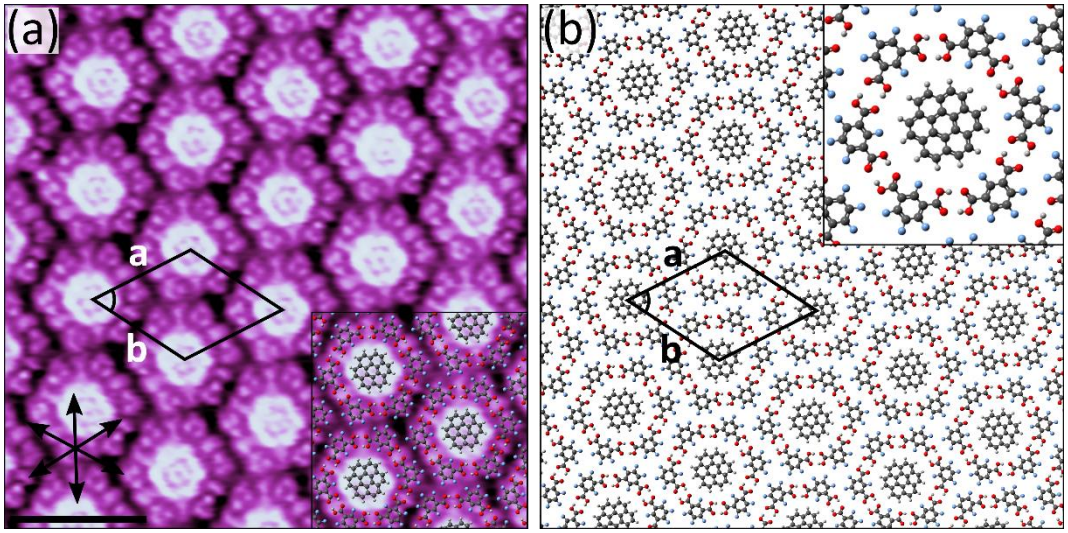

Figure 28: (a) STM image showing the coassembly of F4IPA and coronene at the heptanoic acid/HOPG interface, that emerges upon increasing the relative concentration of F4IPA to coronene. Tunnelling parameters: V_{bias} = −0.9 V, I_{set} = 400 pA. Unit cell parameters: a = b = 2.4 ± 0.1 nm, angle = 60 ± 1°. Scale bar = 3 nm. The radial arrows in the lower left corner show the principle crystallographic directions of the underlying substrate. **(b)** Proposed model for the assembly.

edges of adjacent cyclic hexameric structures in the IPA/coronene system (see section 3.2) are not possible in the analogous F4IPA assembly. The unit cell dimensions for the F4IPA system, a = b = 2.4 ± 0.1 nm and θ = 60 ± 1° (see figure 28), are within error but seemingly fractionally larger than those observed with IPA. Although exchanging fluorine atoms for hydrogen atoms typically has minimal steric impact, the van der Waals radius of fluorine is marginally larger than that of hydrogen. The slightly larger size of F4IPA may account for the slightly larger lattice parameters observed for the F4IPA/coronene system when compared with the analogous IPA/coronene system. A further difference between the two systems is their alignment with the underlying substrate. The angle between the lattice vectors of F4IPA/coronene assembly and the principal lattice vectors of the underlying substrate was investigated for thirteen randomly selected domains. Ten of these domains were found to have a misalignment angle of 5 ± 1°, whilst the angle in the remaining three was 21 ± 1°. Neither of these misalignment angles is the same as the angle of 11 ± 1° observed in the analogous IPA based system (see section 3.2). It should also be noted that although domains with two different substrate alignments were observed, the unit cell dimensions and the arrangement of the molecules are equivalent within both different domain types.

Although slight differences between the discussed IPA/coronene and F4IPA/coronene systems are observed, the basic structural unit, i.e., the cyclic hexameric motif, is essentially equivalent within both systems. The secondary interactions within the two assemblies may differ slightly; however, in this case, these interactions seem to be of limited structural significance. The primary carboxyl functionality present in both IPA and F4IPA allows both molecules to be arranged into the same cyclic hexameric motif. The fact that the precise shape and size complementarity required for coronene to act as an effective template is preserved with F4IPA highlights the minimal steric impact that exchanging hydrogen atoms for fluorine atoms has.

3.5 Conclusions

In conclusion, the self-assembly properties of the simple dicarboxylic acid IPA and its fluorinated analogue F4IPA have been studied at the heptanoic acid/HOPG interface. Whilst IPA readily self-assembles into ordered homomolecular networks, fluorination is found to completely disrupt the homomolecular self-assembly of F4IPA. This occurs despite the close structural similarity between IPA and F4IPA. Although the origin of this behaviour is not entirely clear, the inability of F4IPA to partake in weak C–H···O interactions may be a significant factor.

IPA and F4IPA were also found to differ in their response to the addition of coronene. Whilst IPA was only found to coassemble with coronene into a single structure, with F4IPA two distinct coassembled structures were observed. Which of the two potential coassemblies of F4IPA and coronene that was observed was found to depend on the concentrations of the two components in the solution. One of the two assemblies observed with F4IPA is an unusual structure which lacks translational order, in which the F4IPA molecules are arranged into irregular chains via $\mathrm{R}_2^2(8)$ hydrogen bonds. The F4IPA molecules in the other structure are also arranged via $\mathrm{R}_2^2(8)$ hydrogen bonds; however, in this case the F4IPA molecules are organised into cyclic hexameric arrangements due to the templating influence of the coronene molecules. This latter assembly is isostructural with that formed with the unfluorinated analogue IPA and coronene. For this isostructurality to occur, the dimensions of IPA and F4IPA must match precisely enough that coronene can effectively template the formation of the cyclic hexameric arrangement in both cases. This result highlights the minimal steric impact associated with exchanging hydrogen and fluorine atoms.

Chapter 4: Exploring the self-assembly behaviour of tripyridyltriazine isomers

A large proportion of the remaining discussion in this thesis relates to the formation of complex multicomponent structures based on hydrogen and/or halogen bonding interactions. These networks are constructed by pairing a variety of different hydrogen/halogen bond donors with a range of molecules which can act as effective acceptors for these interactions. Throughout all of the following chapters, the three tripyridyltriazine isomers shown in figure 29 are extensively employed as acceptors. These three molecular building blocks are each composed of four heterocyclic aromatic rings: a central triazine ring surrounded by three pyridyl rings. The three molecules differ only in the position of their pyridyl nitrogen atoms.

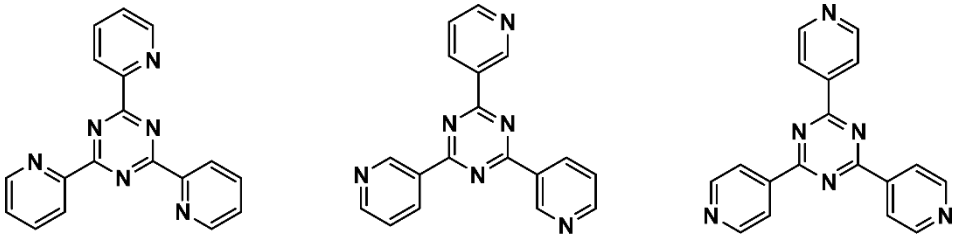

Figure 29: Molecular structures of 2,4,6-tri(2-pyridyl)-*s*-triazine (2TPTZ), 2,4,6-tri(3-pyridyl)-*s*-triazine (3TPTZ) and 2,4,6-tri(4-pyridyl)-*s*-triazine (4TPTZ).

These three molecules were selected as acceptors as pyridyl nitrogen atoms have been shown to be effective acceptor sites for both halogen[49–51] and hydrogen bonds[127–133] under similar conditions to those used here. Furthermore, the three isomers are expected to adopt a planar conformation, which should favour surface adsorption. Although the self-assembly of these molecules on their own is not the focus of this work, knowledge of their homomolecular self-assembly behaviour and the interactions that control this is valuable for comparison with the bimolecular systems that are discussed further in.

With these aims in mind, the self-assembly of the three isomers was investigated via STM measurements conducted under ambient conditions at the solid–liquid interface. Their self-assembly behaviour was explored with two solvents, namely heptanoic acid and 1-phenyloctane. The conditions under which the self-assembly properties of these three isomers were analysed are the same as those under which the bimolecular networks discussed in the remainder of this thesis were studied.

4.1 Potential conformations of the tripyridyltriazine isomers

As is shown in figure 30, the isomer 2TPTZ can adopt two distinct planar conformations. In one of these conformations all of the pyridyl rings are orientated in the same way, such that the molecule adopts a threefold-symmetric conformation (figure 30a). In the alternate conformation, one of the pyridyl rings is flipped such that it is orientated the opposite way relative to the other two (figure 30b). Density functional theory (DFT) calculations were employed to evaluate the relative stabilities of the two conformations. Single gas-phase molecules in both conformations were optimised using Gaussian03[134] at the B3LYP/6-311g(d,p) level. These calculations reveal that, as is consistent with previous results,[135] the threefold-symmetric conformation is 12.2 kJ/mol more stable than the alternate conformation. As this energy difference is approximately five times greater than thermal energy at room temperature, the threefold-symmetric conformation is expected to be essentially exclusively present in the systems studied here.

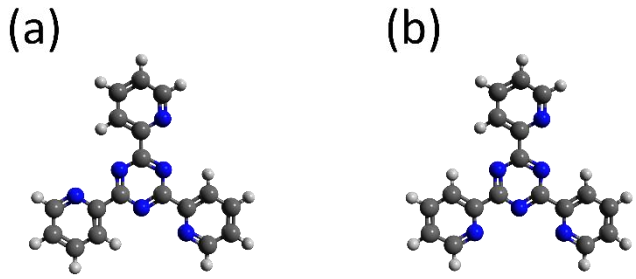

Figure 30: (a) Threefold-symmetric conformation of 2TPTZ. **(b)** Alternate configuration of 2TPTZ.

3TPTZ is also able to adopt two distinct planar conformations in the same manner as 2TPTZ, i.e., a threefold-symmetric conformation in which all of the pyridyl rings are orientated in the same direction (figure 31a) and an alternate conformation in which one of the rings is flipped (figure 31b). DFT calculations were again employed in exactly the same manner as those performed for 2TPTZ. In the case of 3TPTZ, the threefold-symmetric conformation was only found to be favoured by 0.9 kJ/mol. As this energy difference is smaller than thermal energy at room temperature, either conformation should be possible. As is shown throughout this text, the ability of 3TPTZ to readily adopt these two conformations is a significant factor in its self-assembly behaviour. Note that, unlike 2TPTZ and 3TPTZ,

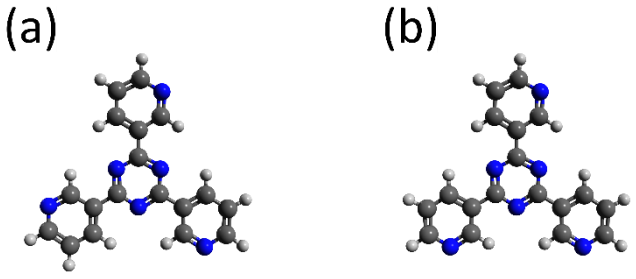

Figure 31: (a) Threefold-symmetric conformation of 3TPTZ. **(b)** Alternate configuration of 3TPTZ.

the isomer 4TPTZ does not have analogous conformational flexibility, with only a single planar conformation being possible.

4.2 Surface-induced chirality of 2TPTZ and 3TPTZ

Although the favourable threefold-symmetric conformation of 2TPTZ is not intrinsically chiral, upon surface adsorption it becomes chiral and can accordingly adopt one of two enantiomorphous configurations (see figure 32). Within one of these configurations, all of the pyridyl nitrogen atoms are positioned at the ortho sites located clockwise relative to the bonds attaching the pyridyl rings to the triazine core. Within the alternate configuration, the pyridyl nitrogen atoms are positioned in the analogous anticlockwise manner.

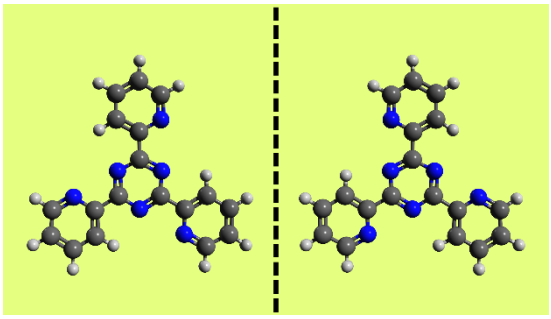

Figure 32: Two enantiomorphous adsorption configurations for the threefold-symmetric conformation of 2TPTZ.

Similarly to 2TPTZ, 3TPTZ also becomes chiral upon surface adsorption. As is shown in figure 33, both possible planar conformations of 3TPTZ have two enantiomorphous adsorption configurations, resulting in a total of four possibilities. Although surface-induced chirality and its influence on the formation of self-assembled monolayers has been exhaustively studied elsewhere and is not the focus of this thesis, the chiral nature of 2TPTZ and 3TPTZ is of particular significance in some of the systems studied throughout this thesis and is discussed in detail where significant.

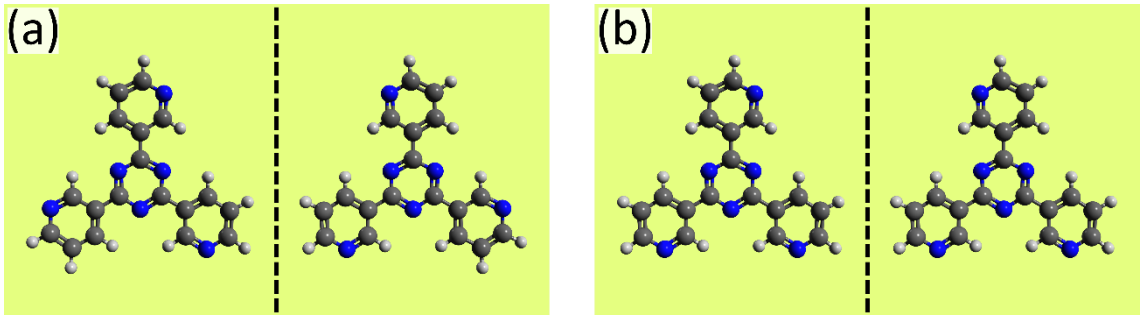

Figure 33: (a) Two enantiomorphous adsorption configurations for the threefold-symmetric conformation of 3TPTZ. **(b)** Two enantiomorphous adsorption configurations for the alternate conformation of 3TPTZ.

4.3 Homomolecular self-assembly behaviour of 4TPTZ

Initially, the homomolecular self-assembly of 4TPTZ was studied at the heptanoic acid/HOPG interface. There are contrasting reports in the literature regarding the self-assembly of this molecule: Kampschulte et al. have previously reported that 4TPTZ does not self-assemble at the heptanoic acid/HOPG interface[127], whilst Li et al. have reported that it does[130]. Within this thesis, the self-assembly of 4TPTZ at the heptanoic acid/HOPG interface was again investigated. Solutions with concentrations ranging from saturated down to 10^{-5} M were tested. The results obtained here are consistent with those of Kampschulte et al., i.e., no evidence for the self-assembly of 4TPTZ was ever observed.

Unlike at the heptanoic acid/HOPG interface, 4TPTZ was observed to self-assemble at the 1-phenyloctane/HOPG interface. The solubility of 4TPTZ in 1-phenyloctane was found to be quite low. Therefore, saturated solutions were used. Deposition of such solutions leads to the formation of extended domains of the homomolecular assembly shown in figure 34.

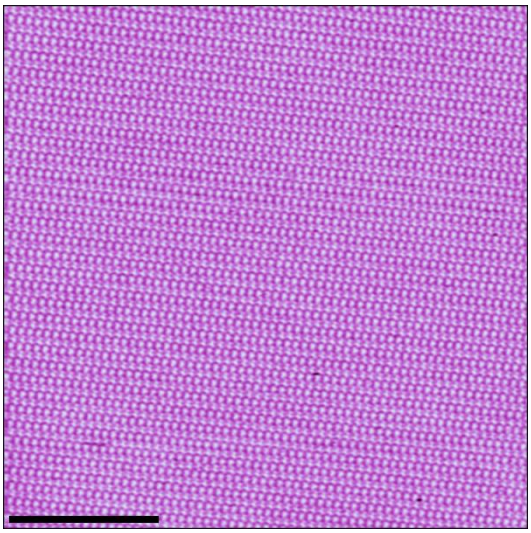

Figure 34: Large-scale STM images showing the assembly of 4TPTZ at the 1-phenyloctane/HOPG interface. Tunnelling parameters: V_{bias} = −1.2 V, I_{set} = 300 pA. Scale bar = 20 nm.

Within high-resolution images of the assembly, such as that shown in figure 35a, the individual 4TPTZ molecules can be clearly resolved as distinct tripodal structures. These molecules are closely packed together on the surface into a rectangular array consistent with the model shown in figure 35b. Although the 4TPTZ molecules are not functionalised such that they can interact via any particularly strong interactions, there may be some stabilising contribution from weak C–H···N(pyridyl) interactions in addition to the van der Waals interactions that seems to dominate the close packing of these molecules.

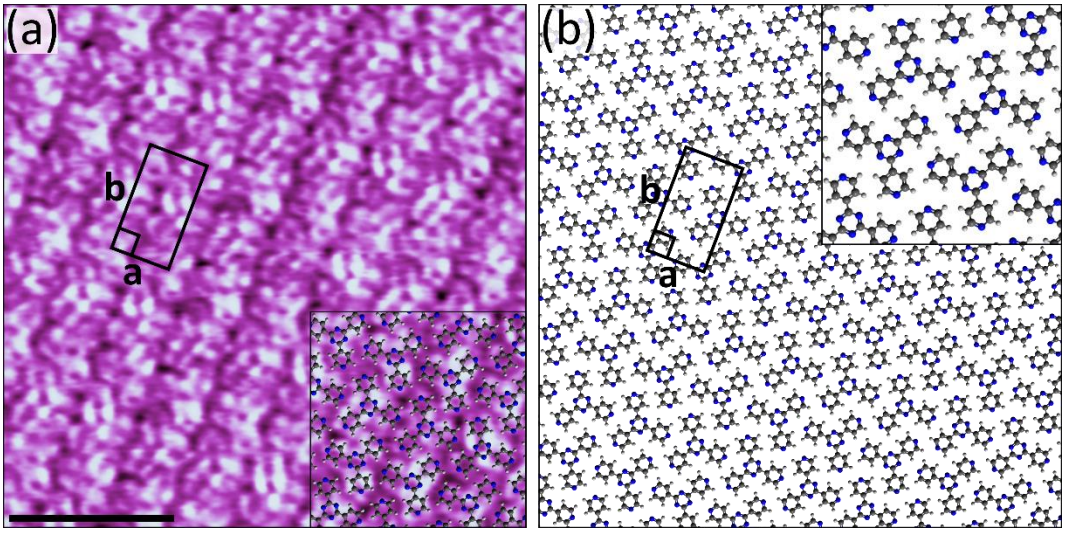

Figure 35: (a) STM image showing the assembly of 4TPTZ at the 1-phenyloctane/HOPG interface. Tunnelling parameters: V_{bias} = −0.9 V, I_{set} = 100 pA. Unit cell parameters: a = 1.1 ± 0.1 nm, b = 2.0 ± 0.1 nm, angle 90 ± 3°. Scale bar = 3 nm. **(b)** Proposed model for the assembly.

4.4 Homomolecular self-assembly behaviour of 3TPTZ

Unlike its isomeric counterpart 4TPTZ, 3TPTZ was found to self-assemble at the heptanoic acid/HOPG interface. Deposition of a 10^{-2} M solution of 3PTTZ was found to lead to the formation of an ordered hexagonal assembly. As is shown in figure 36, extended domains of this network could be observed covering essentially the entire surface of the sample.

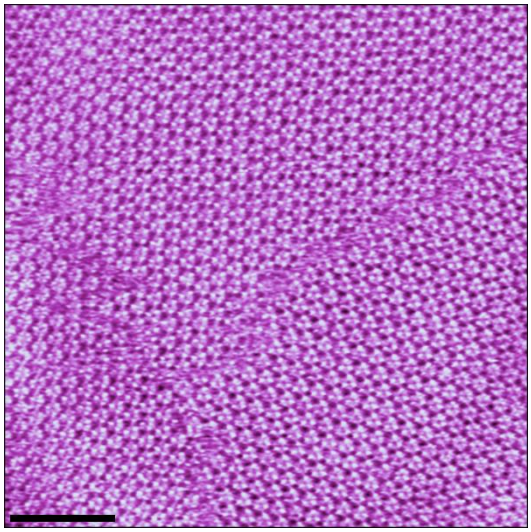

Figure 36: Large-scale STM image showing the assembly of 3TPTZ at the heptanoic acid/HOPG interface. Tunnelling parameters: V_{bias} = −0.9 V, I_{set} = 100 pA. Scale bar = 20 nm.

Within high-resolution images of the assembly, such as that presented in figure 37a, the threefold symmetric 3TPTZ molecules can be clearly resolved. The 3TPTZ molecules are arranged on the surface into a series of cyclic structures, each of which is composed of six 3TPTZ molecules. The arrangement

of these cyclic structures can be clearly rationalised by C−H···N(pyridyl) interactions, with each 3TPTZ molecule being positioned such that it can interact with two adjacent 3TPTZ molecules via these interactions. These weak interactions organise the 3TPTZ molecules into the cyclic arrangements, which are then packed together on the surface into the observed hexagonal array. The pyridyl nitrogen atoms on the periphery of these cyclic structures are not positioned such that they can interact with adjacent 3TPTZ molecules; however, these free pyridyl nitrogen atoms are not likely to be structurally inactive. They likely interact with coadsorbed solvent molecules via strong O−H···N(pyridyl) hydrogen bonds and auxiliary C−H···O interactions. Such interactions are quite favourable and the coadsorbed heptanoic acid molecules are of ideal size to be accommodated in the interstices between the cyclic structures. Although they cannot be clearly resolved, there does appear to be some structure that can be explained by the presence of coadsorbed solvent molecules within these regions. Note that in other studies in which coadsorbed solvent molecules have been proposed, clear resolution of them was similarly not observed.[136–143] A tentatively proposed model for the assembly is presented in figure 37b.

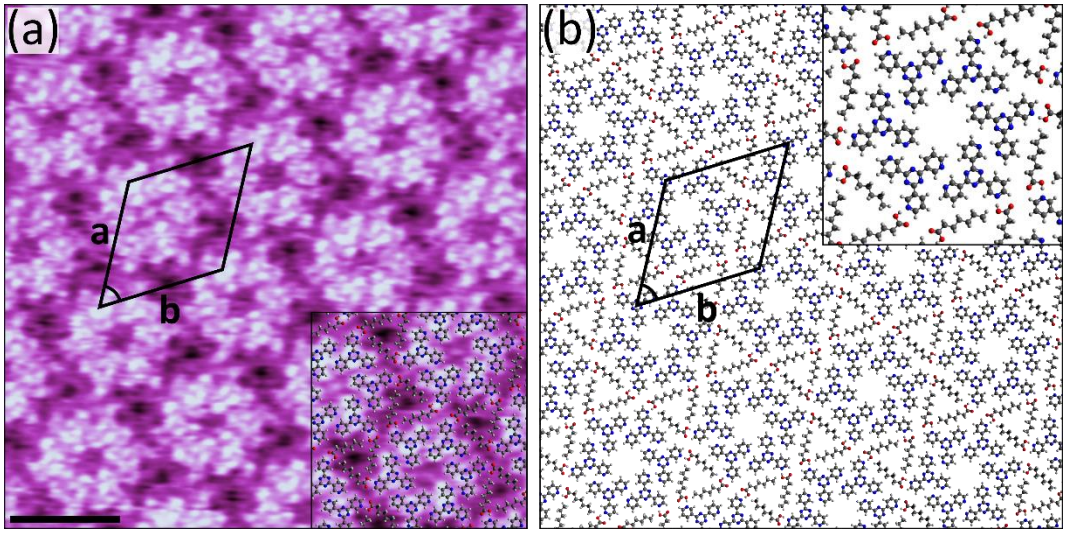

Figure 37: (a) STM image showing the assembly of 3TPTZ at the heptanoic acid/HOPG interface. Tunnelling parameters: V_{bias} = −0.9 V, I_{set} = 100 pA. Unit cell parameters: a = b = 3.5 ± 0.1 nm, angle 60 ± 3°. Scale bar = 3 nm. **(b)** Proposed model for the assembly.

The dependence of the self-assembly behaviour on the concentration of the deposited solution was also investigated. Concentrations of 3TPTZ ranging from 10^{-2} M down to 5×10^{-5} M were explored. No evidence of any concentration-controlled polymorphism was observed in this range. Within the concentration range of 10^{-2} – 2.5 x 10^{-3} M, the hexagonal assembly could be observed covering essentially the entire surface of the sample. At concentrations of 10^{-3} M and below, no evidence of any assembly could be observed on the surface. These observations are summarised in figure 38.

The self-assembly of 3TPTZ at the 1-phenyloctane/HOPG interface was also explored. As was also the case with 4TPTZ, due to the low solubility of 3TPTZ in 1-phenyloctane, saturated solutions were used.

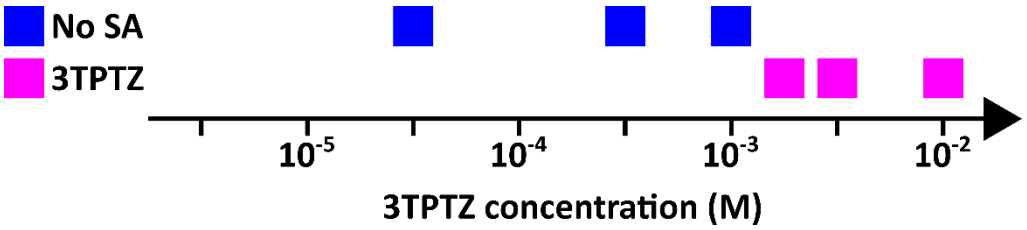

Figure 38: Profile summarising the different observations made at the heptanoic acid/HOPG interface as the concentration of 3TPTZ in solution is changed. Blue squares indicate that no assembly could be observed, and pink squares indicate that the hexagonal assembly of 3TPTZ was observed.

The assembly of 3TPTZ from 1-phenyloctane was found to differ markedly from that observed with heptanoic acid. When 1-phenyloctane is used as the solvent, the assembly is somewhat disordered and cannot be characterised by a unit cell. Figure 39 shows two large-scale images of this disordered assembly, which was observed covering essentially the entire surface of the sample.

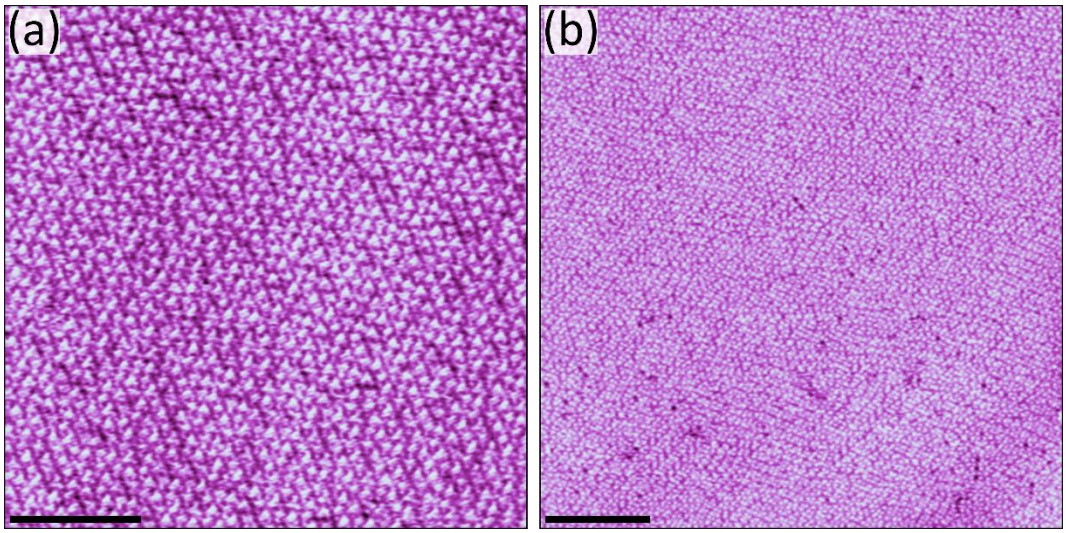

Figure 39: Large-scale STM images showing the assembly of 3TPTZ at the 1-phenyloctane/HOPG interface. Tunnelling parameters for both images: V_{bias} = −0.9 V, I_{set} = 50 pA. For (a) the scale bar = 10 nm, and for (b) the scale bar = 20 nm.

Figure 40 shows an example of a high-resolution image of the assembly within which the individual 3TPTZ molecules can be clearly resolved. These molecules are closely packed on the surface in a semi-disordered manner. As was discussed in section 4.1, there are two distinct planar conformations which 3TPTZ can adopt. Furthermore, as was discussed in section 4.2, these two conformations both have two potential enantiomorphous adsorption configurations. As a result, there are a total of four possible distinct configurations that each of the 3TPTZ molecules within the assembly can adopt. As these four potential configurations are not readily distinguishable via STM and because of the semi-disordered nature of the assembly, precisely understanding the structure of the assembly is extremely challenging. If the exact conformation of the adsorbed 3TPTZ molecules is neglected and only their triangular shape is considered, it appears that the 3TPTZ molecules only adopt two distinct

orientations within a given domain (see overlay in figure 40). These two orientations are related by a 180° rotation. Although this semi-disordered assembly seems to be fairly unusual, very similar anomalous networks of other triangular shaped molecules have been reported.[144–146] The origin of this behaviour within these systems is unclear.

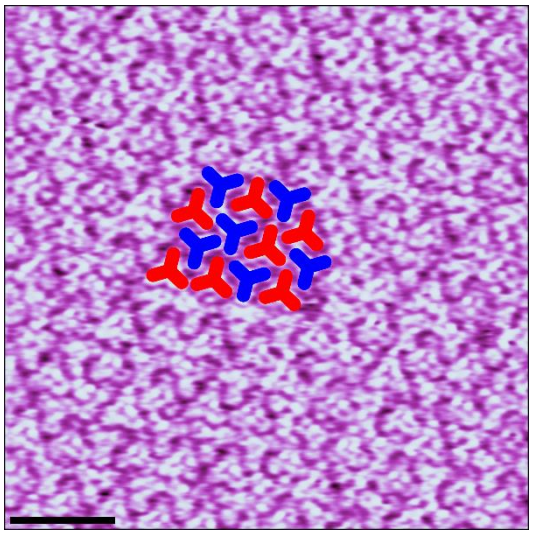

Figure 40: STM image showing the assembly of 3TPTZ at the 1-phenyloctane/HOPG interface. Tunnelling parameters: V_{bias} = −0.9 V, I_{set} = 50 pA. Scale bar = 3 nm. The overlayed tripodal shapes highlight the approximate positions of the 3TPTZ molecules. The two different orientations of the 3TPTZ molecules are shown in red and blue.

4.5 Homomolecular self-assembly behaviour of 2TPTZ

2TPTZ was observed to self-assemble into a seemingly hexagonal assembly at the heptanoic acid/HOPG interface. As is shown in figure 41a, STM imaging could be readily used to observe extended domains of this hexagonal network.

Within high-resolution images of the assembly, such as that shown in figure 41b, the individual 2TPTZ molecules can be clearly resolved. These molecules are seemingly organised into a porous chicken-wire-type structure; however, there are no obvious strong interactions between the adjacent 2TPTZ molecules that could justify the formation of such a porous network. Although it typically cannot be clearly resolved, with certain STM tips some structure can be resolved within the apparent pores of the assembly (see figure 41b). It is very likely that this structure corresponds to coadsorbed solvent molecules present within these regions. These coadsorbed solvent molecules likely interact with the surrounding 2TPTZ molecules via favourable O−H···N(pyridyl) hydrogen bonds. Given that the assembly cannot be rationalised via direct interactions between the 2TPTZ molecules, coadsorbed solvent molecules very likely play a significant structural role.

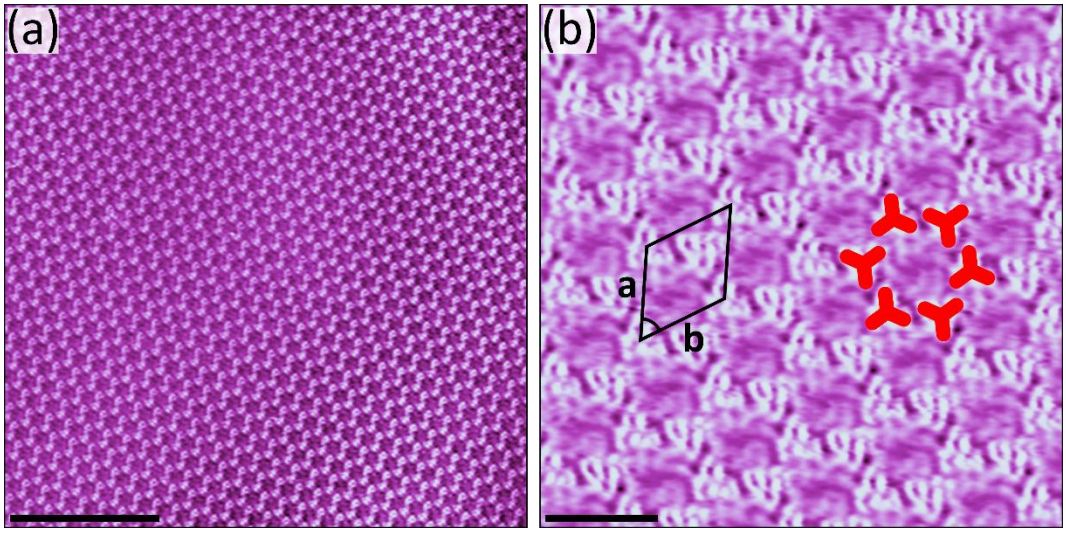

Figure 41: STM images showing the assembly of 2TPTZ at the heptanoic acid/HOPG interface. (a) Tunnelling parameters: V_{bias} = −0.9 V, I_{set} = 100 pA. Scale bar = 20 nm. (b) Tunnelling parameters: V_{bias} = −1.5 V, I_{set} = 50 pA. Unit cell parameters: a = b = 2.5 ± 0.2 nm, angle 60 ± 3°. Scale bar = 3 nm. The overlayed red tripodal shapes highlight the approximate positions of the 2TPTZ molecules.

The influence of the concentration of the solution on the self-assembled properties of 2TPTZ at the heptanoic acid/HOPG interface was also investigated. At concentrations of 10^{-2} – 5 × 10^{-4} M, the hexagonal coassembly was observed covering essentially the entire surface of the sample. Although occasional domains of the hexagonal assembly were still encountered on the surface, the assembly was absent from most of the surface after reducing the concentration of 2TPTZ down to 2.5 × 10^{-4} M. At concentrations of 10^{-4} M and below, no assembly was observed at the heptanoic acid/HOPG interface. The different observations made at the concentrations that were sampled are summarised in figure 42.

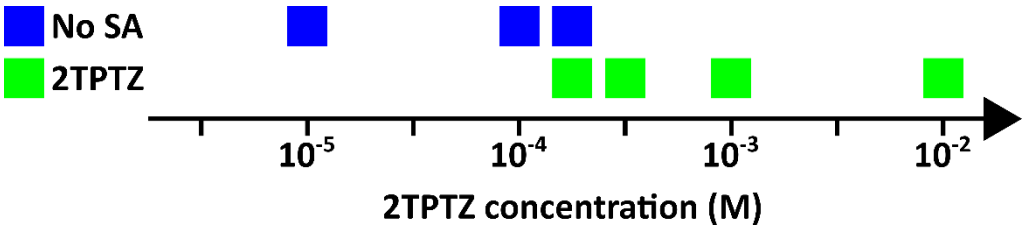

Figure 42: Profile summarising the different observations made at the heptanoic acid/HOPG interface as the concentration of 2TPTZ in solution is changed. Blue squares indicate that no assembly could be observed, and green squares indicate that the hexagonal assembly of 3TPTZ was observed.

As was the case for the two previously discussed tripyridyltriazine isomers, 2TPTZ was also observed to self-assemble from saturated solutions at the 1-phenyloctane/HOPG interface. In this case, two distinct phases were observed coexisting on the surface (see figure 43). One of these structures has

hexagonal symmetry whilst the other is seemingly rectangular. These structures were fairly unstable towards imaging and were readily disrupted at times by the scanning process.

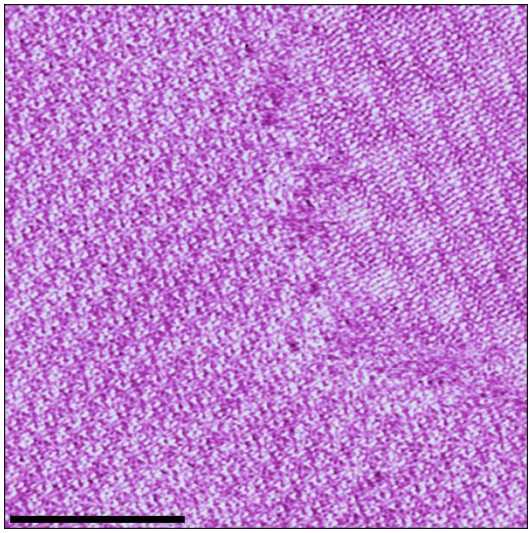

Figure 43: Large-scale STM image showing the assembly of 2TPTZ at the 1-phenyloctane/HOPG interface. The hexagonal (domain on the left side of the image) and seemingly rectangular (domain on the right side of the image) phases can be seen coexisting. Tunnelling parameters: V_{bias} = −0.9 V, I_{set} = 50 pA. Scale bar = 20 nm.

Figure 44 shows an example of a high-resolution STM image of the hexagonal assembly observed at the 1-phenyloctane/HOPG interface. Within this image, the threefold-symmetric shape of the 2TPTZ molecules can be clearly resolved. These molecules are densely packed on the surface. The assembly has a rhombic unit cell in which a 60 ± 2° angle separates two equivalent lattice vectors that have lengths of 4.3 ± 0.2 nm. For a single small molecule in a densely packed network, this unit cell, which

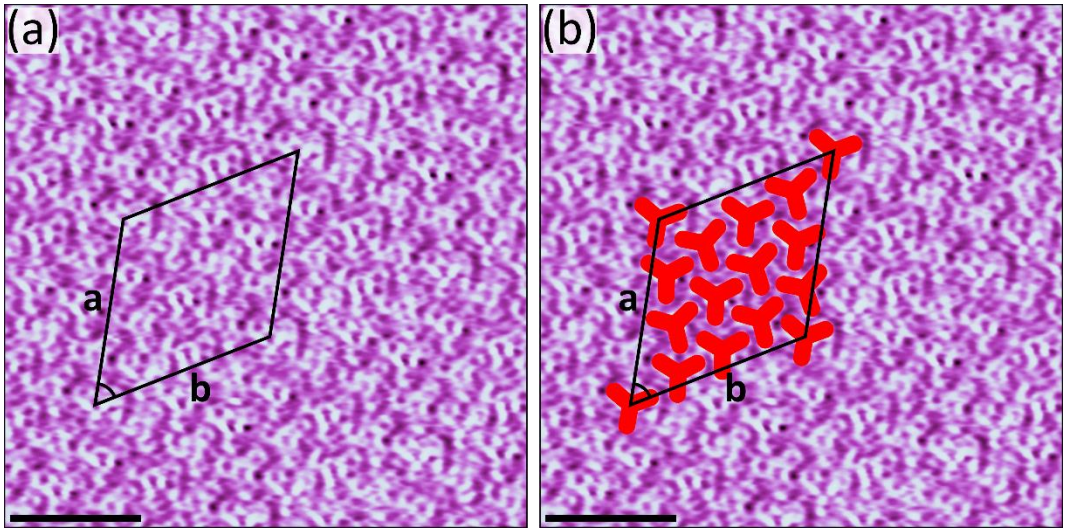

Figure 44: (a) STM image showing the hexagonal assembly of 2TPTZ at the 1-phenyloctane/HOPG interface. Tunnelling parameters: V_{bias} = −0.9 V, I_{set} = 50 pA. Unit cell parameters: a = b = 4.3 ± 0.2 nm, angle 60 ± 2°. Scale bar = 3 nm. **(b)** The same STM image as shown in (a) but with red tripodal shapes overlaid to highlight the approximate positions of the 2TPTZ molecules.

contains a total of thirteen 2TPTZ molecules, is notably large. This hints at the formation of a particularly complex supramolecular structure. As was discussed in section 4.1, the 2TPTZ molecules can adopt two distinct conformations. Although the conformation of the 2TPTZ molecules cannot be unambiguously resolved in the STM images, the adsorbed 2TPTZ molecules are expected to adopt their more energetically favourable threefold-symmetric conformation (see section 4.1). However, as is discussed in section 4.2, this conformation becomes chiral upon surface adsorption, resulting in 2TPTZ being able to adopt two enantiomorphous configurations on the surface. These two enantiomorphous configurations cannot be distinguished within the STM images. Therefore, the configuration of the individual 2TPTZ molecules in the hexagonal assembly is not clear. The assembly could be homochiral in the sense that all the molecules could adopt the same enantiomorphous configuration. However, it is also possible that the assembly is constructed from a mixture of molecules in the two enantiomorphous configurations, in which case, when the large number of molecules in the repeat unit of the assembly is considered, an extensive array of different potential assemblies are viable. The complexity of the assembly coupled with the inability to identify the enantiomorphous configuration of the adsorbed 2TPTZ molecules makes precisely understanding the organisation of the supramolecular structure very challenging. It seems likely that weak C–H···N(pyridyl) interactions combined with the van der Waals interactions that seem to dominate the close-packed nature of the assembly stabilise the hexagonal structure.

As was previously mentioned, an alternate phase was observed coexisting with the hexagonal assembly at the 1-phenyloctane/HOPG interface (see figure 43). Neither phase was particularly dominant, with both being present in roughly equal proportions. As is shown in figure 45, in some

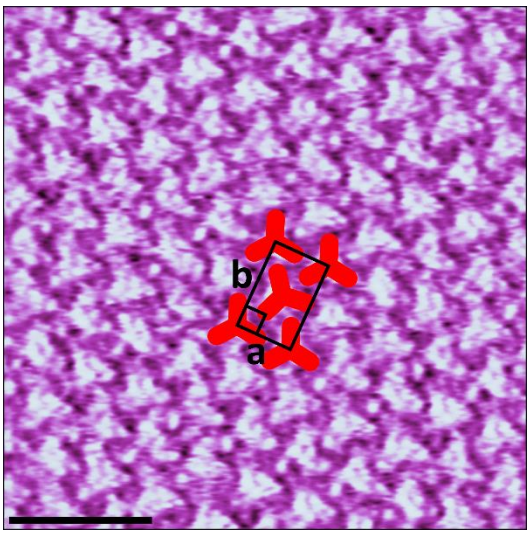

Figure 45: STM image showing the rectangular assembly of 2TPTZ at the 1-phenyloctane/HOPG interface. Tunnelling parameters: V_{bias} = −0.9 V, I_{set} = 50 pA. Unit cell parameters: a = 1.3 nm, b = 2.0 ± 0.1 nm, angle 90 ± 2°. Scale bar = 3 nm. The overlayed tripodal shapes highlight the approximate positions of the 2TPTZ molecules.

regions this assembly seemed to be well ordered, with the molecules being arranged into an approximately rectangular array. The tripodal shape of the 2TPTZ molecules can be resolved; however, as was the case with the coexisting hexagonal assembly of 2TPTZ, their enantiomorphous nature cannot be identified. This again prevents the arrangement of the molecules within the assembly from being precisely understood. The situation is further complicated by the observation of frequent irregularities in the rectangular ordering of the assembly. These irregularities consist of small displacements of the 2TPTZ molecules along the direction of the short lattice vector within the assembly. This effect is highlighted in figure 46. As can be seen in the overlay shown in figure 46b, the molecules in the purple region of the image are organised into the approximately rectangular structure. Within the abutting region highlighted in green, the 2TPTZ molecules are also organised into the same rectangular structure. The short lattice vectors for the purple and green regions are orientated in the same direction. However, between the two regions, there is a small relative displacement of the 2TPTZ molecules along the direction of the short lattice vectors such that the long lattice vectors for the two regions are not aligned (see arrows in figure 46b). Another such displacement is highlighted in figure 46b when comparing the green region to the region to the right of it (highlighted in yellow). These displacements typically occur extremely frequently within the assembly.

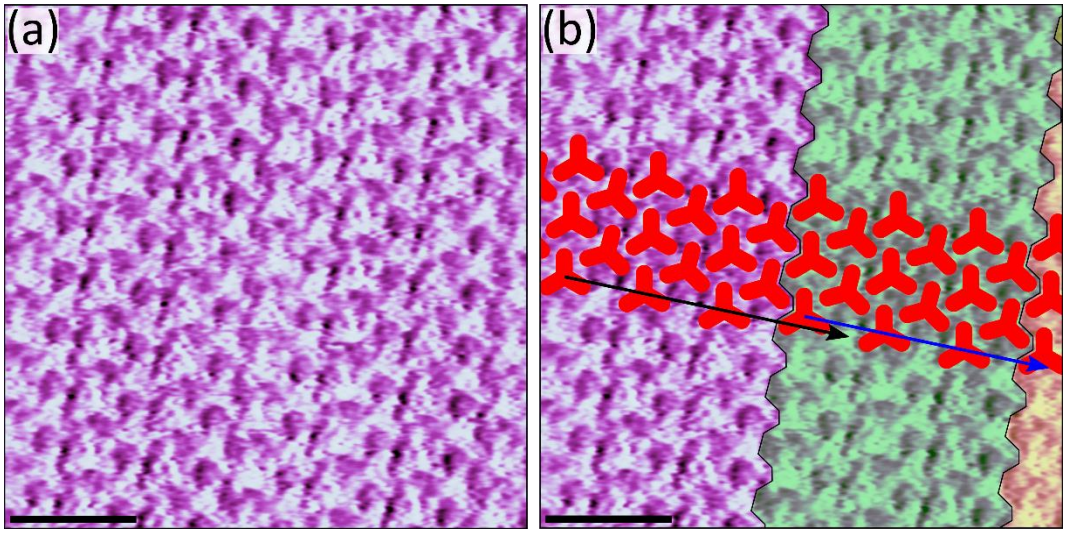

Figure 46: (a) STM image showing the rectangular assembly of 2TPTZ at the 1-phenyloctane/HOPG interface. Tunnelling parameters: V_{bias} = −1.2 V, I_{set} = 50 pA. Scale bar = 3 nm. **(b)** The same STM image as shown in (a) but with red tripodal shapes overlaid to highlight the approximate positions of the 2TPTZ molecules. Misaligned regions of the assembly are highlighted in different colours. The black arrow shows the direction of the long lattice vector for the region highlighted in purple. The blue arrow shows the direction of the long lattice vector for the region highlighted in green.

4.6 Further discussion

Only 2TPTZ and 3TPTZ were observed to self-assemble at the heptanoic acid/HOPG interface whereas all three isomers were observed to self-assemble at the 1-phenyloctane/HOPG interface. The inability of 4TPTZ to self-assemble at the heptanoic acid/HOPG interface indicates that the molecule preferentially remains in the solution phase, which hints at a particularly favourable interaction between 4TPTZ and heptanoic acid. Furthermore, although 2TPTZ and 3TPTZ do self-assemble at the heptanoic acid/HOPG interface, the coadsorption of solvent molecules seems to play a significant role. This again hints at a strong interaction between the tripyridyltriazine isomers and the heptanoic acid molecules. Such a favourable interaction is clearly expected due to the ability of the tripyridyltriazine isomers to interact with heptanoic acid molecules via strong O–H···N(pyridyl) hydrogen bonds. Conversely, 1-phenyloctane cannot interact with the tripyridyl triazine isomers via any strong interactions. Accordingly, all three molecules were observed to readily self-assemble at the 1-phenyloctane/HOPG interface and no evidence for solvent coadsoption was seen in any of the observed networks. These observations are particularly significant in the following chapters where the three tripyridyltriazine isomers are paired with a series of hydrogen and halogen bond donors as, when these experiments are conducted at the heptanoic acid/HOPG interface, the donors essentially have to compete with solvent molecules for the N(pyridyl) acceptor sites. Furthermore, in some of the assemblies discussed in this chapter, molecules of the tripyridyltriazine isomers are observed to directly interact with each other via C–H···N(pyridyl) interactions. Although these interactions are typically quite weak, they also provide a competing interaction mode in which the N(pyridyl) acceptor sites can partake.

4.7 Conclusions

The self-assembly behaviour of three tripyridyltriazine isomers has been explored at the interface between HOPG and two solvents, namely heptanoic acid and 1-phenyloctane. Of the three isomers, only two were observed to self-assemble at the heptanoic acid HOPG interface whereas all three were observed to do so at the 1-phenyloctane/HOPG interface. The ability of heptanoic acid to interact with the three isomers via hydrogen bonds was found to significantly influence their self-assembly behaviour in this solvent. Conversely, the solvent 1-phenyloctane, which cannot strongly interact with the three isomers via any specific intermolecular interaction, was found to play a more passive role. Although exploring the self-assembly behaviour of the three tripyridyl isomers is not the explicit aim of this thesis, the results presented in this chapter provide a useful point of comparison for the

experiments conducted in subsequent chapters, where the three isomers are employed as hydrogen/halogen bond acceptors.

Chapter 5: Exploring the impact of fluorination on the self-assembly behaviour of terephthalic acid in homomolecular and bimolecular systems

Carboxylic acids are highly versatile molecular building blocks which are capable of partaking in a range of intermolecular interactions. However, although carboxylic acids have been exhaustively studied as building blocks for the formation of self-assembled monolayers, most of these studies involve simple $R_2^2(8)$ dimeric hydrogen bonds between carboxyl groups. Other supramolecular uses of carboxyl groups have been somewhat overlooked in the context of surface-confined supramolecular chemistry. Within 3D systems, carboxylic acids are routinely used for the formation of complex multicomponent cocrystals. By pairing a carboxylic acid with an appropriate hydrogen bond acceptor, bicomponent architectures driven by predictable hydrogen bond donor–acceptor interactions can be constructed. One of the most frequently utilised interactions within such systems is the carboxylic acid–pyridine heterosynthon. This heterosynthon occurs when a carboxyl group and a pyridyl group interact via a strong O–H···N(pyridyl) hydrogen bond. This simple and robust interaction has proven to be a highly effective tool for the engineering of 3D crystals.

There have been some efforts to explore the formation of bimolecular self-assembled monolayers by pairing carboxylic acid building blocks with pyridyl type acceptors. Although the formation of such networks has been reported,[127–133] the number of studies is sparse. In order to reliably form such networks, the stability of the bimolecular assembly should be higher than that of the homomolecular assemblies of either of the individual components. This criterion can be difficult to fulfil due to the high propensity of carboxylic acids to self-assemble into homomolecular networks via the aforementioned $R_2^2(8)$ hydrogen bonds. Furthermore, when experiments are conducted at the solid–liquid interface, the solvents used are often carboxylic acids themselves. As a result, solvent molecules can compete for hydrogen bond acceptor sites and thereby prevent the formation of the desired bimolecular network. An ideal carboxylic acid building block in this setting should be a strong enough hydrogen bond donor to form stable networks and outcompete solvent molecules whilst not being inclined towards stable homomolecular self-assembly.

Fluorination represents a potential strategy towards increasing the efficacy of carboxylic acids as building blocks for the formation of bimolecular monolayers. Peripheral fluorination of planar molecules has previously been shown to disrupt their surface-confined homomolecular self-assembly due to electrostatic repulsion between the fluorine atoms.[84,103] A similar effect was also seen in chapter 3, where the molecule IPA was observed to self-assemble into homomolecular monolayers

whilst its fluorinated analogue F4IPA was not. Furthermore, fluorine atoms are highly electron withdrawing and are therefore expected to increase the hydrogen bond donor ability of neighbouring functional groups. Fluorinated compounds such as alcohols[147–151] and carboxylic acids[151,152] have previously been shown to form particularly strong hydrogen bonds. These two complementary properties should allow fluorinated carboxylic acids to act as strong hydrogen bond donating building blocks which are less likely to form stable homomolecular networks than their unfluorinated counterparts.

In order to explore these ideas, the comparative self-assembly properties of the prototypical carboxylic acid terephthalic acid (TPA, figure 47) and its fluorinated analogue tetrafluoroterephthalic acid (F4TPA, figure 47) were investigated. TPA is a simple molecule which has been extensively studied as a building block for the formation of self-assembled monolayers. TPA is composed of a central benzene ring functionalised with two carboxyl groups positioned para to one another. It is a functionally similar structural isomer of IPA (studied in chapter 3) and the two molecules typically self-assemble in a very similar manner. However, due to the para positioning of the carboxyl groups, $R_2^2(8)$ hydrogen bonds cause TPA to self-assemble into linear chains (see schematic representation in figure

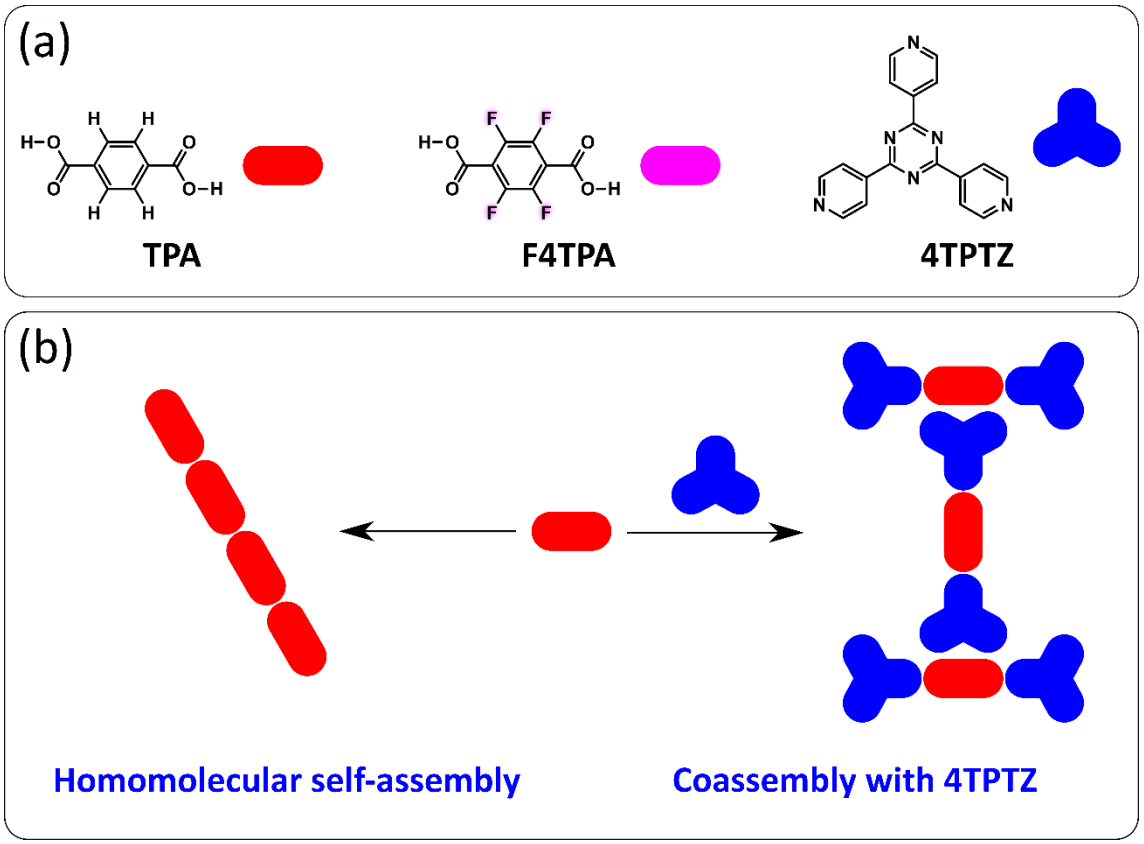

Figure 47: (a) Molecular structures alongside schematic representations of terephthalic acid (TPA), tetrafluoroterephthalic acid (F4TPA) and 2,4,6-tri(4-pyridyl)-s-triazine (4TPTZ). **(b)** Schematic illustration of the homomolecular self-assembly of TPA into linear chains and its coassembly with the molecule 4TPTZ.

47) rather than the zigzag chains that are observed with IPA. TPA has also been shown to be a somewhat effective building block for the formation of 2D carboxylic acid–pyridine cocrystals. As is shown schematically in figure 47, by pairing TPA with the molecule 4TPTZ, Kampschulte et al. demonstrated that bimolecular networks mediated by O−H···N(pyridyl) hydrogen bonds can be formed.[127] 4TPTZ is one of the three tripyridyltriazine isomers which was studied in chapter 4. Here, in order to explore the influence of fluorination on the formation of carboxylic acid–pyridine bimolecular monolayers, both TPA and F4TPA were paired with each of the tripyridyltriazine isomers discussed in chapter 4. The outcomes of each of these pairings was studied using STM operating under ambient conditions at the solid–liquid interface.

5.1 Homomolecular self-assembly behaviour of TPA

As has been widely reported in the literature, deposition of saturated solutions of TPA readily leads to the formation of self-assembled monolayers at the heptanoic acid/HOPG interface.[119,153–155] Extended domains of this homomolecular system could be observed via STM (see figure 48).

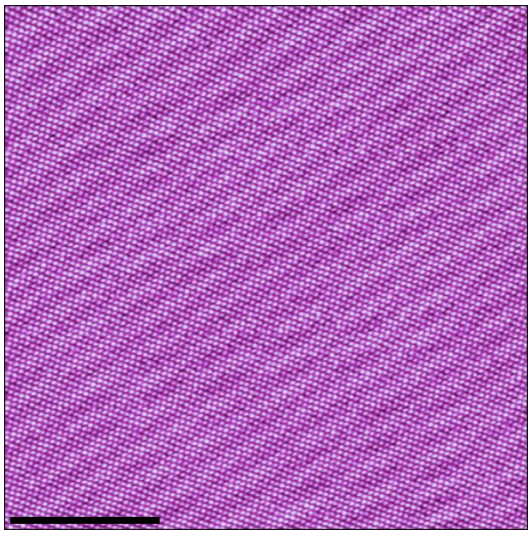

Figure 48: Large-scale STM images showing the assembly of TPA at the heptanoic acid/HOPG interface. Tunnelling parameters: V_{bias} = −1.2 V, I_{set} = 300 pA. Scale bar = 20 nm.

Within high-resolution images of the assembly, the individual TPA molecules can be clearly resolved with submolecular resolution (see figure 49). Each TPA molecule interacts with two neighbouring TPA molecules via the expected $R_2^2(8)$ hydrogen bonds. These interactions organise the TPA molecules into linear chains. These linear chains are packed together side-by-side on the surface, resulting in the formation of a densely packed oblique structure. In addition to the van der Waals interactions that

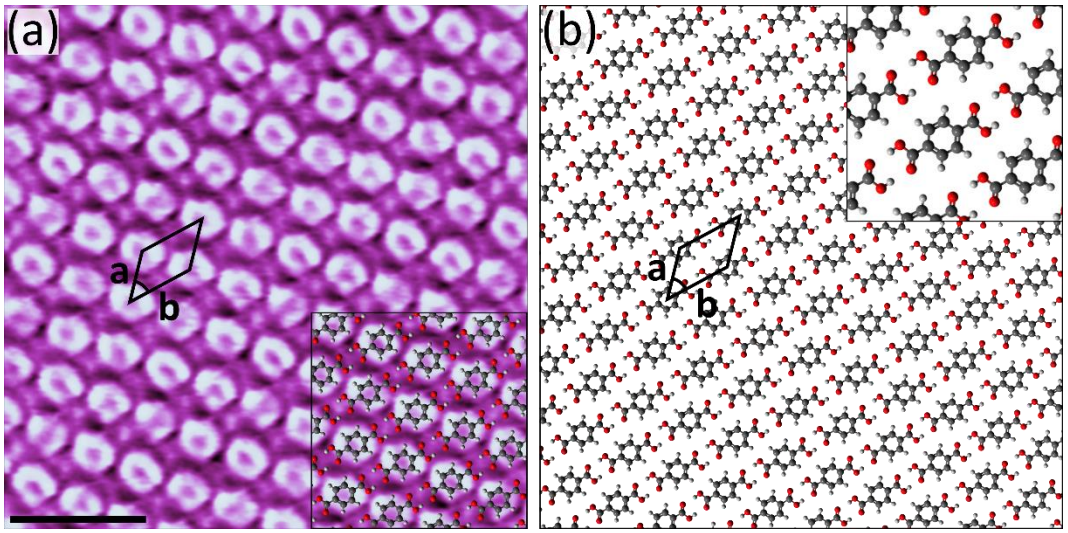

Figure 49: (a) STM image showing the assembly of TPA at the heptanoic acid/HOPG interface. Tunnelling parameters: V_{bias} = −1.2 V, I_{set} = 200 pA. Unit cell parameters: a = 0.77 ± 0.05 nm, b = 1.0 ± 0.1 nm, angle = 48 ± 3°. Scale bar = 2 nm. **(b)** Proposed model for the assembly.

clearly influence the close-packing of these chains, there may also be some stabilising contribution from weak C−H···O interactions between the TPA molecules of adjacent chains. The proposed model for the assembly is shown in figure 49b.

5.2 Homomolecular self-assembly behaviour of F4TPA

Contrastingly to what was observed with TPA, F4TPA was not observed to self-assemble at the heptanoic acid/HOPG interface. Solutions with concentrations ranging from saturated down to 10^{-5} M were tested, and no evidence for the self-assembly of F4TPA was observed under any conditions. This is consistent with the results that were observed for the related IPA/F4IPA system discussed in chapter 3. In that case, fluorination was also found to disrupt the formation of homomolecular monolayers. In principle, F4TPA could self-assemble via $\mathrm{R}_2^2(8)$ hydrogen bonds into the same linear chains observed with IPA; however, the weak C−H···O interactions that seem to influence the side-by-side packing of the chains in the case of TPA are no longer possible with F4TPA. The absence of these weak interactions may be a significant factor in the absence of any homomolecular assembly in the case of F4TPA.

5.3 Bimolecular self-assembly properties of TPA with 4TPTZ

As was discussed in the introduction to this chapter, the coassembly of TPA with 4TPTZ has previously been demonstrated at the heptanoic acid/HOPG interface. By following the procedure outlined by Kampschulte et al., i.e., by depositing mixed solutions prepared by combining equal volumes of

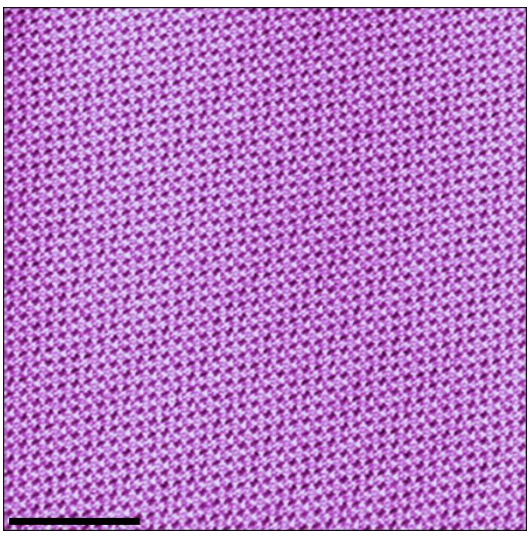

Figure 50: Large-scale STM image showing the coassembly of TPA and 4TPTZ at the heptanoic acid/HOPG interface. Tunnelling parameters: V_{bias} = −1.2 V, I_{set} = 70 pA. Scale bar = 20 nm.

saturated 4TPTZ and saturated TPA solution, these results could be readily reproduced. As is shown in the STM image presented in figure 50, large domains of this ordered bimolecular assembly were observed covering the surface of the sample.

Figure 51a shows an example of a high-resolution STM image showing the coassembly of TPA with 4TPTZ. Within such images, both the tripodal 4TPTZ molecules and the individual TPA molecules can be clearly resolved. The two molecules coassemble into an ordered rectangular network. Each TPA molecule is positioned such that it can bridge two 4TPTZ molecules via strong O−H···N(pyridyl) hydrogen bonds. Only one of the pyridyl nitrogen atoms in each 4TPTZ molecule partakes in these interactions. In addition to the O−H···N(pyridyl) hydrogen bonds, there is also likely a stabilising contribution from secondary C−H···O and C−H···N(pyridyl) interactions. Figure 51b shows the proposed model for the assembly. Although the network of F4TPA and 4TPTZ molecules appears to be porous, the presence of coadsorbed solvent molecules within these pores cannot be ruled out.

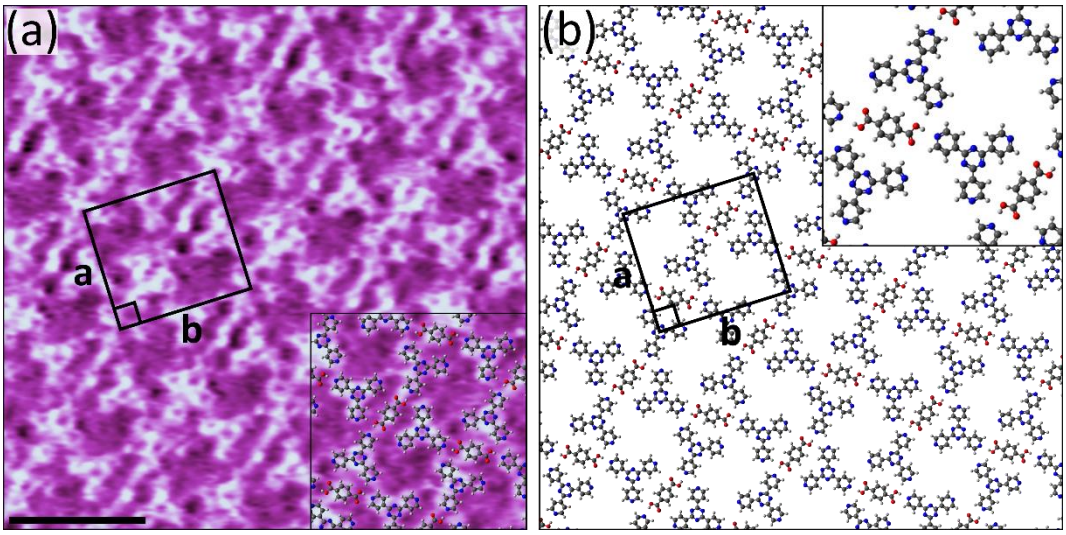

Figure 51: (a) STM image showing the coassembly of TPA and 4TPTZ at the heptanoic acid/HOPG interface. Tunnelling parameters: V_{bias} = −1.2 V, I_{set} = 50 pA. Unit cell parameters: a = 2.7 ± 0.1 nm, b = 3.0 ± 0.1 nm, angle = 90 ± 3°. Scale bar = 3 nm. **(b)** Proposed model for the assembly.

5.4 Bimolecular self-assembly properties of F4TPA with 4TPTZ

As was the case with TPA, F4TPA was also observed to coassemble with 4TPTZ at the heptanoic acid/HOPG interface. Figure 52 shows a large-scale STM image of this bimolecular assembly. The mixed solutions used to prepare this bimolecular network were prepared by combining saturated F4TPA solution with saturated 4TPTZ solution in a ratio of 1:9. Note that the precipitation of what were presumably cocrystals/salt was observed to occur shortly after mixing the two solutions, which hints at the strong affinity that these two molecules have for interacting with one another. The solution that was deposited onto the HOPG substrate was decanted from this precipitate.

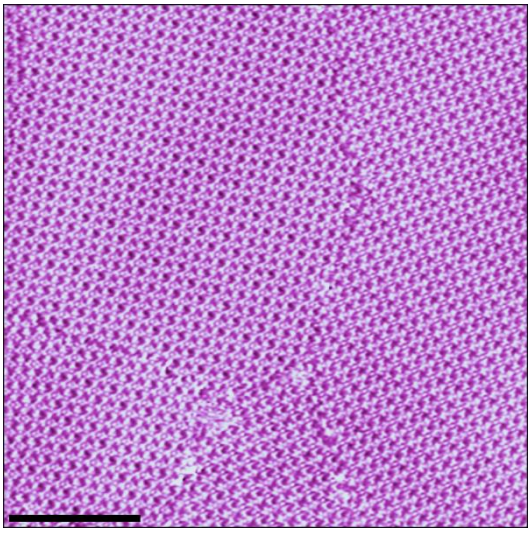

Figure 52: Large-scale STM image showing the coassembly of F4TPA and 4TPTZ at the heptanoic acid/HOPG interface. Tunnelling parameters: V_{bias} = −1.1 V, I_{set} = 70 pA. Scale bar = 20 nm.

Interestingly, the coassembly of F4TPA with 4TPTZ has a rectangular unit cell with lattice parameters that exactly match those observed for the coassembly of TPA with 4TPTZ. Furthermore, high-resolution STM images of the assembly in which both the 4TPTZ and F4TPA molecules can be resolved (see figure 53a), clearly reveal that the two assemblies are isostructural (compare figures 53 and 51). The F4TPA molecules bridge two 4TPTZ molecules via O−H···N(pyridyl) hydrogen bonds in the same manner that was observed with TPA. The same secondary C−H···O and C−H···N(pyridyl) interactions that may stabilise the coassembly of TPA with 4TPTZ are likely also present with F4TPA. Additionally, with F4TPA there may be an extra stabilising contribution from weak C−H···F interactions. The fact that isostructural networks can be formed with both TPA and F4TPA highlights the minimal steric

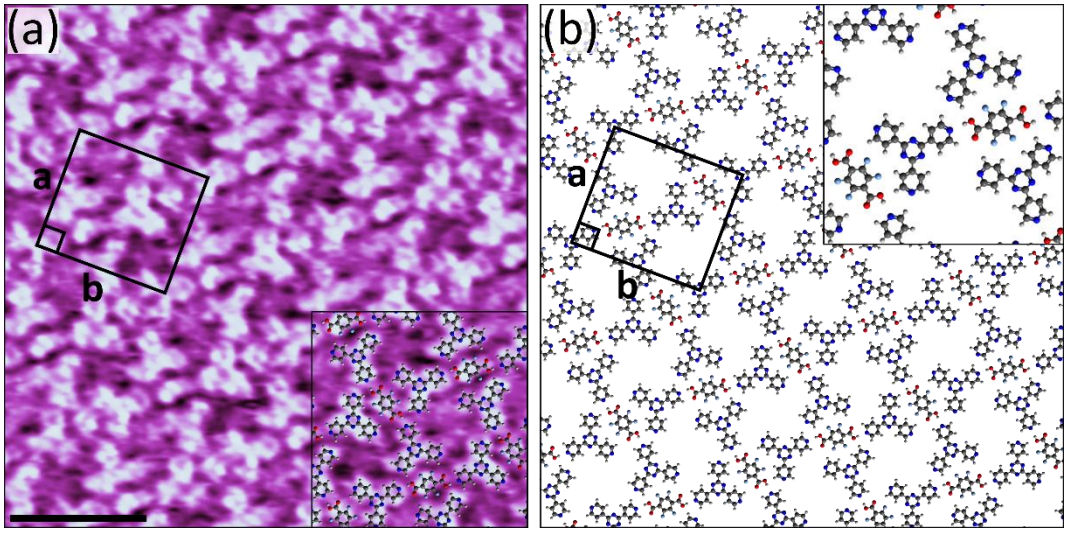

Figure 53: (a) STM image showing the coassembly of F4TPA and 4TPTZ at the heptanoic acid/HOPG interface. Tunnelling parameters: V_{bias} = −1.2 V, I_{set} = 80 pA. Unit cell parameters: a = 2.7 ± 0.1 nm, b = 3.0 ± 0.1 nm, angle = 90 ± 3°. Scale bar = 3 nm. **(b)** Proposed model for the assembly.

impact that exchanging hydrogen atoms for fluorine atoms has. This is consistent with the results presented in chapter 3, where both IPA and its fluorinated analogue F4IPA were observed to assemble into isostructural cyclic hexameric arrangements in the presence of coronene.

5.5 Bimolecular self-assembly properties of TPA with 3TPTZ

Unlike 4TPTZ, 3TPTZ was not observed to coassemble with TPA at the heptanoic acid/HOPG interface. Solutions with a range of different compositions were tested as the formation of a bimolecular structure could depend on the concentrations of the two components. Initially, solutions in which the concentration of TPA was saturated and the concentration of 3TPTZ was 10^{-2} M were deposited and the interface between these solutions and the HOPG surface were surveyed via STM. All that could be observed covering the sample's surface was the hexagonal assembly of 3TPTZ discussed in section 4.4. The concentration of 3TPTZ in the deposited solution was then gradually reduced until the homomolecular assembly of TPA (see section 5.1) could be observed covering the surface. The only ordered assemblies that were observed over the range of tested solution compositions were those formed when only 3TPTZ or TPA are dissolved in solution. No evidence for the formation of any bimolecular structure was ever observed. The observations made with each of the tested solution

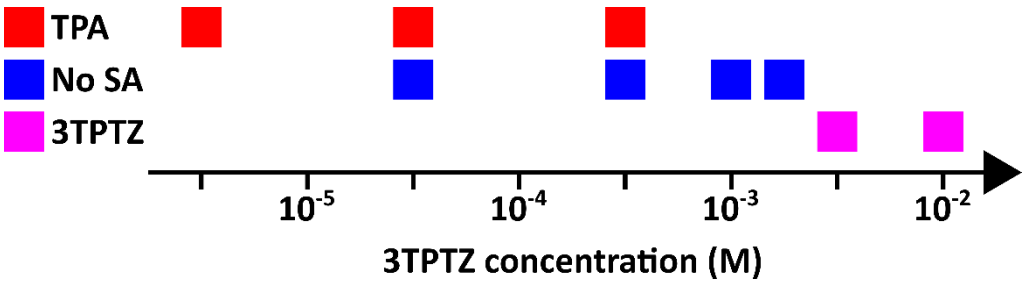

Figure 54: Profile summarising the different observations made at the heptanoic acid/HOPG interface as the concentration of 3TPTZ is adjusted in a saturated solution of TPA. Red squares indicate that the homomolecular assembly of TPA (see section 5.1) was observed, pink squares indicate that the hexagonal assembly of 3TPTZ (see section 4.4) was observed and blue squares indicate that no assembly could be observed. A description of what was observed at each concentration is given below.

- **10^{-2} – 5 × 10^{-3} M:** The hexagonal assembly of pure 3TPTZ could be observed covering essentially the entire surface of the sample.
- **2.5 × 10^{-3} – 10^{-3} M:** No assembly could be observed on the surface of the sample.
- **5 × 10^{-4} M:** There was no assembly present on the vast majority of the surface, but occasional isolated domains of the homomolecular assembly of TPA could be encountered.
- **5 × 10^{-5} M:** The homomolecular assembly of TPA could be observed covering most of the surface of the sample, but occasional regions in which no self-assembly could be observed were also present.
- **5 × 10^{-6} M:** The homomolecular assembly of TPA could be observed covering essentially the entire surface of the sample.

compositions are summarised in figure 54. Each point in the figure is the result of analysing at least five ~0.5 μm^2 regions of a freshly prepared sample's surface.

Although TPA and 3TPTZ were not observed to coassemble at the heptanoic acid/HOPG interface, the two molecules do appear to influence on another's self-assembly behaviour somewhat. In the absence of TPA, 3TPTZ is observed to self-assemble into the expected hexagonal assembly at a concentration of 2.5×10^{-3} M (see section 4.4); however, at the same 3TPTZ concentration in a solution containing a saturated concentration of TPA, the formation of the hexagonal assembly is no longer observed. This indicates that the presence of TPA in the solution disrupts the homomolecular self-assembly of 3TPTZ. Furthermore, as the concentration of TPA is saturated its homomolecular self-assembly should be expected to cover the surface at concentrations where the hexagonal assembly of 3TPTZ is not observed; however, at 3TPTZ concentrations of $2.5 \times 10^{-3} - 5 \times 10^{-5}$ M the homomolecular self-assembly of TPA is either not observed or the extent to which it covers the surface is reduced. This indicates that the presence of 3TPTZ disrupts the homomolecular self-assembly of TPA.

5.6 Bimolecular self-assembly properties of F4TPA with 3TPTZ

Contrastingly to the situation with TPA, F4TPA was observed to readily coassemble with 3TPTZ at the heptanoic/HOPG interface (see figure 55). The binary solutions used to form the observed coassembly were prepared by mixing saturated F4TPA solution with 10^{-2} M 3TPTZ solution in a ratio of 1:9. As was the case with 4TPTZ, precipitation of cocrystals/salt was observed to occur quickly after mixing the two solutions. The solution that was deposited onto the HOPG surface was decanted from this precipitate.

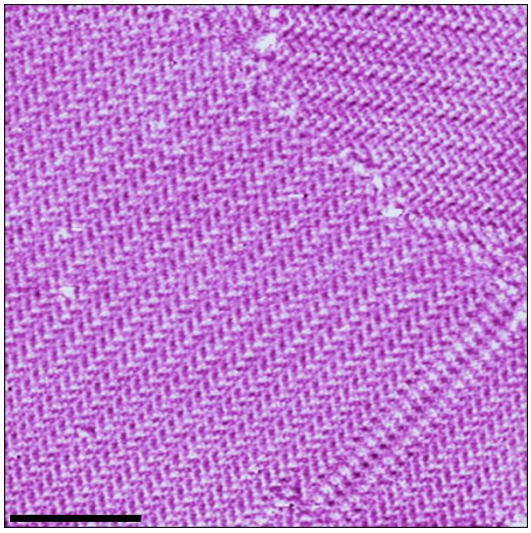

Figure 55: Large-scale STM image showing the coassembly of F4TPA and 3TPTZ at the heptanoic acid/HOPG interface. Tunnelling parameters: V_{bias} = −1.2 V, I_{set} = 100 pA. Scale bar = 20 nm.

Within high-resolution STM images of the assembly, such as figure 56a, the individual 3TPTZ molecules and F4TPA molecules can be clearly resolved. Each F4TPA molecule appears to bridge two 3TPTZ molecules via O−H···N(pyridyl) hydrogen bonds. Each 3TPTZ molecule interacts with two F4TPA molecules via these interactions. Note that in order to maximise the number of favourable hydrogen bonds, the 3TPTZ molecules are required to be in their non-threefold-symmetric conformation (see section 4.1). In addition to the O−H···N(pyridyl) hydrogen bonds, there may also be some stabilising contribution from weak C−H···N(pyridyl), C−H···O and C−H···F interactions.

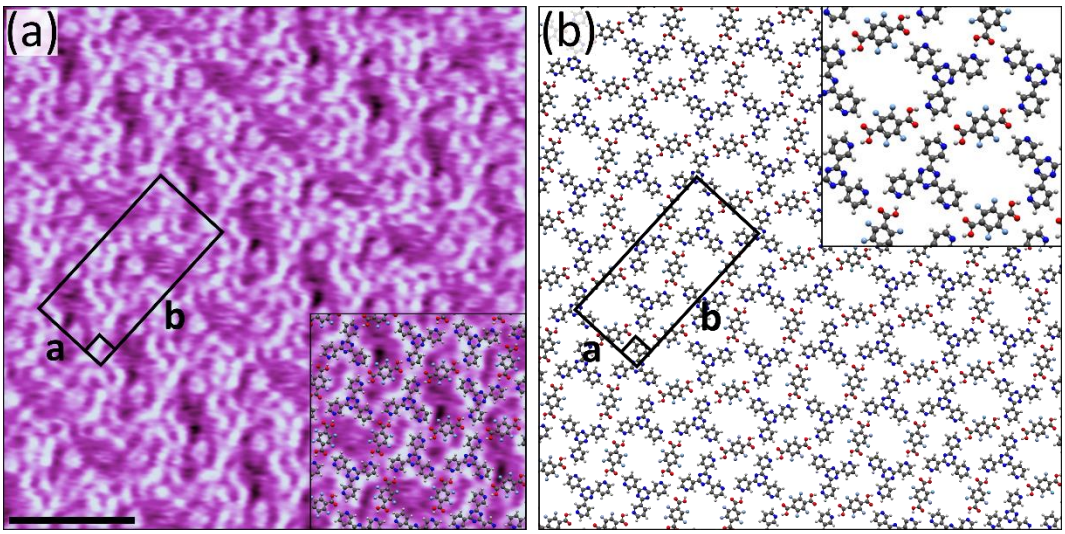

Figure 56: (a) STM image showing the coassembly of F4TPA and 3TPTZ at the heptanoic acid/HOPG interface. Tunnelling parameters: V_{bias} = −1.2 V, I_{set} = 50 pA. Unit cell parameters: a = 2.0 ± 0.1 nm, b = 4.3 ± 0.1 nm, angle = 90 ± 3°. Scale bar = 3 nm. **(b)** Proposed model for the assembly.

5.7 Bimolecular self-assembly properties of TPA with 2TPTZ

As was the case with 3TPTZ, TPA was also found to be an ineffective building block for the formation of bimolecular monolayers when paired with 2TPTZ. Experiments were conducted in exactly the same manner as those used to explore the potential coassembly of TPA with 3TPTZ. Irrespectively of the composition of the deposited solution, the only self-assembled structures that could be observed on the surface were the hexagonal assembly observed when only 2TPTZ is dissolved in solution (see section 4.5) and the homomolecular assembly observed when only TPA is present (see section 5.1). The results obtained for the range of tested solution compositions are summarised in figure 57.

As expected, at relatively high concentrations of 2TPTZ the hexagonal assembly observed when only it is present is observed. Whereas at high relative concentrations of TPA, its homomolecular assembly dominates the surface. The most significant observations were made when the concentration of 2TPTZ in the saturated solution of TPA was 2.5×10^{-4} M. At this concentration, both the homomolecular self-

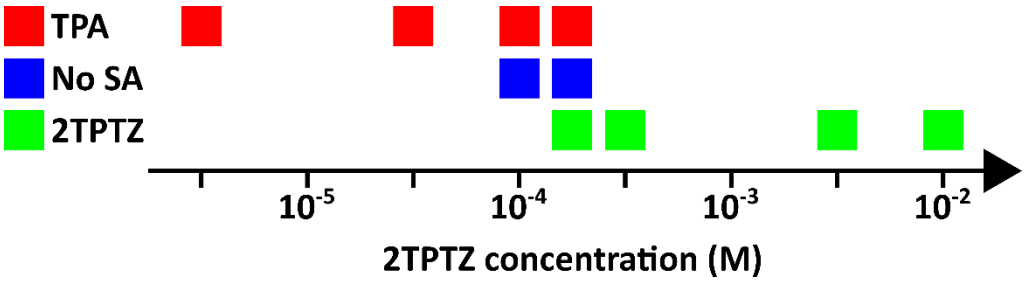

Figure 57: Profile summarising the different observations made at the heptanoic acid/HOPG interface as the concentration of 2TPTZ is adjusted in a saturated solution of TPA. Red squares indicate that the homomolecular assembly of TPA (see section 5.1) was observed, green squares indicate that the hexagonal assembly of 2TPTZ (see section 4.5) was observed and blue squares indicate that no assembly could be observed. A description of what was observed at each concentration is given below.

- **10^{-2} – 5 × 10^{-4} M:** The hexagonal assembly of pure 2TPTZ could be observed covering essentially the entire surface of the sample.
- **2.5 × 10^{-4} M:** Both the homomolecular assembly of TPA and the hexagonal assembly of 2TPTZ were observed coexisting on the surface. Immediately after depositing, assembly was not present on an appreciable amount of the surface, but over the course of a few hours the assemblies of TPA and 2TPTZ began to dominate.
- **10^{-4} M:** Large domains of the pure TPA assembly could be frequently encountered, but assembly was absent from much of the surface.
- **5 × 10^{-5} – 5 × 10^{-6} M:** The homomolecular assembly of TPA could be observed covering essentially the entire surface of the sample.

assembly of TPA and the hexagonal assembly corresponding to 2TPTZ could be observed coexisting on the surface. In most cases, domains of these two structures were separated on the surface by steps or defects in the surface. Instances where domains of the two structures were observed directly interfacing with one another were also observed (see figure 58). The fact that phase-separated

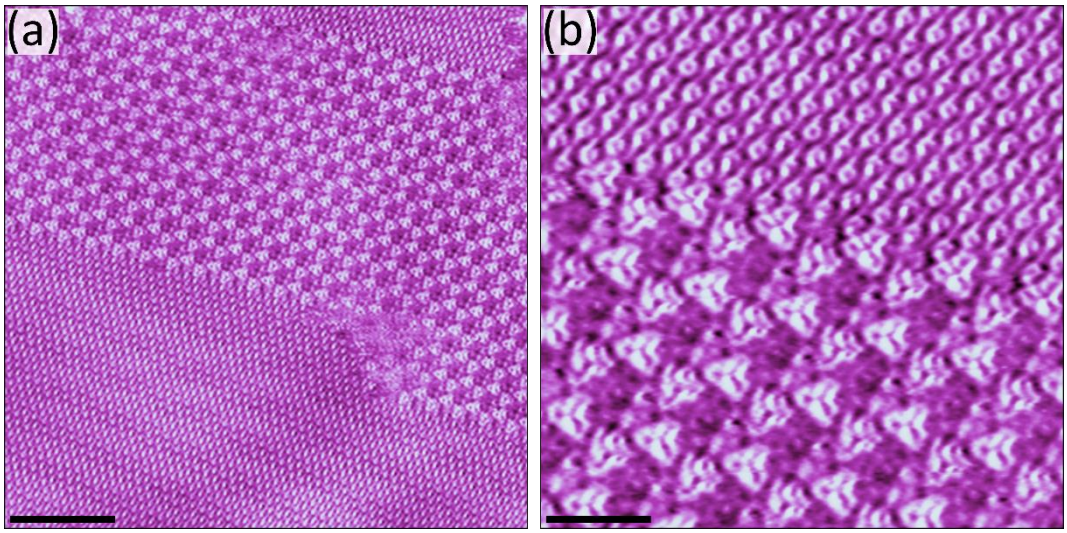

Figure 58: (a) Large-scale STM image showing phase-separated domains of the assembly of 2TPTZ and the assembly of TPA at the heptanoic acid/HOPG interface. Scale bar = 10 nm. **(b)** STM image showing the interface between phase-separated domains. Scale bar = 3 nm. Tunnelling parameters for both images: V_{bias} = −0.9 V, I_{set} = 50 pA.

domains of TPA and 2TPTZ could be observed on the surface is strong evidence that these two molecules are not inclined towards coassembly.

5.8 Bimolecular self-assembly properties of F4TPA with 2TPTZ

Unlike with TPA, the fluorinated analogue F4TPA was found to be an effective building block for the formation of bimolecular networks when paired with 2TPTZ. A large-scale STM image showing the coassembly of F4TPA with 2TPTZ at the heptanoic acid/HOPG interface is shown in figure 59. The solutions used to prepare the bimolecular assembly of F4TPA and 2TPTZ were prepared in an identical manner to those used to prepare the bimolecular network of F4TPA and 3TPTZ discussed in the previous section.

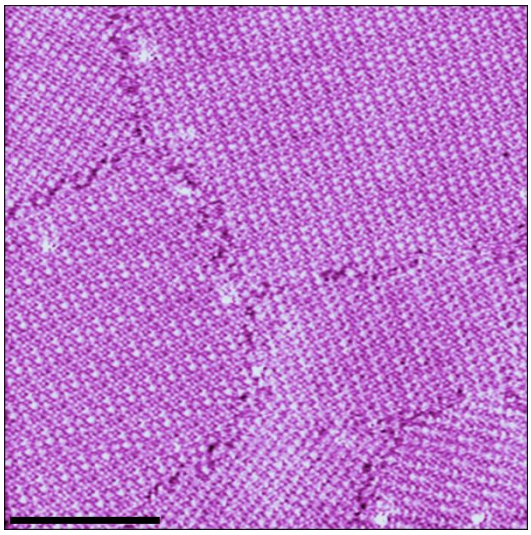

Figure 59: Large-scale STM image showing the coassembly of F4TPA and 2TPTZ at the heptanoic acid/HOPG interface. Tunnelling parameters: V_{bias} = −0.9 V, I_{set} = 50 pA. Scale bar = 20 nm.

Figure 60a shows an example of a high-resolution STM image of the coassembly of 2TPTZ with F4TPA. The 2TPTZ molecules are organised into rows in which the molecules are aligned and orientated in the same direction. These rows are then positioned side-by-side on the surface. Adjacent rows are orientated in an antiparallel fashion. The F4TPA molecules are positioned between the rows such that they can bridge two 2TPTZ molecules in adjacent rows via O−H···N(pyridyl) hydrogen bonds. Each 2TPTZ molecule interacts with two F4TPA molecules in this manner. The proposed model for the assembly is given in figure 60b. In addition to the O−H···N(pyridyl) hydrogen bonds, the F4TPA molecules are also positioned such that they can interact with neighbouring 2TPTZ molecules via auxiliary C−H···O and C−H···F interactions. It should also be noted that this assembly is typically resolved with a characteristic linear moiré pattern. This effect appears as a periodic modulation in

contrast occurring every four lattice spacings along the direction of the short lattice vector (a in figure 60). This effect can be clearly seen in both figures 59 and 60.

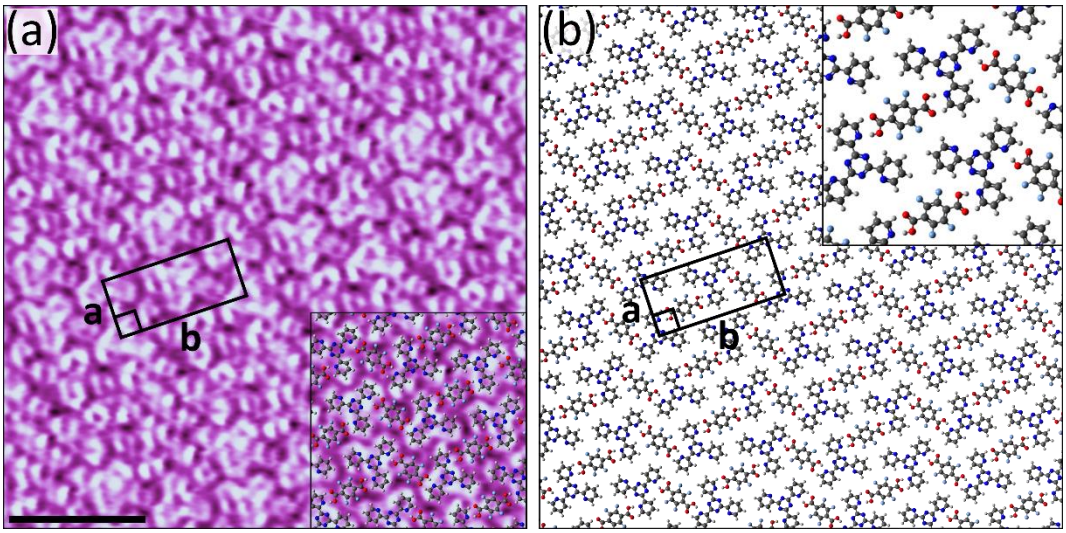

Figure 60: (a) STM image showing the coassembly of F4TPA and 2TPTZ at the heptanoic acid/HOPG interface. Tunnelling parameters: V_{bias} = −1.1 V, I_{set} = 60 pA. Unit cell parameters: a = 1.3 ± 0.1 nm, b = 2.9 ± 0.1 nm, angle = 90 ± 3°. Scale bar = 3 nm. **(b)** Proposed model for the assembly.

5.9 Further discussion

Of the three tripyridyltriazine isomers, only 4TPTZ was observed to coassemble with TPA whilst all three coassemble with its fluorinated analogue, F4TPA. This clearly demonstrates that F4TPA is the superior building block in these bimolecular systems. However, understanding why the fluorinated analogue has such markedly improved performance remains challenging. Both TPA and F4TPA were observed to have comparable solubilities in heptanoic acid. Additionally, the difference in the adsorption energy of these two similarly sized small molecules is expected to be minimal. Therefore, these two factors likely do not significantly contribute to the improved performance of F4TPA. The most obvious difference between the two molecules appears to be the intermolecular interactions in which they partake. The electron withdrawing influence of the fluorine atoms in F4TPA may allow it to form stronger hydrogen bonds with the acceptors when compared with TPA. Additionally, all of the bimolecular systems formed with F4TPA appear to involve stabilising C−H···F interactions between the F4TPA molecules and the tripyridyltriazine isomers. Although these interactions are typically quite weak, they have previously been shown to play a significant stabilising role in other monolayer systems (see section 1.6). The presence of these interactions is clearly not possible with the unfluorinated analogue, TPA. The potentially increased O−H···N(pyridyl) hydrogen bond strength and additional C−H···F interactions which fluorination facilitates may both play a role in the elevated efficacy of F4TPA; however, the relative significance of these factors is not clear.

An additional factor which has not yet been discussed is the potential significance of proton transfer from the carboxylic acid building blocks to the tripyridyltriazine isomers. The interaction between the carboxyl groups of TPA/F4TPA and the pyridyl nitrogen atoms of the tripyridyltriazine isomers have hitherto been considered as simple O–H···N(pyridyl) hydrogen bonds. However, it is also possible that the interaction is actually a salt-bridge in which complete proton transfer from the carboxyl group to the pyridyl nitrogen atom has occurred. The two potential forms of the carboxyl–pyridine interaction are shown in figure 61. In addition to a hydrogen bonding interaction, the salt-bridge interaction is also stabilised by an ionic component. Proton transfer in analogous 3D systems has been extensively explored.[156] In such studies, the difference in the pKa of the carboxylic acid and the conjugate acid of the pyridine base has been shown to be a clear predictor of proton transfer, with the larger the difference in the pKa between the two species increasing the likelihood of proton transfer. Fluorination is well known to reduce the pKa of carboxylic acids, and therefore the pKa values for F4TPA are likely significantly lower than those of TPA. As a result, proton transfer, and therefore formation of the salt-bridge interaction, seems to be much more likely with F4TPA than TPA.

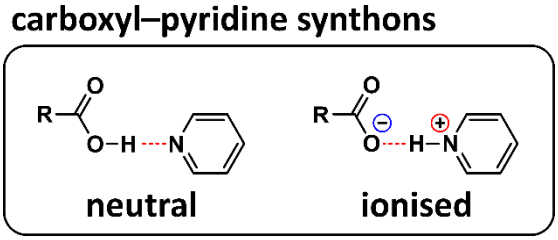

Figure 61: Schematic showing both the neutral and ionised forms of the interaction between a carboxyl group and a pyridyl group. The hydrogen bonds are represented by red dashed lines.

5.10 Conclusions

In conclusion, it has been clearly demonstrated that fluorination can significantly modify the surface-confined self-assembly behaviour of carboxylic acids. Although peripheral fluorination seemingly disrupts the homomolecular self-assembly of F4TPA, it was found to be highly advantageous for the construction of bicomponent carboxylic acid–pyridine networks. Whilst the unfluorinated analogue TPA was only found to coassemble with one of the three tested acceptors, F4TPA was found to do so with all three. These results present a clear strategy towards the reliable formation of these complex, bicomponent architectures.

Chapter 6: Fluorination as a route to the formation of 2D phenol–pyridine cocrystals

As has been extensively discussed in chapters 3 and 5, carboxylic acids are the most frequently explored building blocks for the formation of hydrogen-bond-controlled self-assembled monolayers. Despite their ability to engage in comparable hydrogen bonding interactions, other compounds containing hydroxyl groups, such as phenols, have been comparatively little studied in the context of surface-confined supramolecular chemistry. Furthermore, the studies that have been undertaken primarily focus on simple homomolecular systems in which straightforward O–H···O hydrogen bonds between the hydroxyl groups of adjacent molecules controls their supramolecular organisation.[157–162] Phenolic compounds can be effective hydrogen bond donors, and in principle bimolecular phenol–pyridine networks, analogous to the carboxylic acid–pyridine networks discussed in chapter 5, could be constructed. Although 3D phenol–pyridine cocrystals are routinely observed, their 2D analogues have not been reported.

Within the field of 3D crystal engineering, it has previously been demonstrated that the O–H···N(pyridyl) synthon with carboxylic acids is favoured over that formed with phenolic compounds.[163] Assuming that this trend carries over from 3D crystals to monolayer systems, and given that the unfluorinated carboxylic acid TPA was only found to be a mildly effective building block when paired the three tripyridyltriazine isomers in chapter 5, it is unlikely that a phenolic analogue would have reliable efficacy. Furthermore, when such monolayers are constructed at the solid–liquid interface using commonly employed carboxylic acid solvents, the solvent molecules may outcompete phenolic building blocks for N(pyridyl) hydrogen bond acceptor sites. These considerations indicate that the formation of phenol–pyridine monolayers may be particularly challenging. However, the results presented in chapter 5 highlight a possible strategy towards the reliable formation of such networks: fluorination. Fluorinated phenolic compounds have previously been shown to act as particularly effective hydrogen bond donors when coupled with pyridine-based hydrogen bond acceptors.[164–166] This property could give fluorinated phenols increased efficacy for the construction of phenol–pyridine bimolecular monolayers. Furthermore, the presence of fluorine atoms introduces the potential for additional interactions directly involving the fluorine atoms. These additional interactions may also assist in stabilising the formation of self-assembled monolayers.

With these ideas in mind, the comparative abilities of a simple diphenol and its fluorinated analogue to act as building blocks for the formation of 2D phenol–pyridine cocrystals was investigated. The two diphenols that were investigated are hydroquinone (HQ, figure 62) and tetrafluorohydroquinone (TFHQ, figure 62). These two molecules were coupled with the molecules 2TPTZ, 3TPTZ and 4TPTZ,

i.e., the three tripyridyltriazine isomers discussed in chapter 4, and the outcomes of these combinations were studied at the heptanoic acid/HOPG interface using STM operating under ambient conditions.

Figure 62: Molecular structures of hydroquinone (HQ) and tetrafluorohydroquinone (TFHQ).

6.1 Homomolecular self-assembly properties of TFHQ and HQ

Although it is not the focus of this chapter, the homomolecular self-assembly of both TFHQ and HQ was investigated at the heptanoic acid/HOPG interface. Experiments over a range of different concentrations were not performed; however, saturated solutions of both compounds were tested. In both cases, neither molecule was observed to self-assemble at the heptanoic acid/HOPG interface.

6.2 Bimolecular self-assembly properties of TFHQ with 4TPTZ

STM imaging reveals that the deposition of a solution containing both 4TPTZ and TFHQ does lead to the formation of an ordered multicomponent structure at the heptanoic acid/HOPG interface (see figure 63). The solutions used to form the assembly were prepared by combining equal volumes of saturated 4TPTZ solution and 10^{-2} M TFHQ solution. Soon after mixing the two solutions, cocrystals/salt of TFHQ and 4TPTZ were observed to precipitate from solution. The solution that was deposited onto the HOPG surface was decanted from this precipitate. Precipitation could be avoided by reducing the concentration of both components in solution. These more dilute solutions were prepared by combining equal volumes of 10^{-3} M solutions of each of the components. The observations made at the heptanoic acid/HOPG interface when using these more dilute solutions were identical to those made when using the more concentrated solution decanted from the precipitate.

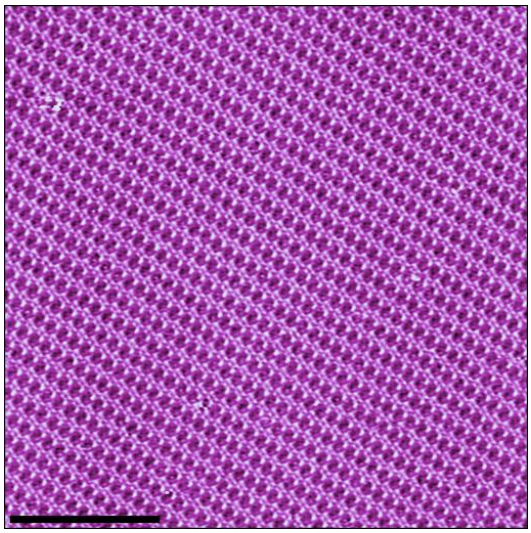

Figure 63: Large-scale STM image showing the coassembly of TFHQ and 4TPTZ at the heptanoic acid/HOPG interface. Tunnelling parameters: V_{bias} = −0.9 V, I_{set} = 100 pA. Scale bar = 20 nm.

Figure 64a shows an example of a high-resolution STM image of the coassembly of TFHQ with 4TPTZ. The 4TPTZ molecules can be clearly resolved as distinct tripodal structures, and the TFHQ molecules appear as approximately circular protrusions. The TFHQ molecules are positioned at the apex of the

tripodal legs of the 4TPTZ molecules such that they can interact with them via O−H···N(pyridyl) hydrogen bonds. The TFHQ molecules bridge two 4TPTZ molecules via these interactions. Two of the three pyridyl nitrogen atoms within each 4TPTZ molecule partake in these interactions. The remaining pyridyl groups are orientated towards what appear to be pores within the assembly. However, were these pores truly unoccupied, the assembly would be extremely loosely packed. Rather, it is expected that coadsorbed heptanoic acid molecules are present within these apparent pores. The proposed model for the assembly, including the coadsorbed heptanoic acid molecules, is shown in figure 64b. As can be seen in this model, the heptanoic acid molecules can be readily incorporated into the apparent pores within the assembly such that they can interact with the free pyridyl nitrogen atoms of the 4TPTZ molecules via favourable O−H···N(pyridyl) hydrogen bonds. These interactions and the additional adsorption energy that the heptanoic acid molecules provide likely makes their presence favourable. Although the solvent molecules cannot be clearly resolved within the STM images, some 'fuzzy' contrast in the regions they occupy can be observed. This is consistent with the coadsorbed heptanoic acid molecules being somewhat mobile and/or loosely bound to the surface. Note that the inability to clearly resolve the heptanoic acid molecules is consistent with numerous previous studies in which the presence of coadsorbed solvent molecules has been proposed.[136–143] In addition to the strong O−H···N(pyridyl) hydrogen bonds between the 4TPTZ and TFHQ/heptanoic acid molecules, there may also be an auxiliary stabilising contribution from weak C−H···O interactions between the same species. Furthermore, it also appears to be likely that weak C−H···F interactions between the 4TPTZ molecules and neighbouring TFHQ molecules are present.

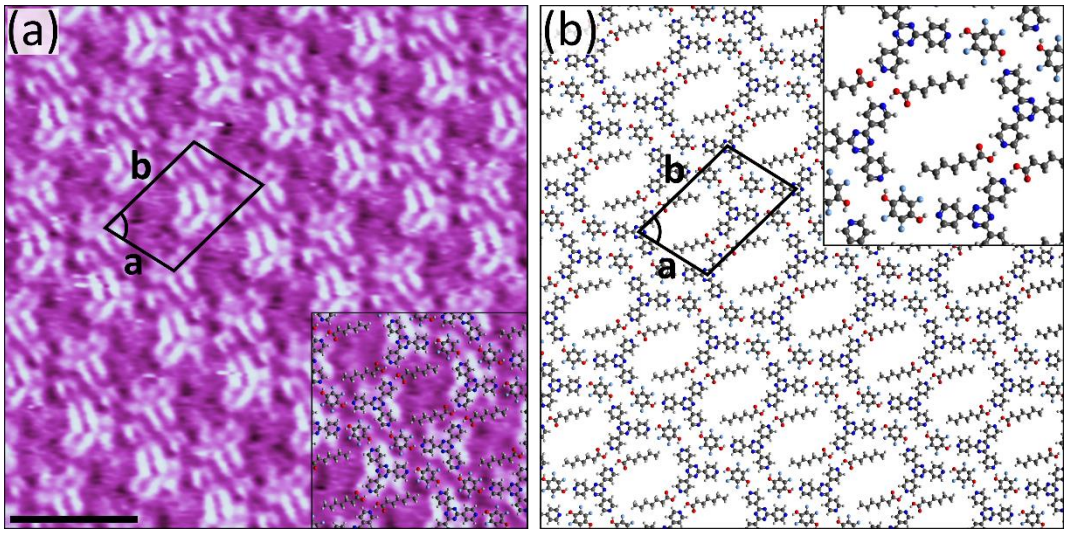

Figure 64: (a) STM image showing the coassembly of TFHQ and 4TPTZ at the heptanoic acid/HOPG interface. Tunnelling parameters: V_{bias} = −1.1 V, I_{set} = 60 pA. Unit cell parameters: a = 1.9 ± 0.1 nm, b = 2.9 ± 0.1 nm, angle = 76 ± 2°. Scale bar = 3 nm. **(b)** Proposed model for the assembly.

6.3 Bimolecular self-assembly properties of HQ with 4TPTZ

Unlike its fluorinated analogue TFHQ, HQ was not observed to coassemble with 4TPTZ at the heptanoic acid/HOPG interface. Initially, solutions prepared by combining saturated 4TPTZ solution with 10^{-2} M HQ solution were tested. Note that this solution composition is similar to that which was successful with TFHQ; however, in the TFHQ case the concentrations of the two components is actually slightly lower due to the precipitation of cocrystals/salt. Unlike with TFHQ, with HQ no precipitation was observed upon combining the two monocomponent solutions, which hints at the interaction between TFHQ and 4TPTZ being stronger than that with HQ. STM imaging did not reveal the formation of any coassembled structures at the heptanoic acid/HOPG interface when using these mixed HQ/4TPTZ solutions. Solutions in which the concentrations of 4TPTZ and HQ were both present at 5×10^{-4} M were also tested as this composition was also successful with TFHQ. Again, with HQ there was no evidence of any assembly on the surface. As is summarised in figure 65, a wide range of different solution compositions were tested. No evidence of any coassembled structure was observed with any of the tested solution compositions.

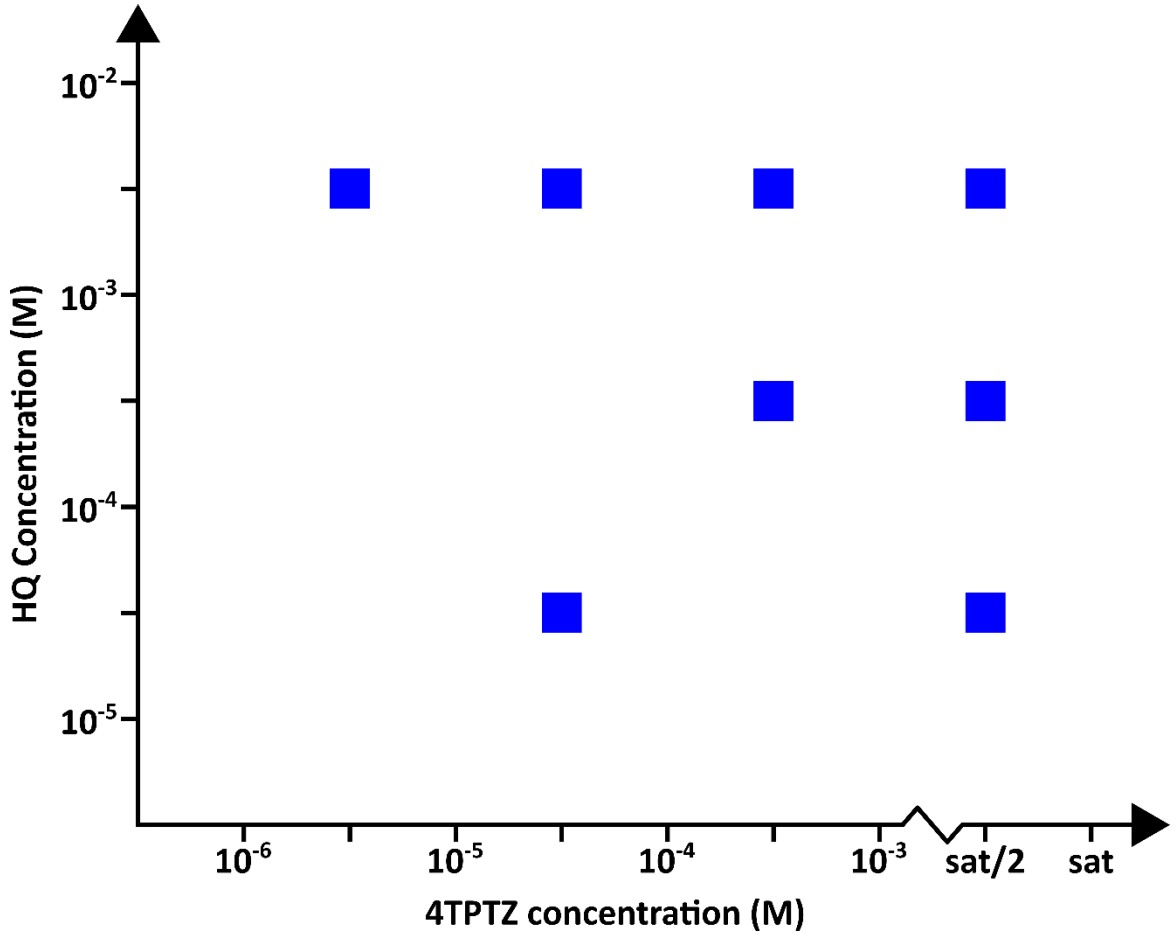

Figure 65: Profile summarising the observations made at the heptanoic acid/HOPG interface for solutions containing both 4TPTZ and HQ at a range of different concentrations. Blue squares indicate that no assembly could be observed.

6.4 Bimolecular self-assembly properties of TFHQ with 3TPTZ

As was the case with 4TPTZ, 3TPTZ was also observed to coassemble with TFHQ. The solutions used were prepared by combining equal volumes of 10^{-2} M 3TPTZ and 10^{-2} M TFHQ solution. As was also the case with 4TPTZ, the precipitation of cocrystals/salt of 3TPTZ and TFHQ was observed to occur after combining the two solutions. However, unlike with 4TPTZ, deposition of the solution decanted from the precipitate only led to the formation of occasional isolated domains of the bimolecular assembly. Fortunately, the precipitation of cocrystals typically did not occur for several hours after preparing the mixed solutions. By depositing freshly prepared solutions, i.e., before any precipitation had occurred, the coassembly of 3TPTZ and TFHQ could be observed covering essentially the entire surface of the sample (see figure 66). This preparation method was adopted as it was much easier to study the coassembly at high coverage. It should be noted that several hours after deposition the assembly was typically observed to disappear from the surface. After this had occurred, either no assembly could be observed on the surface or in some cases the hexagonal assembly observed with just 3TPTZ (see section 4.4) emerged. Additionally, after this had occurred visual inspection of the HOPG surface revealed that bulk 3D cocrystals/salt had precipitated from the deposited solution.

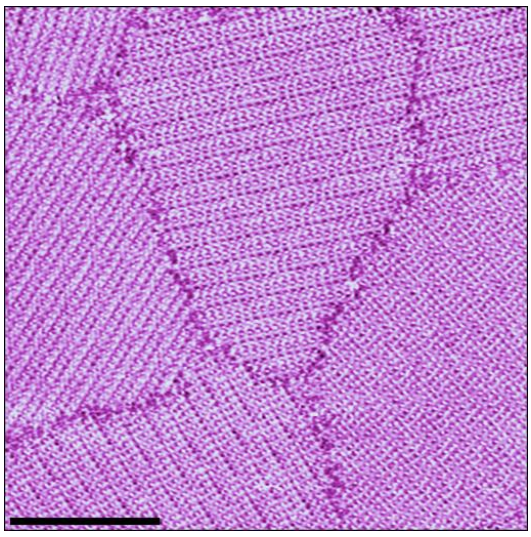

Figure 66: Large-scale STM image showing the coassembly of TFHQ and 3TPTZ at the heptanoic acid/HOPG interface. Tunnelling parameters: V_{bias} = −0.9 V, I_{set} = 50 pA. Scale bar = 20 nm.

High-resolution STM images (see figure 67a) can be used to reveal the details of the assembly. Within such images, both the 3TPTZ and TFHQ molecules can be clearly resolved. The 3TPTZ and TFHQ molecules are arranged on the surface into a densely packed array. The TFHQ molecules are positioned such that they can bridge two 3TPTZ molecules by interacting with them via O–H···N(pyridyl) hydrogen bonds. Figure 67b shows the proposed model for the assembly. Note that the 3TPTZ molecules must be in their non-threefold-symmetric conformation (see section 4.1) to

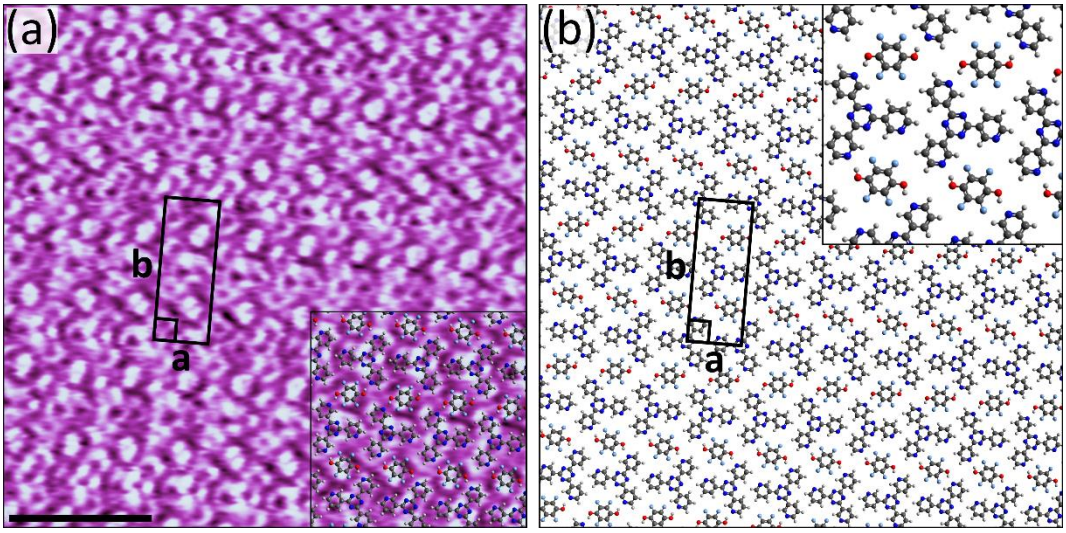

Figure 67: (a) STM image showing the coassembly of TFHQ and 3TPTZ at the heptanoic acid/HOPG interface. Tunnelling parameters: V_{bias} = −0.9 V, I_{set} = 50 pA. Unit cell parameters: a = 1.1 ± 0.1 nm, b = 3.0 ± 0.1 nm, angle = 90 ± 2°. Scale bar = 3 nm. **(b)** Proposed model for the assembly.

maximise the number of favourable O−H···N(pyridyl) hydrogen bonds between them and the TFHQ molecules. In addition to these hydrogen bonding interactions, there may also be a stabilising contribution from weak C−H···F and perhaps C−H···O interactions between the 3TPTZ and TFHQ molecules.

6.5 Bimolecular self-assembly properties of HQ with 3TPTZ

Like its isomer 4TPTZ, 3TPTZ was not observed to coassemble with the unfluorinated analogue HQ. Initially, binary solutions in which the concentrations of both building blocks were 5 × 10^{-3} M were tested. With this solution composition, which is equivalent to the composition that was successful with TFHQ, the hexagonal assembly observed when only 3TPTZ is present (see section 4.4) could be observed covering essentially the entire surface of the sample. Therefore, the concentration of 3TPTZ in the solution was gradually reduced as this is expected to disfavour the formation of the hexagonal assembly and increase the likelihood of coassembly with HQ. However, even when the concentration of 3TPTZ was reduced enough that the hexagonal assembly was no longer observed, the absence of any assembly rather than the coassembly of 3TPTZ with HQ was observed at the heptanoic acid/HOPG interface. These observations are summarised in figure 68. As can be seen by comparison of this figure with the concentration dependence of the self-assembly of 3TPTZ in the absence of HQ (see figure 38, section 4.4), the presence of HQ at a relatively high concentration of 5 × 10^{-3} M appears to have no influence on the self-assembly behaviour of 3TPTZ, i.e., the system simply behaves as if HQ was not present.

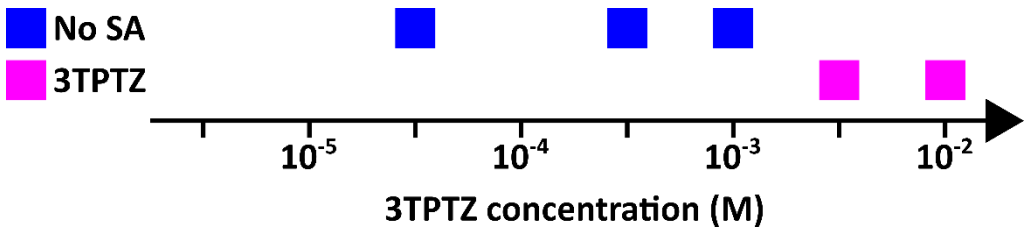

Figure 68: Profile summarising the different observations made at the heptanoic acid/HOPG interface as the concentration of 3TPTZ is adjusted in a solution containing HQ at a concentration of 5×10^{-3} M. Blue squares indicate that no assembly could be observed, and pink squares indicate that the hexagonal assembly of 3TPTZ was observed.

6.6 Bimolecular self-assembly properties of TFHQ/HQ with 2TPTZ

As is discussed later (see section 7.3), the N(pyridyl) atoms of 2TPTZ are sterically inaccessible to the approach of phenolic hydroxyl groups in 2D systems. Accordingly, the formation of 2D networks mediated by O–H···N(pyridyl) hydrogen bonds between TFHQ/HQ and 2TPTZ is not expected to be possible. As such, the potential for the coassembly of TFHQ/HQ with 2TPTZ was not thoroughly explored. However, some preliminary experiments with TFHQ were performed, and the results are consistent with the idea that TFHQ and 2TPTZ do not coassemble. Deposition of mixed solutions in which the concentration of 2TPTZ is 5×10^{-3} M and the concentration of TFHQ is 5×10^{-4} M simply leads to the formation of the hexagonal assembly observed when only 2TPTZ is present (see section 4.5), i.e., the system behaves as if TFHQ was not present. The same observations were made upon reducing the concentration of 2TPTZ to 5×10^{-4} M whilst maintaining the concentration of TFHQ. However, a different result was obtained upon increasing the concentration of TFHQ: deposition of solutions in which the concentration of both TFHQ and 2TPTZ is 5×10^{-3} M does not lead to the formation of any self-assembled structure on the surface. As the assembly corresponding to pure 2TPTZ is expected to be present at this concentration (see figure 42, section 4.5), this indicates that the presence of TFHQ at an elevated concentration disrupts the formation of the hexagonal assembly of 2TPTZ. In no case was any evidence for the coassembly of TFHQ with 2TPTZ observed.

6.7 Further discussion

Whilst TFHQ was observed to coassemble with both 4TPTZ and 3TPTZ, HQ was not observed to coassemble with either of these tripyridyltriazine isomers. These results mirror those presented in chapter 5, where the fluorinated carboxylic acid F4TPA was found to coassemble with all three of the tested tripyridyl triazine isomers, whereas its unfluorinated analogue was only observed to coassemble with one of them. The increased efficacy associated with fluorination in the case of TFHQ

is likely due to similar reasons to those proposed for F4TPA (see section 5.9), i.e., the increased hydrogen bond strength associated with fluorination and additional C−H···F interactions with TFHQ which are not possible with HQ. Calculations on similar phenol–pyridine systems indicate that fluorination increases O−H···N(pyridyl) hydrogen bond strength by ~1.7 kcal/mol, which corresponds to a ~17% increase.[164] Furthermore, DFT calculations on a series of fluorinated azobenzenes have shown that C−H···F interactions have a strength of 0.8–1.0 kcal/mol.[167] In the coassemblies of TFHQ with 4TPTZ and 3TPTZ, each TFHQ molecule is positioned such that it can partake in two O−H···N(pyridyl) hydrogen bonds and multiple C−H···F interactions. The increased hydrogen bond donor strength and additional C−H···F interactions are expected to dramatically increase the net interaction strength between TFHQ and the two acceptors when compared with hypothetical isostructural networks in which TFHQ is exchanged for HQ. This increased net interaction strength may be a significant factor in the improved performance of TFHQ.

Another factor worth considering is the potential for electrochemistry with the molecule HQ. HQ is particularly electrochemically active and is prone to oxidation which converts it to the molecule benzoquinone. Although electrochemistry is not typically considered in conventional ambient STM experiments conducted in insulating solvents, it is possible that the tip and sample could inadvertently act as electrodes at which redox reactions may occur. Such an effect has previously been suggested to occur with a manganese porphyrin under conditions which are extremely similar to those employed here.[168] The oxidation of HQ to benzoquinone could explain why bimolecular networks are not observed with HQ. Note that benzoquinone has ketone groups in place of the hydroxyl groups in HQ and therefore cannot hydrogen bond to either 3TPTZ or 4TPTZ. Also note that the strongly electronegative fluorine atoms of TFHQ should make it much more stable to oxidation than HQ. As such, it may be possible that the increase in resistance to oxidation may be the reason for the apparent improved performance as TFHQ as a hydrogen bond donor, rather than the impact of fluorination on the intermolecular interactions involved in the assembly of the network. However, such a hypothesis seems to be very unlikely to be correct. Firstly, even in the initial stages of imaging no evidence of any bimolecular assembly was observed for any of the solution compositions containing HQ and 3TPTZ/4TPTZ. Were this to be due to the oxidation of HQ depleting its concentration in solution, this oxidation would have to occur at an extreme rate to reduce its concentration sufficiently that no evidence of any bimolecular structure whatsoever could be observed on the surface even immediately after the tip engaged with the surface. Secondly, were such a significant redox process to occur, it is likely that the current generated would likely exceed the typical noise level of the STM measurements, particularly in the initial stages of the experiment, this would interfere with the feedback mechanism and likely result in unstable imaging conditions. Such an effect was not observed.

As was the case with F4TPA (see section 5.9), the potential for proton transfer from HQ/TFHQ to the tripyridyltriazine isomers cannot be eliminated. Figure 69 shows both the neutral and ionised forms of the phenol–pyridine hydrogen bonding interaction. These two forms are entirely analogous to those discussed in section 5.9. Although proton transfer with the phenolic building blocks seems much less likely than with the carboxylic acid building blocks due to the lower acidity of phenols, analogous 3D phenol–pyridine salts in which proton transfer occurs have been reported[169]. As fluorination is expected to increase the acidity of TFHQ relative to that of HQ, proton transfer is more likely to occur with TFHQ.

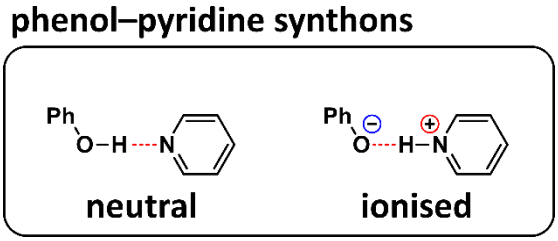

Figure 69: Schematic showing both the neutral and ionised forms of the interaction between a phenol group and a pyridyl group. The hydrogen bonds are represented by red dashed lines.

Another interesting factor which has yet to be discussed is sterics. Within 2D systems, there appears to be particular geometric considerations which may impact upon the formation of O–H···N(pyridyl) hydrogen bonds between phenols and pyridyl groups. Figure 70 shows a schematic illustration of such a hydrogen bond. The phenol and pyridine rings are confined to a coplanar arrangement as both molecules are expected adsorb in this manner within the 2D networks. The optimal geometry for a hydrogen bond typically occurs when the interaction is linear[170,171] and when the position of the partaking hydrogen atom is centred on the projection of the acceptor atom's lone pair[170,172], i.e., when the angles labelled θ_1 and θ_2 in figure 70 both have a value of 180°. Within 3D systems, phenol and pyridyl groups are not typically restricted to coplanar arrangements, and the formation of hydrogen bonds with the optimal linear geometry is possible. However, within 2D systems, such as in hypothetical 2D surface-confined networks formed with HQ and 4TPTZ/3TPTZ, a coplanar arrangement is expected to be enforced by the interaction with the underlying surface. As has previously been studied theoretically,[173] within such an arrangement the optimal linear hydrogen bonding geometry cannot be achieved. This is due to the unfavourable steric interaction between the hydrogen atoms labelled H_a and H_b in figure 70, that would occur were a phenol and pyridine group to be positioned in the optimal linear hydrogen bonding geometry at a reasonable hydrogen bonding distance. Although hydrogen bonding interactions do have some flexibility, deviation from the ideal linear arrangement is associated with a weakening of these interactions[171,172]. This effect may be a contributing factor as to why 2D phenol–pyridine cocrystals have hitherto not been reported.

The influence of sterics on the interaction between TFHQ and 4TPTZ/3TPTZ is less clear. In TFHQ, the hydrogen atom labelled H_a in figure 70 is replaced by a fluorine atom. In principle, this fluorine atom could interact favourably with the hydrogen atom labelled H_b via a weak C−H···F interaction, which should mitigate some of the steric issues associated with HQ. However, this fluorine atom would still have to be extremely close to H_a for a hydrogen bond with the ideal linear geometry to occur. As such, unfavourable steric interactions between these sites are likely still significant with TFHQ. Although STM data alone certainly cannot be used to obtain precise atomic positions, it is clear that the TFHQ molecules do not interact with the 4TPTZ/3TPTZ molecules with an ideal linear hydrogen bonding geometry in the networks observed here (see figures 64 and 67).

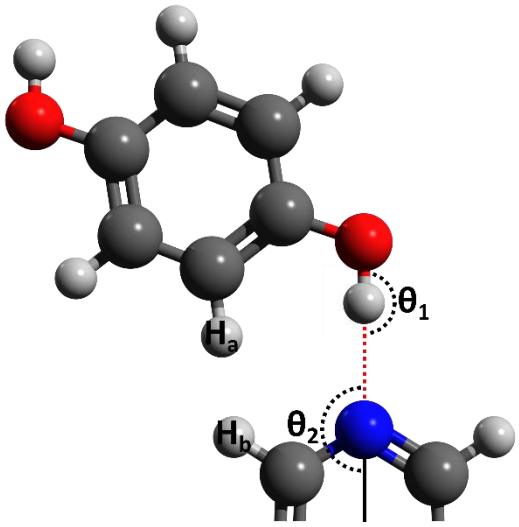

Figure 70: Schematic illustrating the potential O−H···N(pyridyl) hydrogen bond that could occur between HQ and 3TPTZ/4TPTZ when the two molecules are confined to a coplanar arrangement. The hydrogen bond is represented by a red dashed line. The solid black line represents the axis centralised on the projection of the pyridyl nitrogen atom's lone pair of electrons.

6.8 Conclusions

In conclusion, fluorination has been shown to play an essential role in facilitating the coassembly of TFHQ with two pyridine-type acceptors. Although the precise mechanism for this behaviour remains somewhat unclear, the ability of the fluorine atoms to both strengthen the phenol–pyridine hydrogen bonding interactions and to partake in additional stabilising C−H···F interactions are both likely significant. Despite the ubiquity of analogous 3D systems, the formation of 2D surface-confined phenol–pyridine networks has hitherto not been reported. The results presented here demonstrate that fluorination represents a potential route towards the reliable formation of such networks.

Chapter 7: Exploring the interplay between fluorine activated hydrogen bonding synthons in 2D networks

Within most supramolecular systems, the constituent building blocks are theoretically capable of interacting via a range of different intermolecular interactions. Knowledge of which synthons are robust enough to reliably control supramolecular self-assembly is essential for engineering structures with predictable morphologies. Within the field of 3D crystal engineering, significant efforts have been invested into identifying such synthons and establishing hierarchies in their efficacy. Systems in which the molecular building blocks are theoretically capable of interacting via a number of different synthons are of particular interest. In such cases, the different synthons can cooperate such that they synergistically control supramolecular self-assembly or compete such that a limited number of the possible synthons dominate the self-assembly process. Understanding the balance between these cooperative and competitive effects and the factors that influence this balance is essential for the engineering of structures with predictable morphologies. Although the interplay between different synthons has been extensively investigated in the context of 3D crystal engineering, comparable studies on analogous 2D systems have not been reported.

Within the two preceding chapters, it was demonstrated that fluorination provides an effective strategy for increasing the ability of carboxylic acids and phenols to form bimolecular networks when paired with pyridyl functionalised molecules. In both cases, the formation of these bimolecular structures is mediated by similar hydrogen bonding interactions involving hydroxyl and pyridyl groups. The potential structures of the carboxylic acid–pyridine and phenol–pyridine synthons are shown in figure 71. Note that, as was discussed in chapters 5 and 6, there are two possible variations of both synthons: an electrostatically assisted hydrogen bonding interaction in which complete proton transfer from the hydroxyl group to the pyridyl group has occurred and a simple neutral hydrogen bonding synthon in which no proton transfer has occurred. These synthons are routinely utilised in 3D crystal engineering and the balance between them in systems where they are both possible has been extensively explored.[163] As fluorination promotes the interaction between phenolic and carboxylic

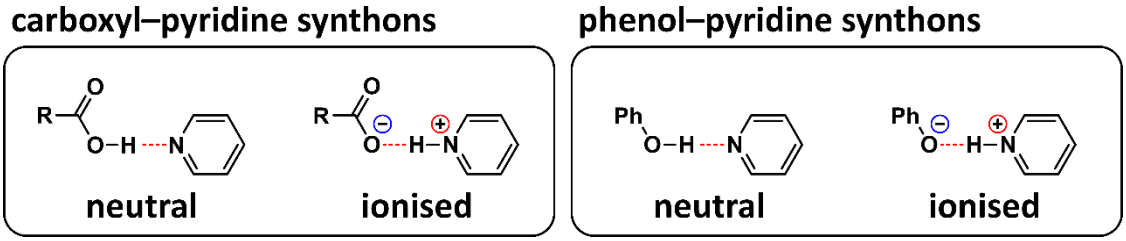

Figure 71: Schematic showing the ionised and neutral forms of the carboxyl–pyridine and phenol–pyridine hydrogen bonding synthons. The hydrogen bonds are represented by red dashed lines.

hydroxyl groups with pyridyl groups in self-assembled monolayers, it provides a unique opportunity to study the interplay between these synthons in 2D systems.

In order to explore these ideas, the coassembly of the molecule 4-hydroxytetrafluorobenzoic acid (4HTFBA, figure 72) with pyridyl functionalised building blocks into self-assembled monolayers at the heptanoic acid/HOPG interface was investigated. As has been the case throughout this thesis, the three tripyridyltriazine isomers discussed in chapter 4 were employed as pyridyl functionalised building blocks. 4HTFBA is a simple aromatic molecule which consists of a perfluorinated aromatic ring functionalised with a hydroxyl group and a carboxyl group positioned para to one another. The bifunctional nature of this molecule means that it can interact with the tripyridyltriazine isomers via its phenolic hydroxyl group and/or its carboxyl group. By exploring the interplay between these two possible interaction modes, the competitive and cooperative balance between them can be investigated in self-assembled monolayers. It should be noted that, as was discussed in chapters 5 and 6, the extent of proton transfer in these two interaction modes, i.e., whether the synthons adopt their ionic or uncharged form (see figure 71), cannot be determined via STM imaging. However, as the ionic and neutral forms typically play the same supramolecular role, differences between them are not considered in this chapter. Only the general nature of the interaction modes is investigated, i.e., if they involve phenolic or carboxylic hydroxyl groups.

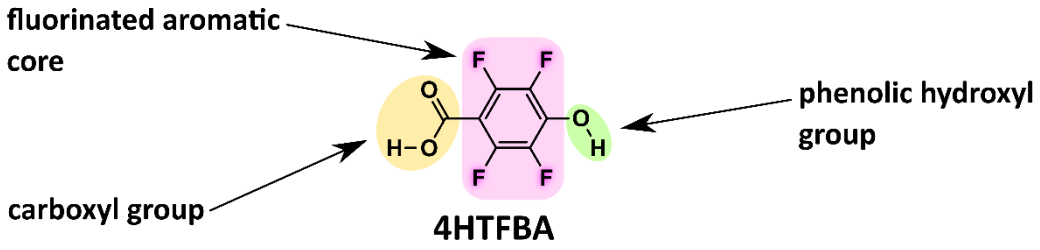

Figure 72: Molecular structure of the bifunctional hydrogen bond donor 4-hydroxytetrafluorobenzoic acid (4HTFBA). The significant structural features are highlighted.

7.1 Homomolecular self-assembly properties of 4HTFBA

Although it is not the focus of this chapter, some efforts to explore the homomolecular self-assembly of 4HTFBA were made. Deposition of 10^{-2} M solutions of 4HTFBA in heptanoic acid did not result in the formation of any self-assembled structures on the surface of the HOPG substrate. Even after increasing the concentration of 4HTFBA to the point of saturation, no evidence of and assembly was observed at the heptanoic acid/HOPG interface.

7.2 Bimolecular self-assembly properties of 4HTFBA with 4TPTZ

Deposition of solutions containing both 4HTFBA and 4TPTZ was observed to result in the formation of bimolecular monolayers at the heptanoic acid/HOPG interface. When the concentration of both components in the solution was 5×10^{-4} M, a distinctive rectangular network was observed covering the surface (see figure 73).

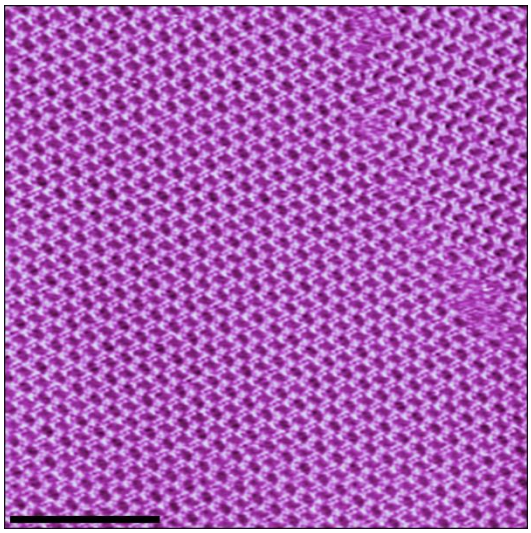

Figure 73: Large-scale STM image showing the rectangular coassembly of 4HTFBA and 4TPTZ at the heptanoic acid/HOPG interface. Tunnelling parameters: V_{bias} = −1.2 V, I_{set} = 50 pA. Scale bar = 20 nm.

Figure 74 shows an example of a high-resolution STM image of the rectangular assembly. Within such images, the individual 4HTFBA and 4TPTZ molecules can be clearly resolved. The 4HTFBA molecules appear as approximately circular protrusions whilst the 4TPTZ molecules are resolved as distinctive tripodal structures. The 4HTFBA molecules are positioned such that they can bridge the pyridyl nitrogen atoms of two 4TPTZ molecules. In order to achieve this, the 4HTFBA molecules must simultaneously hydrogen bond through both their phenolic hydroxyl and carboxyl groups. Figure 74b displays a tentatively proposed model for the assembly. It should be noted that, although the positions of the 4HTFBA molecules can be clearly assigned, the orientation of 4HTFBA molecules cannot be

identified in the STM images. Therefore, it is unclear which of the two pyridyl nitrogen atoms with which each 4HTFBA molecule interacts is orientated towards the phenolic hydroxyl group and which is orientated towards the carboxyl group. The orientation of the 4HTFBA molecules in figure 74b was essentially arbitrarily selected. However, irrespectively of the exact orientation of the 4HTFBA molecules, the significant point in the context of this work is that both the phenol–pyridine and carboxyl–pyridine hydrogen bonding interactions are clearly cooperative in this assembly. In addition to these two strong hydrogen bonding interactions, there is likely also a stabilising contribution from auxiliary C−H···F and C−H···O interactions between neighbouring 4HTFBA and 4TPTZ molecules.

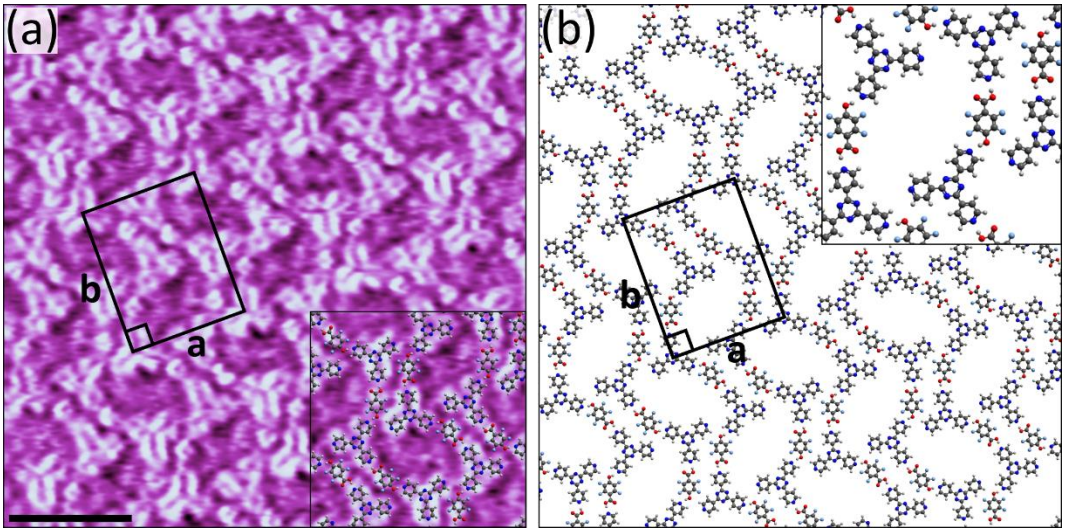

Figure 74: (a) STM image showing the rectangular coassembly of 4HTFBA and 4TPTZ at the heptanoic acid/HOPG interface. Tunnelling parameters: V_{bias} = −1.2 V, I_{set} = 100 pA. Unit cell parameters: a = 2.9 ± 0.1 nm, b = 3.6 ± 0.1 nm, angle = 90 ± 2°. Scale bar = 3 nm. **(b)** Proposed model for the assembly.

The rectangular network of 4HTFBA and 4TPTZ molecules defines a series of what appear to be pores. These pores are certainly large enough to accommodate coadsorbed solvent molecules and this possibility cannot be eliminated. Coronene guest molecules could be readily incorporated into the pores of the rectangular assembly. This was achieved via the following procedure. 10 µL of the solution used to form the rectangular assembly was deposited onto a freshly cleaved HOPG surface. After waiting for approximately five minutes to ensure that the monolayer of the rectangular assembly had fully formed, 2 µL of a 2×10^{-4} M coronene solution was carefully added to the 10 µL droplet on top of the preformed rectangular assembly. Figure 75 shows an example of a large-scale STM image of the surface structure observed following this procedure. Each of the distinctive bright protrusions that can be observed in this image corresponds to a single included coronene molecule. The occupancy of the pores with coronene molecules was observed to be essentially 100%. As is highlighted by the red

arrows in figure 75, pores in which the occupants were particularly bright were occasionally observed. These may correspond to double stacked coronene molecules.

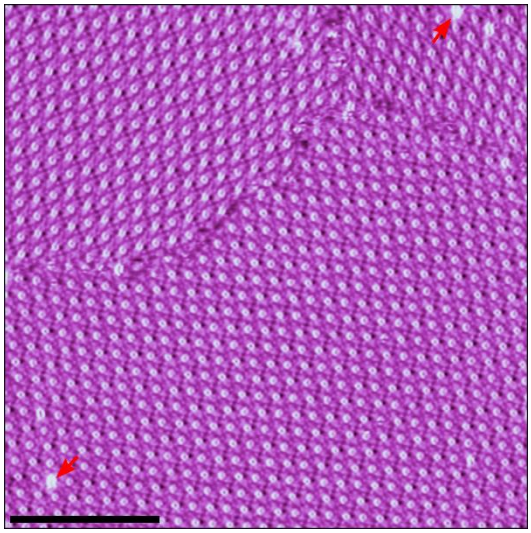

Figure 75: Large-scale STM image showing the rectangular coassembly of 4HTFBA and 4TPTZ at the heptanoic acid/HOPG interface after coronene inclusion. Tunnelling parameters: V_{bias} = −1.2 V, I_{set} = 70 pA. Scale bar = 20 nm.

Figure 76 shows a high-resolution STM image of the coronene-included rectangular assembly within which all three components can be clearly resolved. Not only are the unit cell dimensions of the assembly unperturbed by the inclusion of coronene but such images verify that the arrangement of the 4HTFBA and 4TPTZ molecules is also unaffected. Interestingly, there are technically two

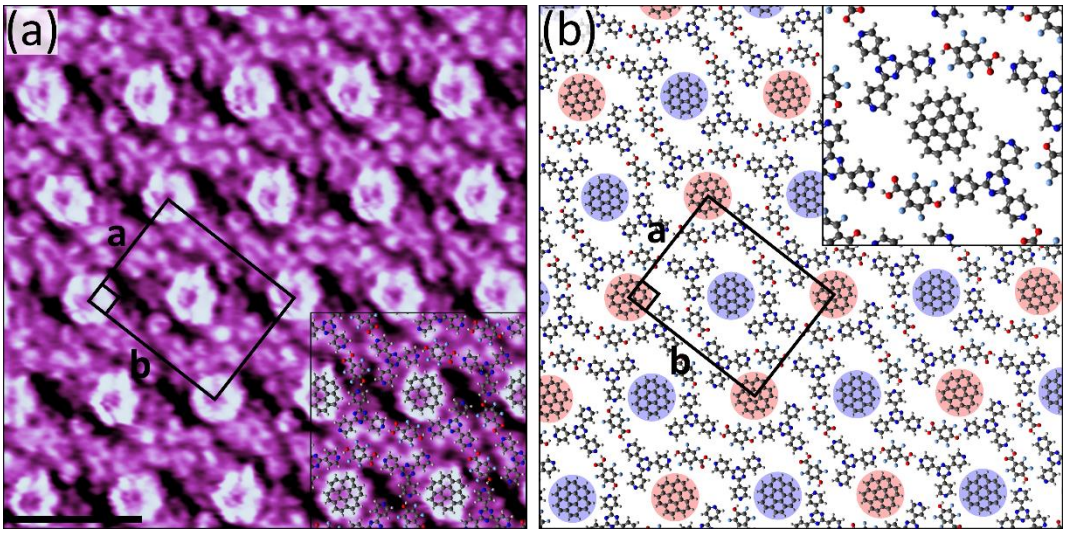

Figure 76: (a) STM image showing the rectangular coassembly of 4HTFBA and 4TPTZ at the heptanoic acid/HOPG interface after coronene inclusion. Tunnelling parameters: V_{bias} = −1.1 V, I_{set} = 100 pA. Unit cell parameters: a = 2.9 ± 0.1 nm, b = 3.6 ± 0.1 nm, angle = 90 ± 2°. Scale bar = 3 nm. **(b)** Proposed model for the assembly. The two different enantiomorphous sites which the coronene molecules occupy are highlighted with red and blue circles.

inequivalent pore structures within the assembly. These two inequivalent sites, which are highlighted by red and blue circles in the model for the coronene-included assembly shown in figure 76b, are enantiomorphs. For an achiral molecule such as coronene, neglecting any potential differences in the atomic structure of the HOPG surface at the position of the pores, these two pore structures are equivalent and coronene guests are accordingly observed to occupy both sites. In order for the coronene molecules to adsorb within the pores, they likely must displace any coadsorbed solvent molecules present within these regions. This indicates that if coadsorbed solvent molecules are present in the absence of coronene, they likely do not play a significant role in controlling the structure of the assembly.

The ratio of 4HTFBA to 4TPTZ molecules with the rectangular assembly is 1:1. It is readily conceivable that structures with alternate stoichiometries could be formed. In particular, given that there are three pyridyl nitrogen atoms in each 4TPTZ molecule with which 4HTFBA molecules could interact, structures with a higher ratio of 4HTFBA to 4TPTZ molecules seem possible. In order to explore this idea, solutions with higher relative concentrations of 4HTFBA were tested. Deposition of solutions in which the concentration of 4HTFBA is 5×10^{-3} M and the concentration of 4TPTZ is $5 \times 10^{-4} - 5 \times 10^{-5}$ M leads to the formation of a distinct hexagonal structure at the heptanoic acid/HOPG interface. A large-scale image of this assembly is shown in figure 77.

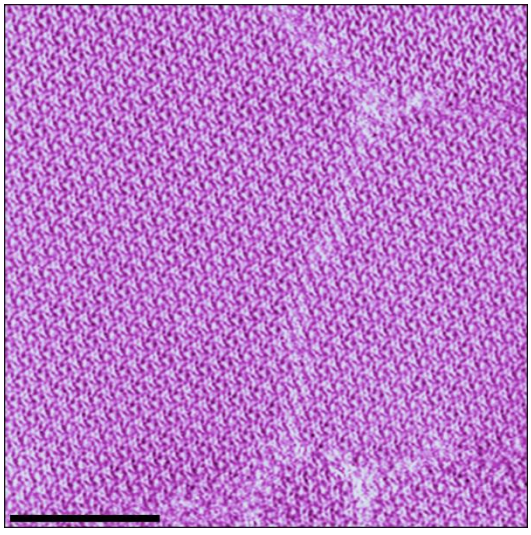

Figure 77: Large-scale STM image showing the hexagonal coassembly of 4HTFBA and 4TPTZ at the heptanoic acid/HOPG interface. Tunnelling parameters: V_{bias} = −0.9 V, I_{set} = 50 pA. Scale bar = 20 nm.

Within high-resolution images of the hexagonal assembly, both the 4HTFBA and 4TPTZ molecules can be clearly resolved. The 4HTFBA molecules are positioned at the apex of the tripodal legs of 4TPTZ molecules such that they can interact with their pyridyl nitrogen atoms. The 4TPTZ molecules that partake in these interactions are saturated with 4HTFBA molecules, i.e., all three of their pyridyl

nitrogen atoms interact with a 4HTFBA molecule. These supramolecular tripodal structures, consisting of one 4TPTZ molecule and three attached 4HTFBA molecules, are then packed together on the surface into porous hexagonal network. As is discussed in detail later, these pores host additional 4TPTZ molecules. The 4HTFBA molecules are only positioned such that they can interact with the pyridyl nitrogen atom of a single 4TPTZ molecule. This situation clearly differs from that observed in the rectangular assembly, where the 4HTFBA molecules bridge two pyridyl nitrogen atom sites. The fact that the 4HTFBA molecules can only interact with a single pyridyl nitrogen atom and that the geometry of all of these interactions appear to be equivalent indicates that either the phenol–pyridine or carboxyl–pyridine interaction mode is favoured in this case. However, as the orientation of the 4HTFBA molecules cannot be resolved in the STM images, it is unclear which interaction mode is favoured. Only detailed theoretical modelling, which is not pursued in this thesis, would be capable of unambiguously elucidating which of these two hydrogen bonding modes is favoured. However, studies on analogous 3D systems indicate that interaction through the carboxyl group may be the favoured interaction mode.[163] Figure 78 shows a tentatively proposed model in which it is assumed that the carboxyl–pyridine interaction mode is also favoured in this 2D system. Secondary C−H···F and C−H···O interactions between neighbouring 4HTFBA and 4TPTZ molecules also appear to be likely.

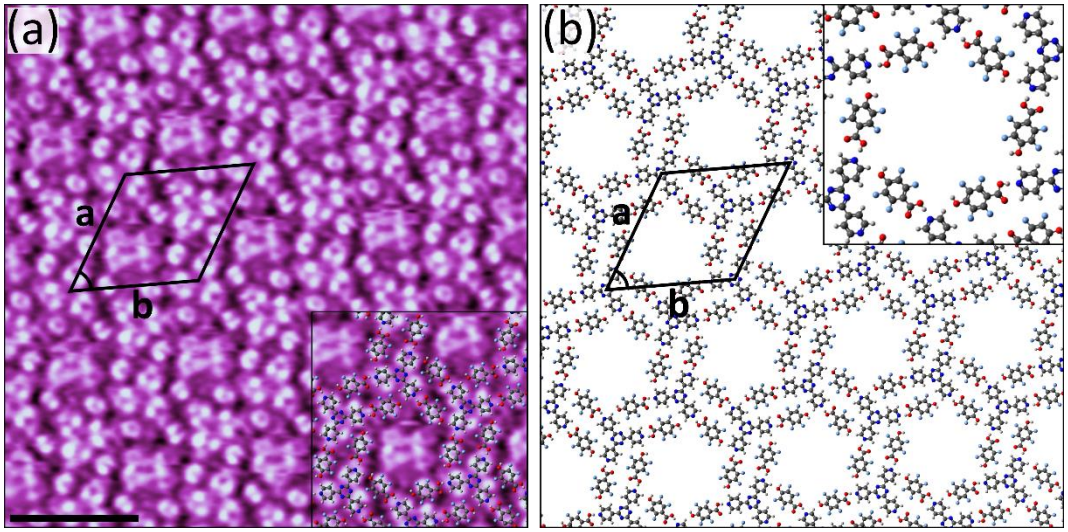

Figure 78: (a) STM image showing the hexagonal coassembly of 4HTFBA and 4TPTZ at the heptanoic acid/HOPG interface. Tunnelling parameters: V_{bias} = −1.2 V, I_{set} = 200 pA. Unit cell parameters: a = 3.0 ± 0.1 nm, b = 3.0 ± 0.1 nm, angle = 60 ± 2°. Scale bar = 3 nm. **(b)** Proposed model for the assembly.

As was mentioned previously, within the pores of the hexagonal assembly additional 4TPTZ molecules are present. As the pores are sixfold symmetric, there are two equivalent orientations which the threefold symmetric pore-confined 4TPTZ molecules can adopt (see figures 79a and 79b). Within some of the pores, the threefold symmetry of the 4TPTZ molecules can be clearly resolved and both possible

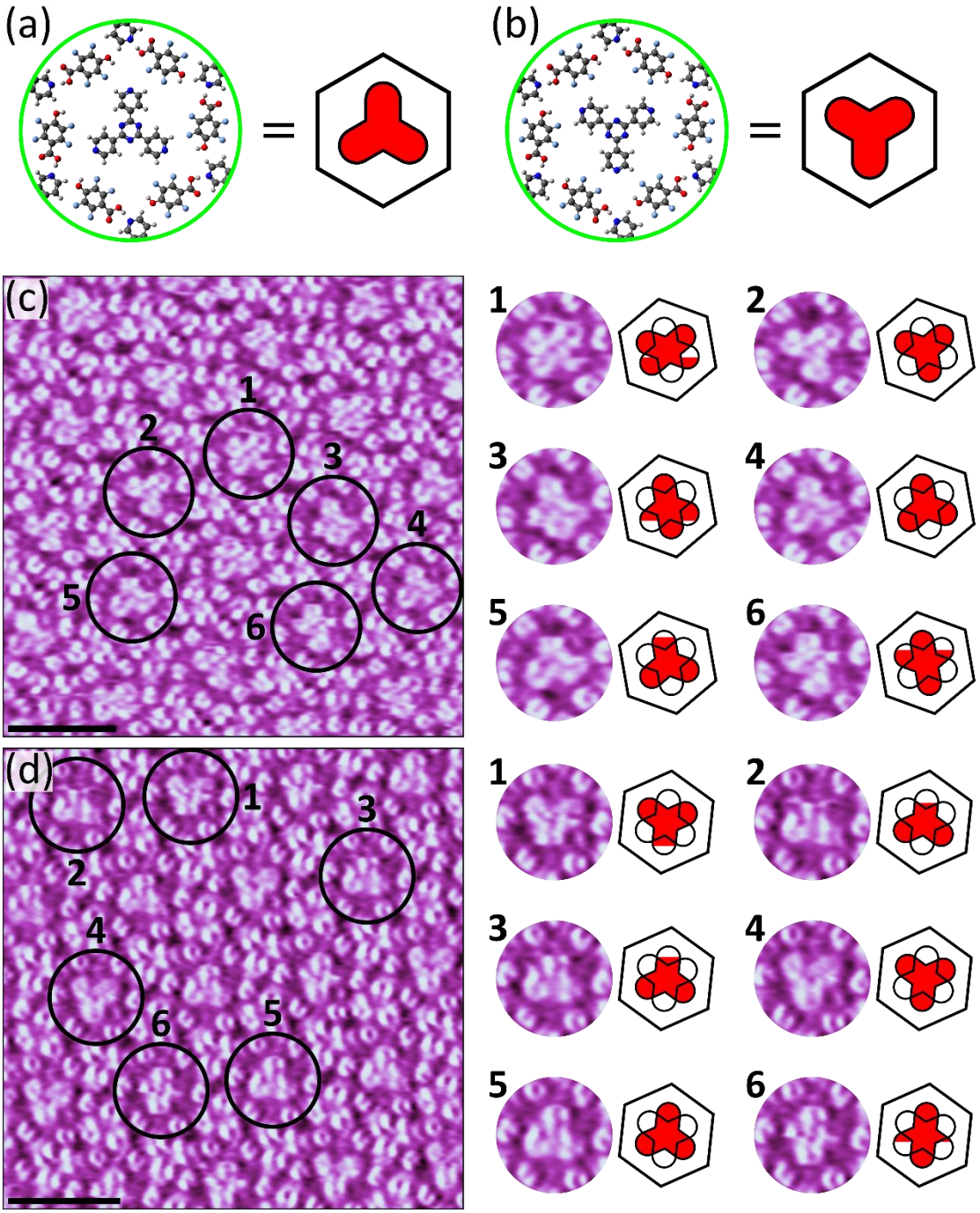

Figure 79: (a) and **(b)** show the two potential orientations of the 4TPTZ molecules within the proposed model for the pores of the hexagonal assembly. These two configurations are both shown alongside simplified schematic representations in which the 4TPTZ molecules are represented by a simple red tripodal shape and the periphery of the pore is represented by a hexagon. **(c)** STM image showing the hexagonal coassembly of 4HTFBA and 4TPTZ at the heptanoic acid/HOPG interface. Tunnelling parameters: V_{bias} = −0.9 V, I_{set} = 200 pA. Scale bar = 3 nm. Six different pores are circled, and the corresponding digital zooms of these pores are shown alongside the image. These digital zooms are shown alongside schematic representations highlighting the regions of the two possible orientations of the pore-confined 4TPTZ molecules that are occupied during imaging. **(d)** STM image showing the hexagonal coassembly of 4HTFBA and 4TPTZ at the heptanoic acid/HOPG interface. Tunnelling parameters: V_{bias} = −1.2 V, I_{set} = 50 pA. Scale bar = 3 nm. The image is analysed in exactly the same manner as that shown in (c).

orientations are observed. However, within most of the pores various structures which do not resemble isolated 4TPTZ molecules are resolved. These observations can be explained if the potential mobility of the pore-confined 4TPTZ molecules is considered. Were these molecules to be immobile or have a mobility which is significantly slower than the STM data acquisition time, each molecule would resolve with clear threefold symmetry in one of the two possible orientations. Conversely, were the 4TPTZ molecules to be mobile on a timescale much faster than the rate at which the STM data is acquired, a sixfold-symmetric structure would be resolved in the pores. Within the STM images shown in figure 79, such a sixfold-symmetric structure is never resolved. Rather, in addition to occasional threefold symmetric 4TPTZ molecules, a variety of different structures which have neither threefold nor sixfold symmetry were resolved. As is highlighted in figure 79, all of the structures observed within the pores can clearly be rationalised as combinations of the two possible orientations of the pore-confined 4TPTZ molecules. All of these structures are consistent with the 4TPTZ molecules occasionally moving between the two possible orientations during imaging, i.e., the pore-confined 4TPTZ molecules having a mobility on a similar timescale as that at which the STM data is acquired. The mechanism for this mobility is unclear: the 4TPTZ molecules may simply rotate within the pores, or alternatively, the mobility may involve the desorption and adsorption of 4TPTZ molecules. Furthermore, the possibility that the scanning process itself may influence the mobility of the 4TPTZ molecules within the pores certainly cannot be eliminated. In addition to the obviously favourable adsorption energy gained by having 4TPTZ molecules adsorbed within the pores, there is also likely some favourable C–H···F interactions between the pore-confined 4TPTZ molecules and the delineating 4HTFBA molecules. It is important to note that the pore-confined 4TPTZ molecules are not positioned such that their pyridyl nitrogen atoms can hydrogen bond with the surrounding 4HTFBA molecules, irrespectively of the preferred orientation of the 4HTFBA molecules (vide supra).

7.3 Bimolecular self-assembly properties of 4HTFBA with 3TPTZ

Like 4TPTZ, 3TPTZ was also observed to coassemble with 4HTFBA at the heptanoic acid/HOPG interface. The solutions used to form the observed network were prepared by combining equal volumes of 10^{-2} M solutions of 4HTFBA and 3TPTZ dissolved in heptanoic acid. Cocrystals/salt were observed to precipitate from this solution composition after leaving it to stand overnight. The solution that was deposited onto the HOPG surface was decanted from this precipitate. Figure 80 shows an example of a large-scale STM image of the assembly. It should be noted that the surface coverage of the assembly was fairly unpredictable: in some experiments, large domains of the coassembly were observed covering the surface, whereas during other experiments significant amounts of disorder

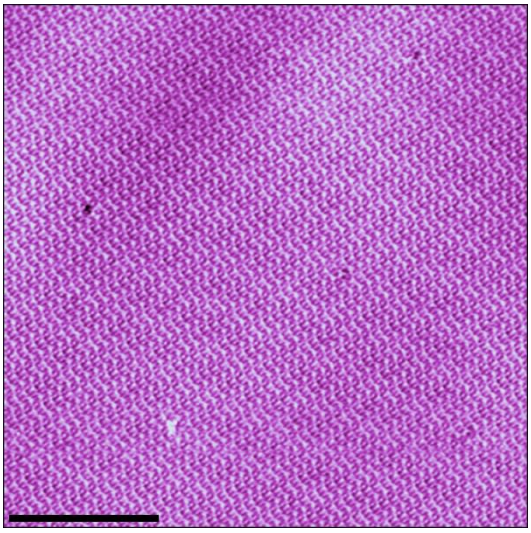

Figure 80: Large-scale STM image showing the coassembly of 4HTFBA and 3TPTZ at the heptanoic acid/HOPG interface. Tunnelling parameters: V_{bias} = −1.2 V, I_{set} = 50 pA. Scale bar = 20 nm.

alongside small regions of the assembly were seen. Furthermore, the situation is further complicated by the fact that the assembly was often observed to be very unstable towards scanning, which made data acquisition particularly challenging at times.

Figure 81a shows a high-resolution STM image in which both the 3TPTZ and 4HTFBA molecules can be clearly resolved. The assembly has a rectangular structure in which the molecules are arranged in a similar manner to that observed in the coassembly of 3TPTZ and TFHQ (see section 6.2), but with 4HTFBA molecules in place of the TFHQ molecules and with slightly different unit cell dimensions (compare figures 81 and 67). Each 4HTFBA molecule is positioned such that it can bridge two 3TPTZ

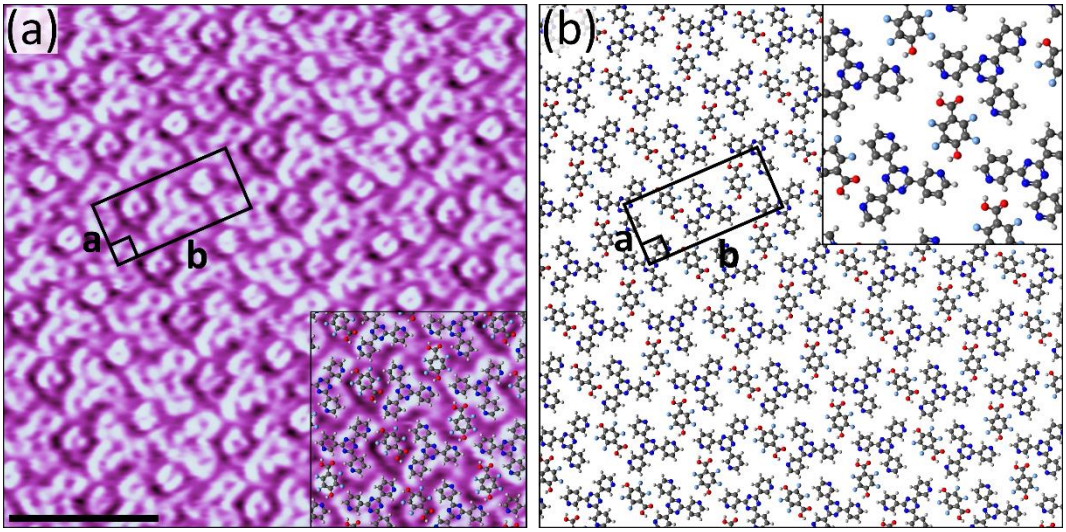

Figure 81: (a) STM image showing the coassembly of 4HTFBA and 3TPTZ at the heptanoic acid/HOPG interface. Tunnelling parameters: V_{bias} = −1.2 V, I_{set} = 200 pA. Unit cell parameters: a = 1.3 ± 0.1 nm, b = 2.9 ± 0.2 nm, angle = 90 ± 3°. Scale bar = 3 nm. **(b)** Proposed model for the assembly.

molecules by interacting with them via a phenol–pyridine interaction at one end and a carboxylic acid–pyridine interaction at the other. A tentatively proposed model for the assembly is shown in figure 81b. However, note that, like in the rectangular coassembly of 4TPTZ and 4HTFBA discussed in the previous section, here the orientation of the 4HTFBA molecules again cannot be resolved in the STM images. As such, the orientation of the 4HTFBA molecules shown in the proposed model in figure 81b is not actually precisely known. Irrespectively of the exact orientation of the 4HTFBA molecules, it is clear that in this assembly the phenol–pyridine and carboxylic acid–pyridine interaction modes are behaving cooperatively in controlling the organisation of the molecules in the assembly. In addition to these hydrogen bonding interactions, weak C−H···F and C−H···O interactions between the 3TPTZ and 4HTFBA molecules may also play an auxiliary stabilising role.

7.4 Bimolecular self-assembly properties of 4HTFBA with 2TPTZ

As was the case with the other two tripyridyl triazine isomers, 2TPTZ was also observed to coassemble with 4HTFBA. Deposition of binary solutions in which both 2TPTZ and 4HTFBA are present at concentrations 5×10^{-4} M leads to the exclusive formation of an oblique structure at the heptanoic acid/HOPG interface. Figure 82 shows an example of a large-scale STM image of this assembly.

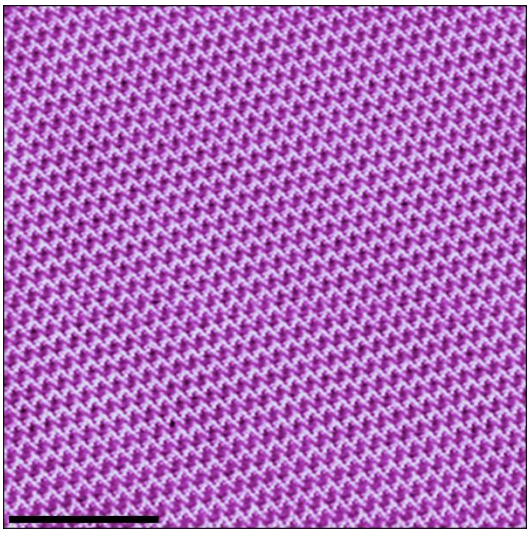

Figure 82: Large-scale STM image showing the oblique coassembly of 4HTFBA and 2TPTZ at the heptanoic acid/HOPG interface. Tunnelling parameters: V_{bias} = −0.9 V, I_{set} = 50 pA. Scale bar = 20 nm.

Within high-resolution STM images of the oblique assembly, such as those shown in figure 83c and 83e, the individual 2TPTZ and 4HTFBA molecules can be clearly resolved. Each 2TPTZ molecule is positioned such that it can interact with a single 4HTFBA molecule, and the positioning of the 4HTFBA molecules clearly indicates that they interact with the pyridyl nitrogen atoms of the 2TPTZ molecules.

As each 4HTFBA molecule only interacts with a single 2TPTZ molecule, the 4HTFBA molecules cannot simultaneously partake in both phenol–pyridine and carboxyl–pyridine hydrogen bonding interactions. Excluding a situation in which there is a mixture of these two interaction modes, this indicates that one of the two alternative interaction modes is preferred in this case. Although the STM images do not have sufficient resolution such that the orientation of the 4HTFBA molecules, and therefore the preferred interaction mode, can be identified, simple steric considerations offer significant insight. In the molecule 2TPTZ, the pyridyl nitrogen atoms are located at the position closest to the triazine core of the molecule; as a result, these sites are much more sterically hindered to the approach of 4HTFBA than the pyridyl nitrogen atoms in either 4TPTZ or 3TPTZ. Planar aromatic molecules, such as 2TPTZ and 4HTFBA, typically adsorb with the plane of their aromatic system approximately parallel to the underlying surface as this maximises their adsorption energy. Assuming that the 4HTFBA and 2TPTZ molecules are adsorbed in such a manner, the two molecules should be approximately coplanar within the assembly. Figures 83a and 83b show simple spacefill representations of the two molecules positioned in the expected coplanar manner. As can be seen in figure 83a, when the carboxyl group of a 4HTFBA molecule is orientated towards a 2TPTZ molecule, the compact carboxyl group is easily able to access the pyridyl nitrogen atoms of the 2TPTZ molecule such that the expected hydrogen bonding interaction can occur. Conversely, as is highlighted in figure 83b, as the phenolic hydroxyl group of 4HTFBA is directly attached to the bulky central aromatic ring, it seems to be particularly difficult for 4HTFBA to interact with 2TPTZ via its phenolic hydroxyl group as this would likely result in there being significant steric clashing between the 4HTFBA and 2TPTZ molecules. Although these simple steric considerations are somewhat crude, they indicate that the 4HTFBA and 2TPTZ molecules within the oblique assembly likely interact via the carboxyl–pyridine interaction mode. The preference for 2TPTZ to partake in carboxyl–pyridine interactions rather than phenol–pyridine interactions is further evidenced by the results present in chapters 5 and 6. In chapter 5, 2TPTZ was shown to readily coassemble with the fluorinated carboxylic acid F4TPA at the heptanoic acid/HOPG interface; however, as is discussed in chapter 6, preliminary experiments indicate that 2TPTZ does not coassemble with the fluorinated diphenol TFHQ under the same conditions. Furthermore, as was discussed for the hexagonal coassembly of 4HTFBA with 4TPTZ, studies on 3D systems indicate that there may be a preference for the formation of the carboxyl–pyridine interaction mode over its phenol–pyridine counterpart irrespectively of the steric factors present with 2TPTZ.[163]

Although the preferred interaction mode between the 4HTFBA and 2TPTZ molecules has been established in the preceding paragraph, this information is not sufficient to fully elucidate the nature of the oblique assembly. The 4HTFBA–2TPTZ dyads adopt two distinct orientations within the assembly, which are related by a 180° rotation. These two different orientations are arranged side-by-

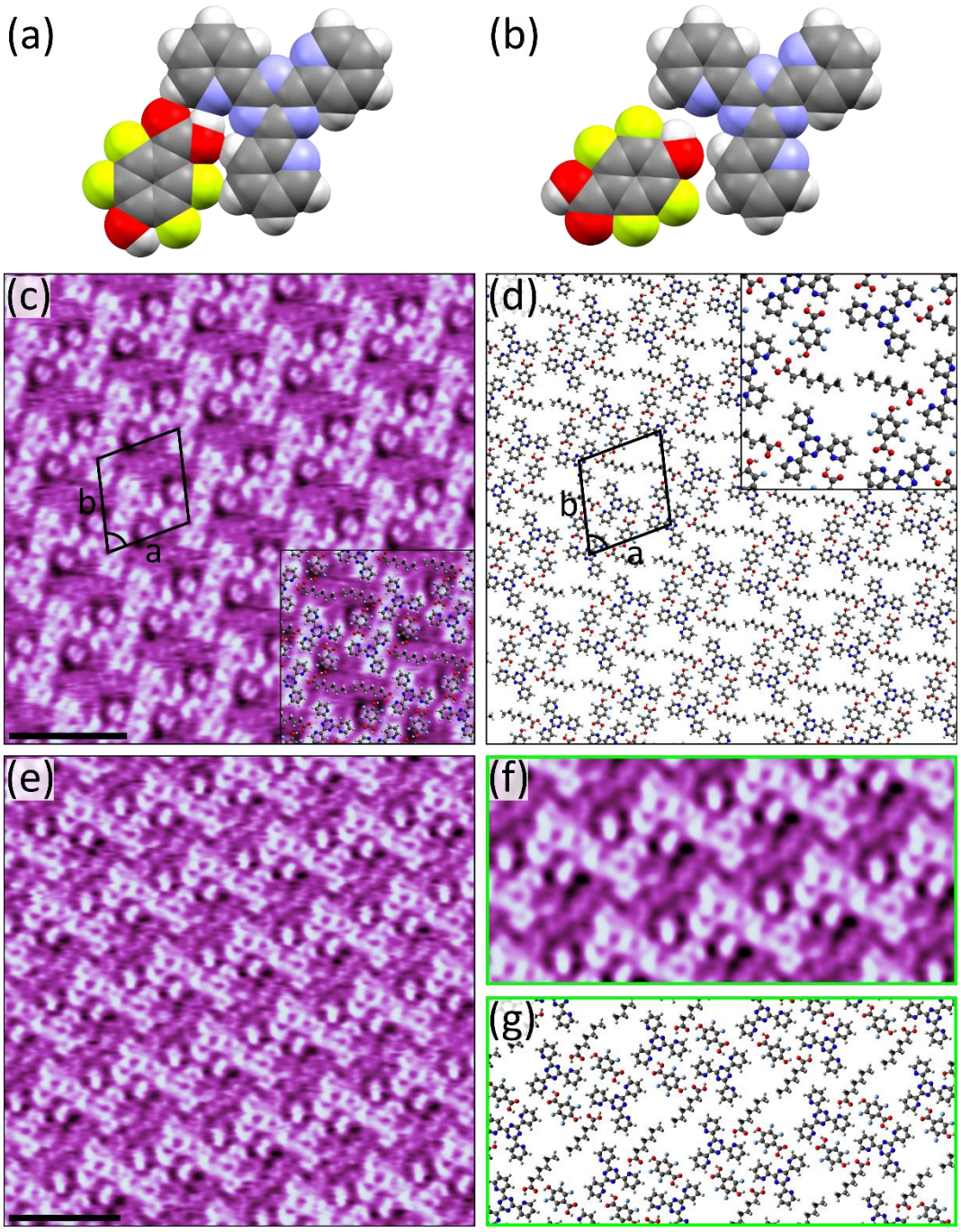

Figure 83: (a) Spacefill representation of 3TPTZ and 4HTFBA, approximately positioned in a reasonable carboxyl–pyridine hydrogen bonding configuration. **(b)** Spacefill representation of 3TPTZ alongside that of 4HTFBA, with the phenol group of 4HTFBA orientated towards one of the N(pyridyl) sites of 2TPTZ. The two molecules cannot be positioned in a reasonable hydrogen bonding geometry without there being significant non-physical overlap between them. The van der Waals radii used in (a) and (b) are those reported by Bondi[114]. **(c)** STM image showing the oblique coassembly of 4HTFBA and 2TPTZ at the heptanoic acid/HOPG interface. Tunnelling parameters: V_{bias} = −0.9 V, I_{set} = 300 pA. Unit cell parameters: a = 2.2 ± 0.1 nm, b = 2.4 ± 0.1 nm, angle = 76 ± 2°. Scale bar = 3 nm. **(d)** Proposed model for the assembly. **(e)** STM image showing the oblique coassembly of 4HTFBA and 2TPTZ at the heptanoic acid/HOPG interface with tip conditions highlighting the presence of coadsorbed solvent molecules. Tunnelling parameters: V_{bias} = −0.9 V, I_{set} = 50 pA. Scale bar = 3 nm. **(f)** Unit cell averaged region of the image shown in (e). **(g)** Model showing the proposed arrangement of the molecules in the region highlighted in (f).

side in an alternating pattern to form the zigzag rows that can be clearly seen in figures 83c and 83e. These rows are positioned parallel to one another on the surface; however, they are not closely packed together and there are no obvious strong interactions between the rows that could justify the spacing between them. This spacing can only be readily understood if the potential influence of solvent coadsorption is considered. As is shown in the proposed model shown in figure 83d, there is sufficient space to incorporate coadsorbed heptanoic acid molecules positioned such that they can hydrogen bond with the pyridyl nitrogen atoms of the 2TPTZ molecules. One of the pyridyl nitrogen atoms in each 2TPTZ molecule appears to interact with a heptanoic acid molecule in this manner. These hydrogen bonds and the favourable adsorption energy that it provides likely makes solvent coadsorption quite favourable. Furthermore, the presence of coadsorbed solvent in the manner proposed also allows for the formation of favourable O−H···O hydrogen bonds between the phenolic hydroxyl groups of the 4HTFBA molecules and the carbonyl oxygen atoms of the heptanoic acid molecules. Although, as is typical in the case coadsorbed solvent molecules, the heptanoic acid molecules ordinarily cannot be clearly resolved within the STM images, under certain tip conditions, structures corresponding to coadsorbed heptanoic acid molecules positioned in a manner consistent with the proposed model could be observed. An example of such an image is shown in figure 83e, and this can be seen even more clearly in the unit cell averaged image shown in figure 83f.

The 4HTFBA and 2TPTZ molecules are present in a ratio of 1:1 within the oblique assembly. As was the case for the coassembly of 4TPTZ with 4HTFBA, it is conceivable that structures with alternate stoichiometries could be formed. In particular, given that there are three pyridyl nitrogen atoms in each 2TPTZ molecule with which a 4HTFBA molecule could interact, it could be expected that structures with a higher ratio of 4HTFBA to 2TPTZ molecules are possible. In order to explore this idea, solutions with a higher molar ratio of 4HTFBA to 2TPTZ were tested. However, deposition of solutions in which the concentration of 4HTFBA is 5×10^{-3} M and the concentration of 2TPTZ is 5×10^{-4} M, i.e., a tenfold molar excess of 4HTFBA, still leads to the formation of the previously discussed oblique assembly.

Although structures in which the ratio of 4HTFBA and 4TPTZ molecules deviates from 1:1 were not realised, an additional 1:1 structure which differs from the oblique assembly was observed. This structure could be observed when the concentrations of both 4HTFBA and 2TPTZ in the solution was increased. Solutions were prepared in which the initial concentrations of both components were 10^{-2} M. These concentrations are described as “initial” because within minutes of preparing such mixed solutions the precipitation of what were presumably cocrystals/salt of 4HTFBA and 2TPTZ was observed to occur. The deposition of the solution decanted from this precipitate was found to lead to the formation of a new rectangular structure at the heptanoic acid/HOPG interface. This new

structure, of which a large-scale STM image is shown in figure 84a, was observed coexisting with the oblique assembly (see figure 84b).

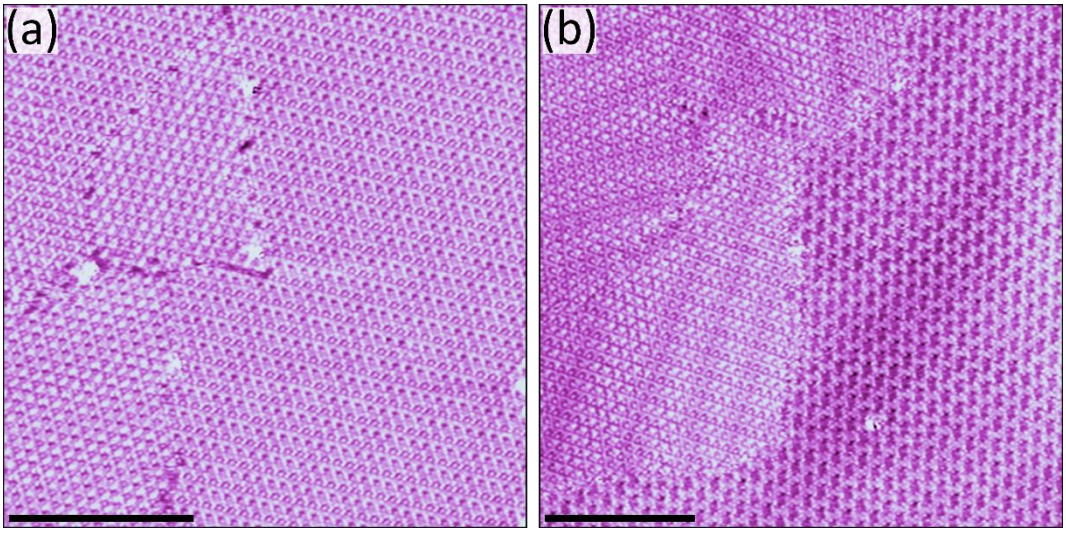

Figure 84: (a) Large-scale STM image showing the rectangular coassembly of 4HTFBA and 2TPTZ at the heptanoic acid/HOPG interface. Tunnelling parameters: V_{bias} = −1.2 V, I_{set} = 100 pA. **(b)** Large-scale STM image showing the coassembly of 4HTFBA and 2TPTZ at the heptanoic acid/HOPG interface. The rectangular (domain on the left side of the image) and oblique phases (domain on the right side of the image) can be seen coexisting. Tunnelling parameters: V_{bias} = −0.9 V, I_{set} = 100 pA. Both scale bars = 20 nm.

Figure 85a shows an example of a high-resolution STM image of the rectangular coassembly of 4HTFBA and 2TPTZ. Both the 4HTFBA and 2TPTZ molecules can be clearly resolved and their appearance is much the same as that observed in STM images of the oblique assembly. As was also the case in the oblique assembly, each 4HTFBA molecule is paired with a single 2TPTZ molecule and the relative positioning of the molecules in these dyads is consistent with hydrogen bond formation. Based on exactly the same steric factors that were discussed for the oblique assembly, within the rectangular assembly, the 4HTFBA molecules are again expected to interact with the 2TPTZ molecules via a carboxyl–pyridine hydrogen bonding interaction. The 4HTFBA–2TPTZ dyads are densely packed together in the assembly and there is no space for coadsorbed solvent molecules. Although the assembly appears to be fairly straightforward at first glance, close inspection reveals some intricacies. As was discussed in section 4.2, the threefold-symmetric conformation that the 2TPTZ molecules adopt has two enantiomorphous adsorption configurations. However, within the STM images the individual 2TPTZ molecules cannot be resolved with sufficient detail such that their enantiomorphous structure can be unambiguously identified. If the chiral nature of the adsorbed 2TPTZ molecules is ignored and only their tripodal shape is considered, the 2TPTZ molecules appear to be arranged into an approximately hexagonal array (see overlay shown in figure 85a). The 4HTFBA molecules are then positioned in the interstices between the 2TPTZ molecules such that they can interact with them via

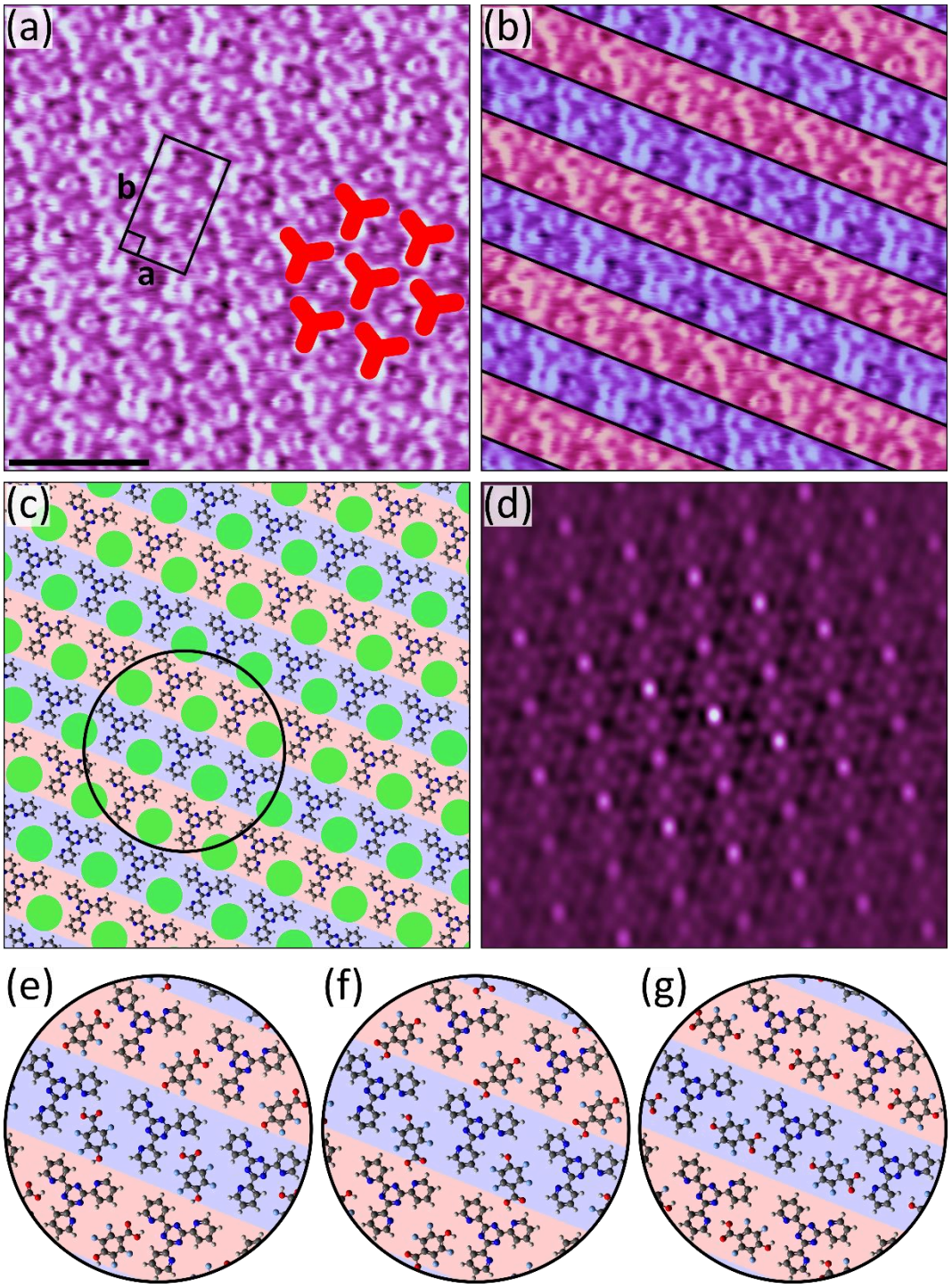

Figure 85: (a) STM image showing the rectangular coassembly of 4HTFBA and 2TPTZ at the heptanoic acid/HOPG interface. Tunnelling parameters: V_{bias} = −0.9 V, I_{set} = 300 pA. Unit cell parameters: a = 1.5 ± 0.1 nm, b = 2.6 ± 0.2 nm, angle = 90 ± 3°. Scale bar = 3 nm. The overlayed red tripodal shapes highlight the approximate positions of the 2TPTZ molecules. **(b)** The same STM image as that shown in (a), but with the alternating pattern of rows in which the 2TPTZ molecules have a different appearances highlighted in red and blue. **(c)** Proposed model for arrangement of the 2TPTZ molecules. The green circles highlight the interstices in which the 4HTFBA molecules are adsorbed. **(d)** Self-correlation of the STM image shown in (a). **(e, f and g)** Proposed models for the three different potential arrangements of the assembly, assuming that each of the 4HTFBA molecules interact with the 2TPTZ molecules in an equivalent manner.

carboxyl–pyridine hydrogen bonds. Were all the 2TPTZ molecules to be in the same enantiomorphous configuration and assuming that the 4HTFBA molecules in the interstices are all equivalent, the assembly would have an approximately hexagonal symmetry. However, careful inspection of the STM images reveals that the 2TPTZ molecules do not all appear to be the same. As is highlighted in figure 85b, the 2TPTZ molecules have two different general appearances and these two different appearance modes are arranged into rows which are packed together in an alternating pattern on the surface. Although, as previously mentioned, the resolution is clearly insufficient for the enantiomorphous configuration of the 2TPTZ molecules to be unambiguously identified, in principle the two enantiomorphs should have different appearances. This has previously been demonstrated using the favourable resolution provided by UHV measurements conducted at low temperature, where the chiral nature of 2TPTZ molecules adsorbed on an Au(111) surface could be resolved.[174] Therefore, it seems possible that the two distinct appearances that the 2TPTZ molecules adopt in the assembly correspond to different enantiomorphs. This would mean that the 2TPTZ molecules in the alternate rows highlighted in figure 85b differ in their enantiomorphous configuration. If only the position of the 2TPTZ molecules is considered, such an arrangement results in the assembly having a rectangular symmetry. The proposed arrangement of the 2TPTZ molecules within the assembly is shown in figure 85c. This arrangement is supported by analysis of the self-correlation of images of the assembly, which clearly indicate that the assembly is rectangular (see figure 85d). Note that this analysis crucially assumes that the slight differences in the appearance of the 2TPTZ molecules between the rows is not the result of a moiré effect. Were a moiré effect to be significant, then precisely understanding the exact arrangement of 2TPTZ molecules would become essentially impossible using only the STM data. The green circles in figure 85c highlight the interstices between the 2TPTZ molecules which host the 4HTFBA molecules. There are three inequivalent pyridyl nitrogen atoms within each of these regions with which the 4HTFBA molecules can interact. The three alternatives are shown in figures 85e, 85f and 85g. From the STM images it is not possible to determine which of the three possibilities the 4HTFBA molecules adopt. All of the 4HTFBA molecules may be positioned in one of the three configurations or any combination of the three may be present. As the three different configurations cannot be reasonably distinguished via STM, the precise arrangement of the molecules within the assembly remains unclear. Although the exact organisation of the molecules in the assembly is unclear, the salient point in the context of this work is that that the carboxyl–pyridine and phenol–pyridine interaction modes are not behaving cooperatively, with only the former playing a structural role within the assembly.

7.5 Conclusions

The interplay between the carboxyl–pyridine and phenol–pyridine hydrogen bonding interaction modes is clearly a complex situation influenced by a variety of different factors. The only clear-cut case occurs when 2TPTZ is employed as an acceptor. The limited steric accessibility of the N(pyridyl) sites of this molecule strictly prohibits the phenol–pyridine interaction mode, whereas the carboxyl–pyridine alternative is still possible. Accordingly, only the latter interaction mode is observed in both of the coassemblies of 4HTFBA with 2TPTZ. Such a clear bias for one of the two interaction modes is not observed when 4TPTZ and 3TPTZ are employed as hydrogen bond acceptors. Although 4TPTZ was observed to coassemble with 4HTFBA into a hexagonal network in which one of the two possible interactions modes seemingly occurs exclusively, an alternate rectangular structure in which the two interaction modes cooperatively influence the organisation of the molecules was also observed. Which of two structures that forms was found to depend on the concentrations of the building blocks in the solution. 3TPTZ and 4HTFBA were only observed to coassemble into a single structure, in which cooperativity between the two interaction modes was again observed. These results indicate that, unlike the situation with 2TPTZ, with 4TPTZ and 3TPTZ there is no strong preference for either of the two interaction modes. This makes the outcome of pairing bifunctional hydrogen bond donors, such as 4HTFBA, with non-sterically hindered acceptors somewhat unpredictable.

Chapter 8: Exploring the interplay between fluorine activated halogen and hydrogen bonds in 2D networks

Within chapter 7, the interplay between two different hydrogen bonding interaction modes, both of which are activated by molecular fluorination, was explored. An additional interaction which has hitherto not been explored experimentally in this thesis is the halogen bond. Like the hydrogen bonding interactions discussed in the preceding three chapters, halogen bond formation is also promoted by molecular fluorination. In this case the mechanism is particularly well studied: the electron withdrawing influence of fluorine atoms can polarise the electron density associated with a nearby halogen atom and thereby amplify its halogen bond donor ability (see sections 1.3.4 and 1.6). Due to the role that fluorination can have in promoting both hydrogen and halogen bond formation, it may be useful in the design of building blocks which can simultaneously partake in both of these interactions. The use of such building blocks could provide a unique multitiered strategy towards controlling the morphology of 2D networks.

Within the field of 3D crystal engineering, the interplay between halogen and hydrogen bonds in systems in which both are possible has been extensively studied. In some of these systems, the two interactions are found to work cooperatively such that both synergistically control the organisation of the molecular building blocks.[175–185] In other systems, these two interactions behave competitively such that one dominates the self-assembly process at the expense of the other.[183–186] Within 2D surface-confined systems, there has also been some explicit efforts to explore the interplay between these two interactions.[155,187–189] However, the true structural significance of the halogen bonding interactions proposed within these studies remains particularly unclear. As was discussed in section 1.3.4, the formation of strong halogen bonds typically requires that the halogen bond donating atom is attached to a strong electron withdrawing group. This criterion is not fulfilled in the current studies in which the interplay between halogen and hydrogen bonds in 2D surface-confined systems is explored. Furthermore, the molecular building blocks within most of these studies are functionalised with long alky chains.[187–189] As was discussed in section 1.3.2, alky chains can have a dominant influence on the arrangement of the molecular building blocks within such systems. As such, the presence of these alkyl chains could mask the true structural role of the proposed halogen/hydrogen bonds.

In order to explore the interplay between halogen and hydrogen bonds in 2D surface-confined systems, the coassembly of the molecule 4-bromotetrafluorobenzoic acid (4BTFBA, figure 86) with the molecules 4TPTZ and 3TPTZ was explored. 4BTFBA is a bifunctional molecular building block, which consists of a fluorinated aromatic ring functionalised with a bromine atom at one end and a carboxyl

group at the other. These two substituents are positioned in a para configuration. The fluorinated aromatic core is expected to promote the formation of carboxyl mediated hydrogen bonds (see chapter 5) and activate the bromine atom towards halogen bond formation (see sections 1.3.4 and 1.6), hopefully allowing 4BTFBA to simultaneously act as an effective halogen and hydrogen bond donor. The molecules 4TPTZ and 3TPTZ, two of the isomers discussed in chapter 4, were employed as complementary building blocks to 4BTFBA as their N(pyridyl) sites are expected to be effective acceptor sites for both halogen and hydrogen bonds. Unlike in the preceding three chapters on similar bimolecular systems, here 1-phenyloctane rather than heptanoic acid is employed as a solvent. This is facilitated by the appreciable solubility that 4BTFBA is observed to have in 1-phenyloctane. Furthermore, as halogen bonds are typically somewhat weaker than hydrogen bonds, the competitive hydrogen bond donating ability of heptanoic acid (see section 4.6) is particularly undesirable in this case. Two additional molecular building blocks, namely 4-methyltetrafluorobenzoic acid (4MeTFBA, figure 86) and coronene, were employed to give insight into the networks formed using 4BTFBA and 4TPTZ/3TPTZ. 4MeTFBA was employed as a structural analogue of 4BTFBA. 4MeTFBA is structurally the same as 4BTFBA but with a methyl group rather than a bromine atom. The two molecules should be able to partake in essentially the same non-covalent interactions other than halogen bonds, which are clearly not possible with 4MeTFBA. Therefore, insight into the significance of any halogen bonding interactions which may be present in systems formed with 4BTFBA can be obtained by studying analogous systems in which 4BTFBA has been exchanged for 4MeTFBA. 4MeTFBA in particular was selected as a structural analogue as it is expected to have essentially the same dimensions as 4BTFBA due to the close size match between the vdW radii of a bromine atom (1.85 Å[115]) and a methyl group (2.0 Å[190]). The minimal steric impact associated with exchanging bromine atoms and methyl groups has previously been exploited in a biochemical setting, where the interchange of these two functional groups can give insight into ligand–protein interactions.[191,192] Similarly, the ease of incorporation of

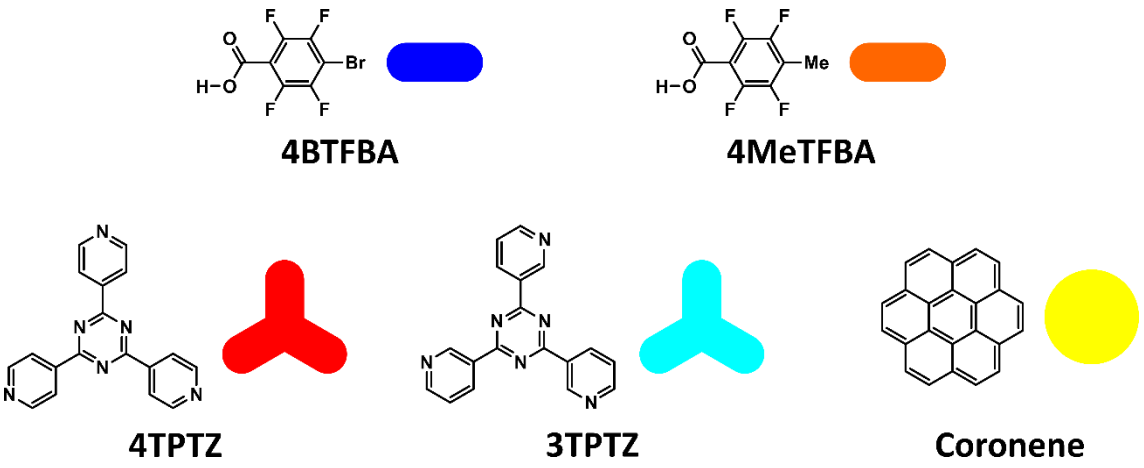

Figure 86: Molecular structures alongside schematic representations of 4BTFBA, 4MeTFBA, 4TPTZ, 3TPTZ and coronene.

the molecule 5-bromouracil into DNA in place of thymine (5-methyluracil) is widely thought to be as a result of the similar dimensions of the two molecules.[191,192] As was the case in section 7.1, here coronene is again employed as a guest molecule. As will be shown, some of the networks formed are porous and guest incorporation gives some insight into the nature of these networks. For clarity, at points throughout this chapter the molecular building blocks will be represented schematically. The simple schematic representations used are shown in figure 86 alongside the corresponding molecular building block.

8.1 Homomolecular self-assembly properties of 4BTFBA

Some efforts were made to explore the homomolecular self-assembly behaviour of 4BTFBA at the 1-phenyloctane/HOPG interface. Solutions with concentrations ranging from 10^{-3} M up to the point of saturation were tested. No evidence for the homomolecular self-assembly of 4BTFBA was observed within this range.

8.2 Bimolecular self-assembly properties of 4BTFBA with 4TPTZ

The deposition of solutions containing both 4BTFBA and 4TPTZ leads to the formation of a hexagonal network at the 1-phenyloctane/HOPG interface (see figure 87). The mixed solutions used to form this hexagonal assembly were prepared by combining saturated 4BTFBA solution with saturated 4TPTZ solution in a ratio of 1:9. Upon being left to stand overnight, cocrystals/salt of 4BTFBA and 4TPTZ were observed to precipitate from the solution. The network from which the hexagonal assembly was formed was decanted from this precipitate.

As is shown in figure 87b, within high-resolution STM images of the hexagonal coassembly, both the 4BTFBA and 4TPTZ molecules can be clearly resolved. As expected, the 4BTFBA molecules are positioned such that they can interact with the pyridyl nitrogen atoms of the 4TPTZ molecules. The 4BTFBA molecules do not bridge two N(pyridyl) sites, i.e., each only interacts with a single N(pyridyl) site. However, as the orientation of the 4BTFBA molecules cannot be resolved, it is unclear if this interaction is mediated via Br···N(pyridyl) halogen bonds or carboxyl–pyridine hydrogen bonding interactions. This issue will be addressed later on. Each 4TPTZ molecule interacts with three 4BTFBA molecules in this manner. The network of 4BTFBA and 4TPTZ molecules delineates a series of pores which appear to be occupied. These occupants are likely either coadsorbed solvent molecules or additional 4BTFBA molecules as the pores are too small to reasonably accommodate 4TPTZ molecules. The typically 'streaky' appearance of these occupants is consistent with them being mobile. The pores appear to be of ideal size to host the molecule coronene and, accordingly, the addition coronene to the system leads to the formation of the expected host–guest network. This was achieved by first depositing 10 µL of the solution used to form the hexagonal coassembly of 4BTFBA and 4TPTZ then, after waiting for a few minutes to ensure that the hexagonal host network had fully formed, 2 µL of 10^{-5} M coronene solution was added to the 10 µL droplet above the preformed host network. High-resolution STM images in which all three components can be clearly resolved, such as that shown in figure 87d, verify that the arrangement of the 4BTFBA and 4TPTZ molecules is seemingly unperturbed by the addition of coronene. These pores are expected to be particularly favourable adsorption sites

as the coronene molecules can interact with the 4BTFBA molecules lining the interior of the pores via favourable C−H···F interactions. Note that in order for coronene incorporation to occur, any species present in the pores must be displaced. This indicates that the mobile pore occupants observed in the absence of coronene likely play no specific role in controlling the structure of the assembly.

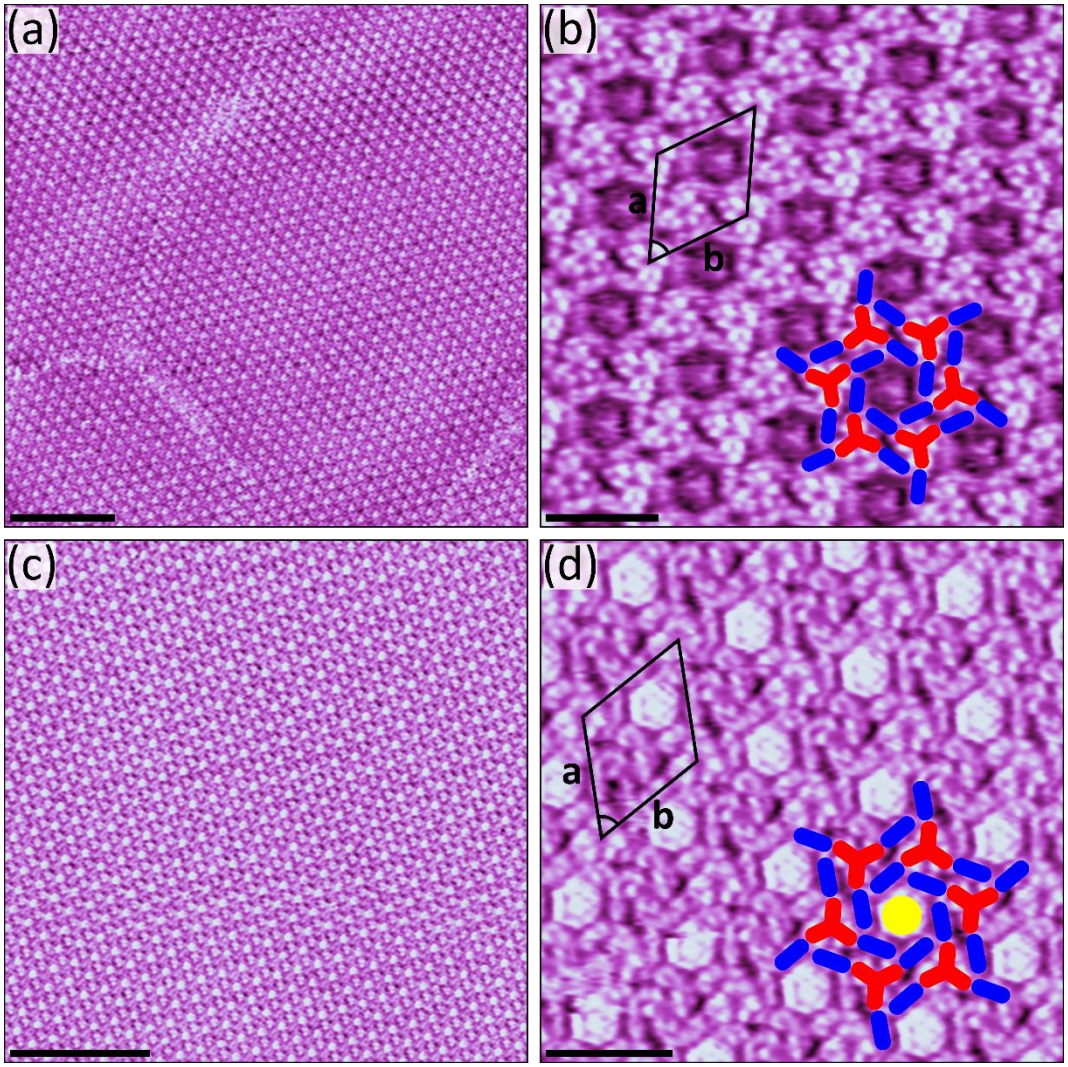

Figure 87: STM images showing the coassembly of 4BTFBA and 4TPTZ at the 1-phenyloctane/HOPG interface without coronene inclusion **(a and b)** and with coronene inclusion **(c and d)**. Tunnelling parameters: (a) V_{bias} = −0.9 V, I_{set} = 50 pA, (b) V_{bias} = −1.2 V, I_{set} = 300 pA, (c) −0.9 V, I_{set} = 50 pA, (d) V_{bias} = −1.2 V, I_{set} = 300 pA. Unit cell parameters shown in both (b) and (d): a = b = 2.9 ± 0.2 nm, angle 60 ± 3°. Scale bars for (a) and (c) are 20 nm and for (b) and (d) are 3 nm. The schematic representations given in figure 86 are overlaid onto images (b) and (d) to highlight the arrangement of the molecules.

As was previously mentioned, the orientation of the 4BTFBA molecules within the assembly cannot be resolved. They could either interact with the 4TPTZ molecules via Br···N(pyridyl) halogen bonds or carboxyl–pyridine hydrogen bonding interactions. Excluding an unusual situation in which a mixture of the two orientations is present, this indicates that there is a preference for one of the two interaction modes. Also note that, based on the STM images, the geometric relationship between the

4BTFBA molecules and the 4TPTZ molecules with which they are halogen/hydrogen bonding is seemingly equivalent in all cases, which is consistent with them all interacting via the same one of the two possible interactions. When the surface-induced chirality of the 4BTFBA molecules is considered, it becomes clear that there are four possible arrangements of the molecules within the assembly. These four possibilities are shown in figure 88. Within two of these arrangements (figures 88a and 88b), the 4BTFBA molecules interact with the 4TPTZ molecules via carboxyl–pyridine hydrogen bonding interactions, whereas in the other two possible arrangements (figures 88c and 88d) Br···N(pyridyl) halogen bonds are present. In order to gain insight into which of these arrangements is preferred, additional experiments were conducted in which 4BTFBA was exchanged for its structural analogue, 4MeTFBA. The deposition of binary solutions prepared by combining saturated 4MeTFBA solution with saturated 4TPTZ solution in a ratio of 1:1 leads to the formation of a hexagonal assembly at the 1-phenyloctane/HOPG interface (see figures 89a and b). Large domains of this assembly could be readily observed covering essentially the entire surface of the HOPG sample. The unit cell dimensions for this hexagonal network were found to be equivalent to those of the hexagonal coassembly of 4BTFBA and 4TPTZ. Further parallels between the two systems can be seen when high-resolution STM images of the two assemblies are compared. Figure 89b shows an example of a high-resolution STM image of the hexagonal coassembly of 4MeTFBA and 4TPTZ in which both components

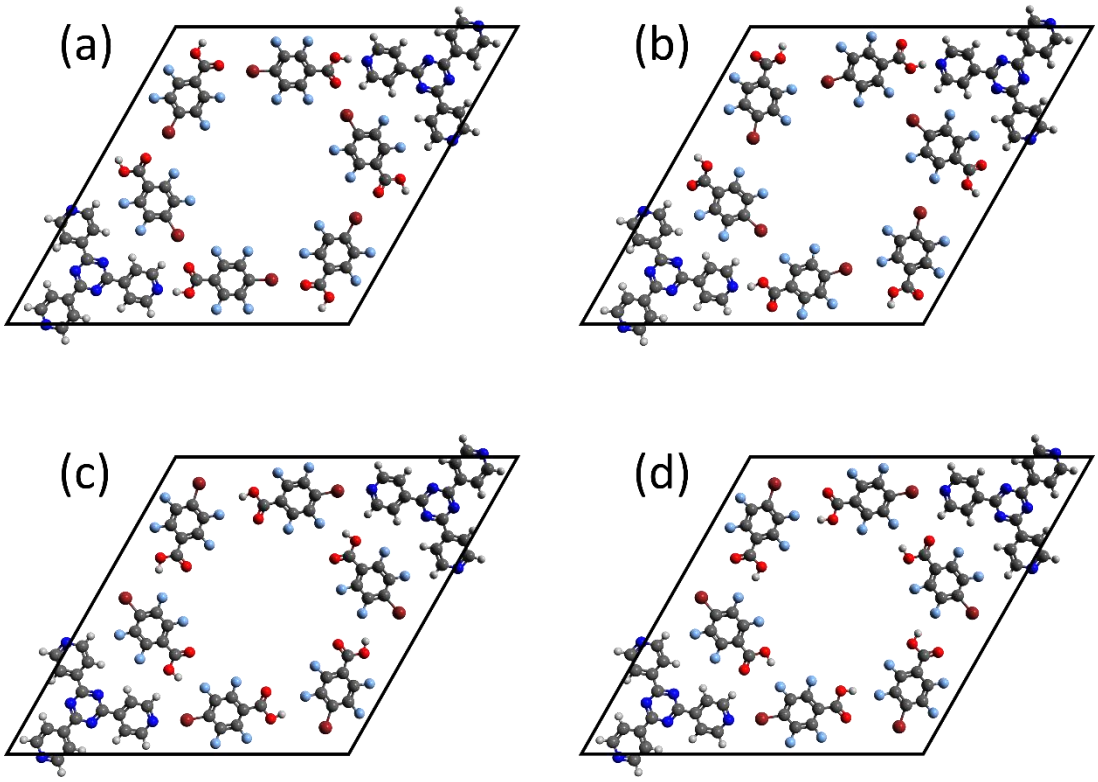

Figure 88: (a–d) Models highlighting the four possible orientations that the 4BTFBA molecules can adopt in its coassembly with 4TPTZ.

can be clearly resolved. By comparison of this figure with that of the hexagonal coassembly of 4BTFBA and 4TPTZ (figure 87b), it becomes clear that the arrangement of the molecules within the two assemblies is entirely analogous, i.e., the two systems are isostructural, with the 4MeTFBA and 4BTFBA molecules occupying equivalent positions within their respective networks. Furthermore, in the 4MeTFBA case, mobile occupants can again be observed within the pores. These occupants, which can be very clearly resolved in figure 89b, likely correspond to either additional 4MeTFBA molecules or coadsorbed solvent molecules. As was also observed in the 4BTFBA case, these could again be displaced by coronene guest molecules without perturbation to the arrangement of the molecules within the assembly (see figures 89c and 89d). Experimentally, this was achieved by depositing a three-

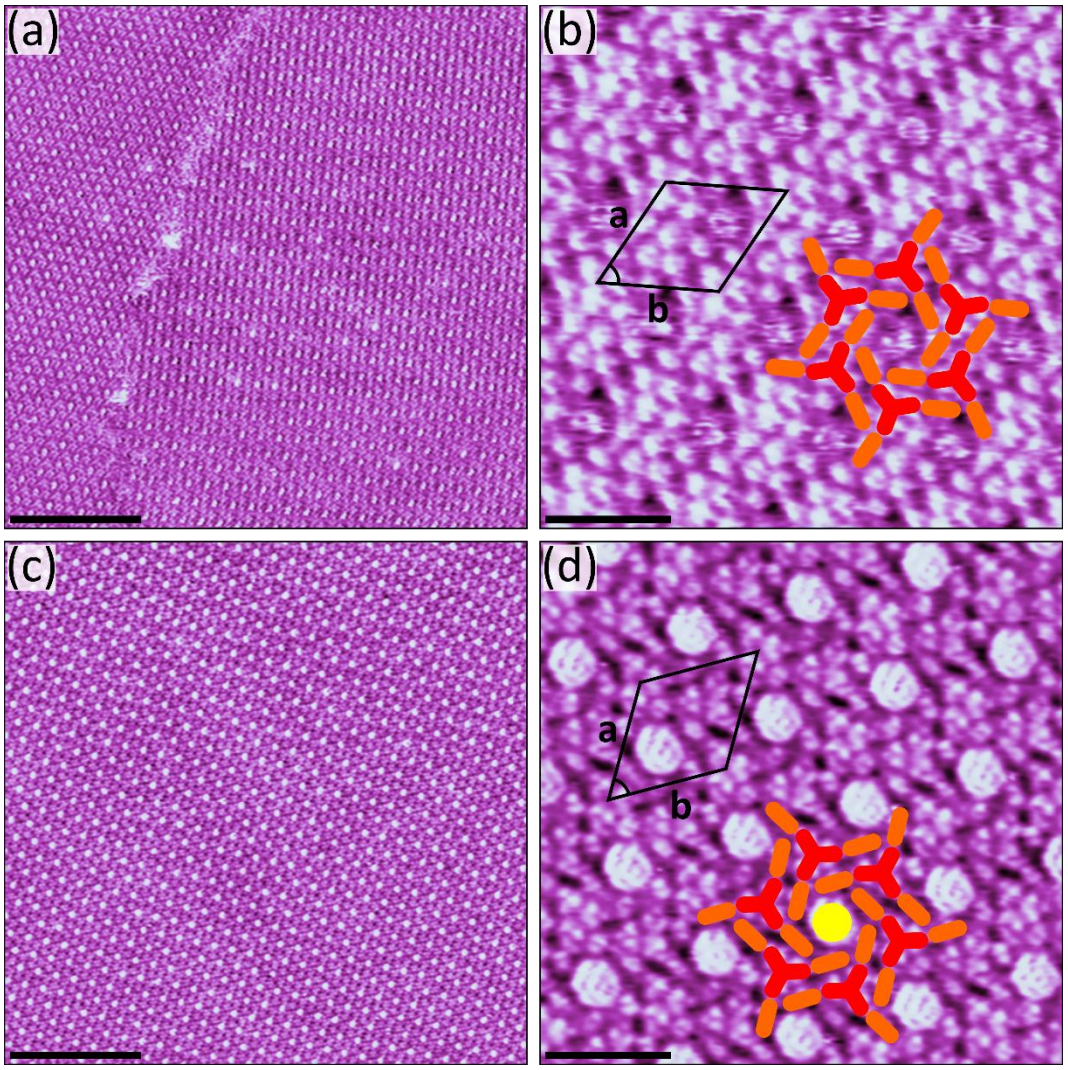

Figure 89: STM images showing the coassembly of 4MeTFBA and 4TPTZ at the 1-phenyloctane/HOPG interface without coronene inclusion **(a and b)** and with coronene inclusion **(c and d)**. Tunnelling parameters: (a) V_{bias} = −0.9 V, I_{set} = 50 pA, (b) V_{bias} = −1.2 V, I_{set} = 300 pA, (c) −1.2 V, I_{set} = 60 pA, (d) V_{bias} = −1.2 V, I_{set} = 300 pA. Unit cell parameters shown in both (b) and (d): a = b = 2.9 ± 0.2 nm, angle 60 ± 3°. Scale bars for (a) and (c) are 20 nm and for (b) and (d) are 3 nm. The schematic representations given in figure 86 are overlaid onto images (b) and (d) to highlight the arrangement of the molecules.

component solution prepared by combining 10–25 µL of saturated coronene solution with 100 µL of the binary stock solution from which the hexagonal coassembly of 4MeTFBA and 4TPTZ was prepared.

The striking parallels between the hexagonal networks formed with both 4BTFBA and 4MeTFBA give significant insight into the ambiguous arrangement of the molecules in the previously discussed 4BTFBA case. With 4MeTFBA, the interaction with the 4TPTZ molecules must be mediated by carboxyl–pyridine hydrogen bonding interactions, i.e., the arrangement is analogous to that in either figure 88a or 88b, simply because 4MeTFBA is not capable of partaking in halogen bonds. This strongly indicates that the interaction between the 4BTFBA and 4TPTZ molecules in the coassembly of these two molecules is also mediated by carboxyl–pyridine hydrogen bonding interactions rather than the alternative Br···N(pyridyl) halogen bonds. Were the 4BTFBA molecules to interact with the 4TPTZ molecules via such halogen bonds, it is unlikely that such clear isostructurality with the coassembly of 4MeTFBA and 4TPTZ would be observed, due to differences that would be expected in both the geometry and strength of Br···N(pyridyl) halogen bonds when compared with carboxyl–pyridine interactions. Furthermore, this result is also consistent with studies on analogous 3D systems, where hydrogen bonds are generally found to be preferred over halogen bonds.[185] Overall, the results with 4MeTFBA indicate that the coassembly of 4BTFBA with 4TPTZ has a structure consistent with either that presented in figure 88a or 88b. Although it remains unclear which of these two alternatives is preferred, the significant point in the context of this work is that carboxyl–pyridine hydrogen bonds are present rather than the alternative Br···N(pyridyl) halogen bonds. In this case halogen bonds seemingly play no role. It should be noted that in the possible arrangement shown in figure 88a, the bromine atoms of the 4BTFBA molecules are positioned such that they could feasibly interact with the carboxyl oxygen atoms of neighbouring 4BTFBA molecules via Br···O halogen bonds; however, the isostructurality observed with the analogous 4MeTFBA based system, where such Br···O halogen bonds are not possible, clearly undermines the potential significance of these interactions. In addition to carboxyl–pyridine hydrogen bonding interactions, the coassembly of 4BTFBA with 4TPTZ is also likely stabilised by secondary C–H···F and C–H···O interactions between neighbouring 4BTFBA and 4TPTZ molecules.

Although the formation of a network cooperatively driven by both halogen and hydrogen bonds was not realised by combining 4BTFBA with 4TPTZ, the results presented in this section do offer some insight. Although in principle the oxygen atoms of the 4BTFBA molecules do represent a viable acceptor site with which the bromine atoms/carboxyl groups of other 4BTFBA molecules could interact, the N(pyridyl) sites of the 4TPTZ molecules are expected to be the preferred acceptor sites for both halogen[193–199] and hydrogen[163,200–202] bonds. Thisplaces the two interactions in direct competition for the preferred N(pyridyl) sites. Evidently, within the coassembly of 4BTFBA and 4TPTZ,

the carboxyl groups dominate this competition, with carboxyl–pyridine hydrogen bonds being formed in preference to Br···N(pyridyl) halogen bonds. The results presented in this chapter also help to validate the experimental approach that has been employed. The isostructurality observed upon exchanging 4BTFBA for 4MeTFBA verifies that 4MeTFBA is an effective structural analogue for 4BTFBA. Accordingly, the approach of using 4MeTFBA as a structural analogue for 4BTFBA is further employed in the subsequent sections of this chapter.

8.3 Bimolecular self-assembly properties of 4BTFBA with 3TPTZ

Like 4TPTZ, 3TPTZ was also observed to coassemble with 4BTFBA at the 1-phenyloctane/HOPG interface. When using a solution composition prepared in exactly the same manner as that used with 4TPTZ in the preceding section, the formation of a hexagonal network was observed. As is shown in figure 90a, large domains of this hexagonal cosssembly were observed covering essentially the entire surface of the sample.

Within high-resolution STM images of the hexagonal coassembly of 3TPTZ and 4BTFBA, such as that shown in figure 90b, both the tripodal 3TPTZ molecules and the rodlike 4BTFBA molecules are resolved. As is highlighted in the overlay shown in in figure 90b, such images can be used to partially elucidate the arrangement of the molecules within the assembly. The 4BTFBA molecules are positioned such that they can interact with the N(pyridyl) atoms of the 3TPTZ molecules; however, as was the case in the coassembly of 4TPTZ and 4BTFBA discussed in the previous section, the orientation of the 4BTFBA molecules cannot be resolved. This makes it unclear if the 4BTFBA molecules interact with the 3TPTZ molecules via either Br···N(pyridyl) halogen bonds or carboxyl–pyridine interactions. The 4BTFBA molecules are again organised in such a manner that they define a series of hexagonal pores that appear to be extremely similar to the pores observed in the coassembly of 4BTFBA and 4TPTZ discussed in the preceding section. These pores are again seemingly occupied by mobile species, thought to be either coadsorbed solvent molecules or additional 4BTFBA molecules, which can clearly be seen in figure 90b. These occupants appear to be of limited structural significance, as is evidenced by the fact that they can be readily displaced by coronene guest molecules (see figures 90c and 90d). This could be easily achieved by depositing three-component solutions prepared by combining saturated 4BTFBA, saturated 3TPTZ and saturated coronene solutions in a ratio of 2:18:5, respectively.

In an effort to gain some insight into the precise orientation of the 4BTFBA molecules, the approach of using 4MeTFBA as a structural analogue for 4BTFBA was employed. The deposition of solutions

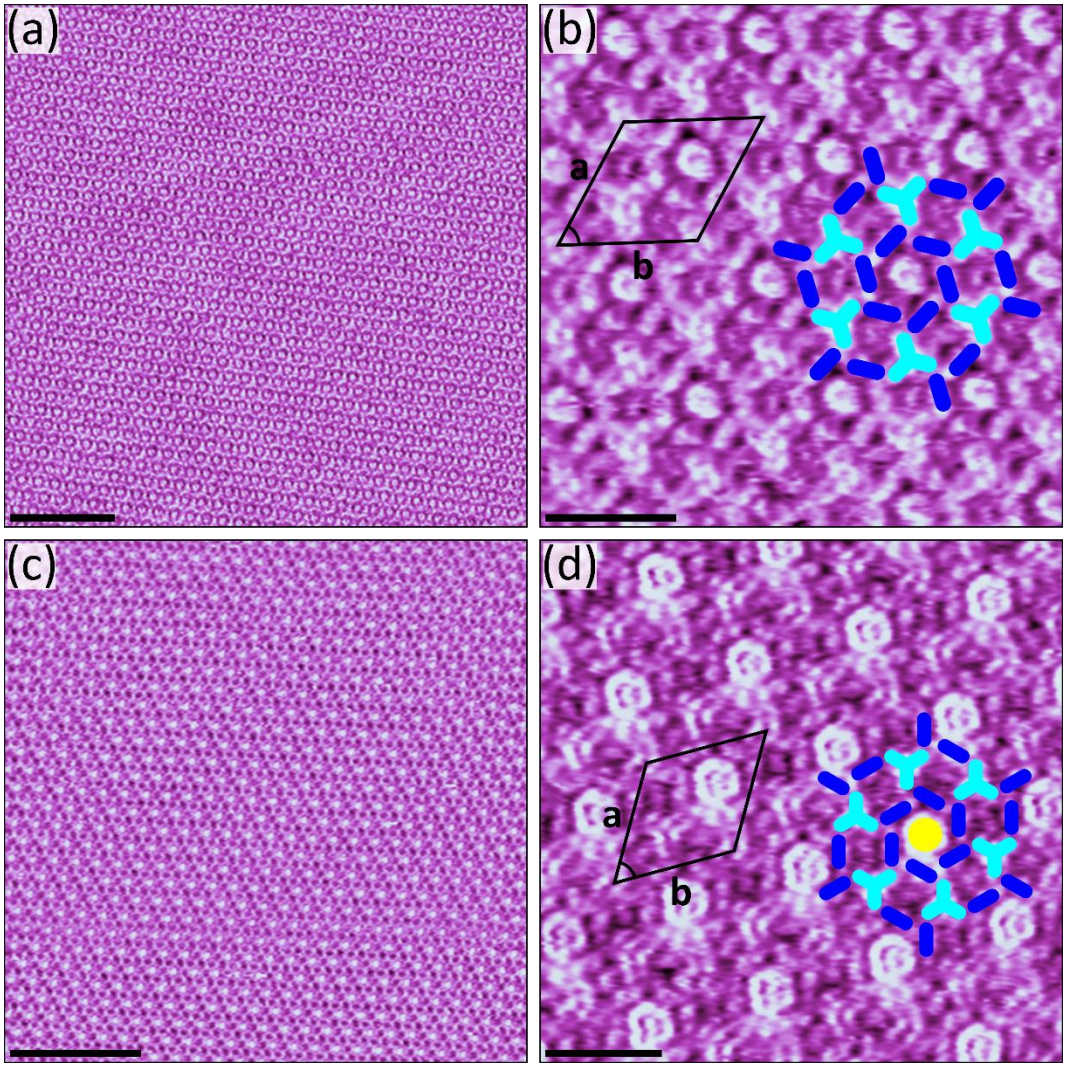

Figure 90: STM images showing the hexagonal coassembly of 4BTFBA and 3TPTZ at the 1-phenyloctane/HOPG interface without coronene inclusion **(a and b)** and with coronene inclusion **(c and d)**. Tunnelling parameters: (a) V_{bias} = −1.2 V, I_{set} = 70 pA, (b) V_{bias} = −1.2 V, I_{set} = 70 pA, (c) −1.2 V, I_{set} = 50 pA, (d) V_{bias} = −1.2 V, I_{set} = 100 pA. Unit cell parameters shown in both (b) and (d): a = b = 3.2 ± 0.3 nm, angle 60 ± 3°. Scale bars for (a) and (c) are 20 nm and for (b) and (d) are 3 nm. The schematic representations given in figure 86 are overlaid onto images (b) and (d) to highlight the arrangement of the molecules.

prepared by combining saturated 4MeTFBA solution and saturated 3TPTZ solution in a ratio of 1:1 leads to the formation of a rectangular network at the 1-phenyloctane/HOPG interface. Large domains of this rectangular network could be observed covering the surface of the sample. It is clear that this network differs from the hexagonal network formed by combining 4BTFBA and 3TPTZ. As can be seen in the high-resolution STM image shown in figure 91b, the 4MeTFBA molecules are positioned such that they can interact with the N(pyridyl) atoms of the 3TPTZ molecules. In this case, the interaction clearly must be mediated by carboxyl–pyridine hydrogen bonding interactions. Each 3TPTZ molecule interacts with two 4MeTFBA molecules in this manner. The rectangular arrangement of the involved molecules is highlighted in the proposed model shown in figure 91c. In addition to the carboxyl–

pyridine hydrogen bonding interactions, the assembly is also likely stabilised by secondary C−H···O and C−H···F interactions between neighbouring 4MeTFBA and 4TPTZ molecules.

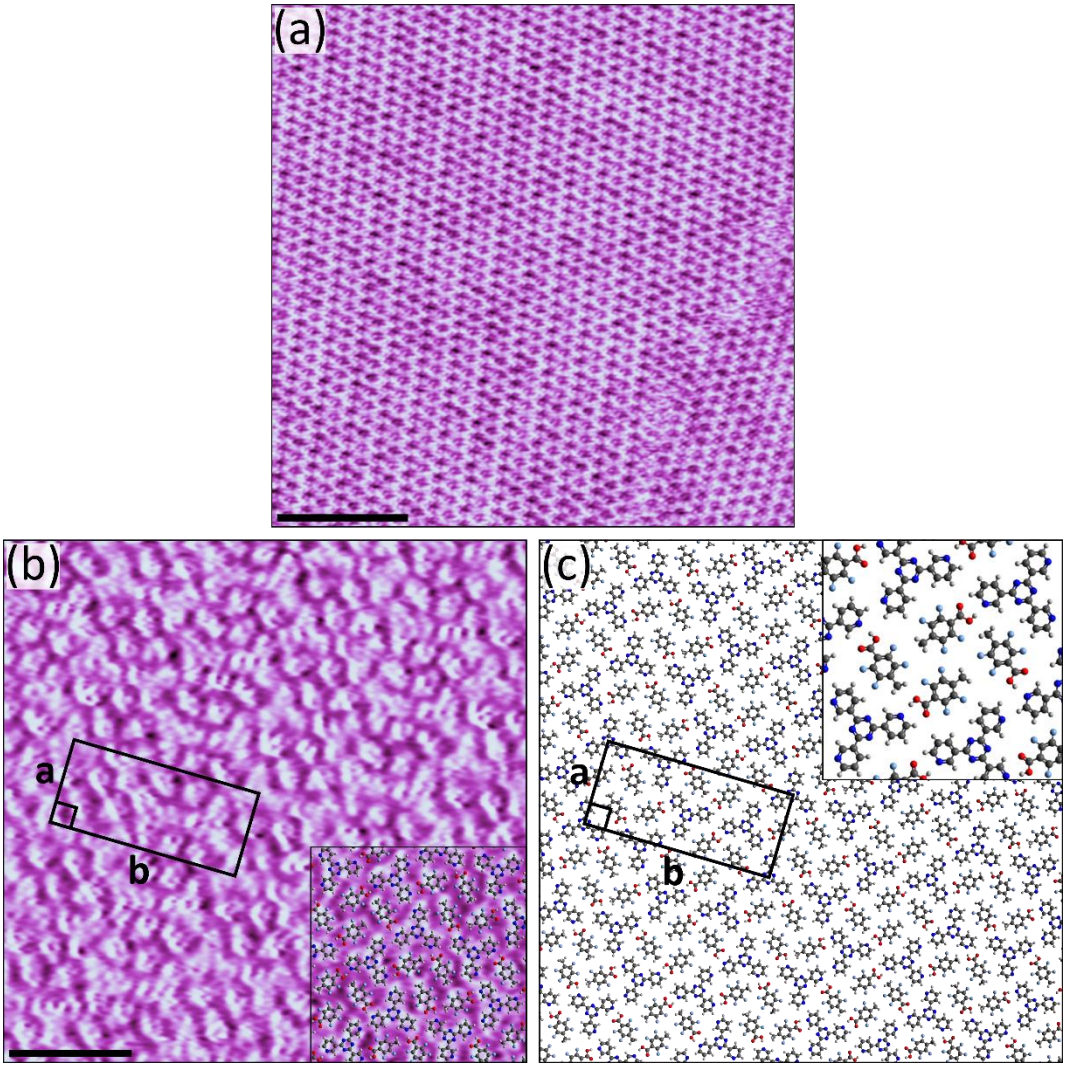

Figure 91: (a and b) STM images showing the rectangular coassembly of 4MeTFBA and 3TPTZ at the 1-phenyloctane/HOPG interface. Tunnelling parameters: (a) V_{bias} = −1.2 V, I_{set} = 300 pA, (b) V_{bias} = −0.9 V, I_{set} = 70 pA. Unit cell parameters: a = 2.1 ± 0.3 nm, b = 4.7 ± 0.3 nm, angle 90 ± 3°. Scale bar for (a) is 20 nm and (b) is 3 nm. **(c)** Proposed model for the assembly.

The 2:1 ratio of 4MeTFBA to 3TPTZ molecules in the rectangular coassembly of these two molecules differs from the corresponding 3:1 ratio (neglecting the identity of the mobile pore occupants) seen in the hexagonal coassembly of 4BTFBA and 3TPTZ. Therefore, in an effort to more fully explore if 4MeTFBA and 3TPTZ can coassemble in an isostructural manner to the hexagonal network observed with 4BTFBA and 3TPTZ, solutions in which the relative concentration of 4MeTFBA was increased were tested. However, even upon increasing the concentration of 4MeTFBA in the solution to its saturation point, whilst maintaining the concentration of 3TPTZ at 0.5 × saturated, the previously discussed rectangular network persists at the 1-phenyloctane/HOPG interface. This indicates that, unlike the situation observed with 4TPTZ in the previous section, 4MeTFBA and 4BTFBA cannot coassemble with

3TPTZ in an isostructural manner. Therefore, the orientation of the 4BTFBA molecules in the hexagonal coassembly of this molecule with 3TPTZ cannot be unambiguously deduced.

Although it is unclear if Br···N(pyridyl) halogen bonds or carboxyl–pyridine hydrogen bonding interactions are present in the hexagonal coassembly of 4BTFBA and 3TPTZ, the fact that each 4BTFBA molecule can only partake in one of these two interactions indicates that one interaction is preferred over the other. It should also be noted that the geometric relationship between the 4BTFBA molecules and the 3TPTZ molecules with which they are halogen/hydrogen bonding appears to be the same in all cases. This supports the idea that the 4BTFBA and 3TPTZ molecules consistently interact via the same one of the two possible interactions. The preference for one of the two interactions hints that there may be some competitive interplay, with one interaction dominating the other for the optimal N(pyridyl) acceptor sites. Although no concrete conclusions can be drawn from the experiments conducted with 4MeTFBA, it should be noted that it seems extremely likely that the preferred interaction in which the N(pyridyl) sites of the 3TPTZ molecules are partaking is the carboxyl–pyridine hydrogen bonding interaction. As was discussed in the previous section, within 3D systems carboxyl–pyridine hydrogen bonds typically occur in preference to halogen bonds. Even more telling though is the extremely obvious structural similarity between the manner in which the 4BTFBA molecules are arranged in the coassembly of 4BTFBA and 4TPTZ (see section 8.1) and in the hexagonal coassembly of 4BTFBA and 3TPTZ. In both cases the 4BTFBA molecules are organised into seemingly identical hexagonal arrangements, which define the pores within which the coronene molecules can be captured. Given that in the coassembly 4BTFBA with 4TPTZ it is clear that carboxyl–pyridine interactions are present rather than Br···N(pyridyl) halogen bonds (see section 8.1), it is likely that this is also true for the hexagonal coassembly of 4BTFBA with 3TPTZ. Were the 4BTFBA molecules to be orientated in a different manner within the two networks, it is unlikely that these molecules would be organised into essentially identical hexagonal arrangements in both cases.

One factor which has not yet been discussed is the stability of the hexagonal coassembly of 4BTFBA and 3TPTZ. Several hours after its formation, the hexagonal network was typically observed to spontaneously convert to a seemingly more thermodynamically favourable rectangular structure. Interestingly, this conversion was never observed during experiments in which coronene was included in the pores of the hexagonal assembly, which indicates that the presence of coronene provides some stabilisation. The rectangular structure could also be directly formed, i.e., without the preceding hexagonal assembly, by depositing solutions with a reduced relative concentration of 4BTFBA. These solutions were typically prepared by combining saturated 4BTFBA solution with saturated 3TPTZ solution in a ratio of 1:99 or by combining 0.01 M 4BTFBA solution with saturated 3TPTZ solution in a

ratio of 1:9. Figure 92a shows an example of a large-scale STM image of the rectangular coassembly of 4BTFBA and 3TPTZ.

Figure 92b shows a high-resolution STM image of the rectangular coassembly of 4BTFBA and 3TPTZ in which both molecules can be clearly resolved. The situation in this case differs markedly from that observed in either of the other networks formed with 4BTFBA in this chapter. Here, the 4BTFBA molecules are positioned such that they can bridge two 3TPTZ molecules by interacting with them via a Br···N(pyridyl) halogen bond at one end and a carboxyl–pyridine hydrogen bonding interaction at the other. Note that for these interactions to occur, the 3TPTZ molecules must be in their non-threefold-symmetric conformation (see section 4.1). It should also be noted that the orientation of the 4BTFBA molecules cannot be identified within the STM images. However, in this case their precise orientation is not significant as the positioning of these molecules is such that they can simultaneously partake in both Br···N(pyridyl) halogen bonds and carboxyl–pyridine hydrogen bonding interactions irrespectively of their exact orientation. Two of the N(pyridyl) sites in each 3TPTZ molecule interact with 4BTFBA molecules via these interactions. The remaining N(pyridyl) sites are positioned such that they can interact with neighbouring 3TPTZ molecules via weak C–H···N(pyridyl) interactions. There is also likely a stabilising contribution from weak C–H···F and C–H···O interactions between the 4BTFBA and 3TPTZ molecules.

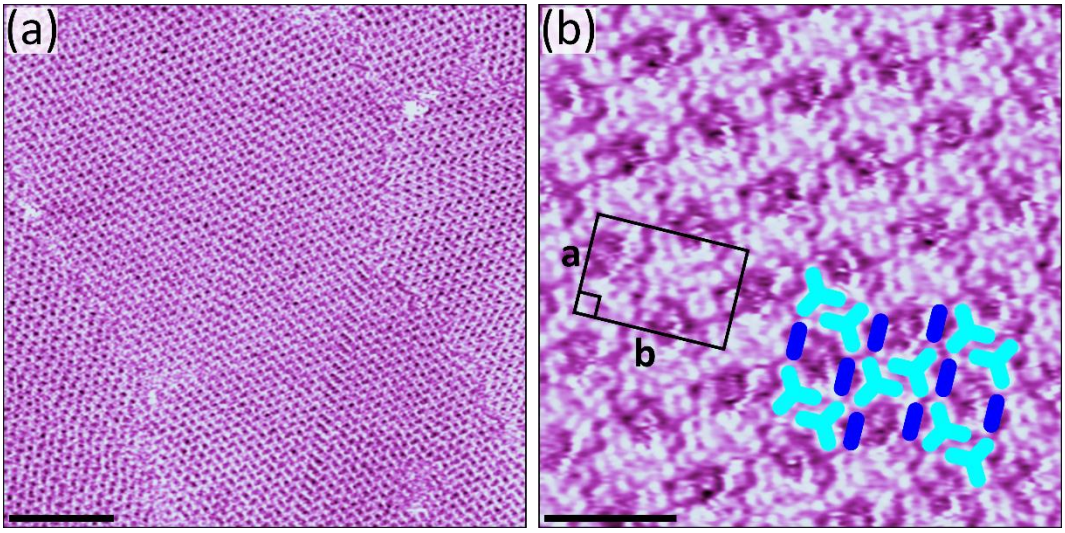

Figure 92: STM images showing the rectangular coassembly of 4BTFBA and 4TPTZ at the 1-phenyloctane/HOPG interface. Tunnelling parameters: (a) V_{bias} = −0.9 V, I_{set} = 50 pA, (b) V_{bias} = −1.2 V, I_{set} = 300 pA. Unit cell parameters: a = 2.3 ± 0.2 nm, b = 3.5 ± 0.3 nm, angle 90 ± 3°. Scale bar for (a) is 20 nm and (b) is 3 nm. The schematic representations given in figure 86 are overlaid onto image (b) to highlight the arrangement of the molecules.

One distinctive structural feature of the rectangular coassembly of 4BTFBA with 3TPTZ, which has hitherto not been discussed, is the extensive presence of defects. As was discussed in section 4.2, the non-threefold-symmetric conformation of 3TPTZ, which is the conformation present in the

rectangular coassembly, becomes chiral upon adsorption. The rectangular assembly of 4BTFBA and 3TPTZ can be described as a series of parallel rows which are closely packed together side-by-side. The arrangement of the molecules in one of these rows is highlighted schematically in figure 93a alongside its mirror image. Due to the chiral nature of the adsorbed 3TPTZ molecules, the row structure and its mirror image are enantiomorphs. However, the chirality does not manifest itself in the arrangement of the molecules on the outer edges of the rows. As a result, any combination of the two different enantiomorphs can be packed together side-by-side, seemingly without significant alteration to the interactions that can occur between the edges of adjacent rows. The assembly can only be accurately described as rectangular when the two enantiomorphous row structures alternate. Such a situation occurs in the region of the assembly shown in figure 92b, and this effect is highlighted clearly in figure

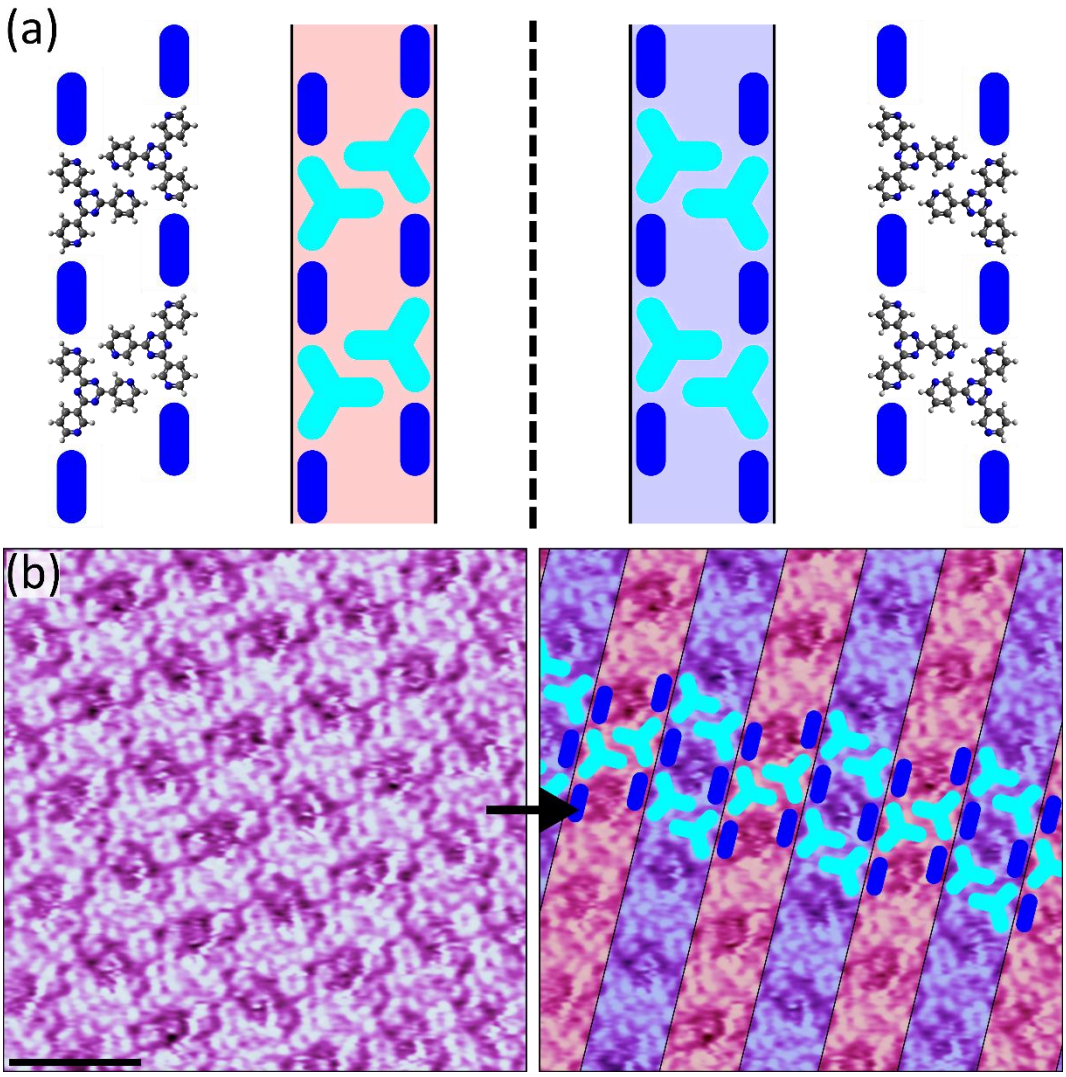

Figure 93: (a) Schematic illustration highlighting the two different enantiomorphous forms of the rows present in the rectangular coassembly of 4BTFBA and 3TPTZ. **(b)** The same STM image as that shown in figure 92b, alongside the corresponding schematic representation, consistent with that shown in (a), which highlights the alternating pattern of enantiomorphous row structures within this region.

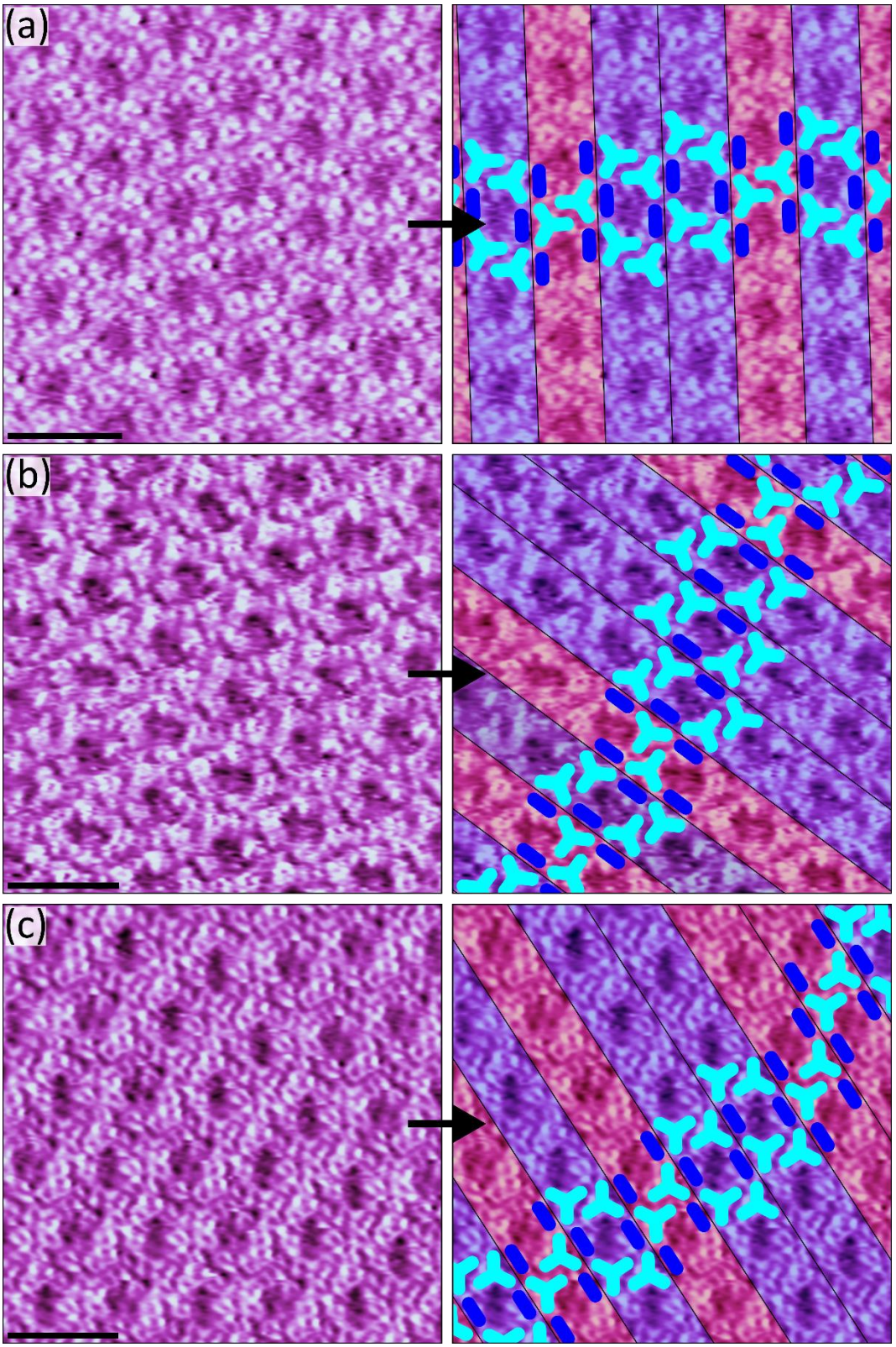

Figure 94: (a–c) A series of STM images showing defective regions of the rectangular coassembly of 4BTFBA and 3TPTZ at the 1-phenyloctane/HOPG interface. These images are shown alongside their corresponding schematic representations, consistent with that shown in figure 93a, which highlights the deviation from the alternating pattern of enantiomorphous row structures within these regions. Tunnelling parameters: (a) V_{bias} = −1.2 V, I_{set} = 50 pA, (b) V_{bias} = −0.9 V, I_{set} = 70 pA. (c) V_{bias} = −0.9 V, I_{set} = 50 pA. All scale bars = 3 nm.

93b. Although such an alternating pattern was generally observed, the presence of defects in which this alternating pattern is broken were very frequently encountered. Figure 94 shows a variety of different STM images in which a range of such defects can be seen.

Irrespectively of the presence of the aforementioned defects, the positioning of the molecules within the assembly visually seems to be consistent with the cooperative action of Br···N(pyridyl) halogen bonds and carboxyl–pyridine hydrogen bonding interactions. The structural role of the carboxyl–pyridine hydrogen bonding interactions seems to be particularly clear-cut. These interactions have been shown to be a highly reliable interaction for controlling the organisation of 2D surface-confined networks throughout this thesis (see chapters 5 and 7 and the preceding discussion in this chapter). However, the true significance of the proposed Br···N(pyridyl) halogen bonds remains unclear. These interactions are expected to be somewhat weaker than the carboxyl–pyridine hydrogen bonding interactions, and their true influence in controlling the organisation of the molecules within the assembly is uncertain. Their apparent presence could simply be a geometric consequence of the other intermolecular interactions within the assembly. In order to explore the significance of the proposed Br···N(pyridyl) halogen bonds, additional experiments using 4MeTFBA as a structural analogue of 4BTFBA were performed. If a network which is isostructural with the rectangular coassembly of 4BTFBA and 3TPTZ can be formed after exchanging 4BTFBA for 4MeTFBA, the proposed Br···N(pyridyl) halogen bonds, which are not possible with 4MeTFBA, are not likely structurally significant. As was shown earlier in this chapter, 4MeTFBA and 3TPTZ coassemble into a rectangular network in which the two components are present in a ratio of 2:1, respectively. As the ratio of 4BTFBA to 3TPTZ in the rectangular coassembly of these two molecules is only 1:1, solutions of 4MeTFBA and 3TPTZ

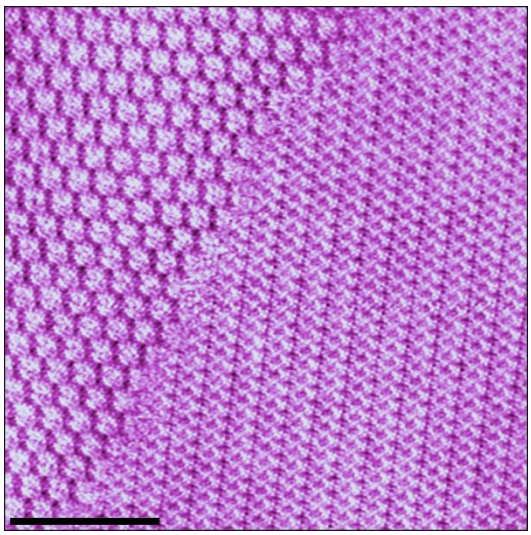

Figure 95: Large-scale STM image showing the coassembly of 4MeTFBA and 3TPTZ at the 1-phenyloctane/HOPG interface. The hexagonal (domain on the left side of the image) and oblique (domain on the right side of the image) phases can be seen coexisting. Tunnelling parameters: V_{bias} = −0.9 V, I_{set} = 50 pA. Scale bar = 20 nm.

containing a lower relative concentration of 4MeTFBA than that used to form the 2:1 rectangular structure were tested. Upon deposition of such a solution, prepared by combining saturated 4MeTFBA solution with saturated 3TPTZ solution in a ratio of 1:11, respectively, two distinct 1:1 stoichiometry structures were observed at the 1-phenyloctane/HOPG interface. One of these structures has hexagonal symmetry, whereas the other is oblique. As is shown in figure 95, these two structures could be observed coexisting on the surface.

Within high-resolution STM images of the hexagonal coassembly, both the 4MeTFBA and 3TPTZ molecules can be clearly resolved (see figure 96). Interestingly, this network appears to be isostructural with the hexagonal assembly formed when 3TPTZ is deposited alone from heptanoic acid (see section 4.4). Here, the 4MeTFBA molecules take the place of the coadsorbed heptanoic acid molecules present in the assembly discussed in section 4.4. The 3TPTZ molecules are organised into the same cyclic structures, composed of six 3TPTZ molecules, via weak C–H···N(pyridyl) interactions. Two of the N(pyridyl) atoms in each 3TPTZ molecule are involved in these interactions. The remaining N(pyridyl) sites interact with the 4MeTFBA molecules via strong carboxyl–pyridine hydrogen bonding interactions. In addition, there is also likely a stabilising contribution from secondary C–H···F and C–H···O interactions between the 4MeTFBA and 3TPTZ molecules.

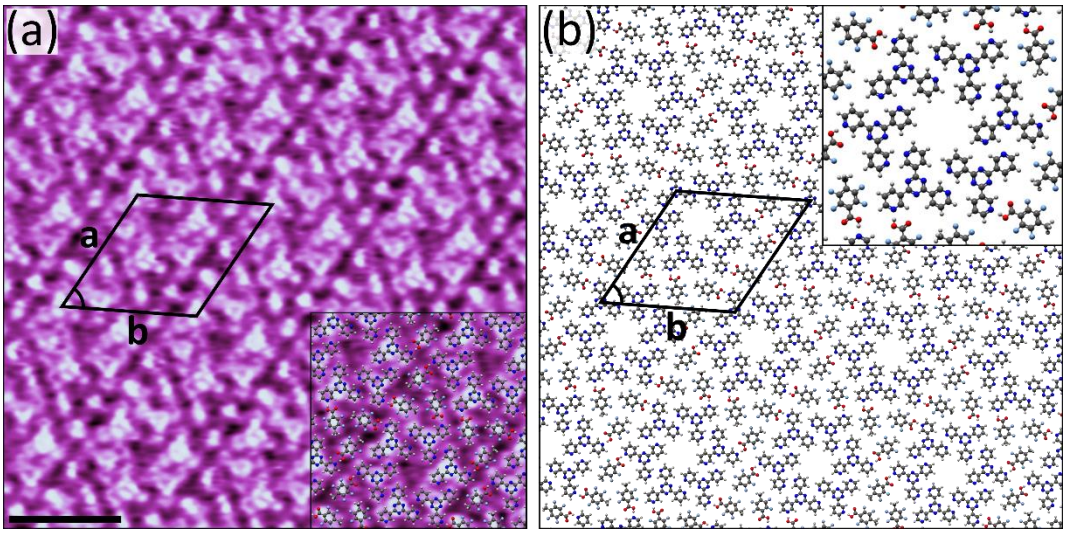

Figure 96: (a) STM image showing the hexagonal coassembly of 4MeTFBA and 3TPTZ at the heptanoic acid/HOPG interface. Tunnelling parameters: V_{bias} = −0.9 V, I_{set} = 70 pA. Unit cell parameters: a = b = 3.6 ± 0.3 nm, angle = 60 ± 3°. Scale bar = 3 nm. **(b)** Proposed model for the assembly.

A high-resolution STM image of the oblique coassembly of 4MeTFBA and 3TPTZ is shown in figure 97. It is worth noting that the unit cell dimensions of this seemingly oblique network are within error of having rectangular symmetry and are not too dissimilar from those of the rectangular coassembly of 4BTFBA with 3TPTZ. Despite this, high-resolution STM images reveal that the arrangement of the

molecules within the two networks differs markedly. Each 3TPTZ molecule is positioned such that it can hydrogen bond to a single 4MeTFBA molecule via a carboxyl–pyridine interaction. The methyl groups of the 4MeTFBA molecules are not orientated towards the N(pyridyl) atoms of neighbouring 3TPTZ molecules, as would be required for the formation of a network isostructural with the rectangular coassembly of 4BTFBA and 3TPTZ. The N(pyridyl) atoms of the 3TPTZ molecules that do not interact with the 4MeTFBA molecules are positioned such that they can interact with neighbouring 3TPTZ molecules via C–H···N(pyridyl) interactions. There is likely also an additional stabilising contribution from weak C–H···F and C–H···O interactions between the 3TPTZ and 4MeTFBA molecules. The proposed model for the assembly is given in figure 97b. Note that the conformation (see section 4.1) and enantiomorphous configuration (see section 4.2) of the 3TPTZ molecules cannot be resolved within the STM images. In the proposed model these were selected such that the number of favourable C–H···N(pyridyl) interactions is maximised.

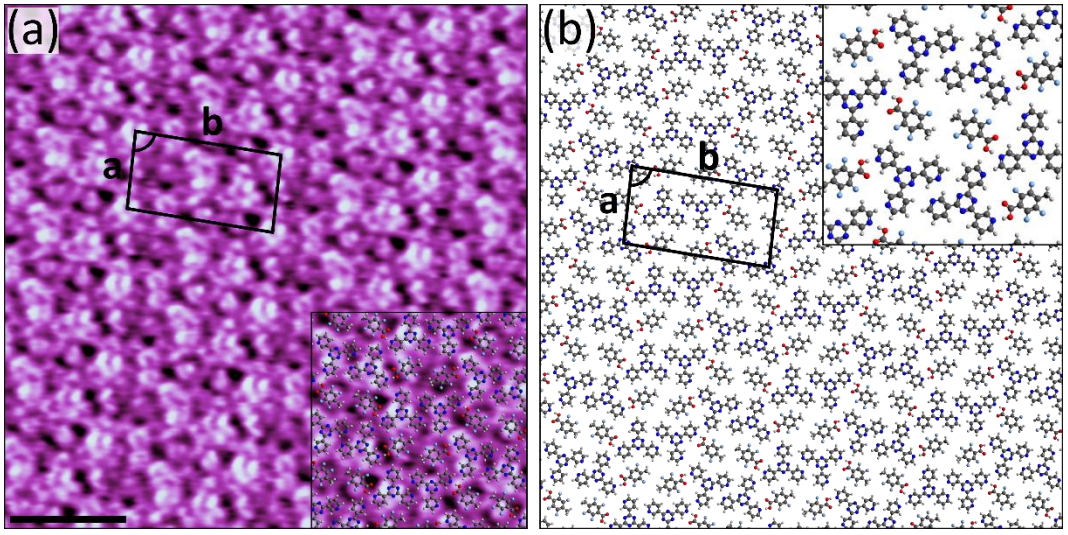

Figure 97: (a) STM image showing the oblique coassembly of 4MeTFBA and 3TPTZ at the heptanoic acid/HOPG interface. Tunnelling parameters: V_{bias} = −0.9 V, I_{set} = 70 pA. Unit cell parameters: a = 2.0 ± 0.3 nm, b = 3.8 ± 0.3 nm, angle 87 ± 3°. Scale bar = 3 nm. **(b)** Proposed model for the assembly.

The hexagonal and oblique networks formed by combining 4MeTFBA and 3TPTZ give significant insight into the rectangular coassembly of 4BTFBA and 3TPTZ. All three systems have equivalent stoichiometry. Furthermore, both networks formed using 4MeTFBA appear to be stabilised by carboxyl–pyridine, C–H···N(pyridyl), C–H···F and C–H···O interactions, i.e., all of the interactions that are seemingly present in the rectangular coassembly of 4BTFBA and 3TPTZ, other than Br···N(pyridyl) halogen bonds. The fact that both networks formed with 4MeTFBA are so structurally different from the rectangular coassembly of 4BTFBA and 3TPTZ, with the only obvious difference being the absence of Br···N(pyridyl) halogen bonds, clearly indicates that Br···N(pyridyl) halogen bonds play a significant structural role in the latter case. This system seems to be a clear-cut example of one in which both

halogen and hydrogen bonds simultaneously play a significant structural role. Rather than one interaction completely outcompeting the other for the optimal N(pyridyl) acceptor sites, these sites are shared.

8.4 Conclusions

The cooperative use of both halogen and hydrogen bonds clearly represents an interesting strategy for controlling the morphology of 2D surface-confined networks. However, understanding the precise interplay between these interactions appears to be somewhat difficult. The presence of the favourable carboxyl–pyridine hydrogen bonding interactions seems to be extremely predictable, with these interactions occurring in all of the networks discussed within this chapter. These results are consistent with those presented in chapters 5 and 7, where the same interaction was observed to occur with extremely high reliability when using fluorinated carboxylic acids which are structurally similar to 4BTFBA. The presence of Br···N(pyridyl) halogen bonds in the systems formed with 4BTFBA does not occur with comparable reliability, with these halogen bonds seemingly only being present in a single one of the three such networks discussed in this chapter.

Chapter 9: Overall conclusions and perspectives

9.1 Conclusions

In this thesis, the self-assembly behaviour of a range of different fluorinated compounds has been explored at the solid–liquid interface. This was done with the aim of gaining insight into the potential value of such compounds in the context of surface-confined supramolecular chemistry. Factors including the steric impact of fluorination and the role of intermolecular interactions both directly and indirectly involving fluorine atoms were considered. Although in a few of the examined systems the supramolecular role of the fluorine atoms was found to be quite subtle, in general, it was shown that the fluorine atoms play a prominent structural role.

One recurring theme discussed in this thesis is the minimal steric impact associated with exchanging fluorine and hydrogen. This is best exemplified in chapter 3, where the precise size and shape complementarity required for coronene to effectively template the formation of cyclic hexameric arrangement of IPA was also observed for the fluorinated analogue F4IPA. This effect was similarly observed in chapter 5, where both TPA and its fluorinated analogue F4TPA were found to coassemble with 4TPTZ into isostructural networks. Although exchanging hydrogen and fluorine atoms can dramatically influence the self-assembly behaviour of a given molecule, in these cases the impact is clearly more subtle. These results indicate that, via the judicious exchange of hydrogen and fluorine atoms, it may be possible to fluorinate certain molecular building blocks without altering the manner in which they organise on the surface.

Particular value was also found in the ability of fluorination to augment other intermolecular interactions which are rarely or hitherto unreported as a driving force for 2D surface-confined self-assembly. This was first explored in chapter 5, where fluorination was shown to significantly promote the formation of bicomponent carboxylic acid–pyridine systems. In chapter 6, this approach was then extended to the formation of analogous phenol–pyridine systems. Fluorination was again found to be advantageous, allowing for the formation of 2D phenol–pyridine networks, which had hitherto not been realised. The precise mechanism for how fluorination promotes the formation of these networks remains somewhat unclear. In both cases, the primary interactions controlling the organisation of the molecular building blocks appear to be hydroxyl–pyridine hydrogen bonding interactions. Although it seems likely that the electron withdrawing influence of the fluorine atoms strengthens these interactions, the introduction of fluorine atoms also allows for the potential formation of additional stabilising C–H···F interactions. It is likely a combination of these two factors that results in the

improved performance of the fluorinated analogues. Regardless of the precise nature of the mechanism at play, these results provide a clear strategy towards the reliable formation of bicomponent carboxyl acid–pyridine and phenol–pyridine 2D surface-confined networks. Analogous 3D structures are amongst the most widely studied systems in the field of crystal engineering, and the results presented here offer a promising route towards extending their diverse supramolecular chemistry from traditional 3D crystals to 2D surface-confined networks.

The knowledge gained in chapters 5 and 6 was then applied in chapter 7, where the interplay between the carboxylic acid–pyridine and phenol–pyridine hydrogen bonding interactions was explored. This was achieved through the use of a simple fluorinated molecular building block, namely 4HTFBA, capable of simultaneously participating in both of these interactions. 4HTFBA was found to coassemble with a range of pyridyl type acceptors into 2D surface-confined networks. Within some of these systems, both carboxyl–pyridine and phenol–pyridine hydrogen bonding interactions are present, with these interactions cooperatively controlling the organisation of the molecules within the assembly; however, in other cases, one of the two interactions occurs in preference over the other. Factors including sterics and the concentrations of the building blocks in solution were found to influence the balance between these two behaviours. A parallel study was also performed in chapter 8, where the interplay between carboxyl–pyridine hydrogen bonding interactions and halogen bonds was explored. This was achieved by coupling the bifunctional molecule 4BTFBA, which is capable of partaking in both halogen and hydrogen bonds, with pyridine functionalised molecules. Fluorination also plays a crucial role in the structure of 4BTFBA as it not only promotes the formation of carboxylic acid–pyridine hydrogen bonding interactions but concurrently activates the molecule towards halogen bond formation. With 4BTFBA, the formation of only a single structure clearly involving the cooperative action of carboxylic acid–pyridine interactions and halogen bonds was realised, with there seemingly being more of a competitive interplay in the other networks that were observed. The results presented in chapters 7 and 8 provide insight into the cooperative and competitive balance between different intermolecular interactions and the factors that influence this behaviour. This is particularly valuable with the strong and directional interactions discussed here, for which identifying asymmetries in their behaviour may present a multitiered strategy towards the formation of more complex 2D surface-confined networks.

Throughout this thesis, diverse array of different systems have been reported in which the presence of fluorine atoms plays a crucial supramolecular role. Many of these are relatively complex multicomponent networks stabilised by intermolecular interactions not typically observed in such systems. Although these ideas are well supported by the experimental data presented in this thesis, a more detailed theoretical understanding would offer significant insight. This is particularly true in

chapters 5, 6 and 7, where the precise role of fluorination in promoting the hydroxyl–pyridine hydrogen bonding interactions that are observed remains somewhat unclear. Future theoretical work should offer significant insight into these issues.

9.2 Perspectives

The results presented in this thesis are rather unprecedented. As such, there is significant room for further development. One consistent observation which could be of value is the negligible steric impact associated with interchanging hydrogen and fluorine atoms. This provides a potential route towards fine-tuning the chemical properties of 2D networks without altering the organisation of their constituent molecules. Such an approach could be particularly effective in the field of host–guest chemistry, where the binding affinity of guest molecules may be adjusted by fluorination of the molecular building blocks of the host network. Crucially, fluorination could allow this to be done without perturbation to the dimensions of the pores, the shape and size of which is often critical for effective guest capture.

In chapters 5 and 6 it was shown that fluorination can be used to promote the formation of bicomponent carboxylic acid–pyridine and phenol–pyridine surface-confined networks. This approach is straightforward, intuitive and is likely to be very general. Accordingly, it seems probable that the foundational work presented here could be readily expanded upon and the construction of other carboxylic acid–pyridine and phenol–pyridine 2D systems could be realised. Furthermore, although this work has focused largely on the ability of fluorination to promote hydroxyl–pyridine hydrogen bond formation, there is no clear reason why this approach could not be applied to other classes of hydrogen bonding interactions. Exploring this could even further expand the toolbox of intermolecular interactions available in the field of 2D supramolecular chemistry.

The use of bifunctional molecular building blocks in the manner explored in chapters 7 and 8 also highlights an area ripe for further expansion. Such building blocks offer a promising multitiered strategy towards the formation of complex supramolecular structures, and the ability of molecular fluorination to simultaneously augment various intermolecular interactions can clearly play a significant role in this area. Furthermore, these studies also provide insight into the factors which influence the cooperative and competitive balance between different intermolecular interactions within 2D supramolecular structures. One significant factor seen in chapter 7 is sterics, where carboxylic hydroxyl groups are readily able to hydrogen bond to the sterically hindered acceptor 2TPTZ whereas phenolic hydroxyl groups are not. This steric bias provides a clear rationale for designing

bifunctional molecular building blocks which can interact with different acceptors in a predictable manner. Establishing similar patterns between other intermolecular interactions would further expand these ideas, potentially allowing for the routine use of multifunctional building blocks for the construction of complex multicomponent networks. As such, further studies on bifunctional building blocks which utilise additional intermolecular interactions and different pairings of the intermolecular interactions explored here would be of significant interest. The methodology outlined here provides a clear guide for such studies.

Overall, the results presented in this thesis highlight the rich supramolecular potential that fluorinated compounds have in the field of surface-confined supramolecular chemistry. This has been shown to extend into prominent areas including multicomponent self-assembly and host–guest chemistry. Further expansion of this foundational work could lead to significant developments in the field of surface-confined supramolecular chemistry.

Chapter 10: Experimental details

Within this chapter, the technical details of the experiments performed are discussed. Details of the precise experimental setup are given. The methods used for sample preparation and data analysis are also discussed.

10.1 STM setup

All STM measurements were performed in constant current mode using a Veeco STM equipped with an A-type scanner head, coupled with an Nanoscope E controller. Measurements were performed under ambient conditions. The temperature at which the measurements were conducted was typically within the range of 21–23°C. The bias voltage was applied to the sample. Considering recent results which demonstrate the profound impact that bias voltage can have on self-assembled networks formed at the solid–liquid interface,[203] it was ensured that a range of different voltages at both polarities were tested. No evidence of any bias-voltage-induced polymorphism was observed. Negative sample bias voltages were generally observed to yield superior resolution images. For the majority of the networks shown in this thesis, positive sample bias voltages often seemed to disrupt the assembly. The tunnelling parameters used to obtain each of the presented images are given in the corresponding figure captions. STM tips were prepared by mechanically cutting 80/20 Pt/Ir wire (Goodfellow). Various measures were taken to eliminate external sources of noise from the setup. As is shown in figure 98, the STM setup was housed in an electrically grounded metallic box. This helps to isolate the apparatus from external sources of electrical noise. Furthermore, the STM is suspended via the use of bungee cords and the interior of the metallic box is lined with soundproof foam. Both of these measures help to isolate the apparatus from mechanical vibrations.

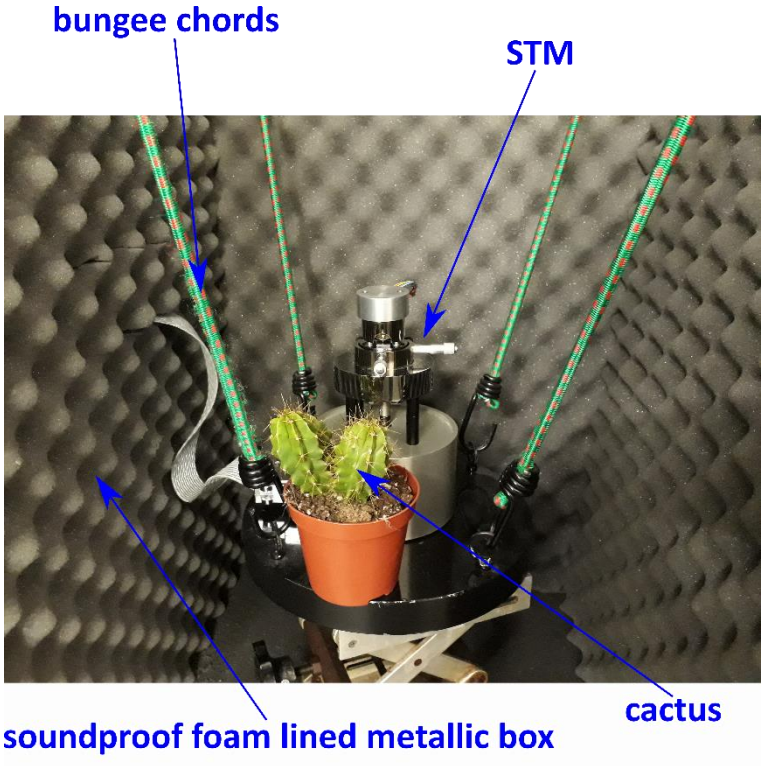

Figure 98: Photograph showing the STM setup used. The key components are labelled.

10.2 Sample preparation

HOPG substrates (TipsNano, ZYB) were freshly prepared prior to each experiment by cleaving the upper layers using adhesive tape. The solutions from which the discussed networks were observed to self-assemble were prepared by dissolving an appropriate quantity of solid material in the corresponding solvent via sonication and, when required, very gentle heating. Unless otherwise stated, the volume of the droplet of solution deposited onto the HOPG substrate for each experiment was approximately 10–15 µL.

10.3 Chemicals

All of the chemicals discussed throughout this thesis, other than 4TPTZ, were obtained from commercial suppliers and used without further purification. The following list gives the source and listed purity for each of the chemicals used.

- IPA (CAS: 121-91-5) Sigma-Aldrich, 99%
- Heptanoic acid (CAS: 111-14-8) Acros Organics, 98%
- Coronene (CAS: 191-07-1) Sigma-Aldrich, 97%
- F4IPA (CAS: 1551-39-9) Fluorochem, 98%
- 2TPTZ (CAS: 3682-35-7) Fluorochem, 99%
- 3TPTZ (CAS: 42333-76-6) Alfa Aesar, 97%
- 1-phenyloctane (CAS: 42333-78-8) Acros Organics, 99%
- TPA (CAS: 42333-78-8) Sigma, 98%
- F4TPA (CAS: 100-21-0) Fluorochem, 97%
- HQ (CAS: 123-31-9) Acros Organics, 99.5%
- TFHQ (CAS: 771-63-1) Alfa Aesar, 96%
- 4HTFBA (CAS: 652-34-6) Alfa Aesar, 97%
- 4BTFBA (CAS: 4707-24-8) Alfa Aesar, 97%
- 4MeTFBA (CAS: 652-32-4) Fluorochem, 97%

4TPTZ (CAS: 42333-78-8) was kindly synthesised by Dr. Graham Pattison according to the following procedure:

A mixture of 4-cyanopyridine (1.0 g, 9.6 mmol), 18-crown-6 (0.1 g, 0.38 mmol) and potassium hydroxide (22.5 mg, 0.40 mmol) was dissolved in decalin (1.0 cm3) and heated with stirring at 200 °C under nitrogen for 3 h. The solvent was evaporated under high vacuum to give a brown solid. This was

washed with hot pyridine (3 x 5.0 cm3) to leave white crystals, which were dissolved in 2.0 M hydrochloric acid (5.0 cm3). Addition of aqueous ammonia led to the precipitation of a white solid which was filtered and dried under high vacuum; yield 0.65 g (65%). 1H NMR (400 MHz, CDCl3,) 8.56 (6 H, d, J = 5.6 Hz) and 8.94 (6 H, d, J = 5.6 Hz)

10.4 Data analysis

All STM images were analysed using WsXM[204] and LMAPper[205]. The effects of thermal drift were eliminated, thereby allowing accurate lattice parameters to be obtained, by using the underlying HOPG surface as an internal calibration grid. Partway through recording an STM image of the molecular overlayer, the tunnelling parameters were adjusted such that atomic resolution of the underlying surface was achieved. The resulting image simultaneously contains both molecular resolution of the overlayer and atomic resolution of the underlying HOPG substrate. These images were then calibrated using the known lattice parameters of the HOPG surface. From these accurately calibrated images, the lattice parameters for the molecular overlayer can be determined. These accurately determined lattice parameters were used to calibrate all of the high-resolution STM images shown throughout this thesis.

References

1. Králik, M. Adsorption, chemisorption, and catalysis. *Chem. Pap.* **68**, 1625–1638 (2014).
2. Xie, Z. X., Xu, X., Mao, B. W. & Tanaka, K. Self-Assembled Binary Monolayers of *n* -Alkanes on Reconstructed Au(111) and HOPG Surfaces. *Langmuir* **18**, 3113–3116 (2002).
3. Katsonis, N., Marchenko, A. & Fichou, D. Substrate-Induced Pairing in 2,3,6,7,10,11-Hexakis-undecalkoxy-triphenylene Self-Assembled Monolayers on Au(111). *J. Am. Chem. Soc.* **125**, 13682–13683 (2003).
4. Kudernac, T. *et al.* Intermolecular Repulsion through Interfacial Attraction: Toward Engineering of Polymorphs. *J. Am. Chem. Soc.* **131**, 15655–15659 (2009).
5. Balandina, T. *et al.* Role of Substrate in Directing the Self-Assembly of Multicomponent Supramolecular Networks at the Liquid–Solid Interface. *ACS Nano* **6**, 8381–8389 (2012).
6. Greenwood, J. *et al.* Covalent Modification of Graphene and Graphite Using Diazonium Chemistry: Tunable Grafting and Nanomanipulation. *ACS Nano* **9**, 5520–5535 (2015).
7. Lei, S. *et al.* One Building Block, Two Different Supramolecular Surface-Confined Patterns: Concentration in Control at the Solid–Liquid Interface. *Angew. Chem. Int. Ed.* **47**, 2964–2968 (2008).
8. Yang, Y. & Wang, C. Solvent effects on two-dimensional molecular self-assemblies investigated by using scanning tunneling microscopy. *Curr. Opin. Colloid Interface Sci.* **14**, 135–147 (2009).
9. Lackinger, M., Griessl, S., Heckl, W. M., Hietschold, M. & Flynn, G. W. Self-Assembly of Trimesic Acid at the Liquid−Solid Interfacea Study of Solvent-Induced Polymorphism. *Langmuir* **21**, 4984–4988 (2005).
10. Dong, L., Gao, Z. & Lin, N. Self-assembly of metal–organic coordination structures on surfaces. *Prog. Surf. Sci.* **91**, 101–135 (2016).

11. Tahara, K., Lei, S., Adisoejoso, J., De Feyter, S. & Tobe, Y. Supramolecular surface-confined architectures created by self-assembly of triangular phenylene–ethynylene macrocycles via van der Waals interaction. *Chem. Commun.* **46**, 8507–8525 (2010).

12. Slater, A. G., Perdigão, L. M. A., Beton, P. H. & Champness, N. R. Surface-Based Supramolecular Chemistry Using Hydrogen Bonds. *Acc. Chem. Res.* **47**, 3417–3427 (2014).

13. De Feyter, S. & De Schryver, F. C. Two-dimensional supramolecular self-assembly probed by scanning tunneling microscopy. *Chem. Soc. Rev.* **32**, 139–150 (2003).

14. Lackinger, M. & Heckl, W. M. Carboxylic Acids: Versatile Building Blocks and Mediators for Two-Dimensional Supramolecular Self-Assembly. *Langmuir* **25**, 11307–11321 (2009).

15. Ivasenko, O. & Perepichka, D. F. Mastering fundamentals of supramolecular design with carboxylic acids. Common lessons from X-ray crystallography and scanning tunneling microscopy. *Chem. Soc. Rev.* **40**, 191–206 (2011).

16. Teyssandier, J., Mali, K. S. & De Feyter, S. Halogen Bonding in Two-Dimensional Crystal Engineering. *ChemistryOpen* **9**, 225–241 (2020).

17. Shi, Z. *et al.* Thermodynamics and Selectivity of Two-Dimensional Metallo-supramolecular Self-Assembly Resolved at Molecular Scale. *J. Am. Chem. Soc.* **133**, 6150–6153 (2011).

18. Groszek, A. J. Selective adsorption at graphite/hydrocarbon interfaces. *Proc. R. Soc. Lond. A* **314**, 473–498 (1970).

19. Rabe, J. P. & Buchholz, S. Commensurability and Mobility in Two-Dimensional Molecular Patterns on Graphite. *Science* **253**, 424–427 (1991).

20. Hentschke, R., Schürmann, B. L. & Rabe, J. P. Molecular dynamics simulations of ordered alkane chains physisorbed on graphite. *J. Chem. Phys.* **96**, 6213–6221 (1992).

21. Liang, W., Whangbo, M.-H., Wawkuschewski, A., Cantow, H.-J. & Magonov, S. N. Electronic origin of scanning tunneling microscopy images and carbon skeleton orientations of normal alkanes adsorbed on graphite. *Adv. Mater.* **5**, 817–821 (1993).

22. Magonov, S. N., Wawkuschewski, A., Cantow, H.-J., Liang, W. & Whangbo, M.-H. Scanning tunneling microscopy study of molecular order at liquid-solid interfaces. *Appl. Phys. A* **59**, 119–133 (1994).

23. Yamada, R. & Uosaki, K. Two-Dimensional Crystals of Alkanes Formed on Au(111) Surface in Neat Liquid: Structural Investigation by Scanning Tunneling Microscopy. *J. Phys. Chem. B* **104**, 6021–6027 (2000).

24. Xie, Z.-X., Huang, Z.-F. & Xu, X. Influence of reconstruction on the structure of self-assembled normal-alkane monolayers on Au(111) surfaces. *Phys. Chem. Chem. Phys.* **4**, 1486–1489 (2002).

25. Zhang, H.-M., Xie, Z.-X., Mao, B.-W. & Xu, X. Self-Assembly of Normal Alkanes on the Au (111) Surfaces. *Chem. Eur. J.* **10**, 1415–1422 (2004).

26. Lopatina, Ya. Yu., Senenko, A. I., Marchenko, A. A. & Naumovets, A. G. Self-Organization of Long-Chain Aliphatic Molecules and Their Derivatives on Atomically Flat Surfaces. *Ukr. J. Phys.* **60**, 153–159 (2015).

27. Ilan, B., Florio, G. M., Hybertsen, M. S., Berne, B. J. & Flynn, G. W. Scanning Tunneling Microscopy Images of Alkane Derivatives on Graphite: Role of Electronic Effects. *Nano Lett.* **8**, 3160–3165 (2008).

28. Chen, Q. *et al.* STM investigation of the dependence of alkane and alkane (C18H38, C19H40) derivatives self-assembly on molecular chemical structure on HOPG surface. *Surf. Sci.* **602**, 1256–1266 (2008).

29. McGonigal, G. C., Bernhardt, R. H. & Thomson, D. J. Imaging alkane layers at the liquid/graphite interface with the scanning tunneling microscope. *Appl. Phys. Lett.* **57**, 28–30 (1990).

30. McGonigal, G. C. Observation of highly ordered, two-dimensional n-alkane and n-alkanol structures on graphite. *J. Vac. Sci. Technol. B* **9**, 1107–1110 (1991).

31. Couto, M. S., Liu, X. Y., Meekes, H. & Bennema, P. Scanning tunneling microscopy studies on *n* -alkane molecules adsorbed on graphite. *J. Appl. Phys.* **75**, 627–629 (1994).

32. Venkataraman, B., Breen, J. J. & Flynn, G. W. Scanning Tunneling Microscopy Studies of Solvent Effects on the Adsorption and Mobility of Triacontane/Triacontanol Molecules Adsorbed on Graphite. *J. Phys. Chem.* **99**, 6608–6619 (1995).

33. He, Y., Ye, T. & Borguet, E. The Role of Hydrophobic Chains in Self-Assembly at Electrified Interfaces: Observation of Potential-Induced Transformations of Two-Dimensional Crystals of Hexadecane by In-situ Scanning Tunneling Microscopy. *J. Phys. Chem. B* **106**, 11264–11271 (2002).

34. Xie, Z. X., Xu, X., Tang, J. & Mao, B. W. Reconstruction-Dependent Self-Assembly of *n* -Alkanes on Au(111) Surfaces. *J. Phys. Chem. B* **104**, 11719–11722 (2000).

35. Askadskaya, L. & Rabe, J. P. Anisotropic molecular dynamics in the vicinity of order-disorder transitions in organic monolayers. *Phys. Rev. Lett.* **69**, 1395–1398 (1992).

36. Bucher, J.-P., Roeder, H. & Kern, K. Thermally induced disorder and conformational defects of alkane monolayers on graphite. *Surf. Sci.* **289**, 370–380 (1993).

37. Cyr, D. M., Venkataraman, B., Flynn, G. W., Black, A. & Whitesides, G. M. Functional Group Identification in Scanning Tunneling Microscopy of Molecular Adsorbates. *J. Phys. Chem.* **100**, 13747–13759 (1996).

38. Watel, G., Thibaudau, F. & Cousty, J. Direct observation of long chain alkane bilayer films on graphite by scanning tunneling microscopy. *Surf. Sci. Lett.* **281**, 297–302 (1993).

39. Uosaki, K. & Yamada, R. Formation of Two-Dimensional Crystals of Alkanes on the Au(111) Surface in Neat Liquid. *J. Am. Chem. Soc.* **121**, 4090–4091 (1999).

40. Yamada, R. & Uosaki, K. In Situ Observation of the Two-Dimensional Crystals of Alkanes on a Reconstructed Au(100) Surface in Neat Liquid by Scanning Tunneling Microscopy. *Langmuir* **16**, 4413–4415 (2000).

41. Marchenko, O. & Cousty, J. Molecule Length-Induced Reentrant Self-Organization of Alkanes in Monolayers Adsorbed on Au(111). *Phys. Rev. Lett.* **84**, 5363–5366 (2000).

42. Xie, Z. X., Xu, X., Tang, J. & Mao, B. W. Molecular packing in self-assembled monolayers of normal alkane on Au(111) surfaces. *Chem. Phys. Lett.* **323**, 209–216 (2000).

43. Marchenko, A., Cousty, J. & Van, L. P. Magic Length Effects in the Packing of *n* -Alkanes Adsorbed on Au(111). *Langmuir* **18**, 1171–1175 (2002).

44. Cousty, J. & Marchenko, A. Substrate-induced freezing of alkane monolayers adsorbed on Au() dependant on the alkane/gold misfit. *Surf. Sci.* **520**, 128–136 (2002).

45. Rabe, J. P. & Buchholz, S. Molecular structure and dynamics in monolayers of long chain alkanes and alkyl-derivatives. *Makromol. Chem., Macromol. Symp.* **50**, 261–268 (1991).

46. Clark, T., Hennemann, M., Murray, J. S. & Politzer, P. Halogen bonding: the σ-hole: Proceedings of "Modeling interactions in biomolecules II", Prague, September 5th–9th, 2005. *J Mol Model* **13**, 291–296 (2007).

47. Brinck, T., Murray, J. S. & Politzer, P. Surface electrostatic potentials of halogenated methanes as indicators of directional intermolecular interactions. *Int. J. Quantum Chem.* **44**, 57–64 (1992).

48. Murray, J. S., Paulsen, K. & Politzer, P. Molecular surface electrostatic potentials in the analysis of non-hydrogen-bonding noncovalent interactions. *Proc. Indian Acad. Sci. (Chem. Sci.)* **106**, 267–275 (1994).

49. Zheng, Q.-N. *et al.* Formation of Halogen Bond-Based 2D Supramolecular Assemblies by Electric Manipulation. *J. Am. Chem. Soc.* **137**, 6128–6131 (2015).

50. Mukherjee, A., Teyssandier, J., Hennrich, G., De Feyter, S. & Mali, K. S. Two-dimensional crystal engineering using halogen and hydrogen bonds: towards structural landscapes. *Chem. Sci.* **8**, 3759–3769 (2017).

51. Kikkawa, Y., Nagasaki, M., Koyama, E., Tsuzuki, S. & Hiratani, K. Hexagonal array formation by intermolecular halogen bonding using a binary blend of linear building blocks: STM study. *Chem. Commun.* **55**, 3955–3958 (2019).

52. Theobald, J. A., Oxtoby, N. S., Phillips, M. A., Champness, N. R. & Beton, P. H. Controlling molecular deposition and layer structure with supramolecular surface assemblies. *Nature* **424**, 1029–1031 (2003).

53. Lei, S. *et al.* Programmable Hierarchical Three-Component 2D Assembly at a Liquid−Solid Interface: Recognition, Selection, and Transformation. *Nano Lett.* **8**, 2541–2546 (2008).

54. Li, Y. *et al.* Thermodynamic Controlled Hierarchical Assembly of Ternary Supramolecular Networks at the Liquid-Solid Interface. *Chem. Eur. J.* **15**, 5418–5423 (2009).

55. Llanes-Pallas, A. *et al.* Trimodular Engineering of Linear Supramolecular Miniatures on Ag(111) Surfaces Controlled by Complementary Triple Hydrogen Bonds. *Angew. Chem. Int. Ed.* **47**, 7726–7730 (2008).

56. Liu, J. *et al.* Chiral Hierarchical Molecular Nanostructures on Two-Dimensional Surface by Controllable Trinary Self-Assembly. *J. Am. Chem. Soc.* **133**, 21010–21015 (2011).

57. Shen, Y.-T. *et al.* The Site-Selective Molecular Recognition of Ternary Architectures by using Supramolecular Nanoporous Networks at a Liquid-Solid Interface. *Chem. Asian J.* **5**, 787–790 (2010).

58. Shen, Y. *et al.* Self-assembling in fabrication of ordered porphyrins and phthalocyanines hybrid nano-arrays on HOPG. *CrystEngComm* **15**, 5526–5531 (2013).

59. Cui, K. *et al.* Multicomponent Self-Assembly with a Shape-Persistent *N* -Heterotriangulene Macrocycle on Au(111). *Chem. Eur. J.* **21**, 1652–1659 (2015).

60. Adisoejoso, J. *et al.* Two-Dimensional Crystal Engineering: A Four-Component Architecture at a Liquid-Solid Interface. *Angew. Chem. Int. Ed.* **48**, 7353–7357 (2009).

61. Velpula, G. *et al.* On the formation of concentric 2D multicomponent assemblies at the solution–solid interface. *Chem. Commun.* **53**, 1108–1111 (2017).

62. Xue, Y. & Zimmt, M. B. Patterned Monolayer Self-Assembly Programmed by Side Chain Shape: Four-Component Gratings. *J. Am. Chem. Soc.* **134**, 4513–4516 (2012).

63. Tahara, K. *et al.* Formation of Multicomponent Star Structures at the Liquid/Solid Interface. *Langmuir* **31**, 7032–7040 (2015).

64. Iritani, K., Tahara, K., De Feyter, S. & Tobe, Y. Host–Guest Chemistry in Integrated Porous Space Formed by Molecular Self-Assembly at Liquid–Solid Interfaces. *Langmuir* **33**, 4601–4618 (2017).

65. Bonifazi, D., Mohnani, S. & Llanes-Pallas, A. Supramolecular Chemistry at Interfaces: Molecular Recognition on Nanopatterned Porous Surfaces. *Chem. Eur. J.* **15**, 7004–7025 (2009).

66. Zhang, X., Zeng, Q. & Wang, C. Host-guest supramolecular chemistry at solid-liquid interface: An important strategy for preparing two-dimensional functional nanostructures. *Sci. China Chem.* **57**, 13–25 (2014).

67. Teyssandier, J., Feyter, S. D. & Mali, K. S. Host–guest chemistry in two-dimensional supramolecular networks. *Chem. Commun.* **52**, 11465–11487 (2016).

68. Griessl, S. J. H. *et al.* Incorporation and Manipulation of Coronene in an Organic Template Structure. *Langmuir* **20**, 9403–9407 (2004).

69. Berger, R., Resnati, G., Metrangolo, P., Weber, E. & Hulliger, J. Organic fluorine compounds: a great opportunity for enhanced materials properties. *Chem. Soc. Rev.* **40**, 3496–3508 (2011).

70. Chopra, D. & Row, T. N. G. Role of organic fluorine in crystal engineering. *CrystEngComm* **13**, 2175–2186 (2011).

71. Reichenbächer, K., Süss, H. I. & Hulliger, J. Fluorine in crystal engineering—"the little atom that could". *Chem. Soc. Rev.* **34**, 22–30 (2005).

72. Howard, J. A. K., Hoy, V. J., O'Hagan, D. & Smith, G. T. How good is fluorine as a hydrogen bond acceptor? *Tetrahedron* **52**, 12613–12622 (1996).

73. Dunitz, J. D. & Taylor, R. Organic Fluorine Hardly Ever Accepts Hydrogen Bonds. *Chem. Eur. J* **3**, 89–98 (1997).

74. Taylor, R. The hydrogen bond between N—H or O—H and organic fluorine: favourable yes, competitive no. *Acta Crystallogr. B* **73**, 474–488 (2017).

75. Thalladi, V. R. *et al.* C–H···F Interactions in the Crystal Structures of Some Fluorobenzenes. *J. Am. Chem. Soc.* **120**, 8702–8710 (1998).

76. Metrangolo, P. *et al.* The fluorine atom as a halogen bond donor, viz. a positive site. *CrystEngComm* **13**, 6593–6596 (2011).

77. Eskandari, K. & Lesani, M. Does Fluorine Participate in Halogen Bonding? *Chem. Eur. J.* **21**, 4739–4746 (2015).

78. Riley, K. E. *et al.* Halogen bond tunability I: the effects of aromatic fluorine substitution on the strengths of halogen-bonding interactions involving chlorine, bromine, and iodine. *J. Mol. Model.* **17**, 3309–3318 (2011).

79. Shimizu, T. K. *et al.* Two-Dimensional Superstructure Formation of Fluorinated Fullerene on Au(111): A Scanning Tunneling Microscopy Study. *ACS Nano* **6**, 2679–2685 (2012).

80. Shu, L., Mu, Z., Fuchs, H., Chi, L. & Mayor, M. A self assembled molecular zipper based on a perfluorophenyl-phenyl diacetylene motif. *Chem. Commun.* 1862–1863 (2006) doi:10.1039/b517759f.

81. Han, Z. *et al.* Imaging the halogen bond in self-assembled halogenbenzenes on silver. *Science* **358**, 206–210 (2017).

82. Huston, S. M. *et al.* Role of Fluorine Interactions in the Self-Assembly of a Functionalized Anthradithiophene Monolayer on Au(111). *J. Phys. Chem. C* **116**, 21465–21471 (2012).

83. Kawai, S. *et al.* Extended Halogen Bonding between Fully Fluorinated Aromatic Molecules. *ACS Nano* **9**, 2574–2583 (2015).

84. Scudiero, L., Hipps, K. W. & Barlow, D. E. A Self-Organized Two-Dimensional Bimolecular Structure. *J. Phys. Chem. B* **107**, 2903–2909 (2003).

85. Hipps, K. W., Scudiero, L., Barlow, D. E. & Cooke, M. P. A Self-Organized 2-Dimensional Bifunctional Structure Formed by Supramolecular Design. *J. Am. Chem. Soc.* **124**, 2126–2127 (2002).

86. Niederhausen, J. *et al.* Subtle Fluorination of Conjugated Molecules Enables Stable Nanoscale Assemblies on Metal Surfaces. *J. Phys. Chem. C* **122**, 18902–18911 (2018).

87. Mu, Z., Shu, L., Fuchs, H., Mayor, M. & Chi, L. Two Dimensional Chiral Networks Emerging from the Aryl−F···H Hydrogen-Bond-Driven Self-Assembly of Partially Fluorinated Rigid Molecular Structures. *J. Am. Chem. Soc.* **130**, 10840–10841 (2008).

88. Huang, Y. L. *et al.* Scanning Tunneling Microscopy Investigation of Self-Assembled CuPc/F_{16}CuPc Binary Superstructures on Graphite. *Langmuir* **26**, 3329–3334 (2010).

89. Jin, X. *et al.* Pinning-down molecules in their self-assemblies with multiple weak hydrogen bonds of C H···F and C H···N. *Chin. Chem. Lett* **28**, 525–530 (2017).

90. Rohde, D., Yan, C.-J. & Wan, L.-J. C−H···F Hydrogen Bonding: The Origin of the Self-Assemblies of Bis(2,2'-difluoro-1,3,2-dioxaborine). *Langmuir* **22**, 4750–4757 (2006).

91. Zhang, X., Yan, C.-J., Pan, G.-B., Zhang, R.-Q. & Wan, L.-J. Effect of C−H···F and O−H···O Hydrogen Bonding in Forming Self-Assembled Monolayers of BF_2-Substituted β-Dicarbonyl Derivatives on HOPG: STM Investigation. *J. Phys. Chem. C* **111**, 13851–13854 (2007).

92. Barrena, E., Oteyza, D. G. de, Dosch, H. & Wakayama, Y. 2D Supramolecular Self-Assembly of Binary Organic Monolayers. *ChemPhysChem* **8**, 1915–1918 (2007).

93. de Oteyza, D. G. *et al.* Balancing Intermolecular and Molecule-Substrate Interactions in Supramolecular Assemblies. *Adv. Funct. Mater.* **19**, 259–264 (2009).

94. Wakayama, Y., de Oteyza, D. G., Garcia-Lastra, J. M. & Mowbray, D. J. Solid-State Reactions in Binary Molecular Assemblies of F_{16}CuPc and Pentacene. *ACS Nano* **5**, 581–589 (2011).

95. Huang, Y. L. *et al.* Tunable Two-Dimensional Binary Molecular Networks. *Small* **6**, 70–75 (2010).

96. Krauss, T. N., Barrena, E., Dosch, H. & Wakayama, Y. Supramolecular Assembly of a 2D Binary Network of Pentacene and Phthalocyanine on Cu(100). *ChemPhysChem* **10**, 2445–2448 (2009).

97. Brewer, A. Y. *et al.* Supramolecular self-assembled network formation containing N···Br halogen bonds in physisorbed overlayers. *Phys. Chem. Chem. Phys.* **16**, 19608–19617 (2014).

98. Oison, V., Koudia, M., Abel, M. & Porte, L. Influence of stress on hydrogen-bond formation in a halogenated phthalocyanine network. *Phys. Rev. B* **75**, 035428 (2007).

99. de Oteyza, D. G. *et al.* Asymmetric Response toward Molecular Fluorination in Binary Copper–Phthalocyanine/Pentacene Assemblies. *J. Phys. Chem. C* **118**, 18626–18630 (2014).

100. Kawai, S. *et al.* Obtaining Detailed Structural Information about Supramolecular Systems on Surfaces by Combining High-Resolution Force Microscopy with *ab Initio* Calculations. *ACS Nano* **7**, 9098–9105 (2013).

101. Viereck, J. *et al.* Rubrene Versus Fluorine-Functionalized Rubrene Molecules on a Metal Surface: Self-Assembly, Electronic Structure, and Energy Alignment of a Monolayer on Ag(100). *J. Phys. Chem. C* **123**, 14382–14390 (2019).

102. Wong, S. L. *et al.* Effect of Fluorination on the Molecular Packing of Perfluoropentacene and Pentacene Ultrathin Films on Ag (111). *J. Phys. Chem. C* **114**, 9356–9361 (2010).

103. Barja, S. *et al.* Self-organization of electron acceptor molecules on graphene. *Chem. Commun.* **46**, 8198–8200 (2010).

104. Glowatzki, H. *et al.* Impact of Fluorination on Initial Growth and Stability of Pentacene on Cu(111). *J. Phys. Chem. C* **116**, 7726–7734 (2012).

105. de Oteyza, D. G. *et al.* Copper-phthalocyanine based metal–organic interfaces: The effect of fluorination, the substrate, and its symmetry. *J. Chem. Phys.* **133**, 214703 (2010).

106. Hirsch, B. E., McDonald, K. P., Flood, A. H. & Tait, S. L. Living on the edge: Tuning supramolecular interactions to design two-dimensional organic crystals near the boundary of two stable structural phases. *J. Chem. Phys.* **142**, 101914 (2015).

107. Mu, Z., Shu, L., Fuchs, H., Mayor, M. & Chi, L. Two-Dimensional Self-Assembly of Linear Molecular Rods at the Liquid/Solid Interface †. *Langmuir* **27**, 1359–1363 (2011).

108. Tahara, K. *et al.* Functionalized Surface-Confined Pores: Guest Binding Directed by Lateral Noncovalent Interactions at the Solid–Liquid Interface. *ACS Nano* **8**, 8683–8694 (2014).

109. Rochford, L. A., Ramadan, A. J., Holliday, S., Jones, T. S. & Nielsen, C. B. The effect of fluorination on the surface structure of truxenones. *RSC Adv.* **6**, 67315–67318 (2016).

110. Gesquière, A., Abdel-Mottaleb, M. M., De Schryver, F. C., Sieffert, M. & Müllen, K. Imaging of a Fluorine-Substituted Isophthalic Acid Derivative on Graphite with Scanning Tunneling Microscopy. *Langmuir* **15**, 6821–6824 (1999).

111. Abdel-Mottaleb, M. M. S. *et al.* In Situ Investigation of Dynamical Nanophase Separation. *Langmuir* **19**, 8256–8261 (2003).

112. Stabel, A., Dasaradhi, L., O'Hagan, D. & Rabe, J. P. Scanning Tunneling Microscopy Imaging of Single Fluorine Atom Substitution in Stearic Acid. *Langmuir* **11**, 1427–1430 (1995).

113. Muller, T., Werblowsky, T. L., Florio, G. M., Berne, B. J. & Flynn, G. W. Ultra-high vacuum scanning tunneling microscopy and theoretical studies of 1-halohexane monolayers on graphite. *Proc. Natl. Acad. Sci. U.S.A.* **102**, 5315–5322 (2005).

114. Feng, C. L. *et al.* Completely interfacial photoisomerization of 4-hydroxy-3′-trifluoromethyl-azobenzene studied by STM on HOPG. *Surf. Sci.* **513**, 111–118 (2002).

115. Bondi, A. van der Waals Volumes and Radii. *J. Phys. Chem.* **68**, 441–451 (1964).

116. Shah, P. & Westwell, A. D. The role of fluorine in medicinal chemistry: Review Article. *J. Enzyme Inhib. Med. Chem.* **22**, 527–540 (2007).

117. Tománek, D. *et al.* Theory and observation of highly asymmetric atomic structure in scanning-tunneling-microscopy images of graphite. *Phys. Rev. B* **35**, 7790–7793 (1987).

118. Batra, I. P. *et al.* A study of graphite surface with stm and electronic structure calculations. *Surf. Sci.* **181**, 126–138 (1987).

119. Lackinger, M., Griessl, S., Markert, T., Jamitzky, F. & Heckl, W. M. Self-Assembly of Benzene−Dicarboxylic Acid Isomers at the Liquid Solid Interface: Steric Aspects of Hydrogen Bonding. *J. Phys. Chem. B* **108**, 13652–13655 (2004).

120. Adisoejoso, J. *et al.* Two-Dimensional Crystal Engineering: A Four-Component Architecture at a Liquid–Solid Interface. *Angew. Chem. Int. Ed.* **48**, 7353–7357 (2009).

121. Destoop, I. *et al.* Solvent-Induced Homochirality in Surface-Confined Low-Density Nanoporous Molecular Networks. *J. Am. Chem. Soc.* **134**, 19568–19571 (2012).

122. Park, K.-W. *et al.* Self-Assembly Behavior of Alkylated Isophthalic Acids Revisited: Concentration in Control and Guest-Induced Phase Transformation. *Langmuir* **30**, 15206–15211 (2014).

123. Tahara, K., Nakatani, K., Iritani, K., De Feyter, S. & Tobe, Y. Periodic Functionalization of Surface-Confined Pores in a Two-Dimensional Porous Network Using a Tailored Molecular Building Block. *ACS Nano* **10**, 2113–2120 (2016).

124. Tahara, K. *et al.* Tailoring Surface-Confined Nanopores with Photoresponsive Groups. *Angew. Chem. Int. Ed.* **52**, 8373–8376 (2013).

125. Blunt, M. *et al.* Directing two-dimensional molecular crystallization using guest templates. *Chem. Commun.* 2304–2306 (2008) doi:10.1039/b801267a.

126. Blunt, M. O. *et al.* Random Tiling and Topological Defects in a Two-Dimensional Molecular Network. *Science* **322**, 1077–1081 (2008).

127. Kampschulte, L., Griessl, S., Heckl, W. M. & Lackinger, M. Mediated Coadsorption at the Liquid−Solid Interface: Stabilization through Hydrogen Bonds. *J. Phys. Chem. B* **109**, 14074–14078 (2005).

128. Zhang, X. *et al.* Two-dimensional networks of an azobenzene derivative: bi-pyridine mediation and photo regulation. *Nanoscale* **4**, 5039–5042 (2012).

129. Cometto, F. *et al.* The STM bias voltage-dependent polymorphism of a binary supramolecular network. *Chem. Commun.* **53**, 11430–11432 (2017).

130. Li, M. *et al.* A dynamic study of the structural change in the binary network in response to guest inclusion. *Phys. Chem. Chem. Phys.* **16**, 8778–8782 (2014).

131. Li, M., Yang, Y.-L., Zhao, K.-Q., Zeng, Q.-D. & Wang, C. Bipyridine-Mediated Assembling Characteristics of Aromatic Acid Derivatives. *J. Phys. Chem. C* **112**, 10141–10144 (2008).

132. Peng, X. *et al.* Pyridine-induced interfacial structural transformation of tetraphenylethylene derivatives investigated by scanning tunneling microscopy. *Nano Res.* **11**, 5823–5834 (2018).

133. Eichhorst-Gerner, K. *et al.* Self-Assembly of a Two-Component Hydrogen-Bonded Network: Comparison of the Two-Dimensional Structure Observed by Scanning Tunneling Microscopy and the Three-Dimensional Crystal Lattice. *Angew. Chem. Int. Ed. Engl.* **35**, 1492–1495 (1996).

134. Frisch, M. *et al. Gaussian 03, Revision C.02*. (2003).

135. Janczak, J., Śledź, M. & Kubiak, R. Catalytic trimerization of 2- and 4-cyanopyridine isomers to the triazine derivatives in presence of magnesium phthalocyanine. *J. Mol. Struct.* **659**, 71–79 (2003).

136. Dienstmaier, J. F. *et al.* On the Scalability of Supramolecular Networks − High Packing Density vs Optimized Hydrogen Bonds in Tricarboxylic Acid Monolayers. *Langmuir* **26**, 10708–10716 (2010).

137. Gatti, R. *et al.* Substrate, Molecular Structure, and Solvent Effects in 2D Self-Assembly via Hydrogen and Halogen Bonding. *J. Phys. Chem. C* **118**, 25505–25516 (2014).

138. MacLeod, J. M., Ben Chaouch, Z., Perepichka, D. F. & Rosei, F. Two-Dimensional Self-Assembly of a Symmetry-Reduced Tricarboxylic Acid. *Langmuir* **29**, 7318–7324 (2013).

139. Sirtl, T. *et al.* Solvent-Dependent Stabilization of Metastable Monolayer Polymorphs at the Liquid–Solid Interface. *ACS Nano* **7**, 6711–6718 (2013).

140. Li, Y. *et al.* Solvent Effects on Supramolecular Networks Formed by Racemic Star-Shaped Oligofluorene Studied by Scanning Tunneling Microscopy. *J. Phys. Chem. C* **112**, 8649–8653 (2008).

141. Gutzler, R. *et al.* Reversible Phase Transitions in Self-Assembled Monolayers at the Liquid−Solid Interface: Temperature-Controlled Opening and Closing of Nanopores. *J. Am. Chem. Soc.* **132**, 5084–5090 (2010).

142. Saiz-Poseu, J. *et al.* Self-assembly of a catechol-based macrocycle at the liquid–solid interface: experiments and molecular dynamics simulations. *Phys. Chem. Chem. Phys.* **14**, 11937–11943 (2012).

143. Kikkawa, Y., Omori, K., Kanesato, M. & Hiratani, K. Two-dimensional Structures of Isobutenyl Ether Compounds Possessing Dodecyl and Tridecyl Chains: Effects of Solvent and Tandem Claisen Rearrangement. *Chem. Lett.* **41**, 1196–1198 (2012).

144. Patera, L. L. *et al.* Crystallization of a Two-Dimensional Hydrogen-Bonded Molecular Assembly: Evolution of the Local Structure Resolved by Atomic Force Microscopy. *Angew. Chem. Int. Ed.* **56**, 10786–10790 (2017).

145. Gao, H.-Y. *et al.* In-plane Van der Waals interactions of molecular self-assembly monolayer. *Appl. Phys. Lett.* **106**, 081606 (2015).

146. Shen, Y. *et al.* Triangular-shaped molecular random tiling and molecular rotation in two-dimensional glassy networks. *Nanoscale* **6**, 7221–7225 (2014).

147. Middleton, W. J. & Lindsey, R. V. Hydrogen Bonding in Fluoro Alcohols. *J. Am. Chem. Soc.* **86**, 4948–4952 (1964).

148. Heger, M., Scharge, T. & Suhm, M. A. From hydrogen bond donor to acceptor: the effect of ethanol fluorination on the first solvating water molecule. *Phys. Chem. Chem. Phys.* **15**, 16065–16073 (2013).

149. Hansen, A. S., Du, L. & Kjaergaard, H. G. The effect of fluorine substitution in alcohol–amine complexes. *Phys. Chem. Chem. Phys.* **16**, 22882–22891 (2014).

150. Juršić, B., Ladika, M. & Sunko, D. E. 1H nmr study of hydrogen bonding of fluorinated alcohols with ethers. *Tetrahedron Lett.* **26**, 5323–5324 (1985).

151. Abraham, M. H. *et al.* Hydrogen bonding. Part 7. A scale of solute hydrogen-bond acidity based on log K values for complexation in tetrachloromethane. *J. Chem. Soc., Perkin Trans. 2* 699–711 (1989) doi:10.1039/p29890000699.

152. Reeves, L. W. HYDROGEN BONDING IN SOLUTIONS OF SUBSTITUTED ACETIC ACIDS. *Can. J. Chem.* **39**, 1711–1720 (1961).

153. Della Pia, A., Luo, D., Blackwell, R., Costantini, G. & Martsinovich, N. Molecular self-assembly of substituted terephthalic acids at the liquid/solid interface: investigating the effect of solvent. *Faraday Discuss.* **204**, 191–213 (2017).

154. Lackinger, M., Griessl, S., Kampschulte, L., Jamitzky, F. & Heckl, W. M. Dynamics of Grain Boundaries in Two-Dimensional Hydrogen-Bonded Molecular Networks. *Small* **1**, 532–539 (2005).

155. Yasuda, S., Furuya, A. & Murakoshi, K. Control of a two-dimensional molecular structure by cooperative halogen and hydrogen bonds. *RSC Adv.* **4**, 58567–58572 (2014).

156. Lemmerer, A., Govindraju, S., Johnston, M., Motloung, X. & L. Savig, K. Co-crystals and molecular salts of carboxylic acid/pyridine complexes: can calculated p K a ’s predict proton transfer? A case study of nine complexes. *CrystEngComm* **17**, 3591–3595 (2015).

157. Clair, S., Abel, M. & Porte, L. Mesoscopic Arrays from Supramolecular Self-Assembly. *Angew. Chem. Int. Ed.* **49**, 8237–8239 (2010).

158. Pawlak, R. *et al.* Robust Supramolecular Network on Ag(111): Hydrogen-Bond Enhancement through Partial Alcohol Dehydrogenation. *ChemPhysChem* **10**, 1032–1035 (2009).

159. Abel, M., Oison, V., Koudia, M. & Porte, L. Conformational change of tetrahydroxyquinone molecules deposited on Ag(111). *Phys. Rev. B* **77**, 085410 (2008).

160. Marele, A. C. *et al.* Some Pictures of Alcoholic Dancing: From Simple to Complex Hydrogen-Bonded Networks Based on Polyalcohols. *J. Phys. Chem. C* **117**, 4680–4690 (2013).

161. Kitaguchi, Y. *et al.* Comparative study of phenol and thiophenol adsorption on Cu(110). *J. Chem. Phys.* **139**, 044708 (2013).

162. Feng, L. *et al.* Supramolecular Tessellations at Surfaces by Vertex Design. *ACS Nano* **13**, 10603–10611 (2019).

163. Shattock, T. R., Arora, K. K., Vishweshwar, P. & Zaworotko, M. J. Hierarchy of Supramolecular Synthons: Persistent Carboxylic Acid···Pyridine Hydrogen Bonds in Cocrystals That also Contain a Hydroxyl Moiety. *Cryst. Growth Des.* **8**, 4533–4545 (2008).

164. Saccone, M. *et al.* Supramolecular hierarchy among halogen and hydrogen bond donors in light-induced surface patterning. *J. Mater. Chem. C* **3**, 759–768 (2015).

165. Saccone, M. *et al. ortho* -Fluorination of azophenols increases the mesophase stability of photoresponsive hydrogen-bonded liquid crystals. *J. Mater. Chem. C* **6**, 9958–9963 (2018).

166. Robertson, Craig. C. *et al.* Hydrogen bonding vs. halogen bonding: the solvent decides. *Chem. Sci.* **8**, 5392–5398 (2017).

167. Karanam, M. & Choudhury, A. R. Study of Halogen-Mediated Weak Interactions in a Series of Halogen-Substituted Azobenzenes. *Cryst. Growth Des.* **13**, 4803–4814 (2013).

168. Habets, T., Speller, S. & Elemans, J. A. A. W. Role of redox-active axial ligands of metal porphyrins adsorbed at solid–liquid interfaces in a liquid-STM setup. *Beilstein J. Nanotechnol.* **11**, 1264–1271 (2020).

169. Huang, K.-S., Britton, D., Etter, M. C. & Byrn, S. R. A novel class of phenol–pyridine co-crystals for second harmonic generation. *J. Mater. Chem.* **7**, 713–720 (1997).

170. Steiner, T. The Hydrogen Bond in the Solid State. *Angew. Chem. Int. Ed.* **41**, 48–76 (2002).

171. Wood, P. A., Allen, F. H. & Pidcock, E. Hydrogen-bond directionality at the donor H atom—analysis of interaction energies and database statistics. *CrystEngComm* **11**, 1563–1571 (2009).

172. Llamas-Saiz, A. L., Foces-Foces, C., Mo, O., Yañez, M. & Elguero, J. Nature of the hydrogen bond: crystallographic versus theoretical description of the O-H···N(sp2) hydrogen bond. *Acta Crystallogr. B* **48**, 700–713 (1992).

173. Ginn, S. G. W. The phenol-pyridine hydrogen bonded complex: a cndo/2 study. *J. Mol. Struct.* **49**, 137–153 (1978).

174. Zhang, J. *et al.* Spontaneous Chiral Resolution in Supramolecular Assembly of 2,4,6-Tris(2-pyridyl)-1,3,5-triazine on Au(111). *J. Am. Chem. Soc.* **131**, 5885–5890 (2009).

175. Saha, B. K., Nangia, A. & Jaskólski, M. Crystal engineering with hydrogen bonds and halogen bonds. *CrystEngComm* **7**, 355–358 (2005).

176. Tothadi, S. & Desiraju, G. R. Designing ternary cocrystals with hydrogen bonds and halogen bonds. *Chem. Commun.* **49**, 7791–7793 (2013).

177. Aakeröy, C. B. *et al.* Combining halogen bonds and hydrogen bonds in the modular assembly of heteromeric infinite 1-D chains. *Chem. Commun.* 4236–4238 (2007) doi:10.1039/b707458a.

178. Aakeröy, C. B., Chopade, P. D., Ganser, C. & Desper, J. Facile synthesis and supramolecular chemistry of hydrogen bond/halogen bond-driven multi-tasking tectons. *Chem. Commun.* **47**, 4688–4690 (2011).

179. Aakeröy, C. B., Chopade, P. D. & Desper, J. Avoiding "Synthon Crossover" in Crystal Engineering with Halogen Bonds and Hydrogen Bonds. *Cryst. Growth Des.* **11**, 5333–5336 (2011).

180. Aakeröy, C. B., Schultheiss, N. C., Rajbanshi, A., Desper, J. & Moore, C. Supramolecular Synthesis Based on a Combination of Hydrogen and Halogen Bonds. *Cryst. Growth Des.* **9**, 432–441 (2009).

181. Zhu, S., Xing, C., Xu, W., Jin, G. & Li, Z. Halogen Bonding and Hydrogen Bonding Coexist in Driving Self-Assembly Process. *Cryst. Growth Des.* **4**, 53–56 (2004).

182. DeHaven, B. A. *et al.* Synergistic effects of hydrogen and halogen bonding in co-crystals of dipyridylureas and diiodotetrafluorobenzenes. *Supramol. Chem.* **30**, 315–327 (2018).

183. Aakeröy, C. B., Fasulo, M., Schultheiss, N., Desper, J. & Moore, C. Structural Competition between Hydrogen Bonds and Halogen Bonds. *J. Am. Chem. Soc.* **129**, 13772–13773 (2007).

184. Aakeröy, C. B., Panikkattu, S., Chopade, P. D. & Desper, J. Competing hydrogen-bond and halogen-bond donors in crystal engineering. *CrystEngComm* **15**, 3125–3136 (2013).

185. Aakeröy, C. B., Spartz, C. L., Dembowski, S., Dwyre, S. & Desper, J. A systematic structural study of halogen bonding versus hydrogen bonding within competitive supramolecular systems. *IUCrJ* **2**, 498–510 (2015).

186. Corradi, E., Meille, S. V., Messina, M. T., Metrangolo, P. & Resnati, G. Halogen Bonding versus Hydrogen Bonding in Driving Self-Assembly Processes. *Angew. Chem. Int. Ed.* **39**, 1782–1786 (2000).

187. Wu, Y. *et al.* Halogen bonding versus hydrogen bonding induced 2D self-assembled nanostructures at the liquid–solid interface revealed by STM. *Phys. Chem. Chem. Phys.* **19**, 3143–3150 (2017).

188. Zha, B., Li, J., Wu, J., Miao, X. & Zhang, M. Cooperation and competition of hydrogen and halogen bonds in 2D self-assembled nanostructures based on bromine substituted coumarins. *New J. Chem.* **43**, 17182–17187 (2019).

189. Dong, M. *et al.* Halogen-bonded building block for 2D self-assembly: Triggered by hydrogen-bonding motifs relative to the terminal functions of the side chains. *Appl. Surf. Sci.* **515**, 145983 (2020).

190. Pauling, L. *The Nature of the Chemical Bond*. (Cornell University Press, 1960).

191. Carlson, E. E., May, J. F. & Kiessling, L. L. Chemical Probes of UDP-Galactopyranose Mutase. *Chem. Biol.* **13**, 825–837 (2006).

192. Park, S. *et al.* Focusing Mutations into the P. fluorescens Esterase Binding Site Increases Enantioselectivity More Effectively than Distant Mutations. *Chem. Biol.* **12**, 45–54 (2005).

193. Metrangolo, P., Panzeri, W., Recupero, F. & Resnati, G. Perfluorocarbon–hydrocarbon self-assembly. *J. Fluorine Chem.* **114**, 27–33 (2002).

194. Řezáč, J. & de la Lande, A. On the role of charge transfer in halogen bonding. *Phys. Chem. Chem. Phys.* **19**, 791–803 (2017).

195. Bertrán, J. F. & Rodríguez, M. Detection of halogen bond formation by correlation of proton solvent shifts 1. Haloforms in n-electron donor solvents. *Org. Magn. Reson.* **12**, 92–94 (1979).

196. Martire, D. E., Sheridan, J. P., King, J. W. & O'Donnell, S. E. Thermodynamics of molecular association. 9. An NMR study of hydrogen bonding of chloroform and bromoform to di-n-octyl ether, di-n-octyl thioether, and di-n-octylmethylamine. *J. Am. Chem. Soc.* **98**, 3101–3106 (1976).

197. Questel, J.-Y. L., Laurence, C. & Graton, J. Halogen-bond interactions: a crystallographic basicity scale towards iodoorganic compounds. *CrystEngComm* **15**, 3212–3221 (2013).

198. Perkins, C., Libri, S., Adams, H. & Brammer, L. Diiodoacetylene: compact, strong ditopic halogen bond donor. *CrystEngComm* **14**, 3033–3038 (2012).

199. Erdélyi, M. Halogen bonding in solution. *Chem. Soc. Rev.* **41**, 3547–3557 (2012).

200. Li, T., Zhou, P. & Mattei, A. Electronic origin of pyridinyl N as a better hydrogen-bonding acceptor than carbonyl O. *CrystEngComm* **13**, 6356–6360 (2011).

201. Aakeröy, C. B., Beatty, A. M. & Helfrich, B. A. "Total Synthesis" Supramolecular Style: Design and Hydrogen-Bond-Directed Assembly of Ternary Supermolecules. *Angew. Chem. Int. Ed.* **113**, 3340–3342 (2001).

202. Steiner, T. Competition of hydrogen-bond acceptors for the strong carboxyl donor. *Acta Crystallogr. B* **57**, 103–106 (2001).

203. Cometto, F. P., Kern, K. & Lingenfelder, M. Local Conformational Switching of Supramolecular Networks at the Solid/Liquid Interface. *ACS Nano* **9**, 5544–5550 (2015).

204. Horcas, I. *et al.* WSXM: A software for scanning probe microscopy and a tool for nanotechnology. *Rev. Sci. Instrum.* **78**, 013705 (2007).

205. LMAPper - The SPM and Mol Viewer. *SourceForge* https://sourceforge.net/projects/spm-and-mol-viewer/.